Wrocław University of Science and Technology

DOCTORAL DISSERTATION

DEVELOPMENT OF METHODS

FOR DETERMINATION OF MECHANICAL

PARAMETERS OF LIPID MEMBRANES

MSc. BEng. Dominik Drabik

Supervisor: Prof. Marek Langner
Department of Biomedical Engineering
Faculty of Fundamental Problems of Technology
Wrocław University of Science and Technology
Wrocław, Poland

Faculty of Fundamental Problems of Technology
Department of Biomedical Engineering

Table of Contents

This PhD dissertation is an article thesis. It is a collection of below three articles:

(page left intentionally blank)

Synopsis of dissertation (ENL/PL)

The development of mechanobiology in recent years has significantly accelerated and gained in importance. This field of science focus on explaining how both mechanical properties of biological structures and external forces or changes in cell or tissue mechanical environment contribute to development, physiology and functioning of the cells. The subject of the dissertation is the development and implementation of experimental methods for determining mechanical parameters of lipid membranes. The development of experimental methods consists of three stages – the implementation of the measurement technique, the verification by investigation of membranes with established in literature parameters and, finally, the use of the method to address the scientific issues. In this dissertation measurement techniques based on the analysis of thermal fluctuation of lipid membranes were developed. Specifically, those were the vesicle fluctuation analysis technique and numerical analysis of the fluctuations using molecular dynamics simulation. The vesicle fluctuation analysis is based on recording the membrane fluctuation in the equatorial plane in order to quantitatively measure the fluctuation as a function of time. The great advantage of the method is its non-invasiveness and the possibility to control experimental conditions. Molecular dynamics simulations are used to determine mechanical parameters requires appropriately long simulations to observe spontaneous fluctuations and then use the appropriate numerical workshop. In this work the full lipid vesicle simulation approach was used, which allows to consider the effect of membrane curvature and then analyze the fluctuation spectrum from the full three-dimensional object. In both techniques, innovative and significant improvements have been introduced. The introduced modifications contributed to increase of the quality and precision of the obtained results leading to reproducible and accurate mechanical parameters of a lipid bilayer. In addition, the method of electroformation, which is used to produce the experimental model of lipid membranes, namely giant unilamellar vesicles, was extensively tested and improved. The core of the dissertation consists of three articles presenting stages of the implementation and improvements of research tools employed for the determination of biologically relevant mechanical properties of model lipid bilayers.

Streszczenie pracy

Rozwój mechanobiologii w ostatnich latach znacząco przyśpieszył i przybrał na znaczeniu. Jest to dziedzina nauki zajmująca się wpływem właściwości mechanicznych struktur biologicznych, wpływem zewnętrznych nacisków oraz zmian w komórce czy tkance w wyniku zmian środowiska mechanicznego na rozwój, fizjologię, funkcjonowanie i patogenezę w komórce. Tematem rozprawy doktorskiej jest opracowywanie i rozwój metod doświadczalnych do wyznaczania parametrów mechanicznych błon lipidowych. W konsekwencji tego prowadzone badania zwykle składają się z trzech głównych etapów – wdrożenia metody pomiarowej, jej weryfikacji poprzez zbadanie dobrze poznanych w literaturze błon i, ostatecznie, wykorzystaniu metody do pomiarów w celu wyjaśnienia zagadnienia naukowego. W ramach pracy wdrożono techniki pomiarowe bazujące na analizie fluktuacji termicznych błon lipidowych - technikę analizy drgań termicznych oraz numeryczną analizę fluktuacji pęcherzyka z wykorzystaniem symulacji dynamiki molekularnej. Technika analizy drań termicznych (flicker-noise) bazuje na rejestrowaniu fluktuacji pęcherzyka w płaszczyźnie ogniskowej w celu ilościowego pomiaru fluktuacji w funkcji czasu. Jej ogromną zaletą jest jej nieinwazyjność i możliwość kontroli warunków eksperymentu. Wykorzystanie symulacji dynamiki molekularnej do wyznaczenia parametrów mechanicznych wymaga przeprowadzenia odpowiednio długich symulacji w celu zaobserwowania spontanicznych fluktuacji, a następnie wykorzystania odpowiedniego warsztatu numerycznego. W ten pracy wykorzystano podejście symulacji pełnego pęcherzyka lipidowego, co pozwala na uwzględnienie efektu krzywizny błony, a następnie analiza spektrum fluktuacji z pełnego trójwymiarowego obiektu. W obu technikach wprowadzono innowacyjne i unikalne usprawniania, które przyczyniły się do zwiększenia jakości otrzymywanych wyników, a w konsekwencji do zwiększenia powtarzalności i zmniejszenia niedokładności wyznaczanych parametrów. Ponadto przeanalizowano i usprawniono metodę elektroformacji, która pozwala na otrzymanie badanych modeli błon lipidowych – gigantycznych jednowarstwowych pęcherzyków lipidowych. Rdzeniem pracy są trzy publikacje naukowe, w których opisano etapy wdrażania, weryfikacji, zastosowania innowacyjnych usprawnień oraz przykłady problemów naukowych, do których wykorzystano powyższe techniki.

Nomenclature (Constants, Symbols and Abbreviations)

Constants

k_B The Boltzmann constant, $k_B = 1.3806 \cdot 10^{-23} \frac{J}{K}$

Symbols

μ	shearing elastic module	u^1, u^2	parameters describing local coordinate system
K_a	compressibility module	$\mathbf{e}_1, \mathbf{e}_2$	surface tangent vectors
κ	bending rigidity coefficient [J]	g_{ij}	induced metric tensor / metric
k_G	Gaussian curvature module	g	determinant of induced metric tensor
T_m	main transition temperature [K]	$\mathbf{n}$	normal vector to the local surface
E_{exp}	the stretching elastic energy per unit area	K_{ij}	extrinsic curvature tensor
A_0	equilibrium area surface	K	total extrinsic curvature
A_d	deformed area surface	K_G	Gaussian curvature
E_{bend}	bending energy per unit area	σ	surface tension
K_1, K_2	principal curvatures, eigenvalues of curvature tensor	F_c	elastic free energy
		$\mathbf{r}$	positional vector of the membrane
κ	the bending elastic modulus	R_{sphere}	reference sphere radius
k_G	the Gaussian elastic modulus	ω_0	static part of perturbation
K_0	spontaneous curvature, local preferred curvature	$\delta\omega$	dynamic part of perturbation
		Y_n^m	spherical harmonics
A	total surface	U_n^m	amplitudes of spherical harmonics
dA	differential area element		

Abbreviations

PC	phosphatidylcholine	DPG	diphosphatidylglycerol/cardiolipin
PE	phosphatidylethanolamine	GUV	Giant Unilamellar Vesicle
PS	phosphatidylserine	SLB	Supported Lipid Bilayer
PI	phosphatidylinositol	VFA	Vesicle Fluctuation Analysis
PG	phosphatidylglycerol	fps	frames per second
SM	sphingomyelin	FF	Force Field
MG	monogalactosyldiglyceride	SPHA	Spherical Harmonics Analysis

Abbreviations of Lipid Molecules

POPC	1-palmitoyl-2-oleoyl-glycero-3-phosphocholine	16:0-18:1 PC
DOPC	1,2-dioleoyl-sn-glycero-3-phosphocholine	18:1c9 PC
DMPC	1,2-dimyristoyl-sn-glycero-3-phosphocholine	14:0 PC
DPPC	1,2-dipalmitoyl-sn-glycero-3-phosphocholine	16:0 PC
DOPE	1,2-dioleoyl-sn-glycero-3-phosphoethanolamine	18:1 (Δ9-Cis) PE
DSPC	1,2-distearoyl-sn-glycero-3-phosphocholine	18:0 PC

Aims of the dissertation

The main aim of this dissertation is the development of methods and numerical tools to determine mechanical properties of lipid bilayers. This main aim consist of below partial aims:

- detailed study of used lipid membrane model, especially in respect to preparation technique, to ensure sufficient quality and repeatability of the investigated sample.

- development of vesicle fluctuation analysis technique in order to determine bending rigidity coefficient as part of mechanical description of lipid bilayers.

- development of numerical tools for analysis of molecular dynamics simulation systems of lipid bilayer in order to determine mechanical properties of lipid bilayers. As a supporting technique, it allows additional insight into molecular processes.

- development of experimental technique for determination of area compressibility to provide full description of mechanical model of lipid membrane.

- application of developed techniques and numerical tools to investigate effects of various factors on mechanical properties as well as solve selected biophysical problems.

Correlation of the dissertation subject to biomedical engineering

Lipid membrane has been acknowledged as a versatile biomaterial, which is known for its biocompatibility and biodegradability. Investigation of mechanical properties of lipid membrane provides crucial information necessary for effective design of lipid drug delivery systems and increase knowledge about the biomaterial itself. As a result it can contribute to various aspects of biomedical engineering such as understanding of pathogenesis origin of various diseases and reasons for physiological disruption, as well as possible solutions to those conditions. Developed tools and methods are known to such fields as bioinformatics, biological imaging, image processing, biomechanics, physics and mathematical modelling. Implementation of those tools to increase knowledge of physiological processes, which in result may lead to finding novel ways for curing of those conditions, are essence of the field known as biomedical engineering.

(page left intentionally blank)

1. Outline/description of dissertation

1.1. Mechanobiology – new trend in biophysics

Over past few years mechanical forces has been recognized as a critical factor to many biological processes at organism, tissue, cell and molecular levels. This have resulted in the emergence of the interdisciplinary field known as mechanobiology [1]. The field focuses on studying the effects of mechanical properties and external forces on behavior of biological structures. Specifically, how do the changes in mechanical environment of cells or tissues contribute to their development, physiology, functioning and occurrence of undesired phenomena such as disease. In order to describe the subject of this dissertation it is necessary to, first of all, outline biomechanical point of view in cell functioning. In general, a single cell is described as a fluid crowded with organelles, macromolecules and structures of various purposes, networked with cytoskeleton and covered by a biological membrane. However, it is sometimes modelled as an encapsulated lipid membrane containing stress-supported structures, which helps its deformation, adhesion, and spreading [2-4]. Cell can also be described as a complex biological machine that constantly consumes energy to maintain its organization [5]. This energy consumption is used to overcome the tendency to maximize entropic disorder and to self-organize itself [6]. Being such molecular machine, the cell can organize and operate complex processes at molecular level. The processes performed by a cell can be looked upon from a variety of perspectives. Some functions are chemical, such as the manufacture of proteins, while others can be classified as information processing, such as cell recognition of another cell as friend or foe. However some, often neglected, functions performed by a cell are of physical/mechanical nature. Examples of such functions are: maintaining and/or changing the shape of a cell, movement of a cells, internal transport of the material, limited adhesion to other cells, stability and resistance [7]. Additionally, numerous membrane components, such as transmembrane proteins, lipid bilayer, cytoskeleton or nuclei, are mechanically sensitive and can contribute to the functioning of whole cell system [8]. Furthermore, cells tend to adjust their mechanical properties to match the substrate [9]. This shows that cell mechanics plays a crucial, yet slightly underestimated, role in many biological processes [10]. A deviation in mechanical properties of cell can be a sign of a variety of pathologies [11]. It is therefore of interest to understand how cells respond to mechanical forces and how these forces influence their life cycle [12]. Furthermore, cells can adopt various of shapes, ranging from smooth-disk erythrocytes, through stretched and triangular skin fibroblasts to branched and highly elongated neurons. Yet the primary mechanical element of all cells is the same: one or more fluid layers surround the cell and its internal compartments while filaments form a flexible scaffolding primarily, but not exclusively, confined within the cell. Again, mechanics of cell plays a crucial part in this process [13].

One of most influential factors on mechanics of cell is biological membrane. It is, at the same time, one of the most important cell structure. It can be described as a barrier surrounding a cell, that additionally facilitates transport of substances into the cell and removal of waste and toxins out of the cell. Since it is a barrier, it is characterized by low permeability for charges particles, which allows to maintain non-equilibrium ion distribution between interior and exterior of the cell, which is crucial for cell functioning. They also fulfil both contact and receptor functions, being responsible for contact between other cells by means of specific structures and being susceptible from environment factors by means of special protein structures incorporated into the membrane [14]. While membranes varies in composition, structure and organization to fulfill mentioned functions, all of the membranes share common general structure, which are usually referred to as *corner stone* of biological membrane. It consist of self-assembled lipids and proteins held together by noncovalent interactions (such as electrostatic interactions) and hydrophobic effect. The plasma membrane of cell is composed of two main layers: the lipid bilayer in the middle and glycocalyx facing the extracellular space. In some descriptions cytoskeleton, which is located on the edge of cytoplasm and membrane is considered as apart of membrane. This whole structure is the mixture of around 50 wt% of lipids, 40 wt% of proteins and 10 wt% of carbohydrates [15]. Serving as a barrier, lipid bilayer consists of several kinds of lipids (with individual lipids types reaching up to thousands) with inserted proteins, that mediate most of the specific functions of membrane. Sketch of lipid bilayer is presented in Figure 1.1. *Outside* of bilayer carbohydrate residues coming from

lateral tails of either glycolipids or glycoproteins are present. This glycocalyx forms a mechanically resistant layer for the cell, as well as participating in adhesion and cell recognition. *Inside* of bilayer tridimensional network of cytoskeleton's filaments can be found. This structure is coupled to the membrane and allows to keep or change the shape of a cell. As a result movement of a cell and rearrangement of the internal organelles are done through the cytoskeleton [15, 16]. As the biological membrane is examined ever more closely, it emerges that it may not just be vertically inhomogeneous (difference in composition between the leaflets), but also spatially inhomogeneous because of the presence of lipid rafts [17, 18]. The difference between the two types of domains commonly involves a difference in phase of lipids and their mechanical properties. The fact that the two phases are different in case of mechanical and structural properties opens up the possibility that preferential incorporation of proteins occurs [19]. Due to composition difference between the individual leaflets of membrane, a constant bend of a whole bilayer may occur, which would result in non-vanishing curvature. Same can happen due to lateral phase separation. Anisotropic structural elements also can influence cell shape. For instance, membrane may stretch more easily in one direction than another if the membrane components have different stiffness or different raft organization [13]. Nevertheless, lipids, with their ability to self-assemble into bilayers due to hydrophobic effect, emerge as an interesting and important part of biological membrane.
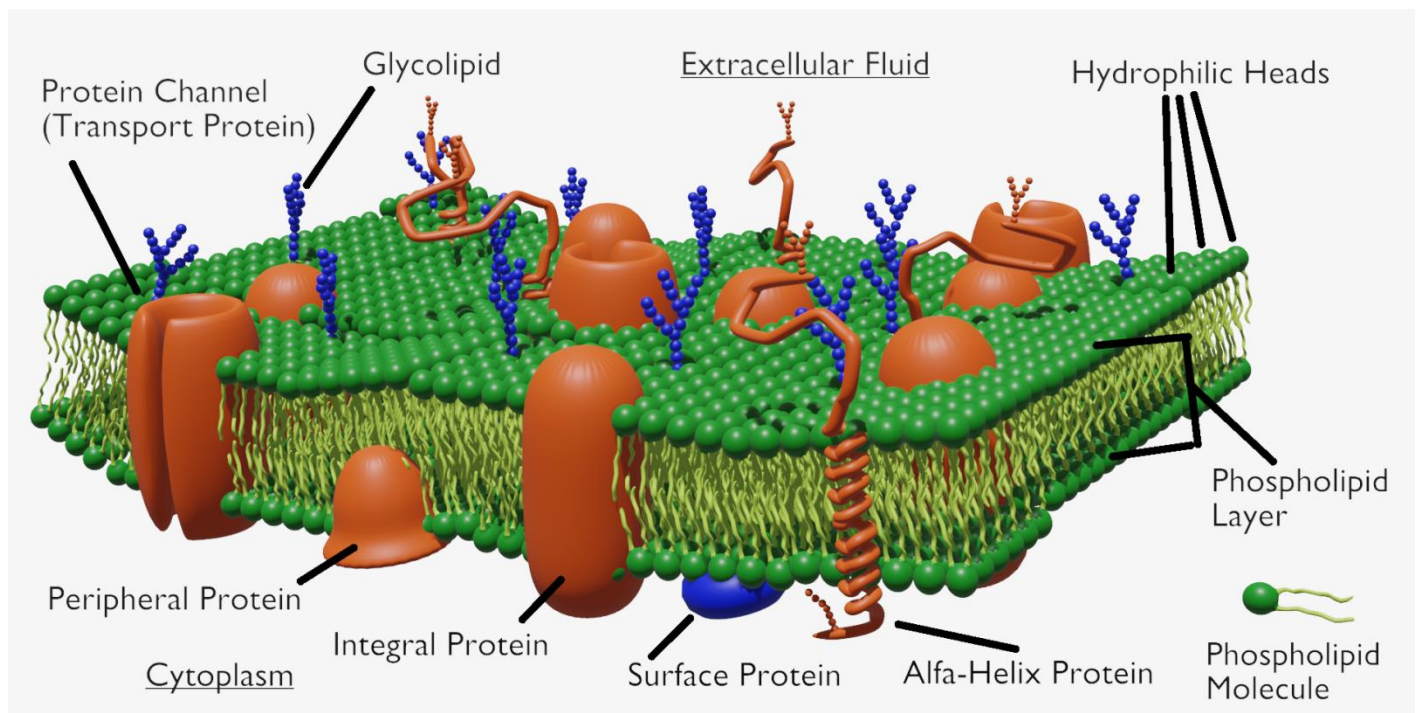

Figure 1.1. A scheme of biological membrane. Common building blocks of biological membrane are: phospholipids formed in layer and various proteins. Cytoskeleton filaments in cytoplasm were omitted for better readability.
Graphic rendered using Blender 2.8 software (GPL license) and is a property of dissertation's author.

Lipids are special class of amphiphilic molecules generally composed of polar head group and two hydrophobic (due to presence of non-polar acyl chains) tails. There exist more than 1000 various lipids that differ in length and composition of hydrophobic chains and polar head groups. Lipids can be divided into three main categories: phospholipids, glycolipids and sterols. Phospholipids are most common among lipids in biological membranes. They can be divided in glycerophospholipids and sphingophospholipids. The glycerophospholipids (phosphatidylcholine (PC), phosphatidylethanolamine (PE), phosphatidylserine (PS), phosphatidylinositol (PI) and phosphatidylglycerol (PG)) have common structure. Structure of selected lipids is visualized in Figure 1.2. It consists of polar head groups and two hydrophobic acyl chains that are connected to the glycerol backbone. The structure of glycerophospholipids and sphingophospholipids differs significantly in the interfacial and hydrophobic part – for instance common base in mammalian sphingomyelin (SM) is sphingosine with trans-double bond between C4 and C5 atoms [14]. Phospholipids play dominantly structural role in the biological membrane. They participate in formation of barrier between the interior and exterior environment and provide special site for functioning of membrane proteins.

Additionally, certain lipids have functional role. Example of such lipid is SM – an important component of eukaryotic cells. Having same shape like PC to minimize free energy in formation of lipid bilayers, it participates in cell signaling. SM is believed to be an important source of ceramides for the nuclear and mitochondrial apoptotic cascades [14, 20, 21]. SM forms stable complexes with cholesterol known as rafts, which makes it an important factor in lipid sorting and cell functioning. Second category of lipids – glycolipids – are localized only on extracellular site of membrane. The sugar residues of glycolipids are exposed to external part of cell and create a film, which serves as recognition sites for cell-cell interactions and facilitates immune responses. Last category – sterols – are constructed on base of sterol backbone. Most common sterol is, exclusive to animal cells, cholesterol, which role together with SM has already been described. In addition to mentioned already lipids, there exist less common lipids that can be found in biological membrane, for instance plasmalogen. It can be found in nervous, immune and cardiovascular cells and is known to protect cells from reactive oxygen species [22]. Another example is cardiolipin (DPG), which can be found in membranes of mitochondria. It has variety of important functions such as regulation of aggregate structures, triggering apoptosis, translocation of cholesterol from outer to inner membrane of mitochondria and/or imports proteins into mitochondrial matrix [23].
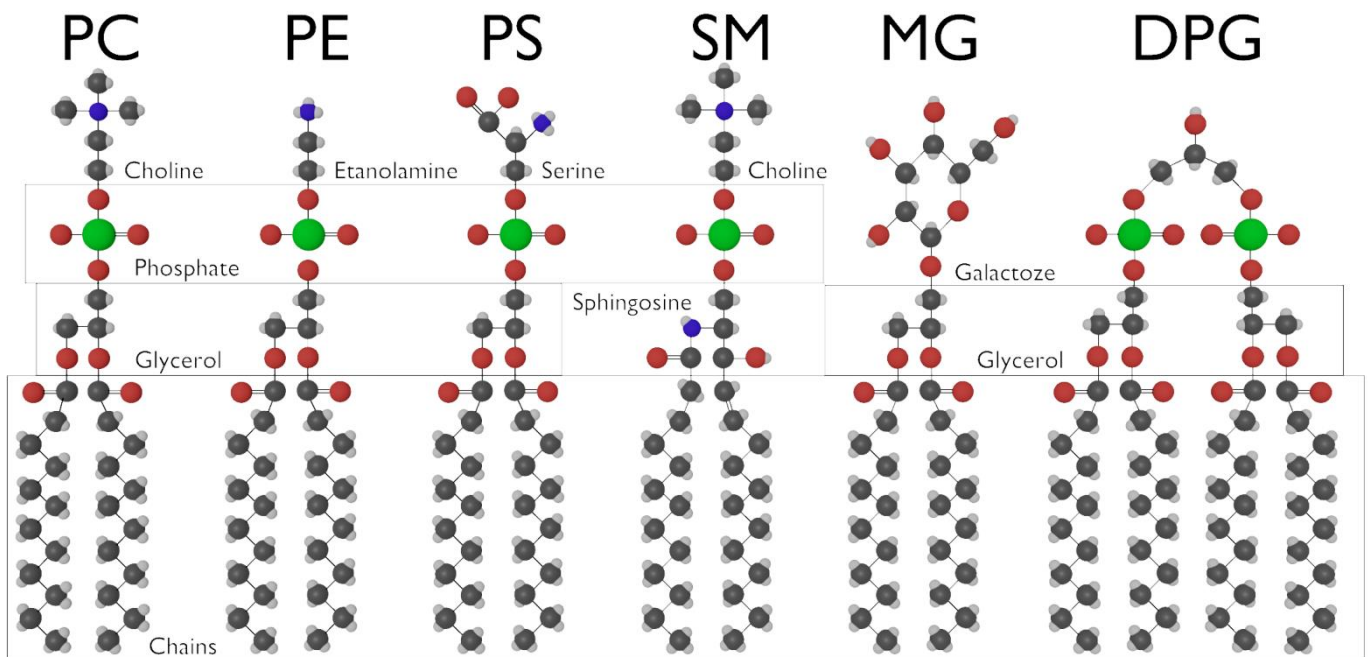

Figure 1.2. Structure of selected lipids present in biological membranes: PC (phosphatidylcholine), PE (phosphatidylethanolamine), PS (phosphatidylserine), SM (sphingomyelin), MG (monogalactosyldiglyceride), DPG (diphosphatidylglycerol, usually referred to as cardiolipin).
Graphic rendered using Blender 2.8 software (GPL license) and is a property of dissertation's author.

Distribution of the lipids in membrane is asymmetric. In mammalian membranes all SM and PC are localized in outer membrane, while the inner membrane consists of PE, negatively-charged PS and PI. Cholesterol was found in both leaflets. Asymmetry can also be observed in bacterial membranes, although it's more difficult to quantify. It was suggested that PG can be found in outer membrane, PI and PE preferentially in inner membrane and cardiolipin in both leaflets in Gram-positive bacteria [24]. Transbilayer movement of lipids is energetically unfavorable because it requires the insertion of the polar groups into the nonpolar region of the bilayer. Flip-flop of some phospholipids (a type of transbilayer movement) is a very time-consuming process (at least 3 hours). Cholesterol is an exception with its transbilayer movement in order of seconds [14].

Membrane proteins are second most common type of molecules that can be found in biological membrane. Proteins that are bound to membrane can be separated into three major groups: integral proteins, peripheral proteins and structural proteins. The structure of those proteins may appear in three forms: α-helical segments, a β-barrel structure and (in case of certain antibiotic peptides) the β-helix. The β-helix is wider than the α-helix, and can therefore function as a channel, transferring monovalent ions through the membrane [25]. Peripheral proteins are

localized in the surface of a membrane and are loosely connected to it either with electrostatic binding, covalent binding or short hydrophobic chains in structure which enable anchoring to membrane. They are responsible for transportation, they allow many molecules to be carried around the cell. Some peripheral membrane proteins carry molecules and electrons between other proteins. Peripheral enzymes participate in metabolism of different membrane components. There also exist peripheral proteins known as lipid-clamps, which are responsible for modification of cell shape [25-27]. Integral membrane proteins are translocated across the lipid bilayer. The main feature of the protein structure is the highly hydrophobic transmembrane segments and tendency to form organized secondary structure. The reason for this is to overcome high energetic cost of incorporating the protein's polar peptide bonds inside hydrophobic hydrocarbon core of the lipid bilayer. Especially that some of the integral proteins, such as bacteriorhodopsin, crosses the membrane even seven times. Second feature of the integral proteins is their length as their transmembrane segments need to correspond to the thickness of hydrocarbon core of the lipid bilayer [25]. The lifetime of peripheral proteins in membrane is from 2 to 5 days. To this end there exist a mechanism that transports to the membrane proteins that were synthesized at the ribosomes inside the endoplasmic reticulum. Generally, the signal peptide on the protein connects to receptor on the membrane, which is then followed by incorporation of protein into the membrane enhanced by the receptor. After the incorporation the signal part is removed and polysaccharides are attached and ribosome is separated from the membrane [14]. Eventually, structural proteins form the membrane cytoskeleton. They are not located near the membrane, but rather connected to it through integral proteins. This type of proteins are the boundary between the cytoskeleton and the membrane. Their functions are stabilization of attachment to other cells or the substrate, regulation of cell locomotion and regulation of cytoplasmic responses to growth factors and other external stimuli. This diversity of cellular functions is matched by the large number of biochemical mechanisms that mediate the connections between membrane proteins and the underlying cytoskeleton [14, 28].

Additional interesting components of membranes are carbohydrates. They are exclusively found in the outer leaflet of the biological membrane of all eukaryotic cells. They are attached to the membrane by either proteins (forming glycoproteins) or to the phospholipids (forming glycolipids). In both cases the carbohydrate portion is exposed to the external surface of the cell. Their role is to protect stability of the membrane by forming a mentioned-earlier coating of the cell surface (glycocalyx). They also are partially responsible for cell defense, since many antigens are cell-surface glycoproteins, and cellular recognition and in connections necessary for tissue forming [27].
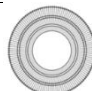
Biological membrane emerges as a complex structure with rich variety of molecules such as lipids, proteins and carbohydrates. Its considerable inhomogeneity (both lateral and spatial) and anisotropy makes it difficult to study separately the properties of lipid bilayers and influence of proteins on the bilayer. As a result, it is challenging to understand and investigate mechanical properties, or any properties, of the membrane. To this end biophysical studies of the membrane properties are performed of various simpler models of membrane structure.

1.2. Lipid bilayer – experimental model for biophysical investigations

The first model of membrane structure was the lipid monolayer. It played considerable role in establishing the bilayer nature of biological membranes during the first third of the XX century. First stable bilayer lipid membrane was reported in 1962 [29]. In 1965 liposomes were discovered [30]. Nowadays there exist various models of membrane structures, which can be divided into two main categories: lipid vesicles and planar lipid models. Lipid membrane models are simplified systems in which almost all physical and chemical parameters can be controlled. These models are frequently associated with various methods providing complementary data [31].

Lipid vesicles (liposomes) are semi-spherical vesicles delimited by a phospholipid bilayer separated by two aqueous compartments. This configuration allows to modify internal water compartment by hydrophilic agents and/or insert hydrophobic agents into the bilayer itself. The vesicle can be delimited by one (unilamellar vesicle) or by multiple bilayers (multilamellar vesicle). There are various of types of vesicles, depending on size and complexity of their topology. Most common cases are summarized in Table 1 [31]. One of the most interesting and widely used model in determination of mechanical parameters is Giant Unilamellar Vesicle (GUV). Its size is similar to eukaryotic cells, which allows visualization of topological and mechanical properties of cell membranes [32].

Table 1. Selected models of liposomes with diameters, description and schemes.

Name	Diameters [μm]	Lipid bilayer	Schemes
SUV (Small Unilamellar Vesicles)	0,02 - 0,05	Single layer	
LUV (Large Unilamellar Vesicles)	0,05 - 1	Single bilayer	
MLV (Multilamellar Vesicles)	0,4 – 10	Concentrically arranged bilayers (5 – 25)	
OLV (Oligolamellar Vesicles)	0,1 - 1	Concentrically arranged bilayer (averagely 5)	
MVV (Multivesicular Vesicles)	>1	Smaller liposomes are surrounded by a common bilayer	
GUV (Giant Unilamellar Vesicles)	5 - 200	Single bilayer	

The advantage of using liposomes is their suitability for vast majority of techniques (such as microscopy, florescence, scattering, surface sensitive techniques). Depending on the vesicle type used they can either allow to visualize the phenomena on the bilayer or investigate the population effect in case of smaller vesicles. Different techniques allow to provide data concerning lipid physical state (fluidity, fluid-gel transition) or membrane permeability. The disadvantages are, depending on the vesicle type used, that only either visual or qualitative data is collected. They also provide limited information about the interactions between the bilayer and its environment [31, 33].

Supported Lipid Bilayers (SLBs) are planar bilayers formed on top of a solid surface. To mimic the cell membrane structure, numerous biomimetic membranes have been developed using solid supports. These include solid-supported bilayer lipid membrane, polymer-cushioned membranes, hybrid bilayer membrane and suspended bilayer membrane. Visualization of those models is presented in Figure 1.3. The main advantage of SLBs is the possibility to vary lipid composition, even locally. It also provides a mean to investigate lipid domain formation, bilayer fluidity, membrane cell attachment and affinities, interaction kinetics and protein absorptions, self-assemblies or functions. Due to high range of possible surfaces, this model remains in agreement with high number of surface analysis techniques. The major disadvantage is lack of the membrane curvature. There is also

possibility of partial loss of functionality, protein denaturation or change of physicochemical properties of membrane due to intense interaction or friction with the substrate [31, 34].
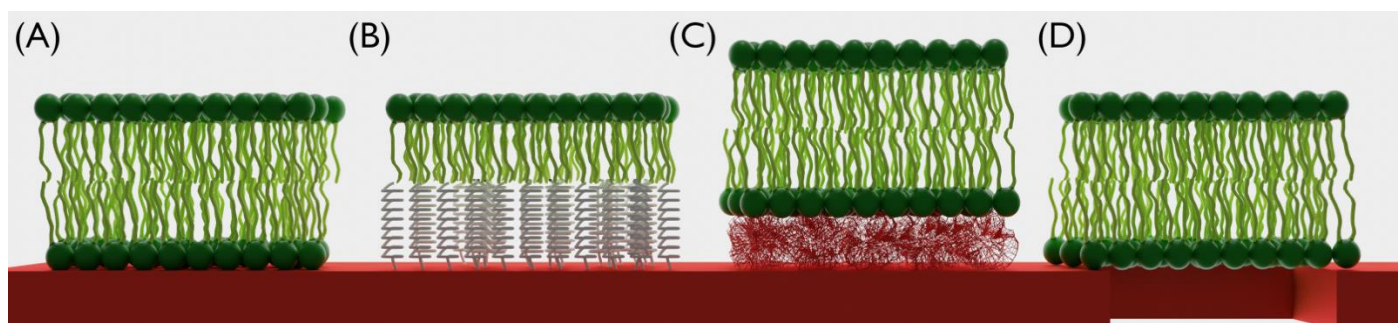

Figure 1.3. Models of planar lipid bilayers formed on surface: (A) classical supported lipid bilayer, (B) Hybrid bilayer lipid membrane, (C) Polymer-cushioned membranes and (D) Suspended bilayer membrane.
Graphic rendered using Blender 2.8 software (GPL license) and is a property of dissertation's author.

Hybrid bilayer lipid membrane are variation of SLBs that is formed on self-assembled monolayer rather than directly on the surface. However, mobility of both lipids and peptides in such membranes is limited, despite increasing stability and robustness of the bilayer. As a result, this model is not mimicking the biological membrane well. To overcome the problem of rigidity and space between the bilayer and the support, polymer-cushioned membrane, were developed. In this approach the bilayer is separated from the rigid surface by soft polymeric material that supports the membrane without the direct linking. This model is superior to previous one in aspect of reducing the effect of rigidity of the surface. Additionally, it allows incorporation of transmembrane proteins. This approach is mostly used to model system of the cell surface glycocalyx. Suspended-lipid bilayers are a model of membrane which is formed over micrometer or nanometer pores. It's a new approach with promising perspectives. There also exist combined approaches of hybrid and suspended bilayer membranes (known as tethered bilayer lipid membranes). In this approach additional layer is added (for instance biotin-streptavidin-biotin-bilayer or carbon chains) to provide sufficient space underneath the membrane for studies of incorporated membrane proteins [33, 34].

Langmuir Monolayers are peculiar case of supported lipid bilayers. They are composed of one lipid leaflet formed at the air/liquid interface. Lipid tails are oriented towards the air and lipid heads, inversely, towards the liquid. Following the deposition of mixture of lipids at the air/liquid interface and evaporation of the solvent, a movable barrier allows the compression of the monolayer. A sensor (such as Withelmy plate) located at the air/water interface allows the measurement of surface pressure change in function of lipid surface area, from which lipid packing and elasticity can be calculated. Scheme of the model is presented in the Figure 1.4 [31, 35, 36].
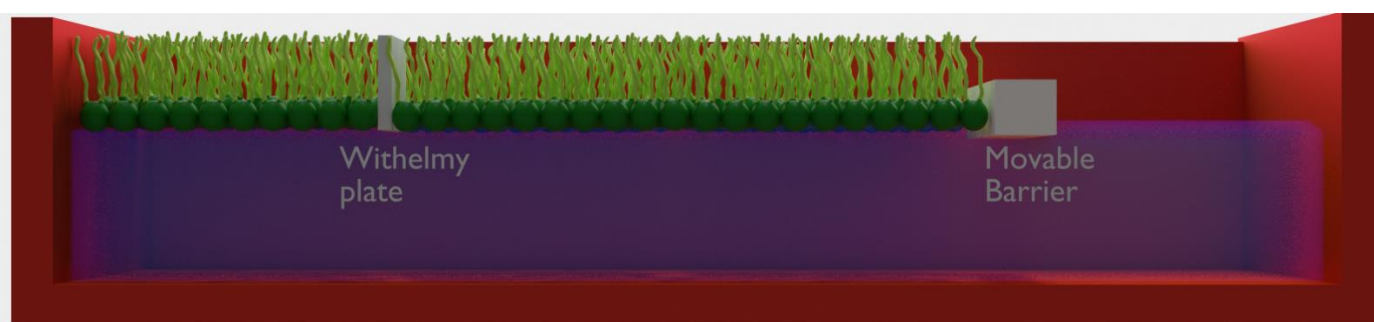

Figure 1.4. Scheme of Langmuir Monolayer.
Graphic rendered using Blender 2.8 software (GPL license) and is a property of dissertation's author.

The main advantage of Langmuir monolayers is their versatility with large variety of lipids – saturated, unsaturated, mixtures, pure, associated (or not) to proteins. They are very easy to handle model in investigation of interactions with different species of compounds spread on the interface or dissolved in the sub-phase. They have also successfully been used to study processes like molecular recognition, cooperative binding, aggregation, signaling,

energy conversion or locomotion. However, this monolayers are usually in a metastable state in condensed phases and are less hydrated than lipid bilayer [35, 36].

GUVs and SLBs are believed to be the most popular and widely used as a mean to study the physical properties, especially mechanical properties, of membrane system. They are chosen due to the fact that characterization of a single membrane is required in those studies. Therefore, they are commonly used to model such phenomena as topology, shape fluctuations, phase behavior, permeability, fission and fusion of biological membranes. The additional advantage of GUVs is the free-standing of the vesicle, which limits any possible effect from the substrate. However, lipid bilayer is an object with certain physical properties that should be considered before establishing their mechanical properties. One of the most important property is the phase transition of a membrane, as it was reported to drastically change mechanical properties determination [37].

Phase transitions of membrane system

One of most interesting property of bilayer is their ability to exist in different phases depending on the water content (lyotropic transitions) and temperature (thermotropic transitions). The phase transition processes typical for biological membranes are connected with hydrocarbon chain. This process has great significance for cell or vesicle fusion.
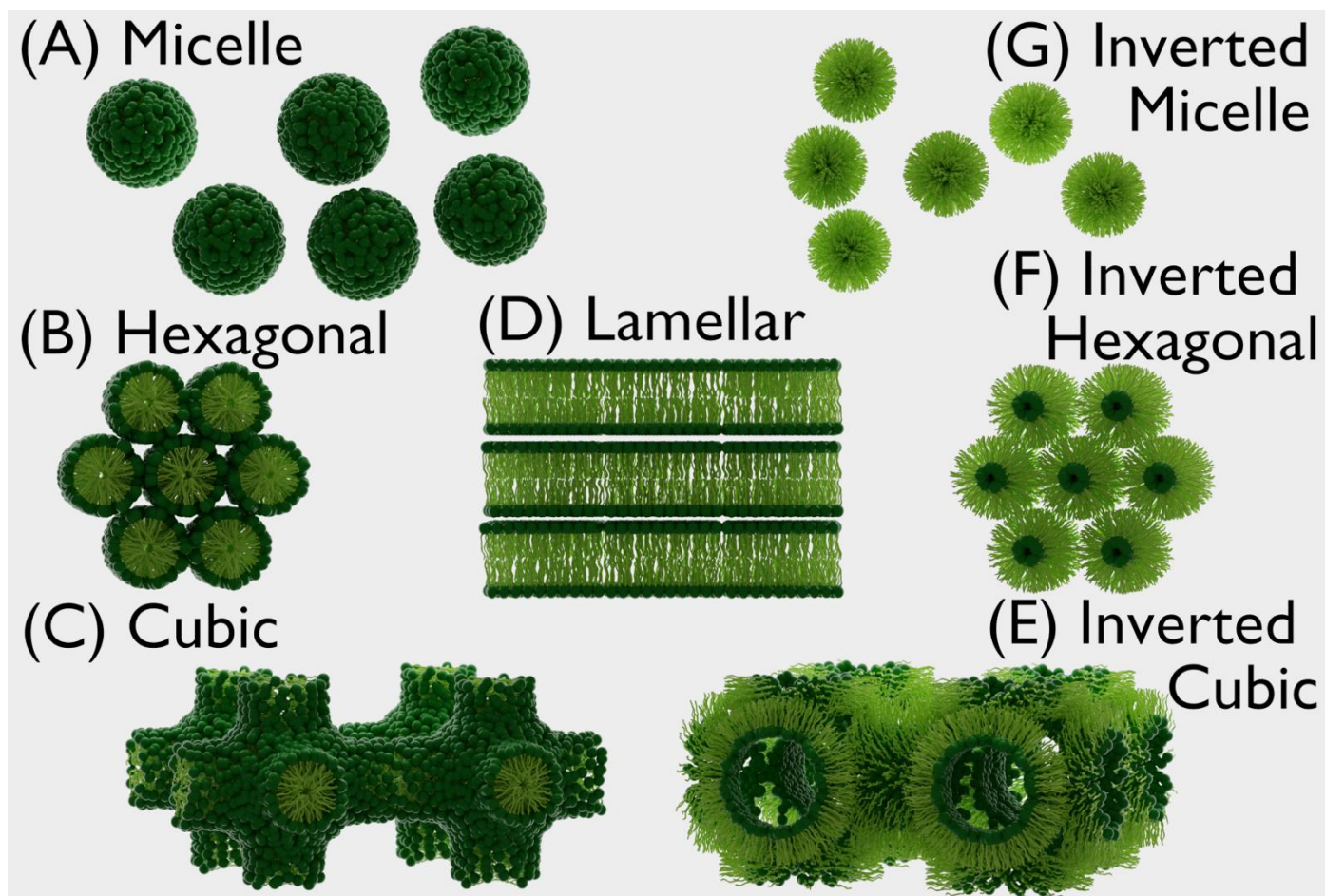

Figure 1.5. Schemes of phases in lyotropic transitions of lipid bilayer. With increase of lipid concentration the structure is transitioning from normal (A) micelle, (B) hexagonal and (C) cubic phases into (D) lamellar phase, which reflect biological membrane model most accurately. Further increase of lipid concentration leads to inverted (E) cubic, (F) hexagonal and finally (G) micelle phases.
Graphic rendered using Blender 2.8 software (GPL license) and is a property of dissertation's author.

Lyotropic transitions depends on lipid concentration. When it is very low, below so-called critical micelle concentration (CMC), the lipids are in form of monomers. With increase in concentration, when it is higher than CMC, lipids starts to form normal micelles (M_l). With further increase of the concentration the system is transformed

into normal hexagonal phase (H$_I$), then into normal cubic phase (Q$_I$) and finally into lamellar phase (L$_\alpha$), which is also often referred to as liquid-phase. With further increase of concentration a transformation into inverted cubic phase (Q$_{II}$) will occur, which go through inverted hexagonal phase (H$_{II}$) to finally reach inverted micelles (M$_{II}$) [14, 38]. Schemes of the individual phases are presented in the Figure 1.5.
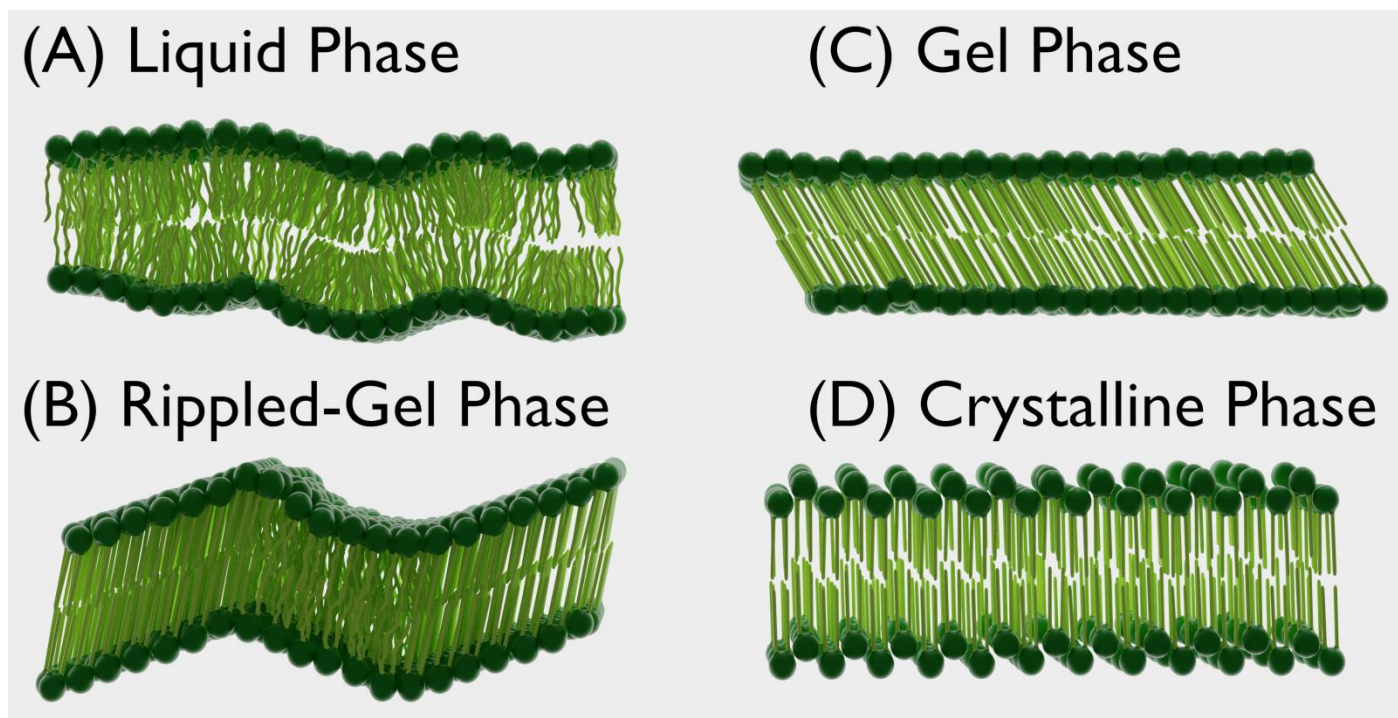

Figure 1.6. Schemes of phases in thermotropic transitions of lipid bilayer. With decrease of temperature the structure is transitioning from (A) liquid (disordered) phase to either (B) rippled-gel phase or (C) gel phase depending on the length of hydrocarbon chains and saturation of lipid molecules. Eventually, structure in gel phase will transition into (D) crystalline (or subgel) phase with further decrease of temperature.
Graphic rendered using Blender 2.8 software (GPL license) and is a property of dissertation's author.

In case of **thermotropic transitions**, typically there are four states in which bilayer can be: crystalline-phase L$_c$, gel-phase L$_{\beta'}$, ripple-phase P$_\beta$ and liquid-phase L$_\alpha$ (sometimes described as liquid disordered L$_d$ phase). With the higher increase of temperature the liquid phase undergo further changes into inverted cubic phase (Q$_{II}$), inverted hexagonal phase (H$_{II}$) and, finally, into inverted micellar phase (M$_{II}$), however such situation does not occur with phospholipids. Each lipid can be characterized by following temperatures – main transition temperature (T$_m$), subtransition temperature and – in some rare cases - pretransition temperature [14, 39, 40]. Those temperatures are determined largely by the hydrocarbon chains length and saturation. When the cell membrane is fully hydrated in biologically-relevant temperature (above T$_m$) it is predominantly in the liquid phase. The liquid phase is characterized by well hydrated lipid and loosely packed lipid heads, lateral movement of lipids and disordered lipid chains. In this phase irregular packing of individual lipid molecules often occurs. If the temperature drops below T$_m$, the membrane will transit into the gel phase. It has to be noted, that only a fraction of lipids will undergo the transition at the beginning but with decrease of the temperature the number of gel phase lipids will increase. The gel phase is mostly observed in long and saturated fatty acid chains. In that phase the individual lipids within the lipid bilayer lose lateral mobility, lipid head groups become more tightly packed and dehydrated, the lipid acyl chains become straighter and ordered, the bilayer thickness increases [40]. If a lipid type exhibits a pretransition temperature, a transition into rippled phase will occur before gel-phase. This ripple-phase is characterized by interdigitated fluid-like regions between the gel regions of the membrane. As a result some regions within the bilayer are more-tightly packed and dehydrated than others [41]. Finally, when subtransition temperature is reached, the bilayer transitions into crystalline-phase (or subgel phase). In this phase a low degree of fluidity, further increase in lipid head density and higher order of chains is also observed. While this phase still remains not-well investigated [42], it was reported to exhibit a staggered structure where the adjacent head groups mutually shift the positions up and down (in comparison to gel phase) [43]. Schemes of described phases in thermotropic transitions are presented in Figure 1.6.

While Gibbs phase rule strictly prohibits coexistence of different phases in homogeneous membranes, both during phase transition and in heterogeneous bilayer such coexistence was observed. A membrane formed from the mixture of lipids with different T_m resulted in such phase coexistence. Since in biological membranes various domains coexist, lipid membranes with phase coexistence has been acknowledge as a good, although in some cases challenging, models to investigate lipid properties. When analyzing heterogeneous bilayer phases, especially in membranes with sterols (such as cholesterol), alternative description of phases is used. In this description there are four phases – solid-ordered S_o (already described gel-phase), solid-disordered S_d, liquid-disordered L_d (already described liquid phase) and liquid-ordered L_o. Cholesterol presence in membrane was reported to induce ordering in liquid phase, which resulted in liquid-ordered L_o phase areas, as shown in Figure 1.7. This phase represents something of a midpoint of the liquid disordered and gel phases. Sufficiently high membrane sterol concentration combined with the relative rigidity of sterol molecules leads to tighter packing of liquid phase membrane. As a result membrane in this L_o phase exhibits solid-like qualities similar to the gel-phase without reducing the high rate of lateral diffusion characteristic to liquid phase [44]. Interestingly, in case of gel-phase, sterols were reported to induce disordering, which resulted in solid-disordered S_d phase. This phase is described as a *disrupted gel*, in which sterol disorders the gel state by breaking up the regular hexagonal chain packing. At the same time it allows more motion [45, 46]. Sterols are especially important molecules in already-mentioned raft hypothesis. Rafts are defined as small areas on the membrane with different ordering (for instance enriched in cholesterol L_o areas on L_d membrane). It is current state of knowledge that only presence of sterols can induce the transition to the liquid-ordered and solid-disordered phases [47].
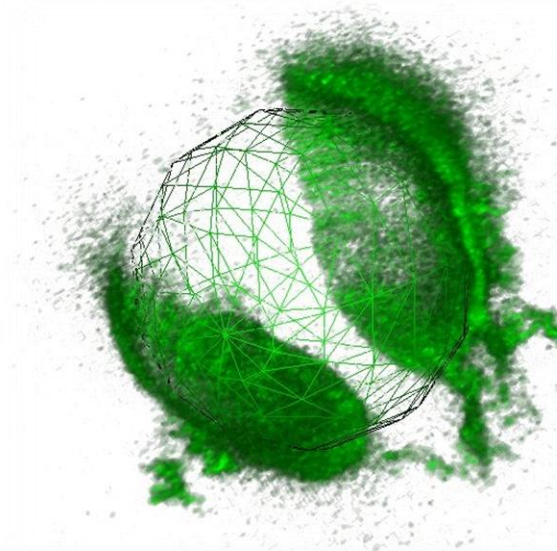

Figure 1.7. Visualization of coexistence of different phases in single GUV formed from POPC/Cholesterol/Sphingomyelin mixture. Due to the usage of specific fluorescence probe only liquid-disordered phase is illuminated. Sphere added for increased readability.
Graphic rendered using ImageJ software (OSS license) and is a property of dissertation's author.

1.3. Mechanical model of a lipid bilayer

Membrane mechanics, surface parametrization and Hamiltonian

In macroscopic scale bilayer can be treated as infinitely thin surface. For such surface properties are given in terms of out-off-plane behavior, area and area difference. Those are related to bending rigidity, stretching elasticity and membrane viscosity. Those macroscopic properties are correlated with microscopic bilayer structure and are dependent on their thermodynamic state and composition. Theoretical considerations presented in this subchapter are based on works of Helfrich[48], Bouvas[15] and Deserno[49].

The collective movement of liposome can be divided into three main components – bending deformations, area expansion/compression and shearing deformation. This categorization was schematically presented in Figure 1.8 and is based on work of Helfrich [48]. In his model it is assumed that area expansion is a response to external pressure and shearing deformations occurs only in liquid-crystalline and/or heterogeneous bilayers. Therefore, the most informative deformation – bending – is responsible for shape and behavior of vesicle in equilibrium state. In general responses of bilayer to deformations are characterized by following constants – shearing elastic module μ, compressibility module K_a, bending rigidity coefficient κ and Gaussian curvature module k_G.

Shear movement is a form of friction between individual lipid particles. It occurs when bilayer is heterogeneous or the bilayer is in solid/gel phase (when tail groups are stiffer). For most of phospholipids the transition temperature T_m is below physiological temperature, therefore most of them naturally occur in liquid phase. In this phase bilayer do not show significant shearing forces (μ=0).
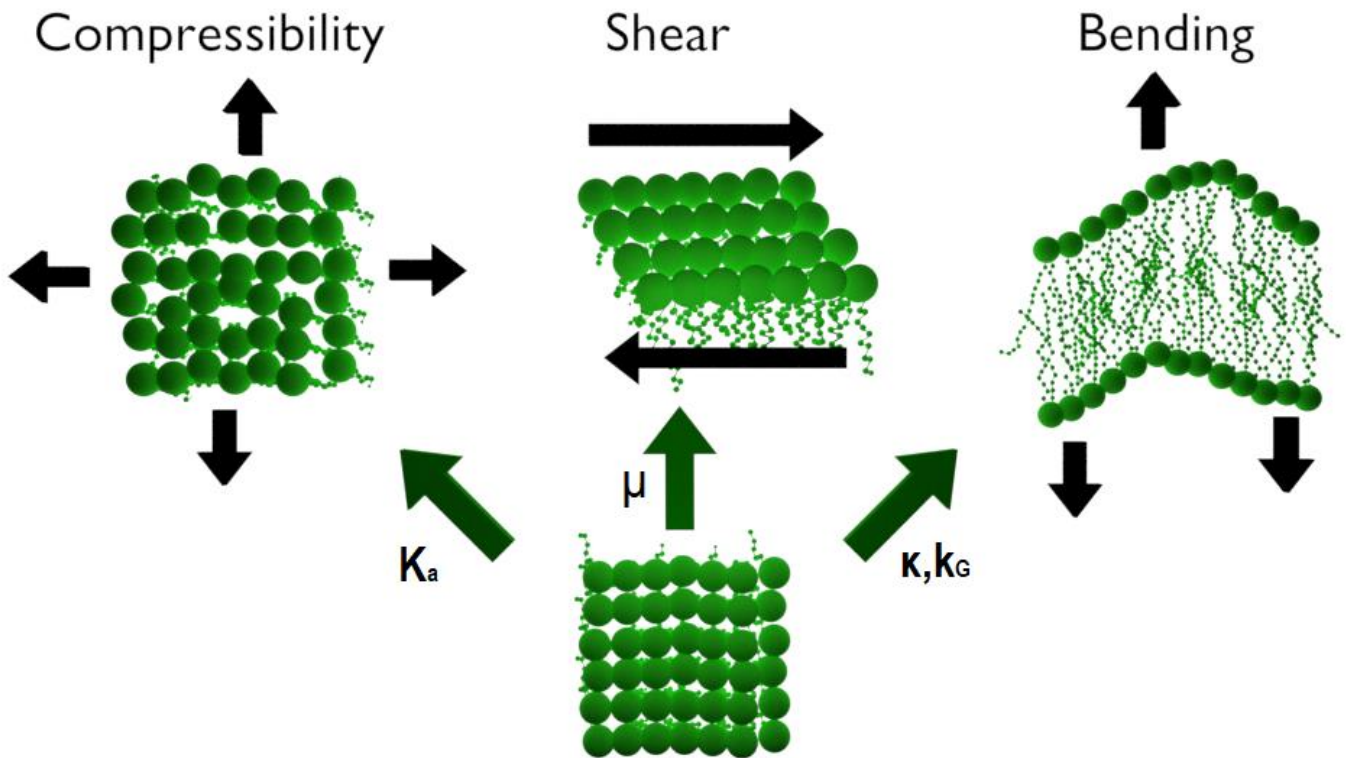

Figure 1.8. Representation of three components of bilayer deformations – area compressibility, shearing deformation and bending. Corresponding symbols characterizing those deformations are included.
Graphic rendered using Blender 2.8 software (GPL license) and is a property of dissertation's author.

The area expansion for lipid bilayers is limited to 4-5% of whole area. According to Equation (1.1) based on Hook's law for elastic spring, the stretching elastic energy per unit area E_{exp} depends on change of relative area $\Delta A/A_0$. The equilibrium area surface is defined by A_0, while deformed area surface is define by A_d.

$$E_{exp} = \frac{1}{2} K_a \left(\frac{A_d - A_0}{A_0} \right)^2 = \frac{1}{2} K_a \left(\frac{\Delta A}{A_0} \right)^2 \tag{1.1}$$

Bending deformations, which energy per unit area E_{bend} is defined according to Helfrich's model by Equation (1.2), is mainly responsible for shape of bilayer. Bending of bilayer is characterized by two main principal curvature axes K_1 and K_2 (describing the local curvature) and three phenomenological parameters:

- the bending elastic modulus κ – correlated with microscopic state of bilayer (rigidity and length of carbon chains of lipids, nature of interaction between lipid heads, etc.),
- the Gaussian elastic modulus k_G – defines the elastic energy associated to the intrinsic curvature,
- spontaneous curvature K_0 – defining an asymmetry in lipid composition of the two leaflets or shape of the bilayer when no constraints are provided.

$$E_{bend} = \frac{1}{2}\kappa(K_1 + K_2 - K_0)^2 + k_G \cdot K_1 K_2 \tag{1.2}$$

When lipid bilayer is in liquid phase (μ=0) only area compressibility and bending have significant impact on mechanics of lipid bilayer. The elastic free energy Hamiltonian $\mathcal{H}$ which describes the deformations of bilayer can be defined according to Equation (1.3).

$$\mathcal{H} = \frac{A_0}{2}K_a\left(\frac{\Delta A}{A_0}\right)^2 + \frac{1}{2}\kappa\int_A (K_1 + K_2 - K_0)^2 dA + k_G\int_A K_1 K_2 dA \tag{1.3}$$

While Hamiltonian can be obtained phenomenologically, it can also by calculated using differential geometry. In order to do that and be able to extract mechanical properties of lipid bilayers, first the parametrization of the surface needs to be performed. In case of vesicle a membrane can be described as a fluctuating two-dimensional surface in three-dimensional space (solvent). Therefore, it can be treated as a smooth surface with a differential area element (dA) and $A = \int dA$ its total area. Since bilayer is a dynamic structure, it cannot be described by coordinates of individual molecules, but a differential geometry with surface invariants are used.
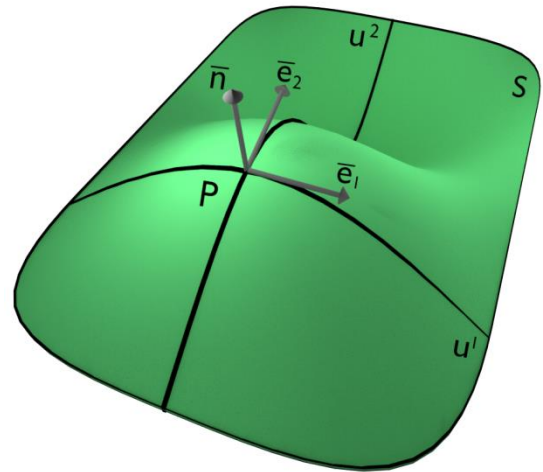

Figure 1.9. Differential geometry scheme: representation of a section of a surface S. The point P, the normal vector **n**, the coordinates u^1 and u^2 as well as vectors $\mathbf{e}_1$ and $\mathbf{e}_2$ are included. *Graphic rendered using Blender 2.8 software (GPL license) and is a property of dissertation's author.*

In order to effectively parametrize the bilayer surface in differential geometry, one should start with adopting a local (two-dimensional) coordinate system $\{u^1, u^2\}$ and find some mapping that assigns coordinate pair (u^1, u^2) to some point in three-dimensional space (described by Cartesian coordinates), as described in Equation (1.4) and visualized in Figure 1.9.

$$\mathbf{R} = \mathbf{R}(u^1, u^2) = \begin{pmatrix} X(u^1, u^2) \\ Y(u^1, u^2) \\ Z(u^1, u^2) \end{pmatrix} \quad , where\ (u^1, u^2) \in \mathbb{R} \tag{1.4}$$

Membranes are parametrized by two variables and the infinitesimal displacements along the surface can be described by Equation (1.5). Tangent vectors can also be constructed according to Equation (1.6). The tangent vectors points into the direction in which the value of the coordinate u^a increases and they express all the local properties of the surface.

$$d\mathbf{R} = \frac{\partial \mathbf{R}}{\partial u^1}du^1 + \frac{\partial \mathbf{R}}{\partial u^2}du^2 \tag{1.5}$$

$$\mathbf{e}_a = \frac{\partial \mathbf{R}}{\partial u^a} = \partial_a \mathbf{R} \quad , where\ a \in \{1,2\} \tag{1.6}$$

The two surface tangent vectors can be used to construct the first fundamental form of surface - induced metric tensor (or just 'metric') g_{ij} defined by Equation (1.7). This metric tensor characterizes the intrinsic geometry of the surface and is used to measure infinitesimal distanced between two points on the surface. The determinant of metric g can be connected to the tangent vectors according to Equation (1.8). Since $\boldsymbol{e}_1 du^1$ and $\boldsymbol{e}_2 du^2$ span the local infinitesimal area element on the surface the determinant of the metric can be connected to it through the definition in Equation (1.9).

$$g_{ij} = \boldsymbol{e}_i \cdot \boldsymbol{e}_j \tag{1.7}$$

$$g = \det(g_{ij}) = g_{11}g_{22} - g_{12}g_{21} = g_{11}g_{22} - (\boldsymbol{e}_1 \cdot \boldsymbol{e}_2)^2 =$$
$$= g_{11}g_{22}[1 - \cos^2(\sphericalangle(\mathbf{e}_1, \boldsymbol{e}_2))] = |\boldsymbol{e}_1|^2 |\boldsymbol{e}_2|^2 \sin^2(\sphericalangle(\mathbf{e}_1, \boldsymbol{e}_2)) = |\boldsymbol{e}_1 \times \boldsymbol{e}_2|^2 \tag{1.8}$$

$$dA = |\boldsymbol{e}_1 du^1 \times \boldsymbol{e}_2 du^2| = \sqrt{g}\, du^1 du^2 \tag{1.9}$$

The normal vector to the local surface **n** can also be constructed from the tangent vectors according to Equation (1.10). It is customary to normalize **n** to unit length. It allows to construct the second fundamental form of surface – the extrinsic curvature tensor K_{ij}. The tensor quantifies the extent of local curvature of the surface in the three dimensional space and is constructed according to Equation (1.11).

$$\boldsymbol{n} = \frac{\boldsymbol{e}_1 \times \boldsymbol{e}_2}{|\boldsymbol{e}_1 \times \boldsymbol{e}_2|} = \frac{\boldsymbol{e}_1 \times \boldsymbol{e}_2}{\sqrt{g}} \tag{1.10}$$

$$K_{ij} = \boldsymbol{e}_i \cdot \frac{\partial}{\partial_j}\boldsymbol{n} = -\boldsymbol{n} \cdot \frac{\partial}{\partial_j}\boldsymbol{e}_i = -\boldsymbol{n} \cdot \frac{\partial}{\partial_i}\frac{\partial}{\partial_j}\boldsymbol{R} \tag{1.11}$$

The curvature tensor is a 2x2 real symmetric matrix and can the diagonalized in an orthonormal basis, where the diagonal elements – eigenvalues K_1 and K_2 – are named principal curvatures of the local surface and define the extrinsic properties of the surface. The curvature tensor has two invariants. First one is called the total extrinsic curvature and is defined by Equation (1.12) as trace K of curvature tensor. In older words extrinsic curvature is sometimes defined as mean curvature H, which is equal to half of K. Second invariant of curvature tensor is calculated as determinant of the matrix K_j^i and is called Gaussian curvature K_G, as in Equation (1.13).

$$K = Tr(K_j^i) = g^{ik}K_{kj} = K_j^j = K_1^1 + K_2^2 = K_1 + K_2 \tag{1.12}$$

$$K_G = \det(K_j^i) = \det(g^{ik}K_{kj}) = K_1 K_2 \tag{1.13}$$

From chemical or atomistic point of view, lipid membranes consist of numerous individual lipid particles giving rise to significant number of inner degrees of freedom summarizing to larger-scale membrane behavior. A lot of models focus on those local physics inside lipid bilayer. However, with increase of scale, the bilayer can be treated in terms of curvature deformation. Almost any peculiar detail, which is responsible for existence of bilayer in the first place, will just vanish providing scale is large enough. The Helfrich Hamiltonian is an example for constructing effective energy functional of membrane based on large-scale phenomenological considerations. As the amplitude of elastic energy depends only on the shape of membrane, the free energy has to be an invariant with respect to a change of parametrization. Therefore, it can be described using both surface invariants – total extrinsic curvature K and Gaussian curvature K_G – and differential area element dA. As a result, the free energy equation can be constructed by multiplicative combinations of principal curvatures leading to four terms: $\int dA$, $\int K dA$, $\int K^2 dA$ and $\int K_G dA$, as shown in Equation (1.14). By relabeling constant with parameters from phenomenological considerations one gets equations presented in Equation (1.15). This results in well-known form of Hamiltonian presented in Equation (1.16). This Hamiltonian has the same physical meaning as the one in Equation 1.3 despite being under another form.

$$\mathcal{H} = \int C^{(0)} dA + \int C^{(1)} K dA + \int C^{(2,1)} K^2 dA + \int C^{(2,2)} K_G dA \tag{1.14}$$

$$C^{(0)} = \sigma + \frac{1}{2}\kappa K_0^2, \quad C^{(1)} = -\kappa K_0, \quad C^{(2,1)} = \frac{1}{2}\kappa, \quad C^{(2,2)} = k_G \tag{1.15}$$

$$\mathcal{H} = \sigma \int dA + \frac{\kappa}{2}\int (K - K_0)^2 dA + k_G \int K_G dA \tag{1.16}$$

The first term in the Hamiltonian is related to area compressibility and describes the energy cost related to an area increase. The symbol σ stands for surface tension. The second term describes the energy cost of bending deformations. It is understood as the energy cost associated with deviations of the equilibrium curvature from local preferred value K_0 based on chemical and structural properties of membrane and environment. The third term describes energy related to topological changes of the surface. Symbol k_G reflects the cost of imposing Gaussian curvature on the surface. In case of unconstrained vesicle in liquid phase both first and the third term in Hamiltonian can be either neglected or omitted. This results in defining relevant elastic free energy F_c by only second term.

Quasi-spherical representation and spherical harmonics function

Two techniques presented in this dissertation are based on spherical harmonics functions. To this end the theoretical background for this approach was also included in model subchapter. Theoretical considerations presented in this subchapters are based on numerous articles focusing on analysis of quasi-spherical vesicle fluctuations [15, 50-52].

Since vesicles are quasi-spherical a natural way to characterize it is to use the polar coordinates. The positional vector of the membrane, defined by Equation (1.17), indicates the position of a given point of the membrane in a given time. The membrane displacement-field is defined by $\omega(\theta, \varphi, t)$, which gives information about deviation from spherical reference radius R_{sphere}. Those relations are presented in Figure 1.10. Fluctuations of the membrane are time-dependent thermal agitations around equilibrium position, therefore can be divided into static part – the average vesicle size at given coordinates or static mean shape $\omega_0(\theta, \varphi, t)$ – and dynamic part of perturbation – deviation from equilibrium or time-dependent deformation of vesicles $\delta\omega(\theta, \varphi, t)$ – as showed in Equation (1.18). Since fluctuations are constrained by equilibrium radius it is assumed that averaged over time fluctuations are balanced, as showed in Equation (1.19).
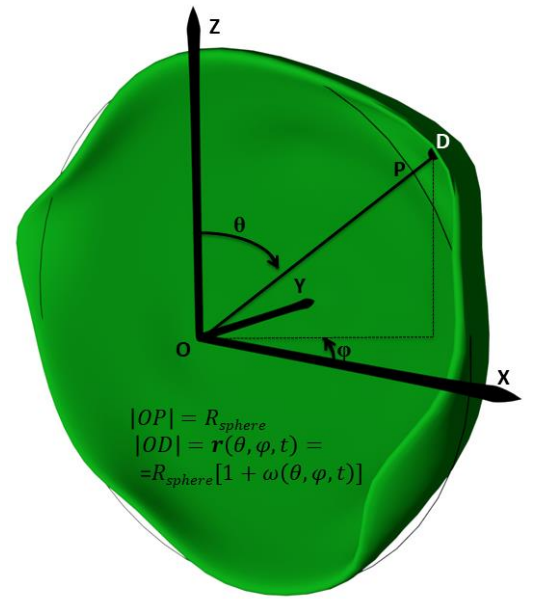

Figure 1.10. Scheme of local radius deformations of a vesicle's membrane.
Graphic rendered using Blender 2.8 software (GPL license) and is a property of dissertation's author.

$$\boldsymbol{r}(\theta, \varphi, t) = R_{sphere}[1 + \omega(\theta, \varphi, t)] \tag{1.17}$$

$$\omega(\theta, \varphi, t) = \omega_0(\theta, \varphi, t) + \delta\omega(\theta, \varphi, t) \tag{1.18}$$

$$\langle \omega(\theta, \varphi, t) \rangle = \omega_0(\theta, \varphi) \implies \langle \delta\omega(\theta, \varphi, t) \rangle = 0 \tag{1.19}$$

Using spherical harmonics Y_n^m as base functions Equations (1.17-1.19) can be rewritten as Equation (1.20), where the only contribution to ω_0 in quasi-sphere shape is a constant term $A_0^0 Y_0^0$.

$$\boldsymbol{r}(\theta, \varphi, t) = R\left[1 + (A_0^0 + U_0^0(t))Y_0^0 + \left(\sum_{n\geq 2, |m|\leq n}^{n_{max}} U_n^m(t)Y_n^m(\theta, \varphi)\right)\right] \tag{1.20}$$

By introducing time-dependent real functions $a_n^m(t)$ and $b_n^m(t)$ described by relation given by Equation (1.21), the Equation (1.20) can be rewritten as Equation (1.22), with $\mathcal{P}_n^m(\cos\theta)$ related to associated Legendre function $P_n^m(\cos\theta)$, as described by Equation (1.23).

$$U_n^m(t) = (a_n^m(t) - ib_n^m(t))/2 \tag{1.21}$$

$$\boldsymbol{r}(\theta, \varphi, t) = R[1 + \left(A_0^0 + U_0^0(t)\right)Y_0^0 +$$

$$+[\textstyle\sum_{n\geq2}^{n_{max}} a_n^0(t)\mathbb{P}_n^m(\cos\theta) + \sum_{0<m\leq n}(a_n^m(t)\cos(m\varphi) + b_n^m(t)\sin(m\varphi))\mathbb{P}_n^m(\cos\theta)]\,] \tag{1.22}$$

$$\mathbb{P}_n^m(\cos\theta) = (-1)^m \sqrt{\frac{2n+1}{4\pi} \cdot \frac{(n-m)!}{(n+m)!}}\, \mathrm{P_n^m}(\cos\theta) \tag{1.23}$$

Which leads to important expression for the spherical harmonics described by Equation (1.24) that is a corner stone for considered techniques based on spherical harmonics functions. Additionally, amplitudes of spherical harmonics function can be rewritten according to Equations (1.25).

$$Y_n^m(\theta, \varphi) = \mathbb{P}_n^m(\cos\theta) \cdot e^{im\varphi} \tag{1.24}$$

$$|U_n^0(t)|^2 = |a_n^0(t)|^2, |U_n^m(t)|^2 |U_n^{-m}(t)|^2 = \frac{1}{2}[|a_n^m(t)|^2 + |b_n^m(t)|^2], 1 \leq m \leq n \tag{1.25}$$

The bending elastic energy $F\{\omega_0, \delta\omega\}$ of a given shape defined by $\omega_0 + \delta\omega$ with respect to the equilibrium one $F_c\{\omega_0\}$ is obtained by Taylor expansion approximation of elastic free energy (middle term of Equation 1.16) up to second order in $\omega(\theta, \varphi)$. It is defined by Equation (1.26), where $\lambda_n(\bar{\sigma})$ is defined by Equation (1.27) and $\bar{\sigma}$ is the reduced membrane tension. Every a_n^m and b_n^m are independent modes, which follow Boltzmann statistics and a time average given by Equation (1.28), where k_B is Boltzmann constant and T is temperature.

$$F_c\{\omega_0, \delta\omega\} - F\{\omega_0\} = \frac{\kappa}{2}\int(K - K_0)^2 dA \cong \frac{\kappa}{2}\textstyle\sum_{n=2}^{n_{max}} \lambda_n(\bar{\sigma}) \left(|a_n^0(t)|^2 + \frac{1}{2}\sum_{1\leq m\leq n}[|a_n^m(t)|^2 + |b_n^m(t)|^2]\right) \tag{1.26}$$

$$\lambda_n(\bar{\sigma}) = (n+2)(n-1)[\bar{\sigma} + n(n+1)] \tag{1.27}$$

$$\langle|a_n^m(t)|^2\rangle = \frac{2k_BT}{\kappa\lambda_n(\bar{\sigma})} \tag{1.28}$$

1.4. Overview of experimental techniques

Techniques for determination of mechanical properties

There are various techniques to determine mechanical properties of lipid bilayers – both experimental and numerical. Commonly, available techniques can be divided into three main categories: (a) techniques based on the analysis of thermal fluctuations, (b) techniques that study the response to mechanical deformation and (c) scattering techniques. The first category focuses on techniques that exercise the dependence of thermal undulations on the membrane bending rigidity. Since two of those techniques are a subject of the dissertation, this category is described in more details later. Second category of techniques exercise the possibility of affecting membrane behavior by applying the external mechanical deformation. This techniques have been commonly used to determine either bending rigidity or area compressibility [15].

Table 2. Overview of techniques that study the response to mechanical deformation of lipid bilayer.

Technique	Determined parameters	Brief description	Literature
Micropipette aspiration	κ, K_A	The idea of the technique is an aspiration of GUV into a small-caliber suction pipette. The analysis of the relative change in the area under the aspiration pressure allows to obtain bending rigidity from the low-tension regime of the tension-area curve.	[53-59]
Tether formation	κ	The idea is the determination of mechanical parameters from the tethers – locally stretched membrane that forms thin cylindrical membrane strands of only 10-100 nm in diameter. Measurements of the tether radius as a function of axial force on the tether gave access to the bending stiffness. This approach has been also used in molecular dynamics simulations.	[60-62]
Optical tweezers	κ	The idea of this approach is similar to the tethered formation with the difference that much larger microsphere are controlled for tether formation which results in their higher diameter. Different approach, using optical tweezers, focus on optical stretching of GUVs with integrated dual-beam optical trap by measuring area strain as a function of applied stress to obtain bending rigidity. This approach was also realized on planar lipids.	[63-66]
Electric field deformation	κ	The idea of this approach is to measure the relative apparent dilatation of the vesicles induced by the electric field as a function of the homogeneous lateral tension to obtain bending rigidity.	[67-70]
Atomic Force Microscopy Force Indentation	κ, K_A	In this approach bilayer, either SLB or tethered vesicle, is indented using tip on the AFM cantilever. Change in force/pressure is recorded during indentation, which is then used to establish either bending rigidity or area compressibility.	[71-74]
Confocal microscope optical deformation	κ	In this approach the membrane is illuminated with a tightly focused low-power laser beam, which is placed slightly above/below the focal plane. As a result the size and divergence of the reflected beam changed with the distance between the membrane and the focal plane. The bending rigidity was directed as a function of work done by optical force, vesicle surface and principle curvatures of an oblate spheroid.	[75, 76]

Abbreviations: κ – bending rigidity coefficient, K_A – area compressibility.

The last category contains scattering techniques. Most widely spread of those techniques are those, which base on either X-ray or neutron scattering. While both techniques are similar in realization, there are principle differences in which they interact with matter. X-rays are electromagnetic waves that primarily interacts with electrons and their amplitude of X-ray scattering length increases linearly with atomic number. Neutrons, on the other hand, are particles that interact with atomic nuclei and neutron scattering amplitudes is a function of the mass, spin and

energy levels of the nuclei that they scatter from [77]. X-ray scattering is usually performed on multilamellar vesicles with highly oriented lipid bilayers to establish bridge to the mechanical coefficients of bulk lamellar phases. These oriented stacks are typically in fully hydrated conditions and with spacing repeat distance quite small so that the systems were in soft confinement regime. The bending rigidity is obtained from scattering data by established dependency between both the Caillé parameter and in-plane correlation length. Both of those parameters can be obtained from scattering data. Caillé parameter is obtained by analyzing the tails of diffraction peaks, while in-plane correlation length is determined from the intensity in the small angle regime [78-80]. Another technique is a combination of Neutron Spin Echo and Dynamic Light Scattering techniques to study shape fluctuations of bilayer vesicle. In this approach Dynamic Light Scattering is first used to obtain values of the translation diffusion coefficient and hydrodynamic radius, which are later used to analyze the neutron spin echo scattering functions. Finally, the relaxation frequency of the fluctuation model is determined from fitting experimental relaxation functions to obtain bending rigidity coefficient [81]. Alternative approach of Neutron Spin Echo measurements of the equilibrium membrane fluctuations that does not require dynamic light scattering data was also developed. In this approach both area compressibility and bending rigidity were calculated [82, 83]. Yet another approach to determine mechanical properties is by using small-angle approach. Small-angle scattering is a popular technique to study biologically relevant material, as it provides detailed information about the size, shape and confirmation of molecular assemblies in solution. As a result, structural biophysics has taken advantage of recent developments to accurately determine the structure of lipid bilayers [84, 85]. Apart from structural details, this approach was also used to establish mechanical properties of membranes – both area compressibility K_A and bending rigidity κ [86].

Development of techniques - Molecular dynamics simulations for the evaluation of membrane mechanical properties

The developed techniques, that are covered by this dissertation, are commonly using giant unilamellar vesicle as a model of lipid membrane. One of the most common technique for producing this lipid membrane model is electroformation. It was originally establish in 1988 [87]. The main advantages of electroformation are that it requires little technical expertise to implement and that it yields spherical, relatively monodisperse and unilamellar lipid vesicles. The idea of the method is to dissolve lipid molecules (either single lipid or lipid mixtures) in organic solvents, such as chloroform or methanol, and deposit it on electrodes' surface (usually platinum or indium tin oxide). This is followed by drying of electrodes to obtain lipid film. This is frequently done in vacuum to ensure full removal of the solvent. Electrodes are then immersed in aqueous buffer and alternative current (AC) field is applied to induce formation of the vesicles. The exact principles and physics behind the formation of GUVs is not well understood despite several contradicting descriptions. It is known, however, that if the bilayer edges are allowed to merge at a faster rate, multi-lamellar vesicles (MLVs) are formed. To increase the rate of bilayer separation the electric field is use. This enables obtaining the unilamellar vesicles. To stimulate swelling process of the hydrated lipid film, the alternating potential difference is applied across the electrodes. There are several studies investigating the effect of both amplitude and frequency on formation of vesicles. In one of such studies the amplitude (from 1V to 10 V) and frequency (from 1 up to 10^3 Hz) are investigated. The best result was observed for 5V and 10 Hz [88]. Similar study showed, that formation of vesicles occurs with amplitude from 0.2 up to 10.5 V and frequency from 1 up to 10^4 Hz. The highest diameters of vesicles were with frequency between 1 and 100 Hz [89]. While most of protocols set frequency in range of 1-12 Hz, some are reporting getting better results with thousands of Hz [90-92]. Interestingly, it has been shown that in 3D electroformation systems frequency order higher (10^4 Hz) than in 2D electroformation system was required to obtain similar quality of GUVs [93]. It was also suggested that geometry, topology, material and wear of the electrodes might be a factor [94]. As a result several different protocols exist with different voltage and frequency of AC field and different duration of electroformation process. They are summed up in Table 3.

To this end I've investigated the effect of electroformation protocol parameters on quality of obtained GUVs population. I especially emphasized the effect of time, frequency and current changes during electroformation

process on the characteristics of final population. The obtained population of vesicles was assessed using three main indicators : means of vesicles' diameter size, ratio of lipid mass in vesicles to total lipid mass placed on electrodes and *oligovesicularity* of the vesicles' population (determination how hollow and unilamellar the vesicles were). Voltage, frequency, duration of electroformation as well as wear of electrodes were investigated as a potential factor. The article with details from this work can be viewed in **PAPER 1** chapter.

Table 3. Various protocols used for electroformation of Giant Unilamellar Vesicles.

Literature	Electric field (AC)	Time	Additional remarks
[95, 96]	1.2V, 10 Hz	2 hours	Most common procedure
[52]	3V, 10 Hz	1 hour	-
[97]	2V, 5 Hz	2 hours	-
[98]	1.1V, 20 Hz	3 hours	-
[99]	5V, 10 Hz	2 hours	Custom design special chamber
[94]	1V -> 4V, 500 Hz	3 hours	Constant voltage increase
[100]	1V -> 4V, 10 Hz	24 hours	Step voltage increase each hour for 1V
[101]	0.15V -> 3.9V, 500 Hz	2 hours	Step voltage increase
[102]	0.02V -> 1.1V, 12 Hz	4 hours	Step voltage increase each 5 min
[103]	0V -> 1.2V, 10 Hz	5 hours	Step voltage increase in first 40 min
[68]	1.1 V, 10 Hz -> 1.5V, 5 Hz	3 hours	Change in protocol after 1 hour
[104]	2.2V, 10 Hz -> 2.2V, 2-4 Hz	1.5 hour	Second – detachment – phase lasts 30 mins; vesicle contain SNARE proteins
[105]	20V -> 250V, 10 Hz (3h) 350V, 10 Hz (2h) 35oV, 10 Hz -> 4 Hz (2h)	7 hours	Special protocol to mimic physiologically relevant conditions
[106]	8V, 10 Hz (2h) 4V, 5 Hz (15min) 2.5V, 2,5 Hz (15min) 1V, 1 Hz (30min)	3 hours	Electroformation with solution exchange
[107]	0.03V -> 0.33V -> 0.8V, 500 Hz	1.43 hour	Phases lasted 6 min, 20 min and 90 min, respectively.

Abbreviations: AC – alternating current, -> - changing to.

Development of techniques – Vesicle fluctuation analysis

In this dissertation methods based on analysis of thermal fluctuation were developed. One of the most widely used technique in this category is vesicle fluctuation analysis (VFA, also sometimes called flicker-noise spectroscopy). The idea of this technique is the analysis of membrane fluctuations - thermally induced shape undulations to be specific – observed on the equatorial surface of a vesicle (see Figure 1.11) as a function of time and measure the amplitudes of those fluctuations, which are later used to determine bending rigidity of the bilayer. This technique was first established in 1989 [51]. In this approach inverted contrast phase microscopy was used. From 500 to 1000 frames for single vesicle was recorded with interval of 1 second. It was based on mechanical model of lipid bilayer by W. Helfrich [48] and average-based approach for numerical analysis is used. Later, in 1990, this approach was used to investigate the effect of temperature on mechanical properties by designing special Peltier chamber [108]. In this approach 5-10 frames per second (fps) was recorded. In 2002 this method is used to investigate the effect of gravitational descend of vesicles on their mechanical properties [52]. Simultaneous development in technology is clearly visible, as the frequency of image capture increased to 25 fps and each vesicle is analyzed for at least 2000 frames. In 2004 three papers regarding flicker noise technique were publish. In two of them phase contrast microscopy was used to observe series of 2000 frames with 30 fps [98] and 300-4000 frames with 25 fps [109]. There was also an attempt to use stroboscopic light to improve the precision of mechanical parameters determination [110], however it resulted in significant decrease in number of frames (down to 400). In 2008 method was used to establish the effect of magainin [101], however no technological nor numerical development were introduced. In 2009 the paper investigating effect of cholesterol and sphingomyelin on mechanical properties of homogeneous

vesicles and vesicles from plasma membrane of human red blood cells were published [68]. The value of fps was increased, depending on the sample, from 60 up to 250 fps. Interestingly, electro-deformation of vesicles is done prior to VFA. In 2010 an effect of fluorescent probes in lipid membrane on mechanical properties was under the investigation [111]. In was shown that up to 2 mol% of fluorescence probes in bilayer the effect in negligible and some probes (such as Rhodamine and NBD-PE) in higher concentrations have stronger effect that others (such as βBodipy). In 2011 a novel way of numerical analysis was developed. It was named as statistical analysis [50], which exhibits certain advantages to the averaged-based approach such as assessment of agreement with mathematical model of recorded vesicle. Furthermore, lack of effect of fluorescence probes (up to 2mol%) on mechanical properties was confirmed in this work. Single vesicle was recorded for 10 minutes leading to 15000 frames (25 fps). In 2013, for the first time, an fluorescent microscope, specifically selective plane illumination microscopy, was used to record thermal fluctuations of the lipid GUVs to measure bending rigidity of POPC vesicles [96]. Fluctuations were recorded with 60-100 fps. In 2014 a review of mechanical properties of POPC vesicles using various techniques, including VFA, was
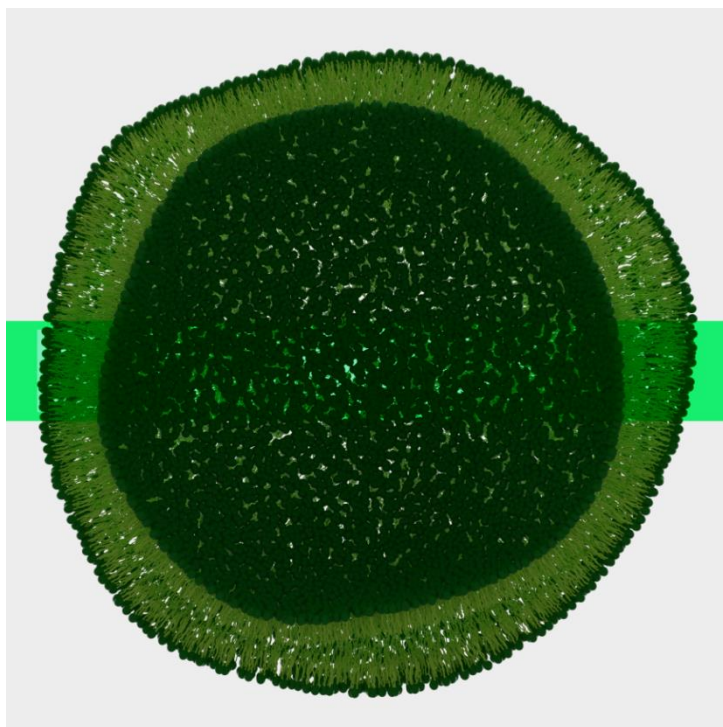

Figure 1.11. Visualization of vesicle. As shown, only small intersection of vesicle at the equatorial part is recorded for the purpose of fluctuation analysis (green area).
Graphic rendered using Blender 2.8 software (GPL license) and is a property of dissertation's author.

published [112]. In 2016 a paper with summarized two years of work was published, in which both fluorescence confocal microscopy and fluorescence microscopy with spinning disk were used to determine bending rigidity of both POPC and DOPC vesicles. The article can be viewed in **PAPER 2** chapter. In that paper fluorescence microscopy was used to improve precision of the location of the bilayer and, as a result, improve determination of the bending rigidity coefficient. Additionally, two numerical approaches are used (both average-based and statistical). Since the development of the method it was commonly used to solve various biophysical problems. In 2017 I used it to determine the effect of doxorubicin drug on bending rigidity of POPC vesicles [113] as well as assess the effect of phenyltin toxins on mechanical properties of lipid membrane [114]. The latter allowed to propose a molecular mechanism of phenyltin interaction with membrane. In 2018 an approach to determine population character of bending rigidity parameter was carried out showing that, instead of expected normal distribution, it follows exponential character [115]. Lately I used VFA to establish the effect of antimicrobial agents (chlorhexidine and octenidine dihydrochloride) on bending rigidity of POPC membranes [data not yet published] and effect of incorporated β-Amyloid peptides on mechanical properties of POPC lipid membranes [116].

Development of techniques - Molecular dynamics simulations for establishing mechanical properties

Second developed technique in this dissertation is SPHA analysis on simulated system of lipid vesicle using molecular dynamics. Molecular Dynamics (MD) is the numerical simulation technique for analyzing physical movement of atoms and molecules. Their trajectories are determined by numerically solving Newton's Law equations of motion for a system of interacting particles. Forces and interactions between the particles and their potential energies are calculated using molecular mechanics force fields. There exist three types of FFs - atomistic, coarse-gain and hybrid (united-atom). Atomistic FF is determined by the sets of force constants, equilibrium bond distances and angles, Lennard-Jones parameters and partial charges for all chemically different atom types involved. This FF allows most detailed interactions between the particles, however, due to number of calculations, it requires substantial amount

of time. When investigation of certain properties of lipid bilayers requires either length or time scales not reachable (or not affordable) in atomistic simulations, so called coarse-grained FFs are used. To make large-scale membrane simulations practically feasible, it is necessary to simplify description of individual lipids or molecules, so that groups of atoms are combined into pseudo-particles resulting in a coarse-grained description of a system. Coarse-grained models are emerging as a practical alternative to full-atomistic simulations when detailed atomistic representation is not necessary while it is important to observe membrane phenomena over long time scales. Finally, a hybrid approach, called united-atom FF, which combines both approaches has been developed. A united-atom is a particle that incorporates a group of atoms but can approximately represent the molecular mechanical properties of the group on a scale of size that is larger than atomic scale. The united-atom model is a good approximation when investigating interactions between the particles that react with each other as a whole group rather than form new compounds or break into smaller submolecules. In this FFs united-atoms are used to represent carbon chains of lipids, namely carbon atom with two bonded hydrogens is replaced with one united-atom reflecting properties of this compound [117, 118]. There exist numerous approaches to determine mechanical properties – both bending rigidity and area compressibility - using molecular dynamics simulations – both based on recreation of experimental conditions or strictly physical determination of the parameters of interest. For MD approaches to determine mechanical properties based on membrane undulations two main approaches can be highlighted.

First approach is usually referred to as Fourier Space methodology. Fluctuation spectrum of thermally excited membrane deformations, which is correlated to bending rigidity, is calculated. It is obtained by applying fast Fourier transformation to the position of lipid molecules in time. The obtained spectrum is plotted as a function of the dimensionless wave number to which a model is fitted to obtain bending rigidity. The area compressibility is defined as a function of bending rigidity and effective thickness of the membrane. This approach was first used on mixture of amphiphiles. After the self-assembly into bilayer and equilibration, the fluctuation spectrum is collected and mechanical parameters are determined [119]. Similar approach was later used on homogeneous DPPC bilayer with united-atom FF [120] and in homogeneous sphingomyelin bilayers using coarse-grained FF [121]. Interestingly, in latter work area compressibility is calculated accordingly to ensemble fluctuation theory, which defines it as a function of bending rigidity and area fluctuations of the system rather than thickness of the membrane. This approach was also used as a reference when establishing different approaches [122]. In 2014 this approach was first used for full-atomistic DPPC, DOPC and DOPE membrane systems [123]. Area compressibility was determined via an analysis of simulation box fluctuations. It was later used to determine mechanical properties of various homogeneous membranes [124].

Second approach is usually referred to as Real Space Fluctuation methodology. Bending rigidity and tilt modulus are obtained from potential of mean force, which is defined as a measure of free energy change associated with molecule tilt under different conditions. For tilt modulus a deviation from membrane normal is considered, while for bending rigidity a divination from surrounding lipid molecules is taken into account (so called lipid splay). Both of those tilts are calculated as a probability distribution, which is then fitted with theoretical model distribution. This approach was first used when the effect of cholesterol in DMPC membranes was investigated using coarse-grained FF DM simulations [125]. It was later improved with calculation of tilt modulus and approach for heterogeneous bilayers [126-128]. It was also used for comparison in full-atomistic DPPC, DOPC and DOPE membrane systems [123]. The methodology was implemented in openly-available software *Openstruct* [129]. It was extensively used to determine mechanical properties of various homogeneous and heterogeneous membranes using full-atomistic CHARMM FF [130].

All of above-mentioned methods were carried out on planar lipid membrane. It is not surprising as planar systems require less computational power. However, the curvature effect is not taken into account, which might be a factor during determination of mechanical properties. However, in 2014, an successful attempt to establish mechanical parameters from full lipid vesicles was carried out using coarse-grained FF [131]. An 34 nm in diameter DMPC lipid vesicle was modelled with different concentrations of surrounding water molecules. The analysis of the vesicle to obtain mechanical parameters, referred to as Spherical Harmonics Analysis (SPHA), is based on Helfrich model [48]

of fluctuations. The fluctuations observed on the surface of vesicle are decomposed into Legendre polynomial modes basis to calculate their amplitudes, as schematically shown in Figure 1.12. The amplitudes are used to determine mechanical properties. I've adapted this approach to determine mechanical properties of POPC, DMPC, DPPC, DSPC and HSPC 10 nm vesicle systems in united-atom FF MD simulations. Additionally, as a reference, I've established mechanical properties of those planar membranes of those lipids using Real Space Fluctuation methodology. Area compressibility was calculated according to published algorithm [132]. This results can be viewed

in **PAPER 3** chapter. Established method was already used for determination of effect of incorporated β-Amyloid peptides on mechanical properties of POPC lipid membranes [116]. Interestingly, a new method based on quantifying compressibility moduli from local thickness fluctuations for determination of area compressibility was introduced lately [133].

Nonetheless, analysis based on undulations is not exclusive approach to determine mechanical properties of lipid bilayers when using MD simulations. Those approaches are based on experimental designs already described at the beginning of this chapter. One of the approaches is based on inducing mechanical deformations during simulation. During a simulation two cylindrical guiding potentials are added to standard FF, which impose a sinusoidal deformation to a planar membrane [134]. The restoring force of the deformed membrane is measured and detected as the mean force exerted on the
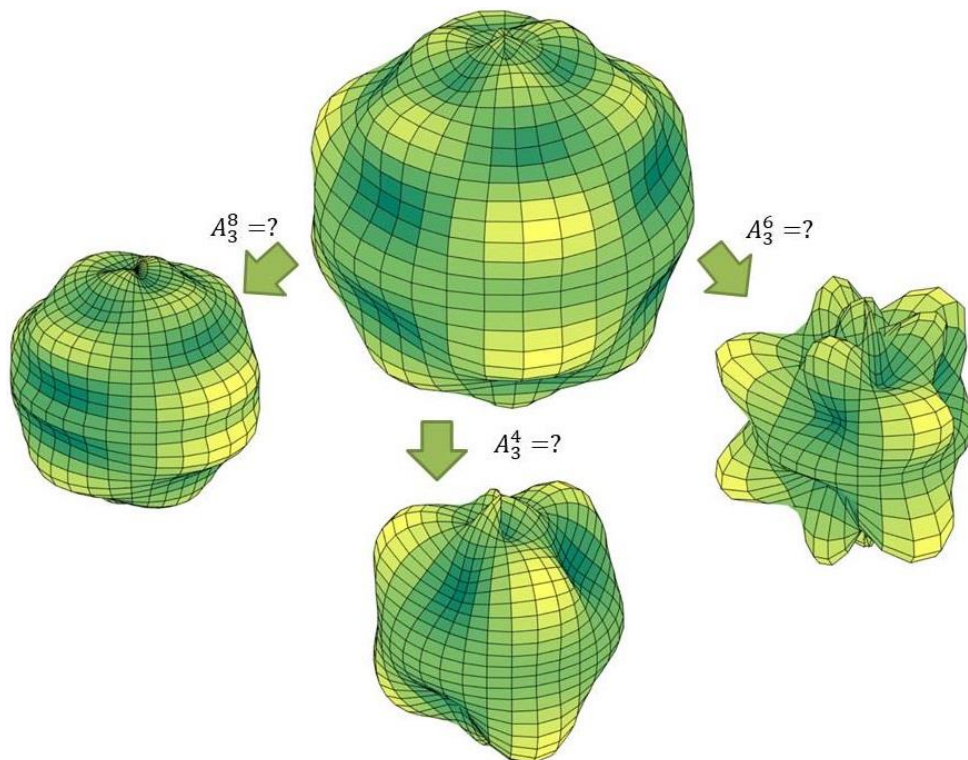
Figure 1.12. Schematic decomposition of observed fluctuations on vesicle's surface into individual modes' amplitudes (described by Legendre polynomials).
Graphic created using GIMP software (GNU license) and is based on a work of dissertation's author.

membrane from the deforming cylinders. The force is determined as a function of the membrane curvature and the bending rigidity is estimated by numerically solving the Helfrich model [48]. Another approach is based on imposing a deformation of the membrane by creating a curbed cylindrical vesicle and measuring the force required to hold this state [61, 122, 135]. This method is practically a numerical simulation of tether formation method. Interestingly, it allows calculation of Gaussian curvature K_G. During simulation a tether is simply stabilized by spanning a cylindrical vesicle through simulation box (across the periodic boundary conditions). As a result simulated system is perfectly cylindrical and the axial pulling force is readily obtained from the stress tensor along the tether direction. Additionally, scattering data was also obtained from MD simulations with coarse-grained FF [136]. A discrete Fourier transform was used to calculate neutron scattering function of the real space density distribution of all lipid molecules. Both planar and vesicle topologies were investigated. Interestingly, bending rigidity was additionally calculated using Fourier Space methodology.

1.5. Summary and perspectives

The main objective of this dissertation was to develop methods to determine mechanical properties of lipid membranes. To this end experimental model of lipid membranes, giant unilamellar vesicles (GUVs) was used. This model was obtained using electroformation method, which was also studied. For determination of mechanical parameters two methods were developed and validated – thermal fluctuation analysis and determination using molecular dynamics simulations. Eventually, developed techniques were used to provide valuable insight into biophysical processes are were used to solve several scientific problems.

The vesicle fluctuation analysis technique was improved by implementation of fluorescence confocal microscopy, which increased the quality of obtained vesicle's contour. This resulted in much precise determination of bending rigidity coefficient. Additionally, a custom analysis software was developed using both OpenCV libraries on C++ and MATLAB. Finally, effect of implementation of various smoothing algorithms on precision of establish parameters was investigated.

Developed method to establish mechanical properties of membranes using molecular dynamics was, also, based on analysis of thermal fluctuations. The difference here was that, in contrary to experimental technique, full three-dimensional vesicle can be analyzed instead of small two-dimensional intersection. This allows not only more precise observation of fluctuation spectra, but also due to nature of molecular dynamics simulations, grants access to microscopic parameters such as membrane thickness, area per lipid and bilayer profiles. It also allows to establish area compressibility from the simulations. This approach was carried out on united-atom force field, which provided more details than commonly used coarse-grain models. This technique allows to include effect of curvature which provided, in some membranes, different parameters than in case of planar membrane topology.

Established techniques were, as described, used to investigate effects of various factors on mechanical properties as well as solve certain biophysical problems. Studies of electroformation resulted in decreasing necessary time of GUVs formation and showed strong effect of electrical field parameters. Vesicle fluctuation analysis technique was successfully used to determine the effect of phenyltin toxins, anti-cancerous drug doxorubicin, neurodegenerative β-amyloid peptides and antimicrobial agents like chlorhexidine and octenidine dihydrochloride on mechanical behavior of lipid membranes. The effect of fluorescence probe incorporated into bilayer, heterogeneity, phase shift and temperature was also investigated. Usage of molecular dynamics studies allowed to provide additional insight into mechanical and structural behavior of investigated lipid membranes. It was used to investigate lipid membranes in uncommonly-investigated lipid phases such as rippled-gel, gel and crystalline (or metastable) phases as well as investigate the effect of neurodegenerative β-amyloid peptides. It was also shown that, contrary to current consensus, established mechanical properties might significantly differ when investigated on planar and spherical systems. This suggest, that solid-phases are not as uniform as it was previously believed.

Nevertheless, an experimental technique should be developed to establish area compressibility, as to confirm results obtained from molecular dynamics simulations. Two techniques were under development during my PhD studies for that purpose – mechanical deformation induced by polystyrene beads controlled by optical tweezers and force spectroscopy during indentation of vesicles using atomic force microscopy. The approaches to establish repeatable results using Optical Tweezers were unsuccessful due to various problems that emerged. On the other hand, a technique using atomic force microscopy was successfully developed [data not yet published], providing an experimental value to confirm area compressibility obtained from molecular dynamics simulations.

1.6. Bibliography

1. Wang, Y., J.Y. Shyy, and S. Chien, *Fluorescence proteins, live-cell imaging, and mechanobiology: seeing is believing.* Annu Rev Biomed Eng, 2008. **10**: p. 1-38.
2. Evans, E. and A. Yeung, *Apparent viscosity and cortical tension of blood granulocytes determined by micropipet aspiration.* Biophys J, 1989. **56**(1): p. 151-60.
3. Stamenovic, D. and D.E. Ingber, *Models of cytoskeletal mechanics of adherent cells.* Biomech Model Mechanobiol, 2002. **1**(1): p. 95-108.
4. Murrell, M., R. Kamm, and P. Matsudaira, *Tension, free space, and cell damage in a microfluidic wound healing assay.* PLoS One, 2011. **6**(9): p. e24283.
5. Mackintosh, F.C. and C.F. Schmidt, *Active cellular materials.* Curr Opin Cell Biol, 2010. **22**(1): p. 29-35.
6. Ahmed, W.W., E. Fodor, and T. Betz, *Active cell mechanics: Measurement and theory.* Biochim Biophys Acta, 2015. **1853**(11 Pt B): p. 3083-94.
7. Boal, D., *Introduction to the cell*, in *Mechanics of the Cell*. 2012, Cambridge University Press: United States of America, New York. p. 1-23.
8. Janmey, P.A. and C.A. McCulloch, *Cell mechanics: integrating cell responses to mechanical stimuli.* Annu Rev Biomed Eng, 2007. **9**: p. 1-34.
9. Discher, D.E., P. Janmey, and Y.L. Wang, *Tissue cells feel and respond to the stiffness of their substrate.* Science, 2005. **310**(5751): p. 1139-43.
10. Moeendarbary, E. and A.R. Harris, *Cell mechanics: principles, practices, and prospects.* Wiley Interdiscip Rev Syst Biol Med, 2014. **6**(5): p. 371-88.
11. Lekka, M., et al., *Elasticity of normal and cancerous human bladder cells studied by scanning force microscopy.* European Biophysics Journal with Biophysics Letters, 1999. **28**(4): p. 312-316.
12. Wang, J., et al., *Mechanomics: an emerging field between biology and biomechanics.* Protein Cell, 2014. **5**(7): p. 518-31.
13. Boal, D., *Part III The whole cell: The simplest cells*, in *Mechanics of the Cell*. 2012, Cambridge University Press: United States of America, New York. p. 371-405.
14. Hianik, T., *Structure and physical properties of biomembranes and model membranes: Membrane structure and composition.* Acta Physica Slovaca 2007. **56**(6): p. 690-700.
15. Bouvrais, H., *Bending Rigidities of Lipid Bilayers: Their Determination and Main Inputs in Biophysical Studies*. Advances in Planar Lipid Bilayers and Liposomes, ed. A. Iglic. Vol. 15. 2012, Oxford, UK: Elsevier Inc. 2-7.
16. Nelson, P., *What's inside cells*, in *Biological Physics: Energy, Information, Life*. 2002, W. H. Freeman: New York. p. 30-61.
17. Simons, K. and E. Ikonen, *Functional rafts in cell membranes.* Nature, 1997. **387**(6633): p. 569-72.
18. Lingwood, D., et al., *Lipid rafts as functional heterogeneity in cell membranes.* Biochem Soc Trans, 2009. **37**(Pt 5): p. 955-60.
19. McIntosh, T.J., A. Vidal, and S.A. Simon, *Sorting of lipids and transmembrane peptides between detergent-soluble bilayers and detergent-resistant rafts.* Biophys J, 2003. **85**(3): p. 1656-66.
20. Slotte, J.P. and B. Ramstedt, *The functional role of sphingomyelin in cell membranes.* Eur. J. Lipid Sci. Technol., 2007. **109**(10): p. 977-981.
21. Slotte, J.P., *Biological functions of sphingomyelins.* Prog Lipid Res, 2013. **52**(4): p. 424-37.
22. Braverman, N.E. and A.B. Moser, *Functions of plasmalogen lipids in health and disease.* Biochim Biophys Acta, 2012. **1822**(9): p. 1442-52.
23. Paradies, G., et al., *Functional role of cardiolipin in mitochondrial bioenergetics.* Biochim Biophys Acta, 2014. **1837**(4): p. 408-17.
24. Marquardt, D., B. Geier, and G. Pabst, *Asymmetric lipid membranes: towards more realistic model systems.* Membranes (Basel), 2015. **5**(2): p. 180-96.
25. Kessel, A. and N. Ben-Tal, *Principles of Membrane Protein Structure*, in *Introduction to Proteins: Structure, Function and Motion*. 2018, CRC Press, Taylor & Francis Group: New York, USA. p. 518-550.
26. Monje-Galvan, V. and J.B. Klauda, *Peripheral membrane proteins: Tying the knot between experiment and computation.* Biochim Biophys Acta, 2016. **1858**(7 Pt B): p. 1584-93.
27. Pignatello, R., *Biological membranes and their role in physio-pathological conditions*, in *Drug-Biomembrane Interaction Studies: The Application of Calorimetric Techniques*. 2013. p. 1-46.
28. Luna, E.J. and A.L. Hitt, *Cytoskeleton--plasma membrane interactions.* Science, 1992. **258**(5084): p. 955-64.
29. Mueller, P. and D.O. Rudin, *Induced excitability in reconstituted cell membrane structure.* J Theor Biol, 1963. **4**(3): p. 268-80.

30.   Bangham, A.D., M.M. Standish, and J.C. Watkins, *Diffusion of univalent ions across the lamellae of swollen phospholipids.* J Mol Biol, 1965. **13**(1): p. 238-52.

31.   Rascol, E., J.M. Devoisselle, and J. Chopineau, *The relevance of membrane models to understand nanoparticles-cell membrane interactions.* Nanoscale, 2016. **8**(9): p. 4780-98.

32.   Zupanc, J., et al., *Lipid vesicle shape analysis from populations using light video microscopy and computer vision.* PLoS One, 2014. **9**(11): p. e113405.

33.   Yee-Hung, M.C. and S.G. Boxer, *Model Membrane Systems and Their Applications.* Curr Opin Chem Biol., 2007. **11**(6): p. 581–587.

34.   Rebaud, S., O. Maniti, and A.P. Girard-Egrot, *Tethered bilayer lipid membranes (tBLMs): interest and applications for biological membrane investigations.* Biochimie, 2014. **107 Pt A**: p. 135-42.

35.   Stefaniu, C., G. Brezesinski, and H. Mohwald, *Langmuir monolayers as models to study processes at membrane surfaces.* Adv Colloid Interface Sci, 2014. **208**: p. 197-213.

36.   Moehwald, H. and G. Brezesinski, *From Langmuir Monolayers to Multilayer Films.* Langmuir, 2016. **32**(41): p. 10445-10458.

37.   Dimova, R., B. Pouligny, and C. Dietrich, *Pretransitional effects in dimyristoylphosphatidylcholine vesicle membranes: optical dynamometry study.* Biophys J, 2000. **79**(1): p. 340-56.

38.   Koynova, R. and B. Tenchov, *Lipids: Phase Transitions*, in *Wiley Encyclopedia of Chemical Biology*. 2008, John Wiley & Sons, Inc. p. 1-15.

39.   Marsh, D., *Phase Transition Temperatures*, in *Handbook of lipid bilayers*. 2013, Taylor & Francis Group: New York. p. 539-600.

40.   Nagle, J.F., *Theory of the main bilayer phase transition.* Ann. Rev. Phys. Chem.. 1980. **31**: p. 157-195.

41.   Akabori, K. and J.F. Nagle, *Structure of the DMPC lipid bilayer ripple phase.* Soft Matter, 2015. **11**(5): p. 918-26.

42.   Tristram-Nagle, S. and J.F. Nagle, *Lipid bilayers: thermodynamics, structure, fluctuations, and interactions.* Chem Phys Lipids, 2004. **127**(1): p. 3-14.

43.   Goto, M., et al., *Study on the subgel-phase formation using an asymmetric phospholipid bilayer membrane by high-pressure fluorometry.* Langmuir, 2012. **28**(33): p. 12191-8.

44.   M'Baye, G., et al., *Liquid ordered and gel phases of lipid bilayers: fluorescent probes reveal close fluidity but different hydration.* Biophys J, 2008. **95**(3): p. 1217-25.

45.   Clarke, J.A., J.M. Seddon, and R.V. Law, *Cholesterol containing model membranes studied by multinuclearsolid state NMR spectroscopy.* Soft Matter, 2009. **5**(2): p. 369-378.

46.   Aufderhorst-Roberts, A., U. Chandra, and S.D. Connell, *Three-Phase Coexistence in Lipid Membranes.* Biophys J, 2017. **112**(2): p. 313-324.

47.   Owen, D.M., et al., *The lipid raft hypothesis revisited--new insights on raft composition and function from super-resolution fluorescence microscopy.* Bioessays, 2012. **34**(9): p. 739-47.

48.   Helfrich, W., *Elastic Properties of Lipid Bilayers: Theory and Possible Experiments.* Z. Naturforsch, 1973. **28**(c): p. 693-703.

49.   Deserno, M., *Fluid lipid membranes: from differential geometry to curvature stresses.* Chem Phys Lipids, 2015. **185**: p. 11-45.

50.   Meleard, P., et al., *Advantages of statistical analysis of giant vesicle flickering for bending elasticity measurements.* Eur Phys J E Soft Matter, 2011. **34**(10): p. 116.

51.   Faucon, J.F., et al., *Bending elasticity and thermal fluctuations of lipid membranes. Theoretical and experimental requirements.* J. Phys. France, 1989. **50**: p. 2389-2414.

52.   Henriksen, J. and J.H. Ipsen, *Thermal undulations of quasi-spherical vesicles stabilized by gravity.* Eur Biophys J, 2002. **9**: p. 365-374.

53.   Evans, E. and W. Rawicz, *Entropy-driven tension and bending elasticity in condensed-fluid membranes.* Phys Rev Lett, 1990. **64**(17): p. 2094-2097.

54.   Henriksen, J.R. and J.H. Ipsen, *Measurement of membrane elasticity by micro-pipette aspiration.* Eur Phys J E Soft Matter, 2004. **14**(2): p. 149-67.

55.   Tierney, K.J., D.E. Block, and M.L. Longo, *Elasticity and phase behavior of DPPC membrane modulated by cholesterol, ergosterol, and ethanol.* Biophys J, 2005. **89**(4): p. 2481-93.

56.   Khadka, N.K., et al., *Modulation of lipid membrane structural and mechanical properties by a peptidomimetic derived from reduced amide scaffold.* Biochim Biophys Acta Biomembr, 2017. **1859**(5): p. 734-744.

57.   Bagatolli, L.A. and D. Needham, *Quantitative optical microscopy and micromanipulation studies on the lipid bilayer membranes of giant unilamellar vesicles.* Chem Phys Lipids, 2014. **181**: p. 99-120.

58. Rawicz, W., et al., *Effect of chain length and unsaturation on elasticity of lipid bilayers.* Biophys J, 2000. **79**(1): p. 328-39.

59. Ibarboure, E., M. Fauquignon, and J.F. Le Meins, *Obtention of Giant Unilamellar Hybrid Vesicles by Electroformation and Measurement of their Mechanical Properties by Micropipette Aspiration.* J. Vis. Exp., 2020. **155**: p. e60199.

60. Waugh, R.E. and R.M. Hochmuth, *Mechanical equilibrium of thick, hollow, liquid membrane cylinders.* Biophys J, 1987. **52**(3): p. 391-400.

61. Baoukina, S., S.J. Marrink, and D.P. Tieleman, *Molecular structure of membrane tethers.* Biophys J, 2012. **102**(8): p. 1866-71.

62. Settles, E.I., et al., *The vesicle trafficking protein Sar1 lowers lipid membrane rigidity.* Biophys J, 2010. **99**(5): p. 1539-45.

63. Shitamichi, Y., M. Ichikawa, and Y. Kimura, *Mechanical properties of a giant liposome studied using optical tweezers.* Chemical Physics Letters, 2009. **479**(4-6): p. 274-278.

64. Solmaz, M.E., et al., *Optical stretching of giant unilamellar vesicles with an integrated dual-beam optical trap.* Biomed Opt Express, 2012. **3**(10): p. 2419-27.

65. Solmaz, M.E., et al., *Optical stretching as a tool to investigate the mechanical properties of lipid bilayers.* RSC Adv., 2013. **3**(37): p. 16632-16638.

66. Dols-Perez, A., et al., *Artificial Cell Membranes Interfaced with Optical Tweezers: A Versatile Microfluidics Platform for Nanomanipulation and Mechanical Characterization.* ACS Appl Mater Interfaces, 2019. **11**(37): p. 33620-33627.

67. Kummrow, M. and W. Helfrich, *Deformation of giant lipid vesicles by electric fields.* Phys Rev A, 1991. **44**(12): p. 8356-8360.

68. Gracià, R.S., et al., *Effect of cholesterol on the rigidity of saturated and unsaturated membranes: fluctuation and electrodeformation analysis of giant vesicles.* Soft Matter, 2010. **6**(7): p. 1472-1482.

69. Aranda, S., et al., *Morphological transitions of vesicles induced by alternating electric fields.* Biophys J, 2008. **95**(2): p. L19-21.

70. Dimova, R., et al., *Vesicles in electric fields: Some novel aspects of membrane behavior.* Soft Matter, 2009. **5**(17): p. 3201-3212.

71. Et-Thakafy, O., et al., *Mechanical Properties of Membranes Composed of Gel-Phase or Fluid-Phase Phospholipids Probed on Liposomes by Atomic Force Spectroscopy.* Langmuir, 2017. **33**(21): p. 5117-5126.

72. Schafer, E., T.T. Kliesch, and A. Janshoff, *Mechanical properties of giant liposomes compressed between two parallel plates: impact of artificial actin shells.* Langmuir, 2013. **29**(33): p. 10463-74.

73. Schafer, E., et al., *Mechanical response of adherent giant liposomes to indentation with a conical AFM-tip.* Soft Matter, 2015. **11**(22): p. 4487-95.

74. Santos, E.B., et al., *Nanomechanical Properties of Phospholipid Microbubbles.* Langmuir, 2012. **28**: p. 5753-5760.

75. Lee, C.H., W.C. Lin, and J. Wang, *All-optical measurements of the bending rigidity of lipid-vesicle membranes across structural phase transitions.* Phys Rev E Stat Nonlin Soft Matter Phys, 2001. **64**(2 Pt 1): p. 020901.

76. Lee, C.H. and J. Wang, *Noninterferometric differential confocal microscopy with 2-nm depth resolution.* Optics Communications, 1997. **135**(4-6): p. 233-237.

77. Kučerka, N., et al., *Structural Significance of Lipid Diversity as Studied by Small Angle Neutron and X-ray Scattering.* Membranes, 2015. **5**(3): p. 454-472.

78. Lyatskaya, Y., et al., *Method for obtaining structure and interactions from oriented lipid bilayers.* Phys Rev E Stat Nonlin Soft Matter Phys, 2001. **63**(1 Pt 1): p. 011907.

79. Kučerka, N., et al., *Structure of fully hydrated fluid phase DMPC and DLPC lipid bilayers using X-ray scattering from oriented multilamellar arrays and from unilamellar vesicles.* Biophys J, 2005. **88**(4): p. 2626-37.

80. Kučerka, N., S. Tristram-Nagle, and J.F. Nagle, *Structure of fully hydrated fluid phase lipid bilayers with monounsaturated chains.* J Membr Biol, 2005. **208**(3): p. 193-202.

81. Arriaga, L.R., et al., *Stiffening effect of cholesterol on disordered lipid phases: a combined neutron spin echo + dynamic light scattering analysis of the bending elasticity of large unilamellar vesicles.* Biophys J, 2009. **96**(9): p. 3629-37.

82. Yi, Z., M. Nagao, and D.P. Bossev, *Bending elasticity of saturated and monounsaturated phospholipid membranes studied by the neutron spin echo technique.* J Phys Condens Matter, 2009. **21**(15): p. 155104.

83. Nagao, M., et al., *Probing Elastic and Viscous Properties of Phospholipid Bilayers Using Neutron Spin Echo Spectroscopy.* J Phys Chem Lett, 2017. **8**(19): p. 4679-4684.

84. Wiener, M.C. and S.H. White, *Fluid bilayer structure determination by the combined use of x-ray and neutron diffraction. I. Fluid bilayer models and the limits of resolution.* Biophys J, 1991. **59**(1): p. 162-73.

85. Heberle, F.A., et al., *Model-based approaches for the determination of lipid bilayer structure from small-angle neutron and X-ray scattering data.* Eur Biophys J, 2012. **41**(10): p. 875-90.

86. Pan, J., et al., *Structural and mechanical properties of cardiolipin lipid bilayers determined using neutron spin echo, small angle neutron and X-ray scattering, and molecular dynamics simulations.* Soft Matter, 2015. **11**(1): p. 130-8.

87. Dimitrov, D.S. and M. Angelova, *Lipid swelling and liposome formation mediated by electric fields.* Journal of Electroanalytical Chemistry and Interfacial Electrochemistry, 1988. **253**(2): p. 323-336.

88. Bi, H., et al., *Electroformation of giant unilamellar vesicles using interdigitated ITO electrodes.* Journal of Materials Chemistry A, 2013. **1**(24): p. 7125-7130.

89. Politano, T.J., et al., *AC-electric field dependent electroformation of giant lipid vesicles.* Colloids Surf B Biointerfaces, 2010. **79**(1): p. 75-82.

90. Wang, Z., et al., *Electroformation and electrofusion of giant vesicles in a microfluidic device.* Colloids Surf B Biointerfaces, 2013. **110**: p. 81-7.

91. Le Berre, M., et al., *Electroformation of giant phospholipid vesicles on a silicon substrate: advantages of controllable surface properties.* Langmuir, 2008. **24**(6): p. 2643-9.

92. Bellon, J.A., M.J. Pino, and N. Wilke, *Low-cost equipment for electroformation of Giant Unilamellar Vesicles.* HardwareX, 2018. **4**: p. e00037.

93. Wang, Q., et al., *Frequency-Dependent Electroformation of Giant Unilamellar Vesicles in 3D and 2D Microelectrode Systems.* Micromachines, 2017. **8**(1): p. 24.

94. Herold, C., et al., *Efficient Electroformation of Supergiant Unilamellar Vesicles Containing Cationic Lipids on ITO-Coated Electrodes.* Langmuir, 2012. **28**: p. 5518-5521.

95. Angelova, M. and D.S. Dimitrov, *A mechanism of liposome electroformation.* Trends in Colloid and Interface Science II, 2007. **76**: p. 59-67.

96. Loftus, A.F., et al., *Robust Measurement of Membrane Bending Moduli Using Light Sheet Fluorescence Imaging of Vesicle Fluctuations.* Langmuir, 2013. **29**(14): p. 588-594.

97. Esposito, C., et al., *Flicker Spectroscopy of Thermal Lipid Bilayer Domain Boundary Fluctuations.* Biophysical Journal, 2007. **93**: p. 3169-3181.

98. Pecreaux, J., et al., *Refined contour analysis of giant unilamellar vesicles.* Eur. Phys. J. E, 2004. **13**: p. 277-290.

99. Pereno, V., et al., *Electroformation of Giant Unilamellar Vesicles on Stainless Steel Electrodes.* ACS Omega, 2017. **2**(3): p. 994-1002.

100. Drabik, D., et al., *The modified fluorescence based vesicle fluctuation spectroscopy technique for determination of lipid bilayer bending properties.* Biochim Biophys Acta, 2016. **1858**(2): p. 244-52.

101. Bouvrais, H., et al., *Softening of POPC membranes by magainin.* Biophysical Chemistry 2008. **137**: p. 7-12.

102. Girard, P., et al., *A New Method for the Reconstitution of Membrane Proteins into Giant Unilamellar Vesicles.* Biophysical Journal, 2004. **87**: p. 419-429.

103. Mathivet, L., S. Cribier, and F. Devaux, *Shape Change and Physical Properties of Giant Phospholipid Vesicles Prepared in the Presence of an AC Electric Field.* Biophysical Journal, 1996. **70**: p. 1112-1121.

104. Witkowska, A., L. Jablonski, and R. Jahn, *A convenient protocol for generating giant unilamellar vesicles containing SNARE proteins using electroformation.* Sci Rep, 2018. **8**(1): p. 9422.

105. Pott, T., H. Bouvrais, and P. Meleard, *Giant unilamellar vesicle formation under physiologically relevant conditions.* Chem Phys Lipids, 2008. **154**(2): p. 115-9.

106. Peterlin, P. and V. Arrigler, *Electroformation in a flow chamber with solution exchange as a means of preparation of flaccid giant vesicles.* Colloids Surf B, 2007. **64**: p. 77-87.

107. dos Santos, J.L., et al., *Portable Proportional-Integral-Derivative controlled chambers for giant unilamellar vesicles electroformation.* Biomedical Physics & Engineering Express, 2019. **5**(4): p. 1-7.

108. Duwe, H.P. and E. Sackmann, *Bending elasticity and thermal excitation of lipid bilayer vesicles: modulation by solutes.* Physica A, 1990. **163**: p. 410-428.

109. Henriksen, J., A.C. Rowat, and J.H. Ipsen, *Vesicle fluctuation analysis of the effects of sterols on membrane bending rigidity.* Eur Biophys J, 2004. **33**: p. 732-741.

110. Genova, J., et al., *Using Stroboscopic Illumination to Improve the Precision of the Bending Modulus Measurement.* Bulg. J. Phys., 2004. **31**: p. 68-75.

111. Bouvrais, H., et al., *Impact of membrane-anchored fluorescent probes on the mechanical properties of lipid bilayers.* Biochimica et Biophysica Acta, 2010. **1798**: p. 1333-1337.

112. Dimova, R., *Recent developments in the field of bending rigidity measurements on membranes.* Advances in Colloid and Interface Science, 2014. **208**: p. 225-234.

113. Fraczkowska, K., et al., *Alterations of biomechanics in cancer and normal cells induced by doxorubicin.* Biomed Pharmacother, 2018. **97**: p. 1195-1203.

114. Przybylo, M., et al., *Changes in lipid membrane mechanics induced by di- and tri-phenyltins.* Biochim Biophys Acta Biomembr, 2017. **1859**(8): p. 1301-1309.

115. Doskocz, J., et al., *Statistical Analysis of Bending Rigidity Coefficient Determined Using Fluorescence-Based Flicker-Noise Spectroscopy.* J Membr Biol, 2018. **251**(4): p. 601-608.

116. Drabik, D., G. Chodaczek, and M. Langner, *Effect β-Amyloid peptides on mechanical properties of POPC lipid bilayers*, in *International Conference on Bioscience, Biochemistry and Bioinformatics (ICBBB 2019)*. 2019, Hong Kong Chemical, Biological & Environmental Engineering Society: Singapure. p. 48.

117. Lyubartsev, A.P. and A.L. Rabinovich, *Force Field Development for Lipid Membrane Simulations.* Biochim Biophys Acta, 2016. **1858**(10): p. 2483-2497.

118. Lee, S., et al., *CHARMM36 united atom chain model for lipids and surfactants.* J Phys Chem B, 2014. **118**(2): p. 547-56.

119. Goetz, R., G. Gompper, and R. Lipowsky, *Mobility and Elasticity of Self-Assembled Membranes.* Physical Letters Review, 1999. **82**(1): p. 221-224.

120. Lindahl, E. and O. Edholm, *Mesoscopic undulations and thickness fluctuations in lipid bilayers from molecular dynamics simulations.* Biophys J, 2000. **79**(1): p. 426-33.

121. Chiu, S.W., et al., *Structure of sphingomyelin bilayers: a simulation study.* Biophys J, 2003. **85**(6): p. 3624-35.

122. Harmandaris, V.A. and M. Deserno, *A novel method for measuring the bending rigidity of model lipid membranes by simulating tethers.* J Chem Phys, 2006. **125**(20): p. 204905.

123. Levine, Z.A., et al., *Determination of biomembrane bending moduli in fully atomistic simulations.* J Am Chem Soc, 2014. **136**(39): p. 13582-5.

124. Venable, R.M., F.L.H. Brown, and R.W. Pastor, *Mechanical properties of lipid bilayers from molecular dynamics simulation.* Chem Phys Lipids, 2015. **192**: p. 60-74.

125. Khelashvili, G., G. Pabst, and D. Harries, *Cholesterol orientation and tilt modulus in DMPC bilayers.* J Phys Chem B, 2010. **114**(22): p. 7524-34.

126. Khelashvili, G. and D. Harries, *How cholesterol tilt modulates the mechanical properties of saturated and unsaturated lipid membranes.* J Phys Chem B, 2013. **117**(8): p. 2411-21.

127. May, S., et al., *Tilt modulus of a lipid monolayer.* Eur Phys J E Soft Matter, 2004. **14**(3): p. 299-308.

128. Khelashvili, G., et al., *Molecular origins of bending rigidity in lipids with isolated and conjugated double bonds: the effect of cholesterol.* Chem Phys Lipids, 2014. **178**: p. 18-26.

129. Johner, N., D. Harries, and G. Khelashvili, *Implementation of a methodology for determining elastic properties of lipid assemblies from molecular dynamics simulations.* BMC Bioinformatics, 2016. **17**: p. 161.

130. Doktorova, M., D. Harries, and G. Khelashvili, *Determination of bending rigidity and tilt modulus of lipid membranes from real-space fluctuation analysis of molecular dynamics simulations.* Phys Chem Chem Phys, 2017. **19**(25): p. 16806-16818.

131. Braun, A.R. and J.N. Sachs, *Determining Structural and Mechanical Properties from Molecular Dynamics Simulations of Lipid Vesicles.* J Chem Theory Comput, 2014. **10**(9): p. 4160-4168.

132. Waheed, Q. and O. Edholm, *Undulation contributions to the area compressibility in lipid bilayer simulations.* Biophys J, 2009. **97**(10): p. 2754-60.

133. Doktorova, M., et al., *A New Computational Method for Membrane Compressibility: Bilayer Mechanical Thickness Revisited.* Biophys J, 2019. **116**(3): p. 487-502.

134. Kawamoto, S., et al., *A guiding potential method for evaluating the bending rigidity of tensionless lipid membranes from molecular simulation.* J Chem Phys, 2013. **139**(3): p. 034108.

135. Hu, M., J.J. Briguglio, and M. Deserno, *Determining the Gaussian curvature modulus of lipid membranes in simulations.* Biophys J, 2012. **102**(6): p. 1403-10.

136. Carrillo, J.Y., et al., *A Computational Approach for Modeling Neutron Scattering Data from Lipid Bilayers.* J Chem Theory Comput, 2017. **13**(2): p. 916-925.

Effects of electroformation protocol parameters on quality of homogeneous GUV populations

Dominik Drabik[a,*], Joanna Doskocz[a], Magda Przybyło[a,b]

[a] *Department of Biomedical Engineering, Faculty of Fundamental Technical Problems, Wrocław University of Science and Technology, 50-377 Wrocław, Pl. Grunwaldzki 13, Poland*
[b] *Lipid Systems sp z o.o., 54-613 Wrocław, ul Krzemieniecka 48C, Poland*

ARTICLE INFO

ABSTRACT

Giant unilamellar vesicles (GUVs) have become one of extensively studied biological bilayer models especially when investigating topological and mechanical properties of cell membranes. They are also used to visualize membrane-related phenomena. However, the method of preparation and the effects of parameters of preparation on the vesicular structure are extensively varied. Therefore, it is important to understand how the process of formation of GUVs influences the outcome population, as it can influence the outcome of the experiment that is planned. Therefore, in this study, we investigated the effects of protocol parameters of electroformation on properties of homogeneous population of POPC GUVs. The parameters investigated in this study are duration of electroformation, usage of electrodes and frequency of applied AC field and its voltage. The properties investigated, which can be used to describe GUV populations are average diameter of vesicle, the amount of lipid molecules in population, and structure of vesicles. According to our results, prolonged time (greater than 4 h) does not influence outcome; however, parameters of applied electrical field (voltage and frequency) did significantly influence the properties of obtained POPC GUV populations.

1. Introduction

Giant unilamellar vesicles (GUVs), lipid vesicles with diameter ranging from 5 to 50 μm, are the extensively studied membrane-related model system. Their size is similar to eukaryotic cells, which allows visualization of topological and mechanical properties of cell membranes by using light and fluorescence microscopy (Zupanc et al., 2014). Thus, they serve as a model system to mimic a freestanding lipid bilayer. Furthermore, due to their size, the curvature of lipid bilayer on molecular level is negligible (Kozlov, 2010; Yesylevskyy et al., 2014). GUVs have been widely used to study different aspects of lipid membranes such as fundamental membrane thermodynamics (Almeida et al., 2005), membrane curvature (Baumgart et al., 2014), membrane domains (Lipowsky and Dimova, 2003), fusion (Micheletto et al., 2016), lateral structure (Kubiak et al., 2011), and bending rigidity (Nagle et al., 2015). One of the primary advantages of using GUVs as model systems is the ability to precisely control molecular composition of the membranes as well as their environmental conditions. Furthermore, they allow to obtain parameters for each individual vesicles instead of averaged values obtained from large number of liposomes, as in case of large and small unilamellar vesicles.

There are several techniques used for the preparation of GUVs; however, the most common one, due to its convenience, is electroformation (Dimitrov and Angelova, 1988). In this method, lipid molecules dissolved in organic solvents, such as chloroform or methanol, were deposited on electrodes' surface. This is followed by drying of electrodes to obtain dry lipid film, which is then immersed in aqueous buffer and then, AC field is applied. As the principle behind the formation of GUVs is not well understood, several different protocols exist. Furthermore, to the best of our knowledge, there are no studies focusing on finding the most optimal protocol for GUV electroformation. The first and the most common procedure involves applying of 1.2 V AC field with 10 Hz frequency for up to 2 h (Angelova and Dimitrov, 2007; Herold et al., 2012; Loftus et al., 2013). But, the method of electroformation are commonly modified to vary the voltage, frequency, and duration. Several variations in the protocol have already been published. For instance, GUVs were electroformed for 1 h with 3 V and 10 Hz AC field (Henriksen and Ipsen, 2002), for 2 h with 2 V 5 Hz AC field (Esposito et al., 2007), and for 3 h with 1.1 V 20 Hz AC field (Pecreaux et al., 2004). Another modification of electroformation is to increase voltage during the process, such as 3 h electroformation with frequency of 500 Hz and stepped voltage increasing from 1 V up to 4 V

---

* Corresponding author.
  E-mail address: dominik.drabik@pwr.edu.pl (D. Drabik).

(Herold et al., 2012) and 24 h electroformation with frequency of 1 Hz and stepped voltage increasing from 1 V up to 4 V (Drabik et al., 2016), 2 h electroformation with 500 Hz and stepped voltage increasing from 0.15 V up to 3.9 V (Bouvrais et al., 2008), 4 h electroformation with 12 Hz and stepped voltage increasing each 5 min from 0.02 V to 1.1 V (Girard et al., 2004), or 5 h electroformation with 10 Hz and stepped voltage increasing in first 40 min from 0 up to 1.2 V (Mathivet et al., 1996). There are also a few more advanced protocols including changing frequency as well as voltage such as 1 h of electroformation in 1.1 V with 10 Hz frequency AC field followed by 2 h of 1.5 V and 5 Hz (Gracia et al., 2009), 3 h of 10 Hz and increasing continuously voltage from 20 V up to 350 V followed by 2 h of 10 Hz and 350 V AC field and completed with 2 h of 350 V with continuously decreasing frequency from 10 Hz down to 4 Hz (Pott et al., 2008), or 2 h of 10 Hz and 8 V, followed by 15 min of 5 Hz and 4 V, followed by 15 min of 2.5 Hz and 2.5 V and completed with 30 min of 1 Hz and 1 V AC field (Peterlin and Arrigler, 2007). Furthermore, changing electrode material (Morales-Penningston et al., 2010) and adsorption on lipid film (Tao and Yang, 2015) does significantly influence the outcome.

The purpose of this study was to investigate the effect of parameters of electroformation on quality of GUVs. The investigated parameters were duration of process, voltage, frequency of applied AC field and usage of electrodes on the following topological properties of the obtained vesicles: size of the vesicle, population of lipid molecules, and structure of the vesicle. Based on previously listed protocols, the duration of electroformation can vary from 0.5 h to 7 h. In rare cases, it can extend even up to 24 h, depending on the protocol used. Frequency can vary from 1 Hz to 12 Hz, and in rare cases, it can even go up to 500 Hz. Voltage usually varies from 2 mV to 5 V with different ways of increasing it during the process. In this article, we have investigated the effect of parameters on geometrical properties of vesicles as well as efficiency of the process itself. The size of investigated vesicles is crucial for experimental setup. Therefore, we analyzed the average size of vesicles by using both fluorescent microscopic images and flow cytometry. The amount of lipid film that is used in the process is considered, as it can affect the outcome. Therefore, we analyzed the amount of lipid molecules in GUV suspension, which corresponds to the efficiency of electroformation technique, by using both photometer- and fluorimeter-based methods. It allows to assess effect of protocol parameters on efficiency of the process by quantification of lipid molecules from lipid film used for GUV formation. In addition, the structure of the vesicles is assessed as a ratio of oligovesicular vesicles (OVVs)–vesicles similar in size to GUVs but containing smaller unilamellar vesicles within–to GUVs in electroformed population. The results of this study should help to optimize protocol parameters of GUV electroformation and should provide a starting point for the GUV-based research by answering some of the important questions that scientists might encounter.

2. Materials and methods

2.1. Materials

Lipid 1-palmitoyl-2-oleoyl-sn-*glycero*-3-phosphocholine (POPC) and fluorescent probes namely, NBD-PC (1-acyl-2-(6-[(7-nitro-2,1,3-benzoxadiazol-4-yl)amino]hexanoyl)-sn-*glycero*-3-phosphocholine) and Rhodamine PE (18:1 Liss Rhod PE 1,2-dioleoyl-sn-*glycero*-3-phosphoethanolamine-*N*-(lissamine rhodamine B sulfonyl) ammonium salt) were purchased from Avanti Polar Lipids (USA). Concentrations of fluorophores were determined using UV/Vis spectroscopy with excitation wavelength and the extinction coefficient obtained from the probe specification sheets. Polystyrene spheres were purchased from Polysciences (Germany). Ferric chloride and ammonium thiocyanate were purchased from VWR (USA). Triton X-100 was purchased from Amresco (USA). Sodium dithionite was purchased from Hadron Scientific (Poland). We used 18 MW deionized water in all our

experiments (PolWater, Poland).

2.2. Preparation of giant unilamellar vesicles (GUVs)

A modified electroformation method was used to model the formation of lipid membranes (Drabik et al., 2016). Briefly, 15 μl of POPC in chloroform (1 mM) was deposited in small quantities (as 2 μl droplets) onto platinum electrodes. Electrodes were set parallel to each other at a distance of 5 mm. The electrodes were kept for 1 h under reduced pressure to remove traces of organic solvents. Next, the electrodes were immersed in pure aqueous solution. Basic electroformation protocol consists of 4 h electroformation with 1 Hz AC electrical field applied in a PTFE (polytetrafluoroethylene) electroformation chamber (Lipid Systems, Poland) with the electrical field voltage set to 1 V for first hour, 2 V for second hour, 3 V for third hour, and finally 4 V for the remaining time of electroformation. However, depending on the protocol parameter under investigation, the aforementioned values were modified as described below. After electroformation, the chambers were left for 1 h without electrical field applied to allow descent of vesicles from electrodes. For a control sample, electrical field was not applied each time to one of the chambers.

2.3. Acquisition and assessment of microscopic images

Images were collected using Leica TCS SPE microscope equipped with 63×/1.30 ACS APO oil-immersion objective (Leica, Germany). We recorded 1392 × 1040 pixel images with Leica DFC310 FX camera using 0.102 μm pixel size. Samples were illuminated with fluorescence illuminator EL6000 and fluorescence emission was detected using appropriate cutoff filters. GUVs prepared for microscope were labeled with 1 mol% Rhodamine-PE fluorescent probe and electroformed in sucrose solution. After electroformation, glucose solution was externally added to make the vesicles fall in Z axis and to allow recording of all vesicles of different radii in one plane. Unlike within other microscopic studies, when recorded samples were being carefully selected, in our study, recorded images were consecutively collected over whole liposome population and then thoroughly analyzed (there were no lower limit in GUV size). Furthermore, at least 200 vesicles were considered, which provides greater insight into population parameters. Individual vesicles in recorded images were detected on collected images using discrete differential evolution optimization for circle detection approach (Cuevas et al., 2011).

2.4. Flow cytometry

BD FACS Calibur flow cytometer was used to study GUVs. Both forward scattering (FSC) and side scattering (SSC) values are correlated with the size of the vesicles (van der Pol et al., 2014) and therefore can be used as a mean to relatively assess radii of the vesicles. In the measurement the events were triggered by the light scattering of vesicles. The applied voltage for SSC was equal to 268 in logarithmic mode, and the applied voltage for FSC was set to E01 with 3.0 Amp Gain and linear mode. Each measurement took 3 min with 10,000 events finishing the measurement. Similar samples' measurements may differ depending on the status of the cytometer (Simonsen, 2016); therefore, polystyrene beads were measured and used as a correction factor for SSC and FSC values for each of the measurements of GUVs (this process has been described in detail in Supplementary information 2.2).

2.5. Lipid amount assessment

The amount was lipid in GUV suspension was measured using two methods: first, we used colorimetric method based on the formation of a complex between phospholipids and ammonium ferrothiocyanate (Charles and Stewart, 1980). The solution of GUV was kept under

pressure until complete evaporation of water, leaving behind only lipid film in the vial. This was followed by the addition of 1 ml chloroform to dissolve lipid. Next, we added 1 ml thiocyanate reagent dissolved in water. Samples were vortexed for 1 min and then the chloroform layer was removed using glass syringe. Subsequently, absorbance was measured at 488 nm using Nicolet evolution 100 spectrophotometer. Calibration curve was prepared before measuring samples of interest. In the second method, we measured the intensity of fluorescent probe in GUVs and used it to determine the amount of lipid molecules. This is because each of the suspension of GUVs is labeled with 2 m% of Rh-PE following the assumption that ratio of probe to lipid is constant throughout the whole population. But, GUVs are not uniform in shape; therefore, light scattering can be different. To this end, micellization process was used to obtain similarly sized particles. GUVs labeled with 2 m% of Rh-PE were treated with 10% triton-X solution. After 10 min, fluorescence intensity was measured using Fluoromax-4 Spectrofluorometer (Horriba, Japan). Then, the samples were read at an excitation wavelength of 560 nm and emission wavelength of 570–630 nm. The obtained spectra were then integrated to obtain total intensity values, which was next converted to the amount of lipid in suspension, based on calibration curve.

2.6. Oligovesicular vesicle fraction assessment

To determine the fraction of oligovesicular vesicles in the suspension of GUVs, we assessed the ratio between outer layer and inner layers of the vesicles. In this method, NBD-labeled bilayer was quenched using bilayer-impenetrable sodium dithionite resulting in significant drop in fluorescence intensity related to fraction of lipids located in the outer layer. Two approaches to the quenching of dithionite were used: (i) measurement of fluorescence intensity prior to and after quenching and (ii) recording initial quenching rate. In first case, GUV suspension fluorescence was measured using Fluoromax-4 Spectrofluorometer (Horriba, Japan) based on measurement protocol (Langner and Hui, 1993). Base sample was excited at 460 nm wavelength and emission was detected from 500 to 600 nm wavelength. This was followed by the addition of 50 µl of 1 M dithionite dissolved in 1 M Tris Base (pH = 11.21 ± 0.05). After 2 min, the intensity was measured again and relative drop in intensity was calculated as the fraction of lipids located in the outer membrane. In second case, initial rate of quenching of NBD was used as a mean to determine fraction of lipids in the outer layer. Initial rate, for dithionite impermeable membranes, is proportional to the amount of NBD-labeled lipids in the outer membrane (Angeletti and Nichols, 1998). In this instance, the higher the initial rate, the better the quality of obtained populations. The quenching kinetics were measured using stopped-flow instrument (BioLogic, Grenoble, France) in transmission configuration, equipped with a xenon–mercury lamp, a monochromator slit of 0.5 nm and quartz flow cuvette of 1.5 mm optical path length. The chamber was illuminated with wavelength of 436 nm, and a 475 nm long-pass filter was placed prior to the detector. Samples were mixed with injection speed of 4 ml/s and a total volume of 281 µl with 5:1 lipid:dithionite solutions ratio. Quenching of sample was recorded for 80 s with constant time step equal to 20 ms. The obtained quenching kinetics were fitted with monoexponential function. Initial rate was calculated by multiplying initial value with rate. Initial rate of quenching kinetics are correlated with ratio of lipids in outer and inner layers, especially in case of impenetrable dithionite in artificial lipid bilayers (Angeletti and Nichols, 1998).

2.7. Statistics

The results are presented as mean ± standard deviation calculated from different number of population sampling of GUVs. In case of quenching measurements using spectrofluorometer, the standard deviation was calculated from three independent populations. One-way

analysis of variance (ANOVA) was performed to determine the significance of difference between measurements from three independent measurements as well as the controls. While ANOVA provides information on whether the difference in data points is significant, it does not provide more details about difference between individual data points. Thus, a more detailed analysis (*ad hoc*) of significance of mean values was performed using Tukey test. Confidence level of $\alpha = 0.03$ ($p < 0.03$) for measurements was used in statistical tests. The calculations were performed using OriginLab OriginPro 9 software.

3. Results and discussion

3.1. The effect of electroformation duration on liposomes' size

In this study, we used two methods to investigate the effect of electroformation on the size of liposomes: fluorescence microscopy and flow cytometry. In fluorescence microscopy, 150 mOsm sucrose/glucose solution was added to induce the fall of liposomes on gravity, which enabled the observation of vesicles in the same plane. This concentration was selected as the lowest one that induced the proper descent of strong vesicles. Keeping the osmotic balance prevented the unattended vesicular rupture (Figs. S2–S4). At least 200 vesicles were measured for each sample to obtain viable statistical set. Final results are presented in Fig. 1 (detailed data in Figs. S5–S7). Control population had no AC voltage applied during the process. The average radius of each population set obtained from each of electroformation durations was not statistically different. Prior to measurements of GUVs using Flow Cytometry, polystyrene beads of diameters 1.5, 4.5, and 11 µm were used as the markers for optical correction described previously (see Section 2.2 and Fig. S9 in Supplementary information). Forward scattered light (FSC) was used to compare the sizes of GUVs. Final results are presented in Fig. 2 (for detailed information see Figs. S10-S11). The average FSC voltage corresponding to each of electroformation durations was not statistically different.

Both methods showed no relation between sizes of obtained vesicles and duration of electroformation. In both methods, there was difference between control samples and electroformed samples; however, the difference was less visible in case of flow cytometry. Furthermore, when electroformation was run for 24 h in flow cytometry experiment, control and electroformed samples overlapped. We can explain this phenomenon using two reasons. First, while FSC is correlated with sizes of recorded objects, the magnitude of scattering change can be small; therefore, even relatively large (for instance 2 µm) change in size can correspond to small change in voltage. This is not, however, the case in
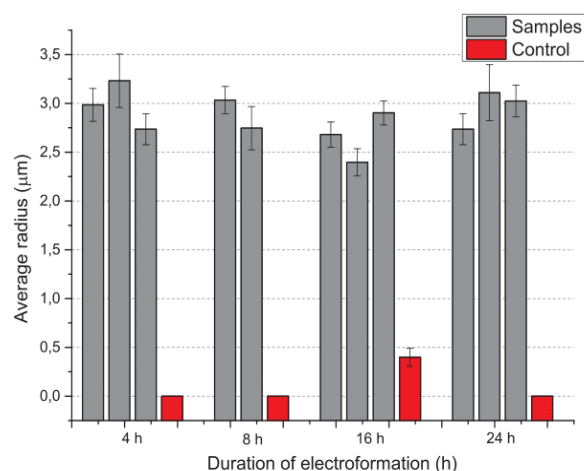
Fig. 1. Average radii of POPC GUVs as a function of electroformation duration obtained using fluorescent microscopy. Error bars represent uncertainty of Gaussian peak value fit. Average radii of vesicles are not statistically significant ($p < 0.03$). Control sample had no AC voltage applied at all.
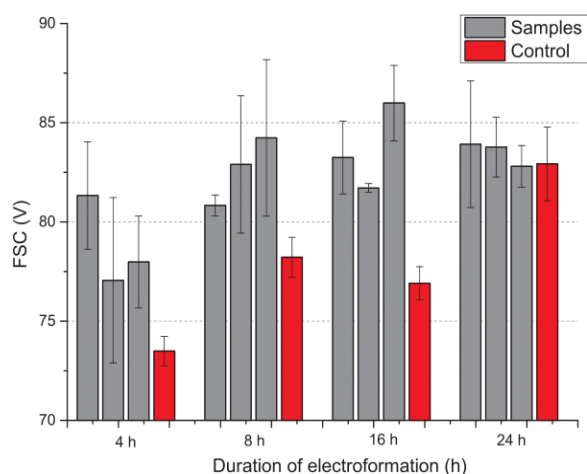
Fig. 2. Peak FSC value as a function of electroformation duration obtained by measuring POPC GUVs using flow cytometry. Error bars represent uncertainty of Gaussian peak value fit. FCS voltage between different durations of electroformation is not statistically significant ($p < 0.03$). Control sample had no AC voltage applied.
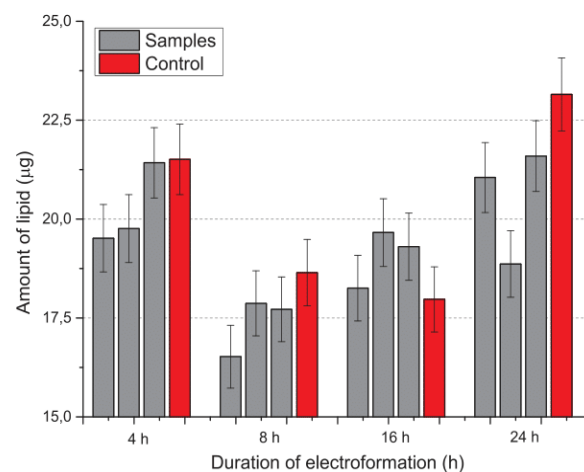

Fig. 4. The amount of lipid molecules in GUVs suspension in function of electroformation duration obtained using micellization method. Error bar represents uncertainty of linear fit from calibration curve (standard error). The amount of lipid molecules in different duration of electroformation was not statistically significant ($p < 0.03$). Control sample had no AC voltage applied.

microscopic studies. Second, small vesicles can aggregate and therefore be treated as bigger ones during cytometer measurement, since similar effect has been observed in case of polystyrene beads. This is again not the case in microscopic studies where each of the recorded GUV is being verified prior to analysis. The increase in duration of electroformation did not affect size of the vesicles. Consequently prolonged duration (longer than 4 h) of electroformation cannot be considered as a factor influencing the quality of obtained vesicles.

3.2. The effect of electroformation duration on process efficiency

In this study, we used two methods to investigate the effect of duration of electroformation on its efficiency in GUVs population: classical colorimetric method and fluorescence intensity method combined with micellization. In this instance, efficiency of electroformation is understood as the amount of lipid molecules which is present in GUV solution, related to the amount of lipid molecules in primary lipid film deposited on electrodes. Fig. 3 presents the results of colorimetric test. The calibration curve is presented in Fig. S12 along with individual absorbance spectra (Figs. S13-S14). According to our results, the average amount of lipid molecules of GUV population obtained from each of electroformation durations was statistically different. However
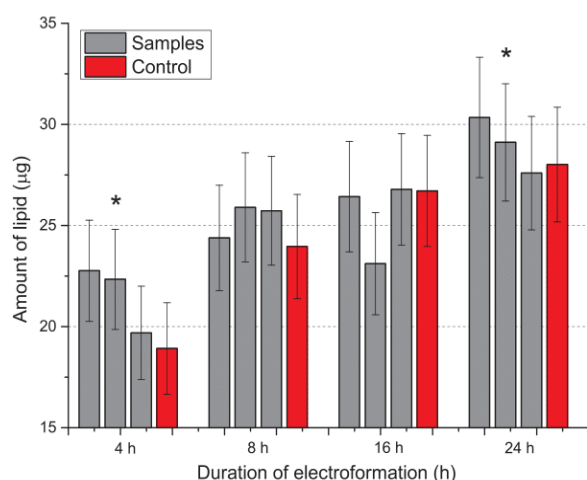
Fig. 3. Amount of lipid in suspension of GUVs as a function of electroformation duration obtained using colorimetric method. Error bars represent uncertainty of linear fit from calibration curve (standard error). Only the amounts obtained between 4 h and 24 h of electroformation were statistically significant (marked by *). Control sample had no AC voltage applied.

further comparison of means using Tukey test showed that there was a statistical difference only between the amounts obtained from 4 h and 24 h of electroformation. The test did not take into account uncertainties resulting from the experiment, which might have resulted in much lower uncertainties of investigated time points than expected and therefore overestimation of significance.

Fig. 4 presents the results of fluorescence analysis. The calibration curve is presented in Fig. S15 as well as the fluorescence spectra for individual durations of electroformation (Figs. S16-S17). According to our results, the average amount of lipid molecules for a given population obtained from each of electroformation durations was not statistically different.

With respect to the results obtained from fluorescence and colorimetric analysis, it can be stated that both methods show no correlation between the amount of lipid molecules in GUVs suspension and duration of electroformation. This suggest that after 4 h, at least 95% of the lipid molecules have already been used to form GUVs and further electroformation does not alter the amount of lipid molecules used in GUV formation significantly. Furthermore, there was no difference between control samples and measurement samples. This shows that electroformation is not a process which increase the amount of lipid used for GUVs formation, but rather to increase their diameters. While there is no dependency between the amount of lipid molecules on duration of electroformation, other factors have been observed to influence the outcome, such as the state and surface roughness of electrodes (Herold et al., 2012). This is especially visible in fluorescence method where order of measurement was 24, 4, 16, and 8 h one after the other.

3.3. The effect of duration of electroformation on structure of liposome

To investigate the effect of duration of electroformation on structure of liposomes, we performed two selected quenching analysis, differing slightly between them in approach. After electroformation, two types of vesicles can be observed: (i) GUVs and (ii) OVVs. The size of OVVs is similar to GUVs, but they contain smaller vesicles inside them. The structure of liposome can be expressed as a ratio of lipid molecules in outer and inner membranes of a lipid bilayer. However, if additional smaller vesicles are located inside, the ratio will be different. This can serve as an indicator of fraction of OVVs in GUVs population. Fig. 5 presents the results of assessment using fluorimeter and the recorded quenching. First, we successfully tested whether quenching of NBD-PE reflects parameter in question (Supplementary information Section 5.1
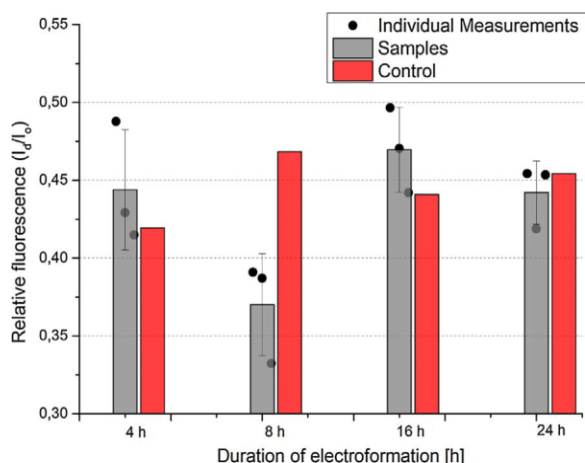
Fig. 5. Ratio of recorded intensity of fluorescence after addition of dithionite (I_d) to fluorescence before addition (I_o) as a function of electroformation duration. Error bar represents standard deviation from individual results. Relative fluorescence values were not statistically significant ($p < 0.03$). Control sample had no AC voltage applied.

and Fig. S18). This was followed by investigation of GUVs population obtained after different duration of electroformation process. Individual spectra are presented in Figs. S19 and S20 . Relative fluorescence is calculated as the ratio between fluorescence intensity after and prior to dithionite addition. According to our results, the relative values of fluorescence were not statistically different in function of electroformation duration.

In the second experimental approach to dithionite quenching, kinetics of the process itself were used as an indicator of ratio of outer and inner layers. Initial rate parameter is, for dithionite-impenetrable membranes, proportional to the amount of NBD-labeled lipids in the outer membrane. The greater the initial rate, the fewer lipid vesicles are enclosed in vesicles. Fig. 6 presents the obtained initial rates of GUVs, which electroformation duration was performed for investigated time intervals. Prior to the evaluation of GUVs, the measurement setup was tested on LUV and MLV populations (Fig. S21). Individual kinetics of the investigated GUV population are presented in Fig. S22. According to the results, the average initial rates recorded for GUVs with different electroformation duration were not statistically different. Both methods showed no correlation between the ratio of lipid quantity in inner/outer membrane and duration of electroformation. This ratio correlates with number of vesicles inside other vesicles for dithionite-impenetrable
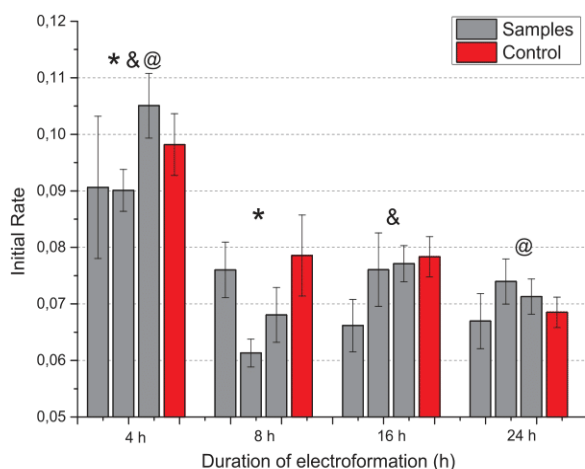
membranes. Presence of vesicles inside other vesicles is an unfavorable situation for analysis. Furthermore, there was no difference between control samples and samples of interest. Only initial rate measurement in case of 4 h outlines itself. However, it has to be emphasized that this measurement was performed first, which means that the electrodes were least damaged from all initial rate measurements. In addition, the results suggest that enhanced electroformation duration do not influence structure of the vesicles and cannot be considered as a factor influencing the structure of obtained vesicles.

3.4. The effect of electroformation current frequency on formation of liposomes

Apart from the most time-consuming protocol parameter–duration of electroformation–two protocol parameters of this process can be easily adjusted. Frequency of applied AC voltage was verified first. Difference between investigated parameters of GUVs populations are presented in Fig. 7, with electroformation time fixed to 4 h. Using One-way ANOVA, we found that the average radii of liposomes' population obtained from each of tested frequencies were statistically different. Furthermore, ad hoc Tukey test confirmed that the statistical difference is present between each of investigated frequencies. In case of the amount of lipid molecules, ANOVA test showed that means were statistically different to the point that the state of the electrodes should not influence the outcome. Ad hoc test confirmed statistical difference both between 10/1 Hz and 100/1 Hz, however, there were no statistical difference between 100 and 10 Hz. Finally, in case of vesicle topology, ANOVA test showed that the values were statistically different. However, *ad hoc* Tukey test clarified that significance in difference is only present in case of 100 Hz and 1 Hz populations. This shows that setting AC frequency to 1 Hz yielded bigger vesicles with higher use of lipid material deposited on electrodes. In case of vesicle topology, the difference between 1 Hz and 10 Hz was not statistically significant suggesting that such small deviation may not cause additional formation of small vesicles inside GUVs. However, greater increase in frequency changed the quantity of lipid inside vesicles. To sum up, the results suggest that the use of 1 Hz frequency is preferable for AC electric field applied in electroformation process (Fig. 8).

3.5. The effect of electroformation voltage increment on formation of liposomes

Voltage is the last easily adjustable parameter that is set when using electroformation technique to obtain GUVs. However, two ways of modifying the voltage are possible: first is by changing the values of voltage itself; however, as stated in Introduction section, most of the electroformation protocols use 1–4 V. In our opinion, a more interesting factor is whether the increase of voltage during the process influences the outcome population. Thus, we electroformed populations in two distinct ways: once with stepped voltage increase each hour from 1 V up to 4 V by 1 V and second with constant 2.5 V over all 4 h of electroformation, which is an average voltage applied in first case. One-way ANOVA revealed that the average radii of liposomes population obtained from these two approaches were statistically different. This was confirmed by Tukey test. The results were not found to be significantly different in case of amount of lipid molecules and initial rate (confirmed using both ANOVA and ad hoc Tukey tests). This suggests that changes in voltage preferentially influence the size of vesicles but not the efficiency of electroformation process and/or vesicles topology.

3.6. The effect of state of electrodes on formation of liposomes

State and surface roughness of electrodes is pointed out as a crucial factor influencing the quality of obtained GUVs populations. It has been reported that when using ITO-coated coverslips as electrodes the maximal radius of vesicles decreased from initial 100 um–25 um in fifth

Fig. 6. Initial rate obtained for GUV populations quenched with dithionite in function of electroformation duration. Error bar represents standard deviation from individual results. Initial rates for 4 h electroformation duration were statistically significant from other durations (marked as *,& and @, $p < 0.03$). Control sample had no AC voltage applied.
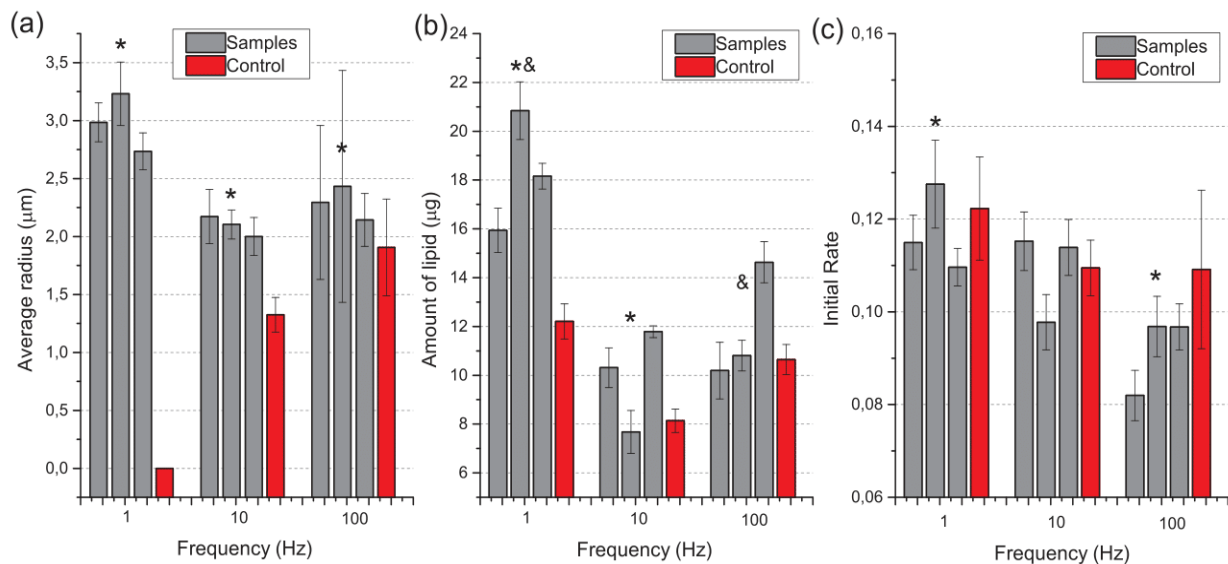
Fig. 7. (a) Average radius, (b) amount of lipid and (c) initial rates obtained for GUV populations as a function of frequency of applied AC voltage during 4 h of electroformation. Error bars are calculated as stated in Sections 3.1–3.3. Control sample had no AC voltage applied. Symbols * and & mark statistical significance ($p < 0.03$).

electroformation on the same electrodes (Herold et al., 2012). To this end we have investigated the changes in GUVs population electroformed from newly-bought electrodes. The results were summarized with GUVs population obtained from electrodes on their fifteenth use. Difference in investigated parameters is presented in Fig. 9. One-way ANOVA revealed that average radius of liposome was not statistically different with each subsequent use of electrodes. This results is somewhat contradicted to those stated by Herold et al. (2012). However two factors are different. Material, of which electrodes are made, is platinum, contrary to ITO used in mentioned publication. This might make the electrodes less susceptible to defects and alternations of electrode's surface. Furthermore there was no lower limit of sizes applied when taking vesicles into statistics. This makes the whole population's statistic less sensitive to changes at its edges. There was also no statistical significance in amount of lipid used for electroformation, as calculated using one-way ANOVA. The most striking change was observed in initial rate values. One-way ANOVA showed that initial rate values are statistically significant. Ad-hoc Tukey test showed, that initial rate obtained from both fifth and fifteenth use of electrodes was statistically

significant from other populations. Furthermore initial rates from both third and fourth use were statistically significant from first use. This results show that the topology of GUVs vesicles is most sensitive parameter to state of electrode's surface. A slight change in electrode's topology, not even changing significantly average radius, can change the hollowness of vesicles in electroformed population. These results suggest that if in obtained GUVs population majority of vesicles are filled with other lipid structures one should either buy new electrodes or anneal the current ones.

4. Conclusion

In this study, we investigated the effect of prolonged (more than 4 h) duration of electroformation, frequency of applied AC field, state of electrodes used in the process and the effect of increase in voltage during the process of electroformation on geometrical parameters of GUV population. Specifically, we investigated the average size of the vesicles, quantity of lipid molecules used to form the GUV population, and fraction of OVVs in GUV population. Using both flow cytometry
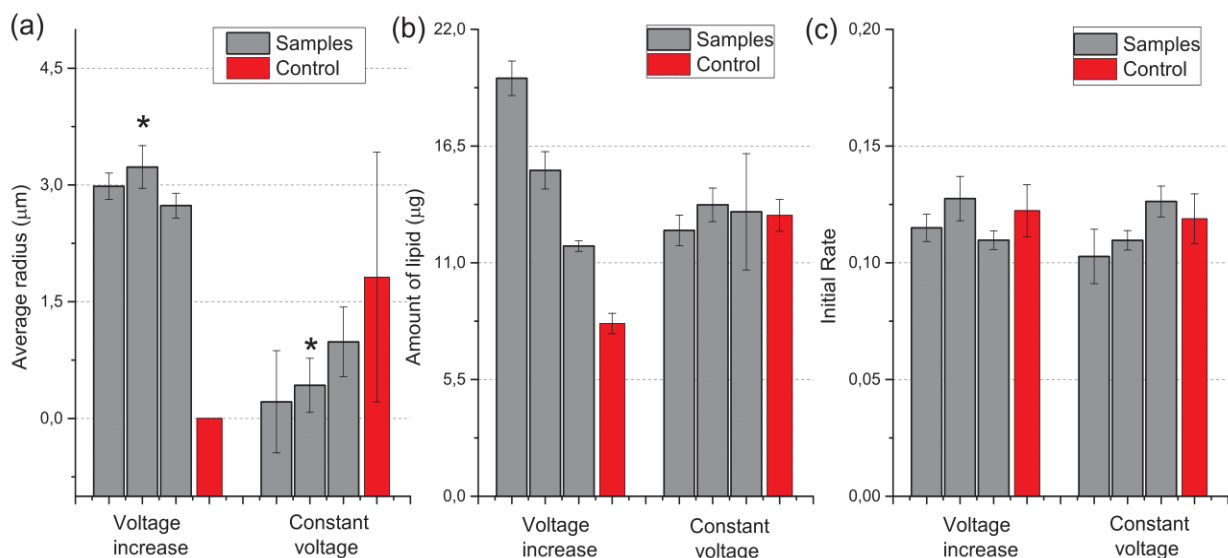
Fig. 8. (a) Average radius, (b) amount of lipid and (c) initial rates obtained for GUV populations after 4 h electroformation with voltage increase from 1 V to 4 V (described in figure as "voltage increase") or with constant 2.5 V (described as "constant voltage"). Error bars are calculated as stated in Sections 3.1–3.3. Control sample had no AC voltage applied. Symbol * marks statistical significance.
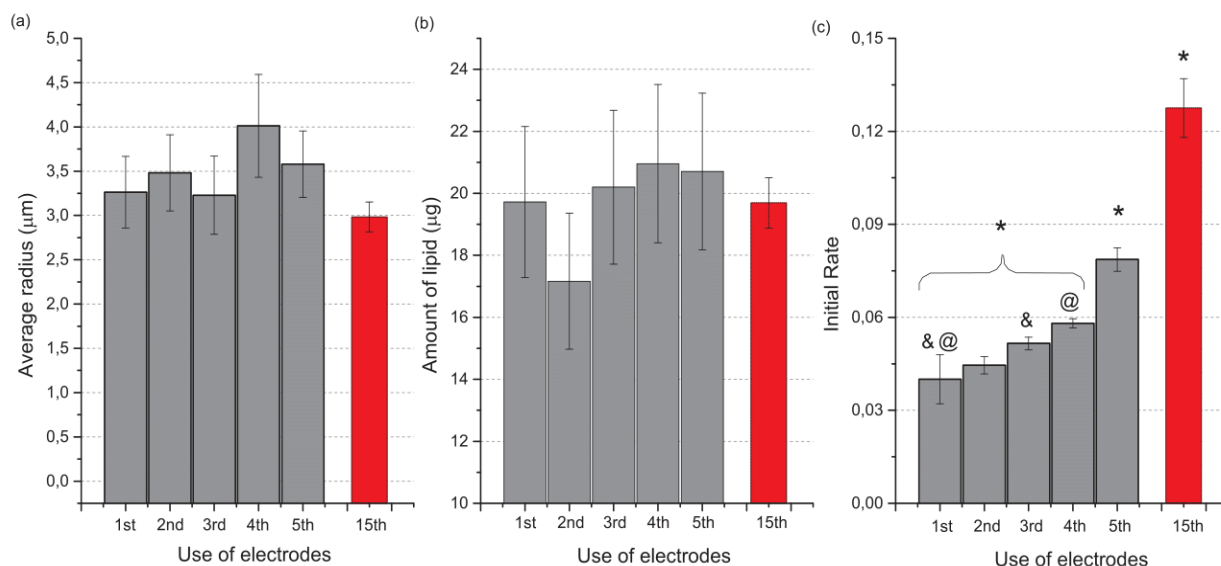
Fig. 9. (a) Average radius, (b) amount of lipid and (c) initial rates obtained for GUV populations after 4 h electroformation with voltage increase from 1 V to 4 V in function of electrode use. Error bars are calculated as stated in Sections 3.1–3.3. The results were summarized with previous results after fifteenth electrode use (red bars). Symbols *, &, @ mark statistical significance. (For interpretation of the references to colour in this figure legend, the reader is referred to the web version of this article.)

and fluorescence microscopy, we showed no significant difference in diameter of obtained vesicles for prolonged duration of formation. Using colorimetric- and fluorescence-based approaches, we showed that there was no significant difference in the amount of lipid between investigated samples (also with reference to the control samples). Furthermore, we performed two different approaches on NBD-PE quenching using dithionite, and the results showed that the ratio of lipids in the outer and inner membrane remains unchanged when electroformation was performed for longer than 4 h, even in control samples. This confirms that duration does not influence fraction of OVVs in GUV population. Using selected three of the previous methods–fluorescence microscopy, colorimetric method, and NBD-PE quenching in stopped-flow instrument–we showed the effect of another two protocol parameters on GUVs population over chosen 4 h of electroformation. According to our results, the use of 1 Hz frequency resulted in bigger vesicles and with slightly smaller fraction of OVVs in population. Furthermore, the usage of lipid material on electrodes was higher when 1 Hz AC voltage frequency was applied. We have also showed that increasing the voltage during whole process of electroformation, instead of applying constant and predefined voltage value, increased the size of the vesicles, but did not influence the forming efficiency or the fraction of OVVs in population. The study of usage of electrodes on parameters of GUVs population showed that fraction of OVVs increases with each usage of electrodes. These results show that electroformation is a complex process, which is more influenced by parameters of applied electrical field (both voltage and frequency) and the state of electrode's surface used in the formation rather than the time of process itself. Changing the duration of electroformation did not change any of the investigated parameters significantly. Furthermore, it is noteworthy that additional factors influencing the parameters can be present, which was not taken into account in this study. Such factors are related to construction of electroformation chamber, for instance the distance between the electrodes or area of active surface of electrodes, or the type of electrode material. We hope that this work will provide valuable information about the process of electroformation and will increase the speed of formation of GUVs when deciding on the duration of the process itself.

Acknowledgements

Appendix A. Supplementary data

References

Almeida, P.F.F., Pokorny, A., Hinderliter, A., 2005. Thermodynamics of membrane domains. Biochim. Biophys. Acta 1720, 1–13.
Angeletti, C., Nichols, J.W., 1998. Dithionite quenching rate measurement of the inside-outside membrane bilayer distribution of 7-nitrobenz-2-oxa-1,3-diazol-4-yl-labeled phospholipids. Biochemistry 37, 15114–15119.
Angelova, M., Dimitrov, D.S., 2007. A mechanism of liposome electroformation. Trends Colloid Interface Sci. II 76, 59–67.
Baumgart, T., et al., 2014. Thermodynamics and mechanics of membrane curvature generation and sensing by proteins and lipids. Annu. Rev. Phys. Chem. 62, 483–506.
Bouvrais, H., et al., 2008. Softening of POPC membranes by magainin. Biophys. Chem. 137, 7–12.
Charles, J., Stewart, M., 1980. Colorimetric determination of phospholipids with ammonium ferrothiocyanate. Anal. Biochem. 104, 10–14.
Cuevas, E., et al., 2011. Circle detection using discrete differential evolution optimization. Pattern Anal. Appl. 14 (1), 93–107.
Dimitrov, D.S., Angelova, M., 1988. Lipid swelling and liposome formation mediated by electric fields. J. Electroanal. Chem. Interfacial Electrochem. 253 (2), 323–336.
Drabik, D., et al., 2016. The modified fluorescence based vesicle fluctuation spectroscopy technique for determination of lipid bilayer bending properties. Biochim. et Biophys. Acta (BBA)–Biomembr. 1858 (2), 244–252.
Esposito, C., et al., 2007. Flicker spectroscopy of thermal lipid bilayer domain boundary fluctuations. Biophys. J. 93, 3169–3181.
Girard, P., et al., 2004. A new method for the reconstitution of membrane proteins into giant unilamellar vesicles. Biophys. J. 87, 419–429.
Gracia, R.S., et al., 2009. Effect of cholesterol on the rigidity of saturated and unsaturated membranes: fluctuation and electrodeformation analysis of giant vesicles. Soft Matter 6, 1472–1482.
Henriksen, J.R., Ipsen, J.H., 2002. Thermal undulations of quasi-spherical vesicles stabilized by gravity. Eur. Phys. J. E 9, 365–374.
Herold, C., et al., 2012. Efficient electroformation of supergiant unilamellar vesicles containing cationic lipids on ITO-coated electrodes. Langmuir 28, 5518–5521.
Kozlov, M.M., 2010. Biophysics: joint effort bends membrane. Nature 463, 439–440.
Kubiak, J., et al., 2011. Lipid lateral organization on giant unilamellar vesicles containing lipopolysaccharides. Biophys. J. 100 (4), 978–986.
Langner, M., Hui, S.W., 1993. Dithionite penetration through phospholipid bilayers as a measure of defects in lipid molecular packing. Chem. Phys. Lipids 65, 23–30.
Lipowsky, R., Dimova, R., 2003. Domains in membranes and vesicles. J. Phys.: Condens. Matter 15 (S31–S45), S31.
Loftus, A.F., et al., 2013. Robust measurement of membrane bending moduli using light sheet fluorescence imaging of vesicle fluctuations. Langmuir 29 (14), 588–594.
Mathivet, L., Cribier, S., Devaux, F., 1996. Shape change and physical properties of giant phospholipid vesicles prepared in the presence of an AC electric field. Biophys. J. 70,

1112–1121.

Micheletto, Y.M.S., et al., 2016. Electroformation of giant untilamellar vesicles: investigating vesicle fusion versus bulge merging. Langmuir 32 (32), 8123–8130.

Morales-Penningston, N.F., et al., 2010. GUV preparation and imaging: minimizing artifacts. Biochim. Biophys. Acta 1798 (7), 1324–1332.

Nagle, J.F., Jablin, M.S., Tristram-Nagle, S., 2015. Sugar does not affect the bending and tilt moduli of simple lipid bilayers. Chem. Phys. Lipids 196, 76–80.

Pecreaux, J., et al., 2004. Refined contour analysis of giant unilamellar vesicles. Eur. Phys. J. E 13, 277–290.

Peterlin, P., Arrigler, V., 2007. Electroformation in a flow chamber with solution exchange as a means of preparation of flaccid giant vesicles. Colloids Surf. B 64, 77–87.

Pott, T., Bouvrais, H., Meleard, P., 2008. Giant unilamellar vesicle formation under physiologically relevant conditions. Chem. Phys. Lipids 154, 115–119.

Simonsen, J., 2016. A liposome-based size calibration method for measuring microvesicles by flow cytometry. J. Thromb. Haemost. 14, 186–190.

Tao, F., Yang, P., 2015. Ca-mediated electroformation of cell-sized lipid vesicles. Sci. Rep. 5, p9839.

Yesylevskyy, S.O., Kraszewski, S., Ramseyer, C., 2014. Determination of the shape and curvature of nonplanar lipid bilayers that are bent in a single plane in molecular dynamics simulations. J. Mol. Model. 20 (4), 2176.

Zupanc, J., et al., 2014. Lipid vesicle shape analysis from populations using light video microscopy and computer vision. PLoS One 9 (11), pe113405.

van der Pol, E., et al., 2014. Particle size distribution of exosomes and microvesicles determined by transmission electron microscopy, flow cytometry, nanoparticle tracking analysis, and resistive pulse sensing. J. Thromb. Haemost. 12 (7), 1182–1192.

Supplementary Information : Effects of electroformation protocol parameters on quality of homogeneous GUV populations

Dominik Drabik,[a] Joanna Doskocz,[a] and Magda Przybyło[a,b]

[a] Department of Biomedical Engineering, Faculty of Fundamental Technical Problems, Wrocław University of Science and Technology, 50-377 Wrocław, Pl. Grunwaldzki 13, Poland.
[b] Lipid Systems sp z o.o., 54-613 Wrocław, ul Krzemieniecka 48C, Poland

ABSTRACT : Giant unilamellar vesicles (GUVs) have become one of extensively studied biological bilayer models especially when investigating topological and mechanical properties of cell membranes. They are also used to visualize membrane-related phenomena. However, the method of preparation and the effects of parameters of preparation on the vesicular structure are extensively varied. Therefore, it is important to understand how the process of formation of GUVs influences the outcome population, as it can influence the outcome of the experiment that is planned. Therefore, in this study, we investigated the effects of protocol parameters of electroformation on properties of homogeneous population of POPC GUVs. The parameters investigated in this study are duration of electroformation, usage of electrodes and frequency of applied AC field and its voltage. The properties investigated, which can be used to describe GUV populations are average diameter of vesicle, the amount of lipid molecules in population, and structure of vesicles. According to our results, prolonged time (greater than 4 h) does not influence outcome; however, parameters of applied electrical field (voltage and frequency) did significantly influence the properties of obtained POPC GUV populations.

1. Microscopy

1.1. Vesicle detection using DDEO

Recorded images were analyzed using discrete differential evolution optimization (DDEO) for circle detection. This approach is described in details elsewhere [1]. In figure S1 the result of such analysis is presented along with recorded image.
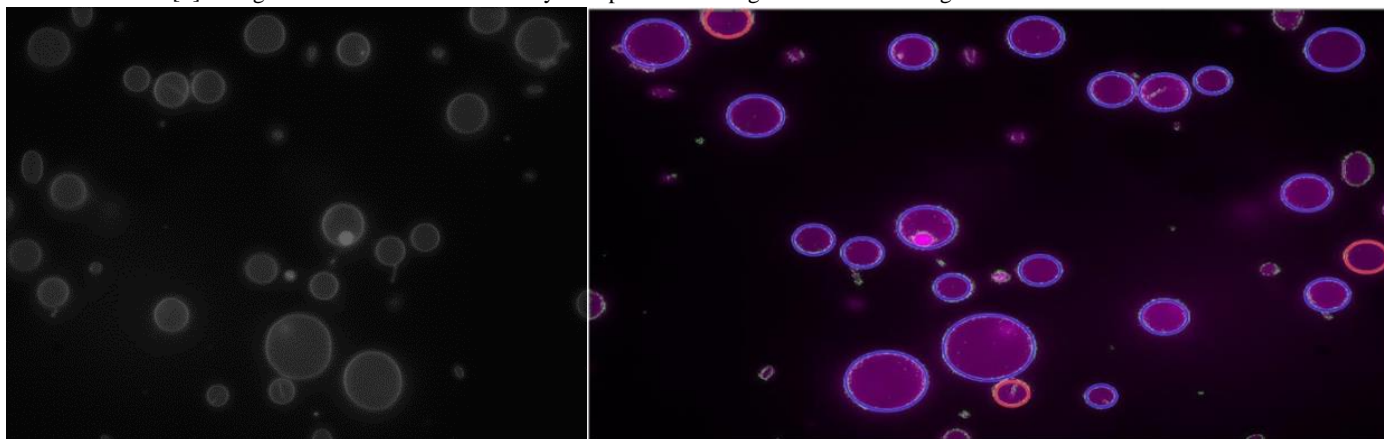
Figure S1. (Left) Recorded POPC vesicles in 150mOsm sucrose/glucose solution, (Right) result of analysis using DDEO for circle detection. Blue circles represent very good accuracy in circle detection while red ones slightly worse (due to absence of part of vesicles or noise).

1.2. Sugar concentration

In order to be able to observe whole population of vesicles in one plane appropriate concentration of sucrose/glucose had to been applied. The presence of sucrose inside vesicles and sucrose/glucose mixture outside vesicles cause gravity effect making larger vesicles descent [2]. Three sugar concentrations have been tested – 75mOsm, 150mOsm and 300mOsm (which translates directly to 75mM, 150mM and 300mM respectively). Results suggest that 75mOsm sugar concentration was too small to cause descent of larger vesicles while both 150 mOsm and 300 mOsm are similar in recorded sizes. To this end 150 mOsm was selected in order to prevent any possible ruptures of vesicles due to high pressure.
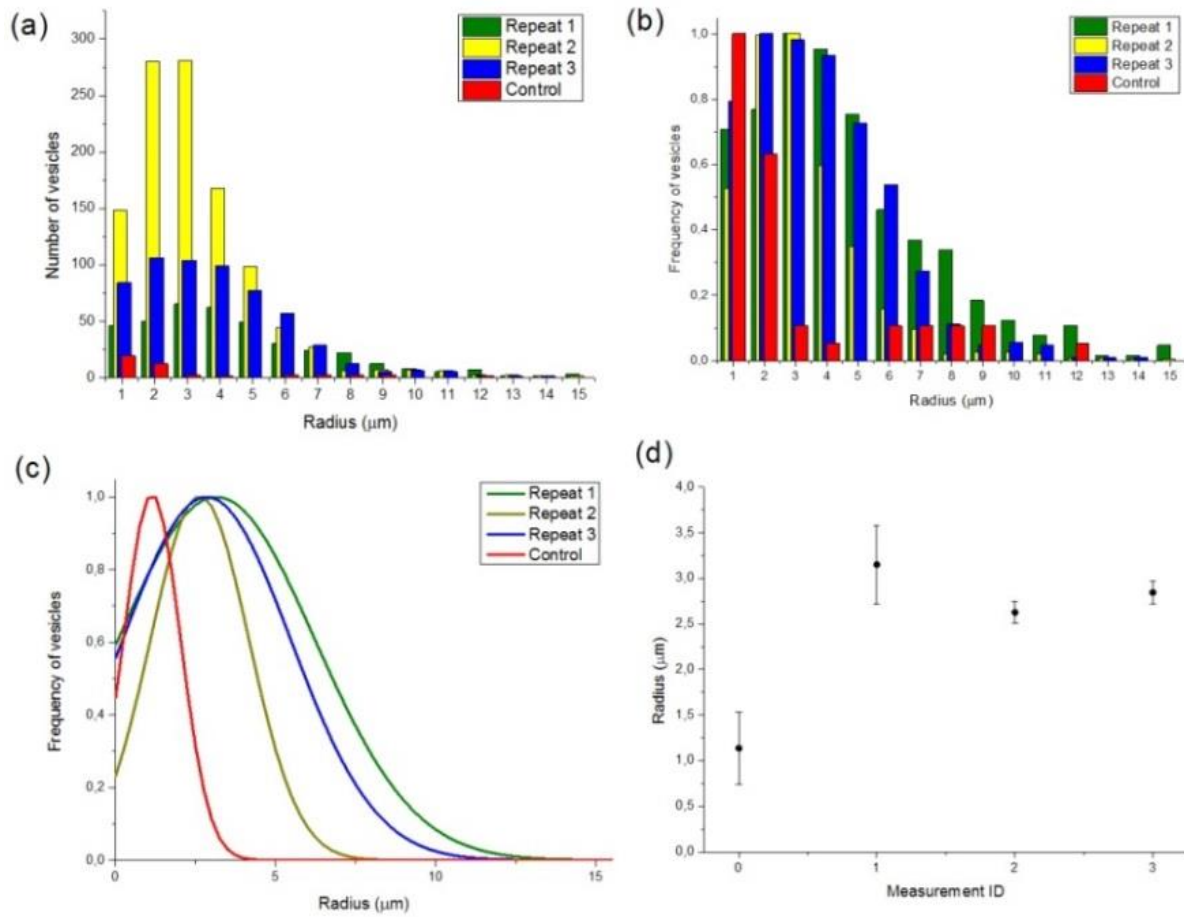
Figure S2. Vesicles formed in 75mOsm for 24h. Panels (a) and (b) represents number of vesicles and frequency of vesicles at given radius size bin, panel (c) represents Gauss fit and panel (d) represents average radii of vesicles with Measurement ID=0 being control.
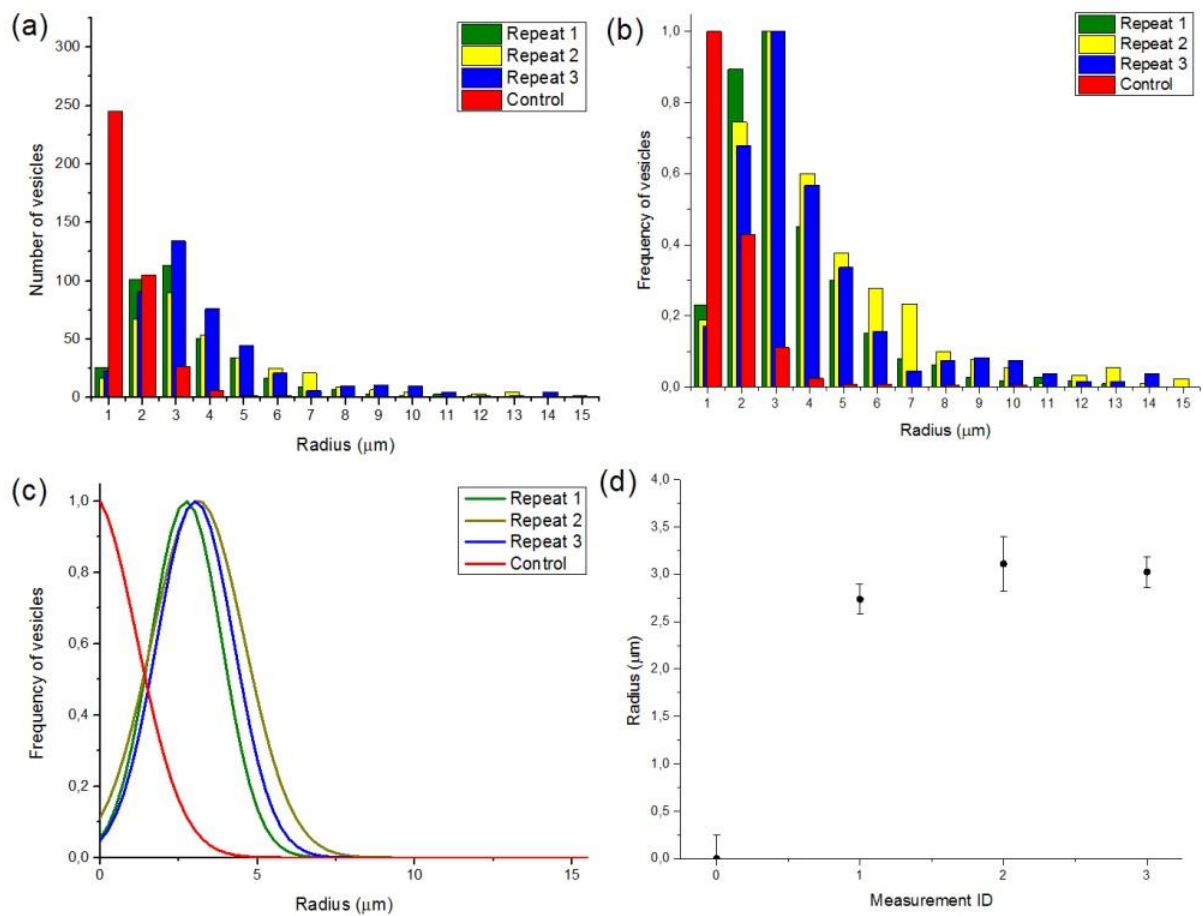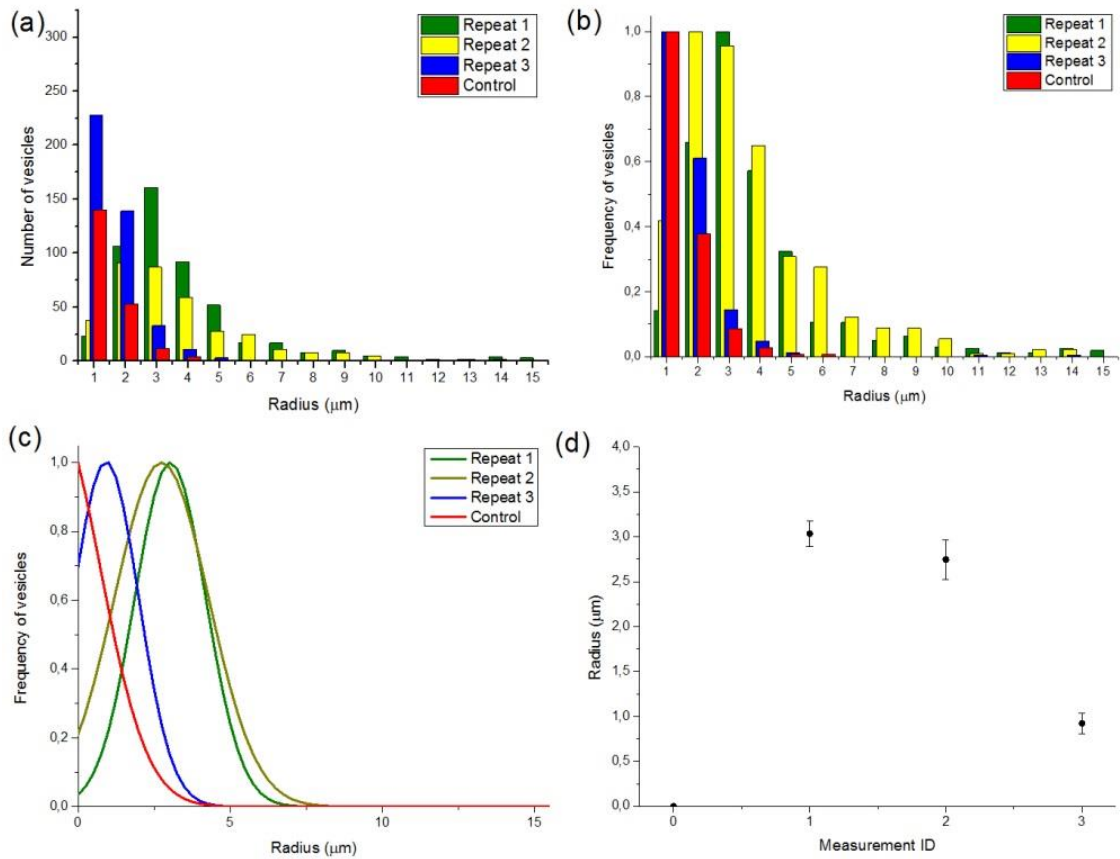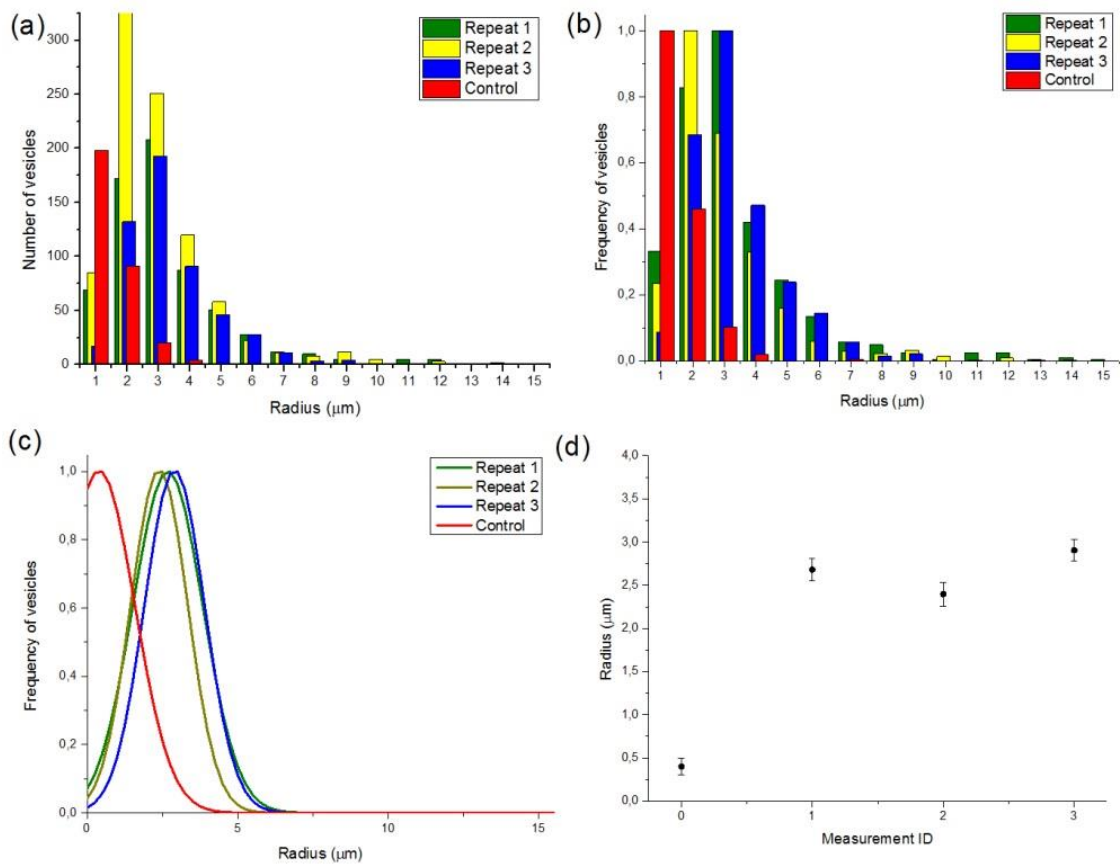

Figure S3. Vesicles formed in 150mOsm for 24h. Panels (a) and (b) represents number of vesicles and frequency of vesicles at given radius size bin, panel (c) represents Gauss fit and panel (d) represents average radii of vesicles with Measurement ID=0 being control.
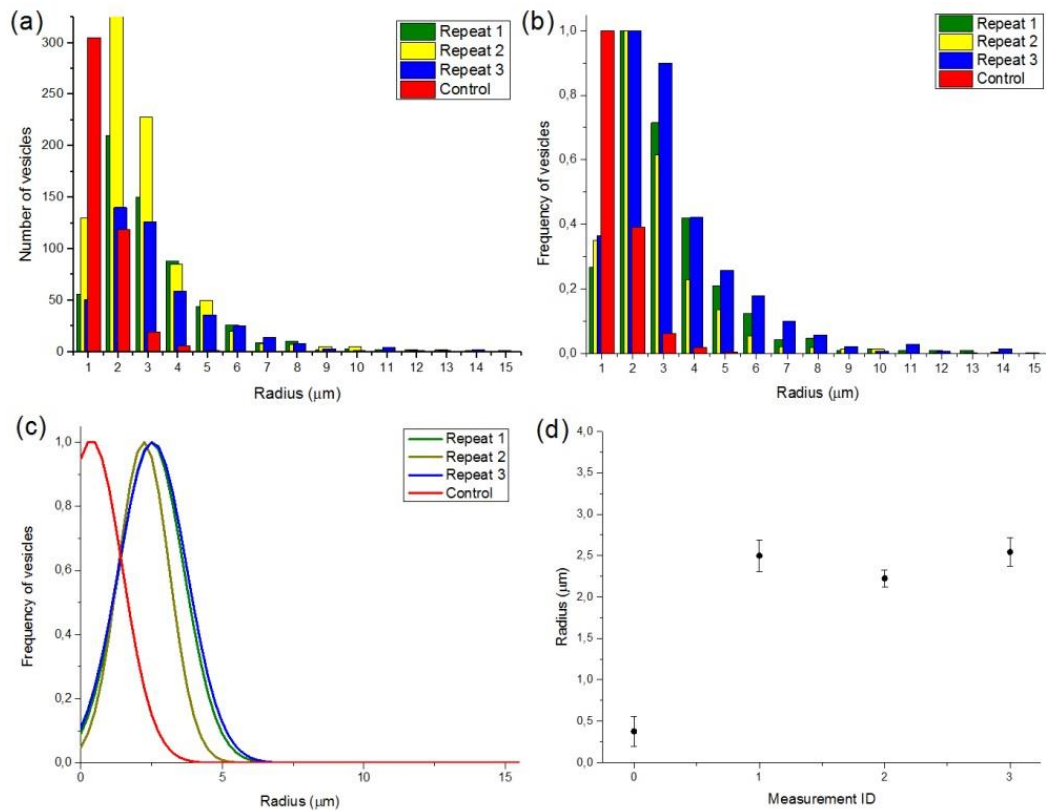
Figure S4. Vesicles formed in 300mOsm for 24h. Panels (a) and (b) represents number of vesicles and frequency of vesicles at given radius size bin, panel (c) represents Gauss fit and panel (d) represents average radii of vesicles with Measurement ID=0 being control.

1.3. Individual results for each duration of electroformation

For statistical purposes in each measurement at least 200 vesicles were recorded. Below are presented individual results for 4 h, 8 h and 16 h of investigated electroformation duration, while 24 h electroformation is presented in Figure S3. Control is understood as a sample with electrodes immersed in water solution for same time but with no AC applied. In repeat 3 in 8h clearly there was a fault during electroformation.
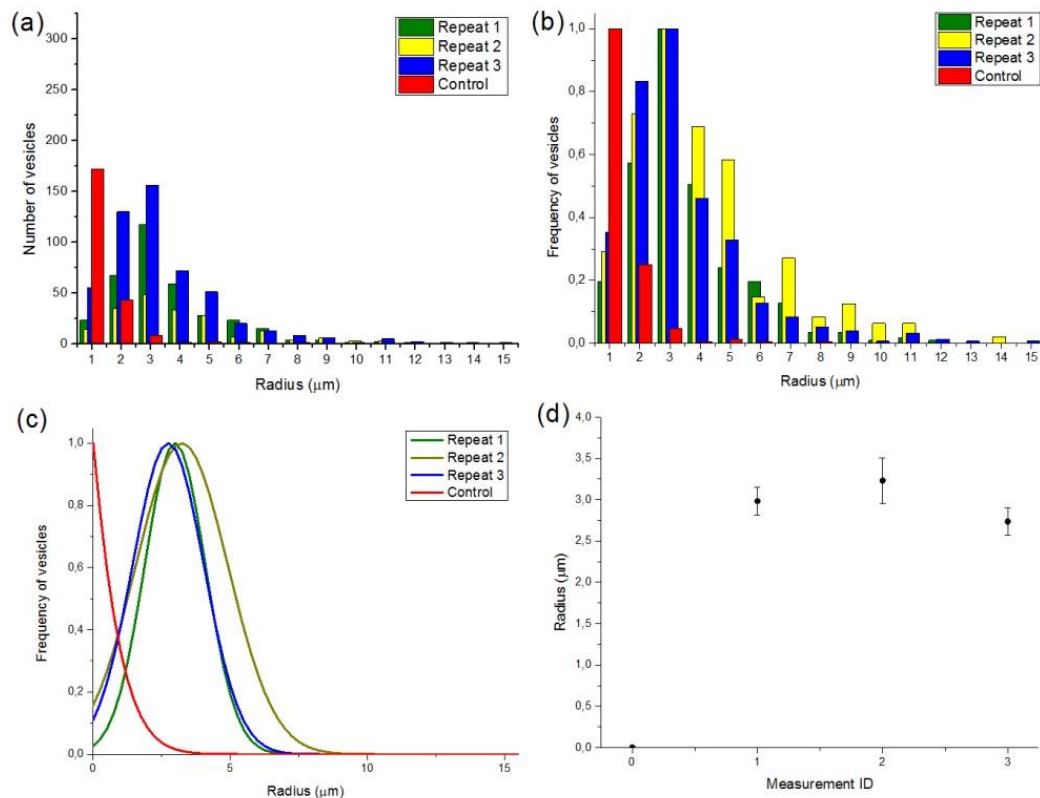
Figure S5. Vesicle sizes obtained in populations electroformed for 4h in 150mOsm sucrose/glucose solution. Panels (a) and (b) represents number of vesicles and frequency of vesicles at given radius size bin, panel (c) represents Gauss fit and panel (d) represents average radii of vesicles with Measurement ID=0 being control.

Figure S6. Vesicle sizes obtained in populations electroformed for 8h in 150mOsm sucrose/glucose solution. Panels (a) and (b) represents number of vesicles and frequency of vesicles at given radius size bin, panel (c) represents Gauss fit and panel (d) represents average radii of vesicles with Measurement ID=0 being control.

Figure S7. Vesicle sizes obtained in populations electroformed for 16h in 150mOsm sucrose/glucose solution. Panels (a) and (b) represents number of vesicles and frequency of vesicles at given radius size bin, panel (c) represents Gauss fit and panel (d) represents average radii of vesicles with Measurement ID=0 being control.

2. Flow cytometry

2.1. Vesicle detection using flow cytometry

Flow cytometer has been reported as a viable method to investigate GUVs [3-5]. For purpose of this studies both polyester beads and GUVs vesicles were recorded. In figure 1 example of SSC(FSC) dot plots were presented. It should be noted, that several polystyrene beads are sometimes recorded as one object providing false positive data points (Figure S8.a).
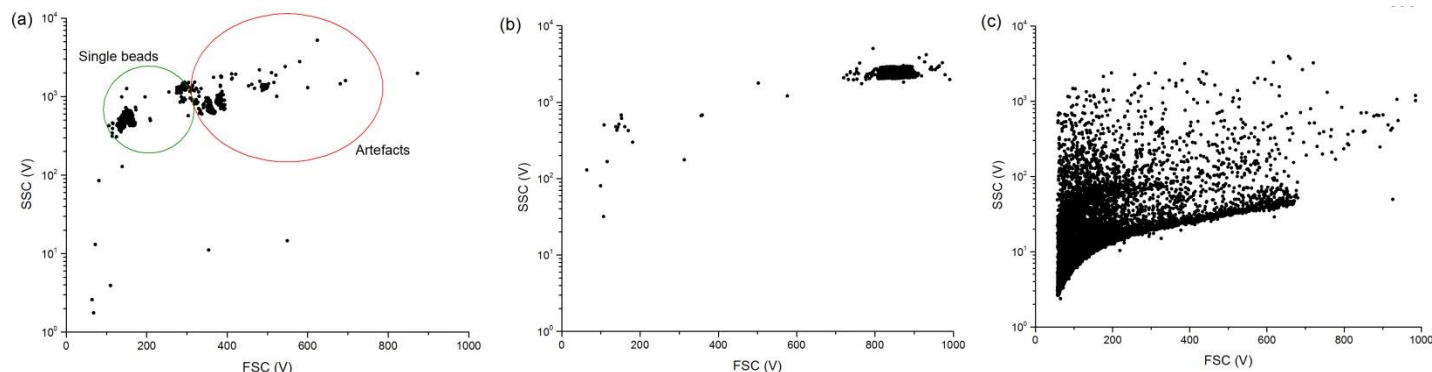
Figure S8. Examples of SSC(FSC) dot plots for (a) 4.5µm diameter polystyrene beads, (b) 11µm diameter polystyrene beads and (c) GUVs electroformed for 8h. In case of small particles sometimes several events were measured as one resulting in recorded larger particles marked as artefacts in panel (a). Second curve can be observed in liposome plot (panel c), however we believe those are OVVs rather than GUVs.

2.2. Polystyrene beads scattering as a correction factor

In order to take into account any possible differences in recorded intensities of FSC and SSC, prior to each measurement series polystyrene beads of sizes 1.5, 4.5 and 11 µm were measured. Each polystyrene beads were measured 3 times and Gaussian function was fitted in order to obtain peak value for each of beads sizes. This was followed by averaging those peak values and obtaining three marker values for each of GUVs measurements. Finally function minimization was carried out in order to find correction factor for both FSC and SSC which would result in minimal differences between markers from each of GUVs measurements. All measurements were compared to those with 4h electroformation duration. For FSC correction factors were equal to 1.042, 1.06 and 1.064 for 8h, 16h and 24h of electroformation duration respectively. For SSC correction factor was in all cases equal to 1.5. In figure S9(a) obtained histograms for polystyrene beads are presented along with averaged marker from three measurements. In figure S9(b) differences in obtained histograms of 4.5 µm beads recorded in different measurement days are presented (legend represents GUVs associated with the day of measurement).
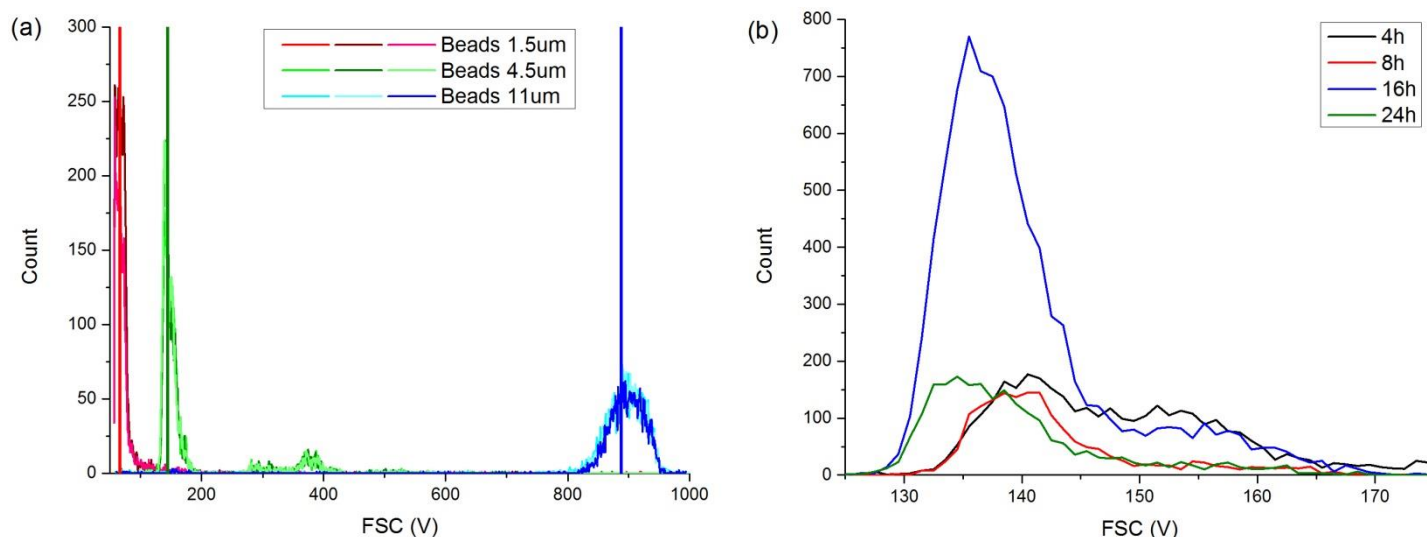
Figure S9. Polystyrene beads measured in flow cytometry. In panel (a) beads recorded prior to 4h electroformation duration GUVs are presented along with markers used for determination of correction factor. In panel (b) histograms of 4.5 µm beads recorded prior to measurements of different electroformation duration GUVs are presented. Note the difference in peak positions of given populations.

2.3. Individual results for each of investigated durations of electroformation

Below are presented individual results for each investigated electroformation duration. Control is also understood as a sample with electrodes submerged in water solution for same time but without AC applied. In order to obtain population parameter, Gaussian function was fitted to the data and peak value was obtained. In figures S10 and S11 histograms for FSC are presented. Each sample was measured 3 times, however, to keep figures clean, only first repeats were plotted.
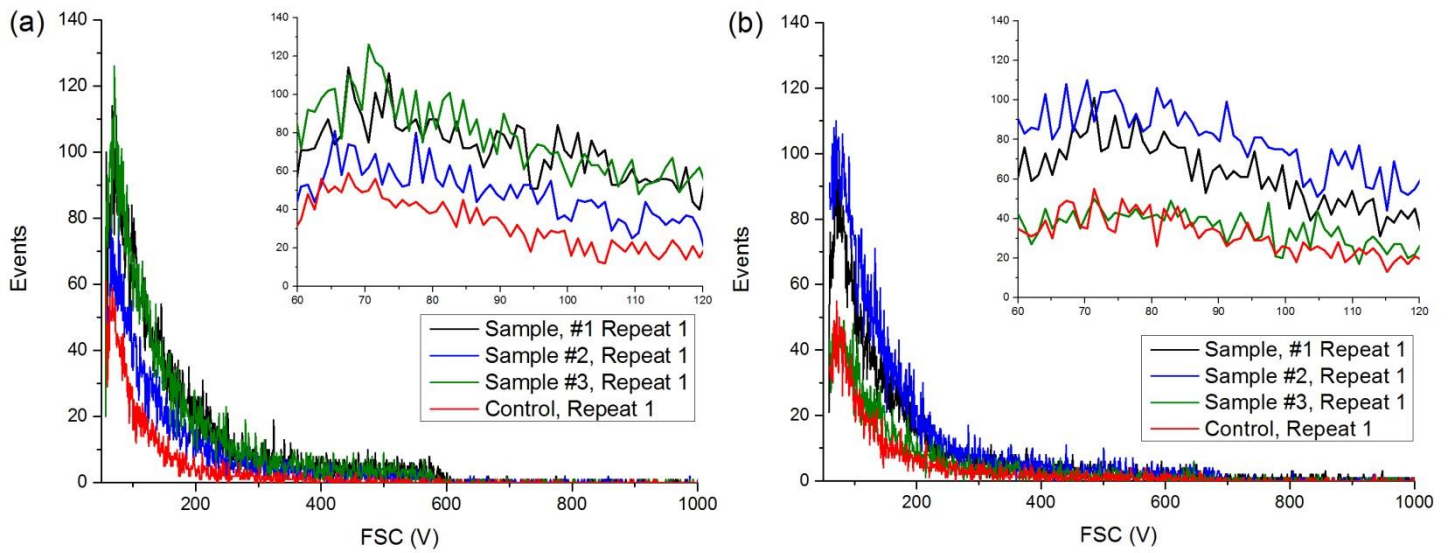
Figure S10. Histograms of FSC for GUV vesicles electroformed for (a) 4h and (b) 8h recorded using flow cytometry. Inset in figure reflects magnification on the FSC range where peak value is present.
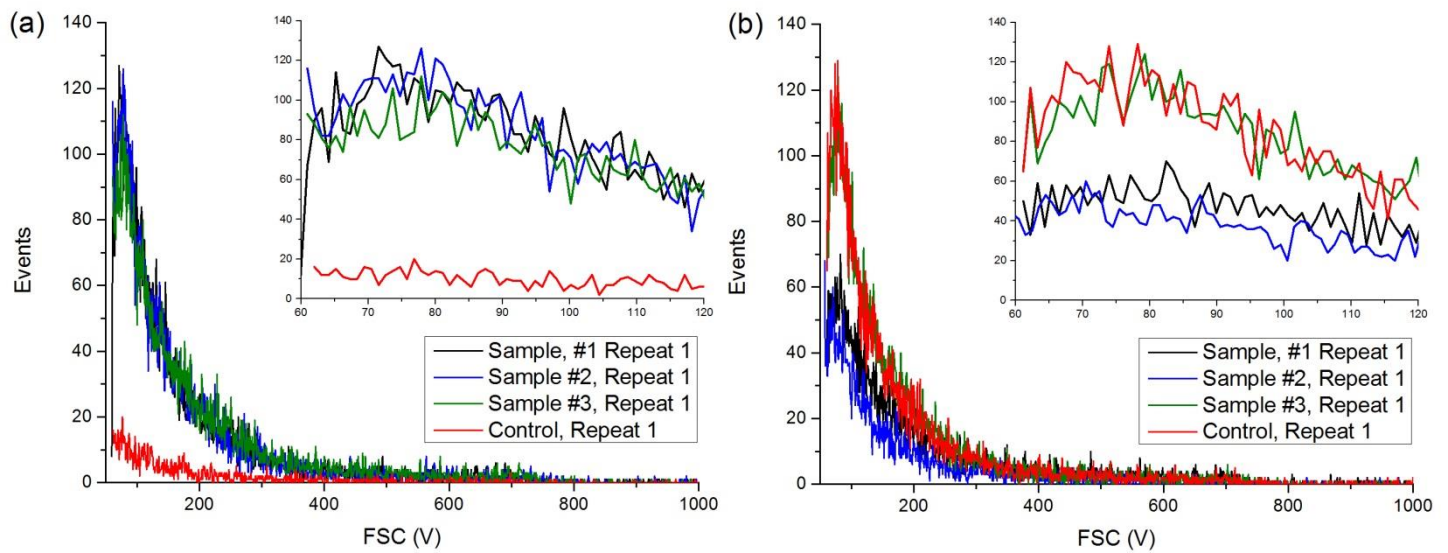

Figure S11. Histograms of FSC for GUV vesicles electroformed for (a) 16h and (b) 24h recorded using flow cytometry. Inset in figure reflects magnification on the FSC range where peak value is present.

3. Lipid amount assessment using colorimetric method

3.1. Calibration curve for lipid mass determination using colorimetric method

In order to correctly assess the amount of lipid calibration curve for lipid used in studies had to be measured. For each calibration curve for each lipid amount three samples were measured to verify measurement protocol. Calibration curve was obtained independently two times to ensure repeatability of measured values. Both absorbance spectra and linear fit used for determination of lipid amount are presented in figure S12.
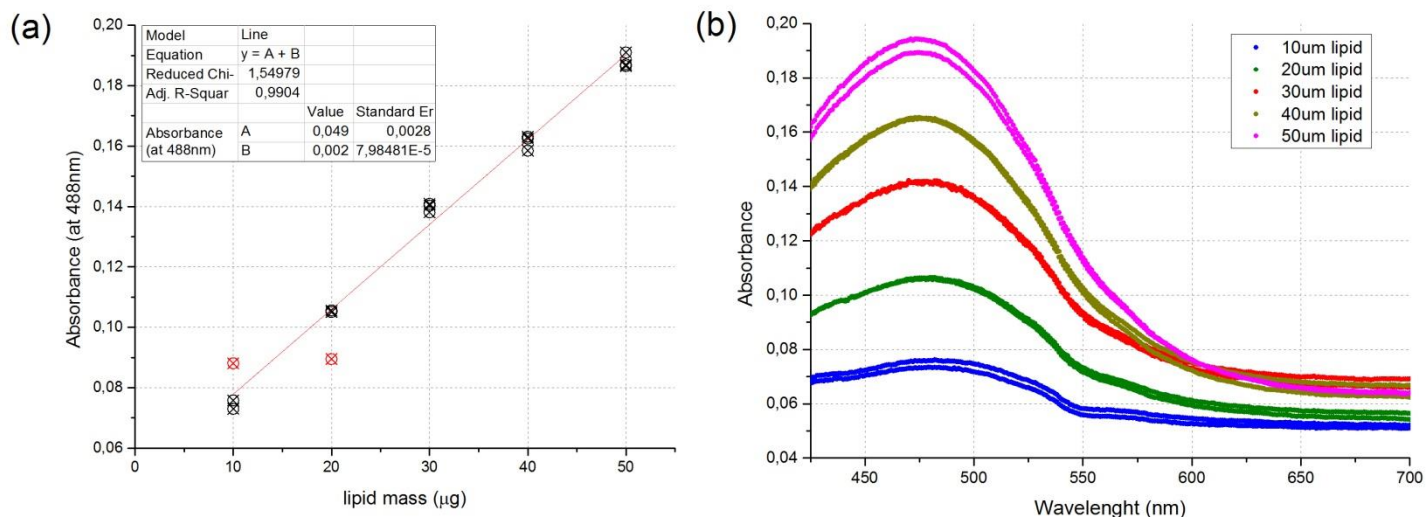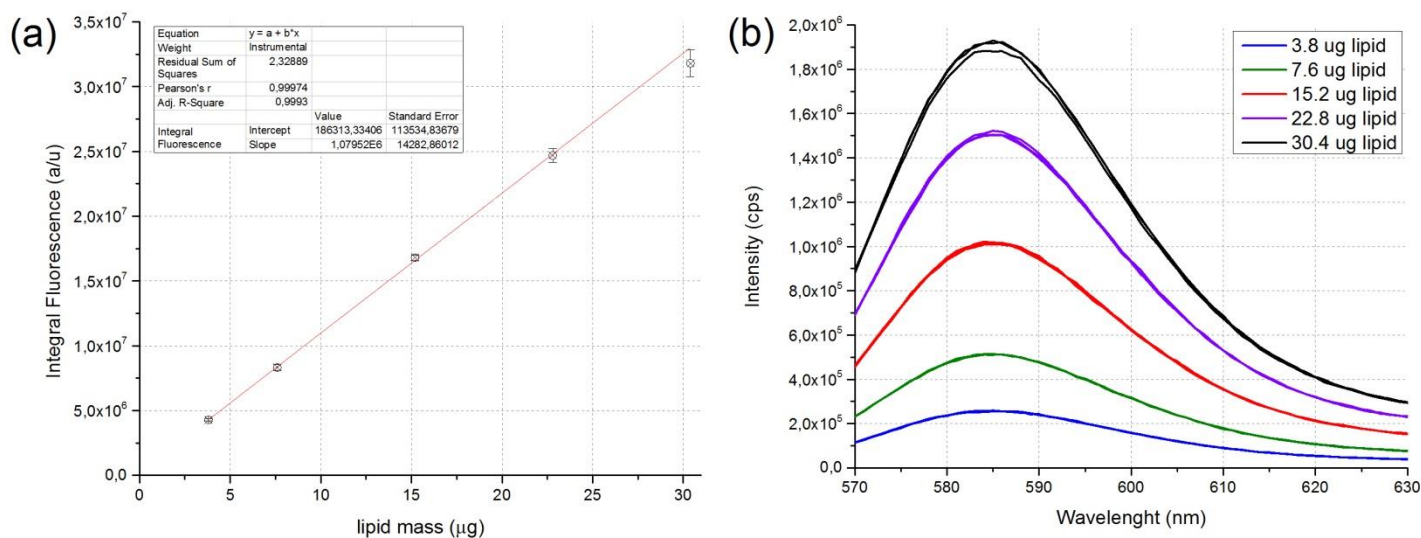
Figure S12. In panel (a) calibration curve for determination of lipid mass in GUV samples is presented along with linear fit. In panel (b) raw absorbance spectra from first calibration curve measurement is presented.

3.2. Individual results for each duration of electroformation

Below are presented individual results for each of investigated electroformation duration. Control is also understood as a sample with electrodes submerged in water solution for same time but without AC applied. GUV solution was evaporated under low pressure conditions. Lipid film was then dissolved in 1ml chloroform and 1ml of thiocyanate reagent was added. Samples were vortexed for 2minutes prior to absorbance measurement. Value of absorbance at 488nm was used to determine the mass of lipid molecules in solution. In figure S13 and S14 absorbance spectra for each of electroformation duration is presented. Each sample was measured 3 times, however results were identical in each repeat.
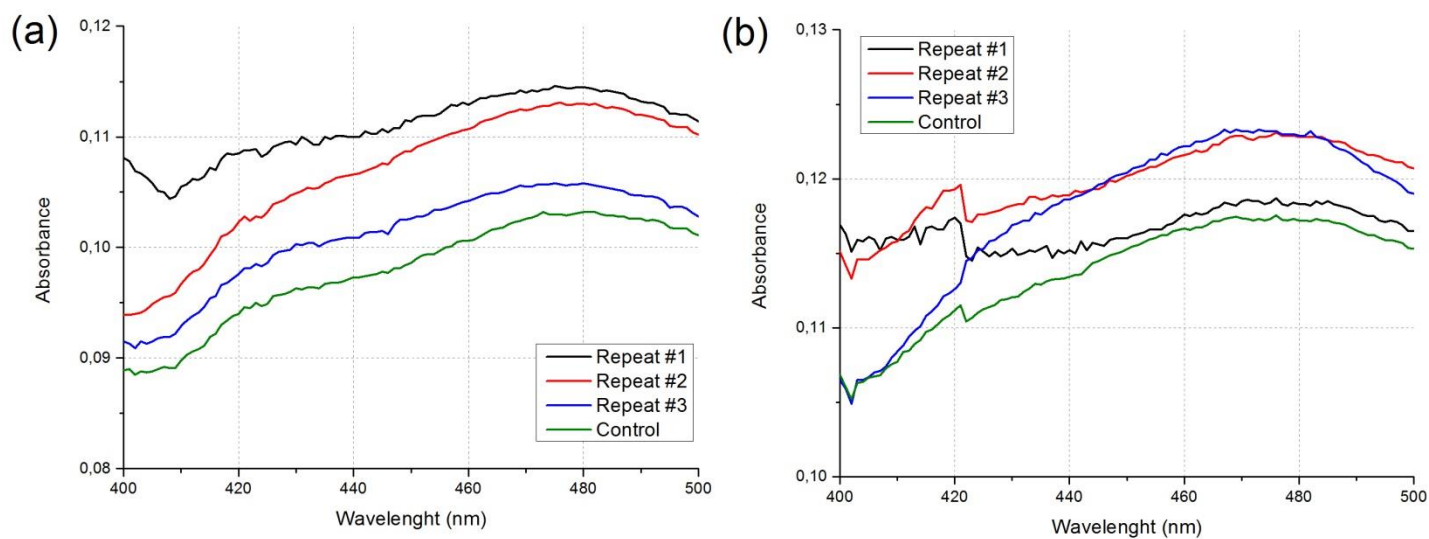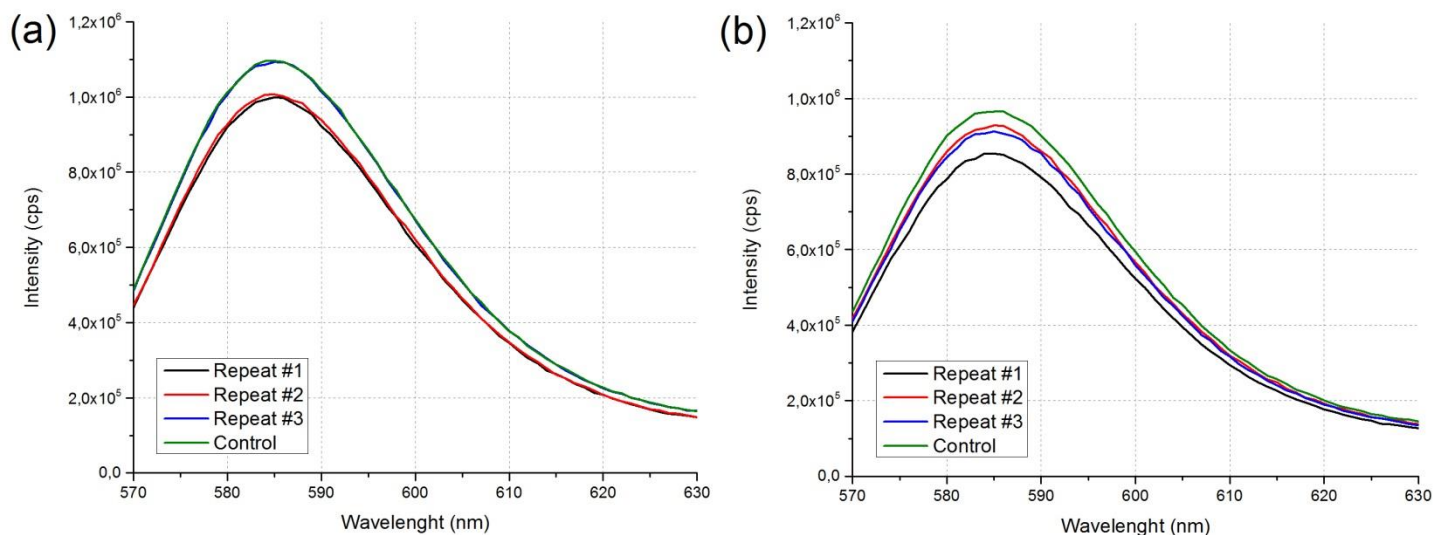

Figure S13. Absorbance spectra for GUV solution obtained after (a) 4h and (b) 8h of electroformation.
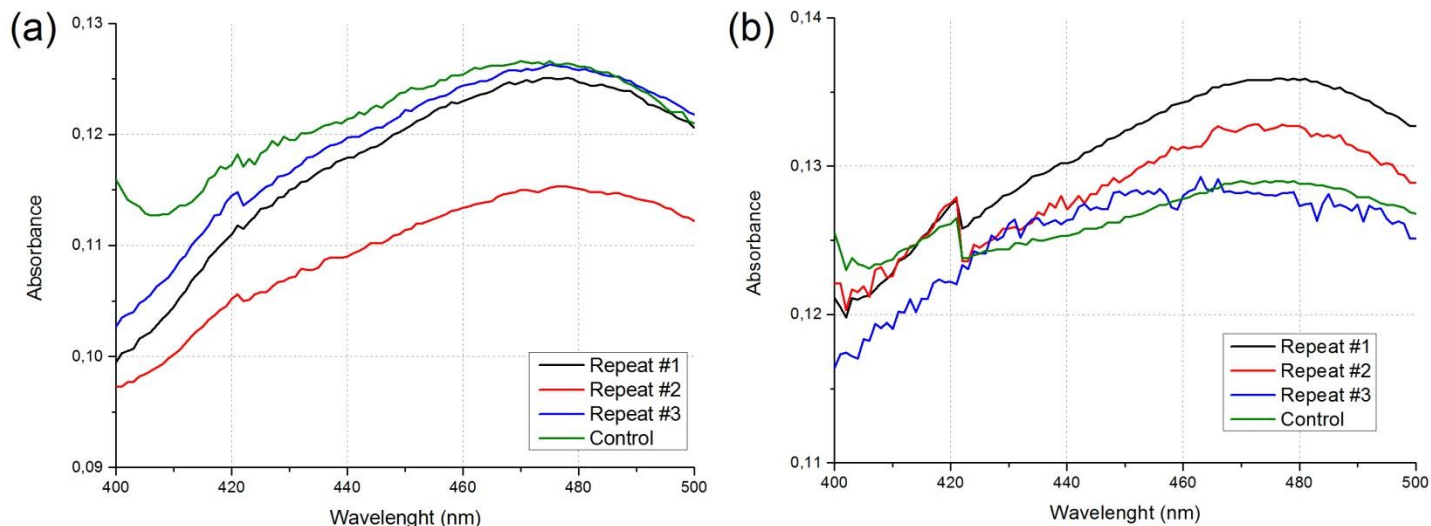
Figure S14. Absorbance spectra for GUV solution obtained after (a) 16h and (b) 24h of electroformation.

4. Lipid amount assessment using fluorescence method

4.1. Calibration curve for lipid mass determination using fluorescence method

In order to correctly asses amount of lipid based on the intensity of fluorescent dye calibration curve had to be measured. We assume that lipid/dye concentration is always constant therefore one sample of LUVs labelled with 1m% of Rhodamine-PE was prepared and then diluted into five different concentrations of lipid. This was followed by adding 70ul of 10% triton-x solution to induce micellization. After 10 minutes samples were measured 3 times. Whole process has been repeated 3 times. In figure S15 obtained calibration curve with linear fit is shown along with raw fluorescence spectra from first measurement series. The final value is integration of fluorescence intensity from 570 to 630 nm after subtracting base curve.

Figure S15. In panel (a) calibration curve of integral fluorescence for determination of lipid mass in GUV samples is presented along with linear fit. In panel (b) raw fluorescence spectra from first calibration curve measurement is presented.

4.2 Individual results for each duration of electroformation

Below are presented individual results for each of investigated electroformation duration. Control is also understood as a sample with electrodes submerged in water solution for same time but without AC applied. GUVs were converted into micelles by adding 70ul of 10% triton-x solution. It was verified using dynamic light scattering whether all lipid from GUVs has been converted into micelles (data not shown). Measured fluorescence spectra are presented in figures S16 and S17.

Figure S16. Fluorescence spectra for GUV solution obtained after (a) 4h and (b) 8h of electroformation.
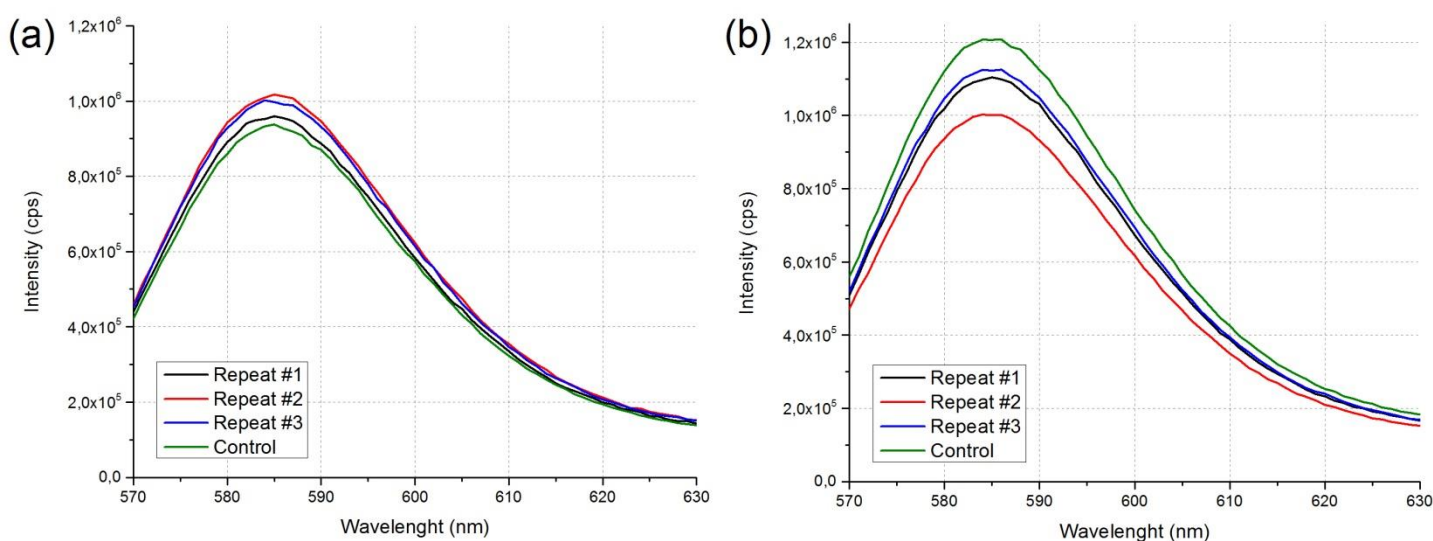
Figure S17. Fluorescence spectra for GUV solution obtained after (a) 16h and (b) 24h of electroformation.

5. OVVs presence evaluation using fluorescent quenching level method

5.1 Calibration quenching for LUVs and MLVs

In order to ensure both impenetrability of dithionite in lipid bilayers and certainty that recorded parameter describe property in question, a series of tests were carried out on populations of LUVs and MLVs. In latter case recorded fluorescence should be significantly higher, since MLVs are known to contain vesicles inside them. Each population was also micellized using Triton-X to perform a positive test – all fluorophore particles should be reachable for dithionite after micellization. The experiment was repeated 3 times to ensure obtained results were not a matter of random environment - first repeat is presented in Figure S18.
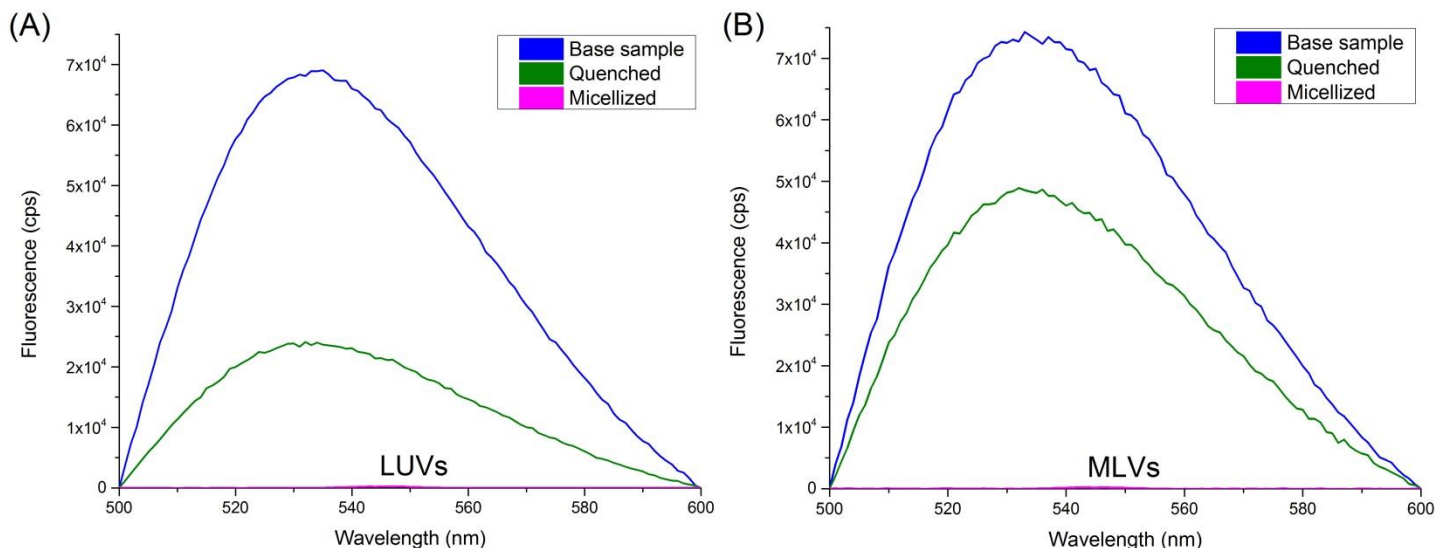
Figure S18. Fluorescence spectra for NBD-labelled (A) 100nm LUV and (B) MLV in water. The effect of quenching using 50 µl of 1M dithionite solution in 1M TRIS-Base is presented along the effect of micellization on fluorescence spectra.

**5.2 Individual results for each duration of electroformation**

Below are presented individual results for each of investigated electroformation durations. Control is also understood as a sample with electrodes submerged in water solution for same time but without AC applied. Each sample was measured prior and after 2 minutes of addition of 50 µl of 1M dithionite dissolved in 1M Tris base (pH = 11.21±0.05). Relative drop in intensity is understood as fraction of lipids located in outer membrane. Measured fluorescence spectra are presented in figures S19 and S20.
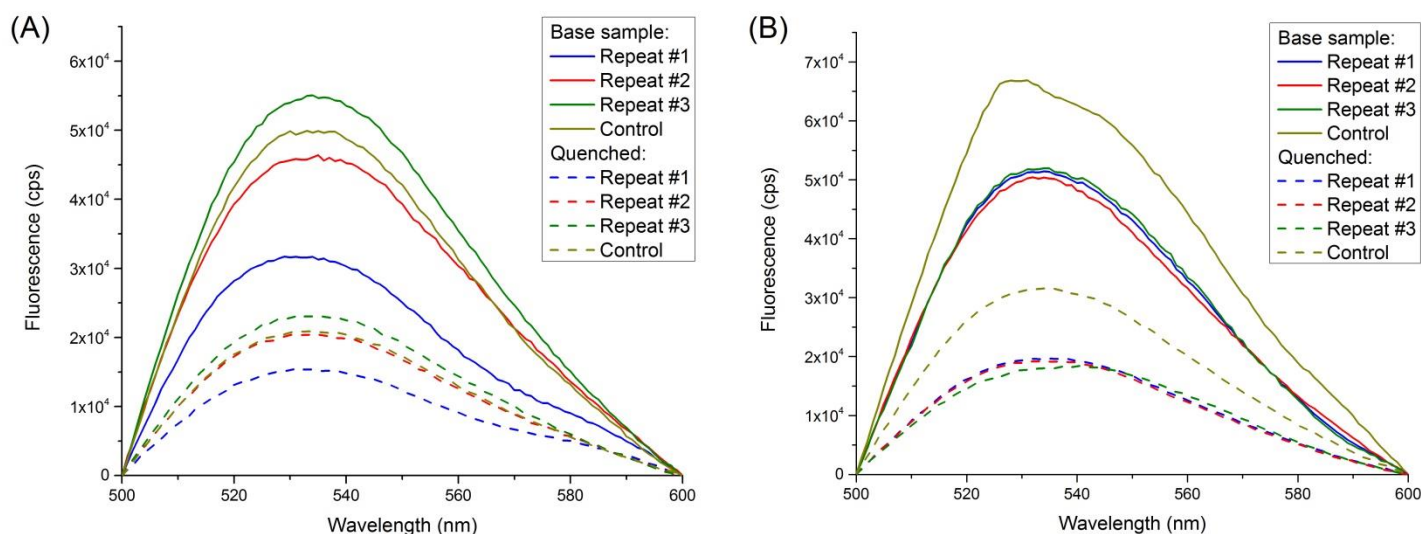
Figure S19. Fluorescence spectra for NBD-labelled GUVs in water electroformed for (A) 4h and (B) 8h. The effect of quenching using 50 µl of 1M dithionite solution in 1M Tris base is presented along the effect of micellization on fluorescence spectra.
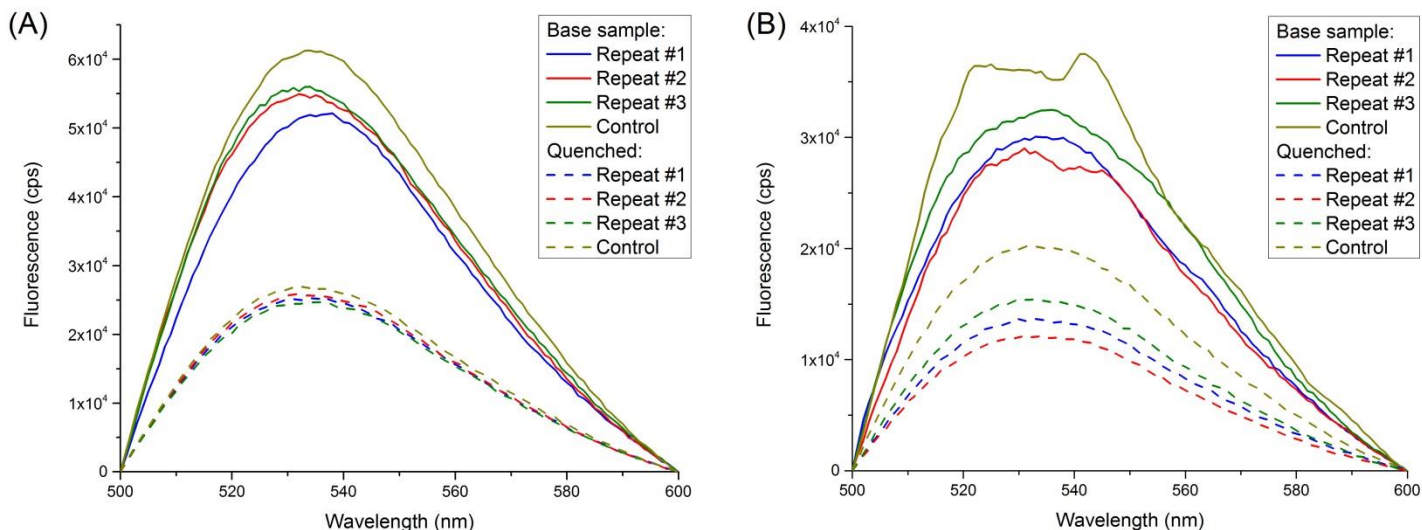
Figure S20. Fluorescence spectra for NBD-labelled GUVs in water electroformed for (A) 16h and (B) 24h. The effect of quenching using 50 µl of 1M dithionite solution in 1M TRIS-Base is presented along the effect of micellization on fluorescence spectra.

6. OVVs presence evaluation using fluorescent quenching ratio method

6.1 Calibration quenching for LUVs and MLVs

In order to ensure whether sensitivity of Stopped-Flow instrument is sufficient to determine ratio of lipids in inner/outer bilayer a series of tests were carried out on populations of LUVs and MLVs. The initial rate was obtained by fitting single-exponential equation to decay of NBD fluorescence and multiplying initial value times rate. The parameter therefore is correlated with quenching, meaning the greater the value of initial rate, the greater is quantity of lipids in outer bilayer (which means that fewer vesicles are located inside other vesicles). Several initial values for both LUVs and MLVs populations as well as averaged values are presented in figure S21(A). The kinetics of quenching are presented in figure S21(B).
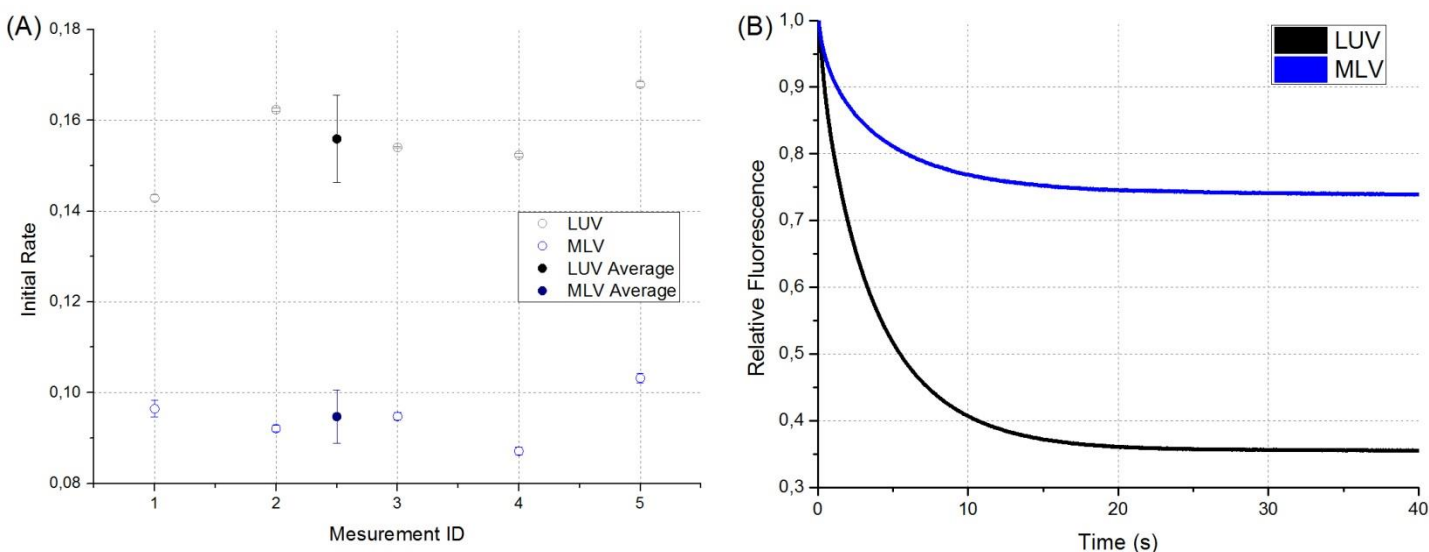
Figure S21. Comparison of LUVs and GUVs population labelled with NBD-PE when quenched with dithionite solution. In panel A both individual results and averaged are presented for both population. For individual measurements error bars represent the uncertainty of fit while for averaged values error bars represent standard deviation. In panel B kinetics of quenching for both LUVs and GUVs population are presented.

6.2 Individual results for each duration of electroformation

Below are presented representative kinetics for each of investigated electroformation durations and repeats. Control is also understood as a sample with electrodes submerged in water solution for same time but without AC applied. Each measurement reflects mixing of GUVs solution with dithionite solution with volume ratio 4:1. Results for 4h and 8h are presented in figure S22 while results for 16h and 24h are presented in figure S23.
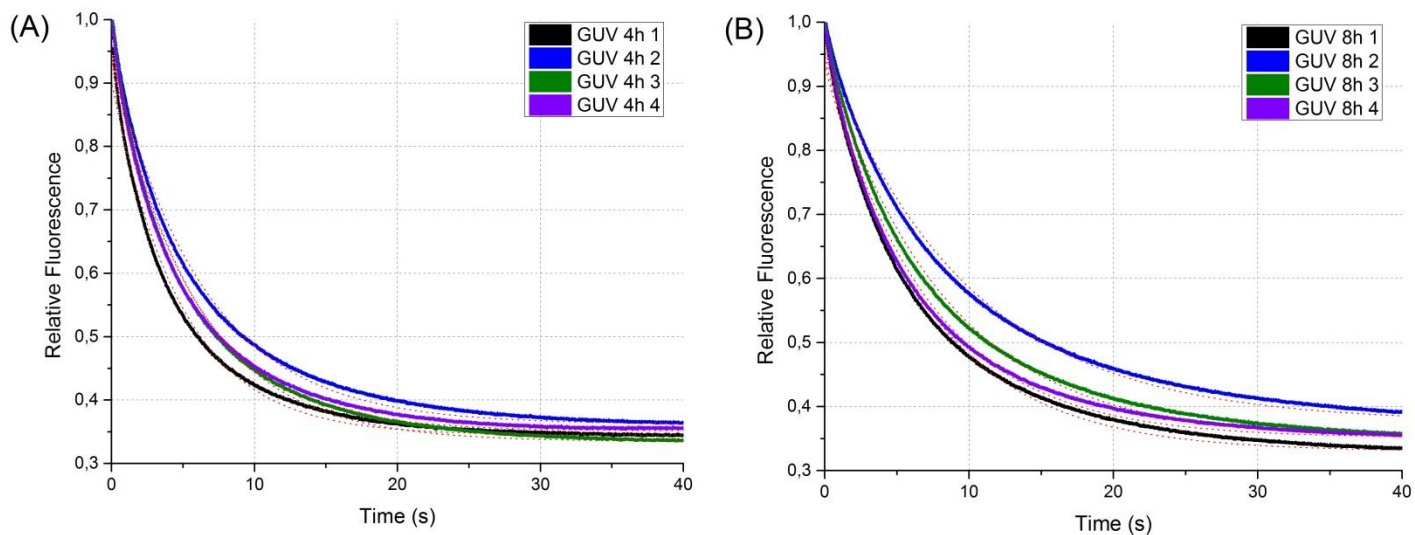
Figure S22. Quenching ratio for GUVs labelled with NBD-PE electroformed for (A) 4 hours and (B) 8 hours.
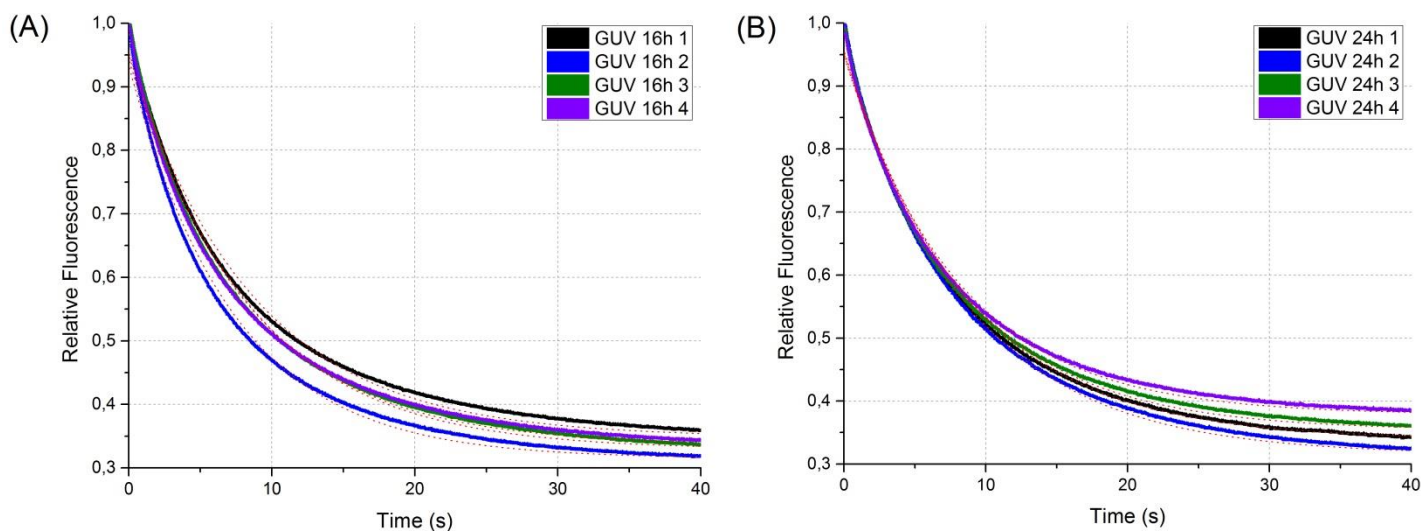

Figure S23. Quenching ratio for GUVs labelled with NBD-PE electroformed for (A) 16 hours and (B) 24 hours.

Notes and references

1. Cuevas, E., et al., Circle detection using Discrete Differential Evolution Optimization Pattern Analysis and Applications 2011. 14(1): p. 93-107.
2. Henriksen, J.R. and J.H. Ipsen, Thermal undulations of quasi-spherical vesicles stabilized by gravity. Eur. Phys. J. E, 2002. 9: p. 365-374.
3. Simonsen, J., A liposome-based size calibration method for measuring microvesicles by flow cytometry. J Thromb Haemost, 2016. 14: p. 186-90.
4. Uhl-Vorauer, K., et al., Determination of Liposome Size Distribution by Flow Cytometry. Cytometry, 2000. 39: p. 166-171.
5. Childers, N.K., et al., Characterization of liposome suspensions by flow cytometry. Journal of Immunological Methods, 1989. 119: p. 135-143.

The modified fluorescence based vesicle fluctuation spectroscopy technique for determination of lipid bilayer bending properties

Dominik Drabik [a,b,*,1], Magda Przybyło [a,b,1], Grzegorz Chodaczek [c], Aleš Iglič [d], Marek Langner [a,b]

[a] Laboratory for Biophysics of Lipid Aggregates, Department of Biomedical Engineering, Wrocław University of Technology, 50-377 Wrocław, Pl. Grunwaldzki 13, Poland
[b] Lipid Systems sp. z. o. o., ul. Duńska 9, 54-427 Wrocław, Poland
[c] Wrocław Research Centre EIT +, ul Stabłowicka 147, 54-066 Wrocław, Poland
[d] Laboratory of Biophysics, Faculty of Electrical Engineering, University of Ljubljana, Tržaška 25, SI-1000 Ljubljana, Slovenia

A R T I C L E I N F O

A B S T R A C T

Lipid bilayer is the main constitutive element of biological membrane, which confines intracellular space. The mechanical properties of biological membranes may be characterized by various parameters including membrane stiffness or membrane bending rigidity, which can be measured using flicker noise spectroscopy. The flicker noise spectroscopy exploits the spontaneous thermal undulations of the membrane. The method is based on the quantitative analysis of a series of microscopic images captured during thermal membrane fluctuations. Thus, measured bending rigidity coefficient depends on the image quality as well as the selection of computational tools for image processing and mathematical model used. In this work scanning and spinning disc confocal microscopies were used to visualize fluctuating membranes of giant unilamellar vesicles. The bending rigidity coefficient was calculated for different acquisition modes, using different fluorescent probes and different image processing methods. It was shown that both imaging approaches gave similar bending coefficient values regardless of acquisition time. Using the developed methodology the effect of fluorescent probe type and aqueous phase composition on the value of the membrane bending rigidity coefficient was measured. Specifically it was found that the bending rigidity coefficient of DOPC bilayer in water is smaller than that determined for POPC membrane. It has been found that the POPC and DOPC bending rigidities coefficient in sucrose solution was lower than that in water. Fluorescence imaging makes possible the quantitative analysis of membrane mechanical properties of inhomogeneous membrane.

© 2015 Elsevier B.V. All rights reserved.

1. Introduction

The mechanics of biological structures is a critical property for proper functioning of any biological system. [1–3] Whereas most of research is devoted to the mechanics of protein networks alone or together with associated cellular membranes, the mechanics of lipid bilayer component of biological membranes is less frequently studied as it is widely viewed as a passive and mechanically irrelevant element of biological systems. There are, however, circumstances where the lipid bilayer mechanics is of critical importance. The flow and redistribution of intracellular membranes requiring continuous shape and topology transformations, accompanied by the lipid and membrane protein sorting, depend on the flexibility of the lipid bilayer alone and/or the lipid bilayer combined with associated proteins [4–7]. Similarly the

control of cell volume or signal transduction facilitated by mechano-sensors requires involvement of mechanically well-defined lipid bilayers [8]. Lipid phase and topology as well as functioning of membrane-associated proteins are all affected by intra-membrane pressure that is manifested by the extent of the bilayer undulation dynamics [9,10]. Membrane thermal fluctuations are necessary element of cell mobility and protein fibre-based trafficking of endo-membranes [11]. The mechanics of lipid bilayer is a complex material property that can be described by different theoretical models used for the identification of quantitative parameters, which experimentally determined values depend on the quality of technical infrastructure and type of methodology used [12]. The conceptual perception of the biological membrane used to formulate a quantitative biophysical theory is a direct consequence of model first proposed by of the Singer and Nicolson (fluid mosaic model [13]). In this model the lipid bilayer is a scaffold in which various proteins are immersed in or associated with. Consequently, the most simple theoretical model of the biological membrane assumes that its mechanical properties can be reduced to these of the lipid bilayer [14]. In most of the cases the lipid bilayer can be considered as a two-dimensional surface, since its thickness (about 5 nm) is orders of magnitude smaller than the size of closed a biological membranes

---

* Corresponding author at: Lipid Systems sp. z. o., ul. Duńska 9, 54-427 Wrocław, Poland.
  E-mail address: Dominik.Drabik@pwr.edu.pl (D. Drabik).
[1] Authors contributed equally.

like cells or giant unilamellar vesicles (3–100 μm). In this representation the elastic energy of the membrane can be described by Helfrich Eq. (1).

$$E_{el} = 2\kappa(H-C_0)^2 + \kappa_G K \tag{1}$$

where κ is the bending rigidity constant, κ_G is Gaussian bending constant, related to the resistance to deformation during membrane topological transformation, c_0 is the spontaneous curvature of the membrane and H and K are the mean and Gaussian curvatures of the membrane surface, respectively [14,15]. To measure mechanical properties of the lipid bilayer, the membrane deformation, caused by various stimuli, needs to be visualized. To perform such experiments the giant unilamellar vesicles (GUV) have been used [16–18]. Typically, the vesicle topology is altered by external stimulus, followed by acquisition of microscopic images of GUVs and image analysis allowing for the determination of membrane mechanical properties [17,19,20]. When thermally induced membrane fluctuations are analysed (the flicker noise spectroscopy technique [21,22]) a large number of rapidly acquired images is required. These images are usually produced with the phase contrast microscopy [17,23–28] or occasionally with the light sheet fluorescence microscopy [29]. Phase contrast images of membranes can be rapidly acquired, contrary to the fluorescence confocal laser scanning microscopy (CLSM), where the image acquisition is slow. However, the CLSM has the capacity to visualize membrane inhomogeneity or its intrinsic biophysical properties (charge, fluidity) making possible the correlation between membrane mechanics and other membrane affecting factors [30,31]. In the paper two fluorescence imaging techniques, several image processing procedures and calculation methods, have been evaluated with the respect to their capacity to produce reliable values of the bending rigidity coefficient. Specifically, the slow but delivering high-contrast CLSM was compared with the fast but producing low-contrast images spinning disk confocal microscopy (SDM). The latter delivers almost instantaneously the images of the entire vesicle, while the former produces images, which are smeared in time. The aim of presented studies was to estimate the effect of an image acquisition technique and image processing method on the experimentally determined bending rigidity coefficient of POPC and DOPC lipid bilayers. In addition, the effect of sucrose of the bending rigidity coefficient of the two membranes was measured.

2. Materials and methods

2.1. Materials

Lipids (1-palmitoyl-2-oleoyl-sn-glycero-3-phosphocholine (POPC) and 1,2-dioleoyl-sn-glycero-3-phosphocholine (DOPC)), NBD-PC (1-acyl-2-(6-[(7-nitro-2-1,3-benzoxadiazol-4-yl)amino]hexanoyl)-sn-glycero-3-phosphocholine) and Rhodamine PE (18:1 Liss Rhod PE 1,2-dioleoyl-sn-glycero-3-phosphoethanolamine-N-(lissamine rhodamine B sulfonyl) ammonium salt) were purchased from Avanti Polar Lipids (USA). β-BODIPY FL DHPE and Atto 488 DOPE were purchased from Life Technologies (USA) and AttoTech (Germany), respectively. Stocked solutions of lipids with fluorescent probes in chloroform were analysed with HPLC (Knauer, Germany) equipped with ELSD detector (Grace, USA) before each experiment. [32,33] Concentrations of fluorophores were determined with UV/VIS spectroscopy using the excitations wavelengths and the extinction coefficient from probe specification sheets. The 18 MΩ deionized water was used in all experiments (ELGA system, Poland).

2.2. Preparation of giant unilamellar vesicles (GUV)

A modified electroformation method, originally developed by Angelova and Dimitrov, [16] was used for model lipid membranes formation. Specifically, 10 μl of POPC in chloroform (0.75 mM) mixed with 1 mol% or 0.5 mol% of fluorescent probe (for SDM or CLSM measurements, respectively) was deposited in small quantities (as 2 μl droplets) onto platinum electrodes. The organic solvent was evaporated with a stream of nitrogen and the electrodes covered with lipid film were kept for 1 h under reduced pressure to remove traces of organic solvents. Next, the electrodes were immersed in aqueous solution and exposed to the AC 1 Hz electrical field for 24 h in a PTFE (Polytetrafluoroethylene) electroformation chamber (Lipid Systems, Poland). Finally, vesicles were transferred into a PTFE observation chamber (Lipid Systems, Poland). The observation chamber design prevents the convection of liquids, therefore enabling extended microscopic observations. Typically, the average diameter of liposomes was equal to 13 ± 6 μm.

2.3. Acquisition of microscopic images

Two confocal microscopic modalities were employed in this study: spinning disk microscopy (SDM) and confocal laser scanning microscopy (CLSM). The Cell Observer SD spinning disk confocal microscope (Zeiss, Germany) was equipped with α Plan-Apochromat 100×/1.46 oil immersion objective (Zeiss, Germany). 512 × 512 pixels images were recorded with an EMCCD camera (iXon3 885, Andor, UK) using 2 × 2 binning with 0.133 μm pixel size at a rate of 33 frames per second (fps) with a video integration time of 30 ms. Samples were illuminated with 488 nm (NBD-PC, Atto 488 DOPE and β-BODIPY FL) and 561 nm (Rhodamine-PE) lasers and emitted light was passed through 527/54 and 629/62 filters, respectively. The LSM 510 Meta laser-scanning microscope (Zeiss, Germany) was equipped with a 40×/1.2 water immersion objective (Zeiss, Germany) and PMT detectors. 300 × 300 pixel images were acquired with 0.13–0.25 μm pixel size at a rate of 3–4 fps with a video integration time of 229–343 ms. Samples were illuminated with excitation wavelengths equal to 477 nm (NBD-PC), 488 nm (Atto 488 DOPE) and 514 nm (Rhodamine PE and β-BODIPY FL) and fluorescence emission was detected using appropriate cut-off filters. All samples were measured at 24 ± 1 °C. All measurements have been performed in dedicated observation chamber to reduce the effect of uncontrolled vesicle movements. SDM has the value of depth of focus equal to 0.85 μm, while the depth of focus of CLSM equals to 1.38 μm. To improve further the quality of analysis the radius of vesicle was calculated for each image and when the fluctuations of radius was unacceptable large the series of images were discarded from further analysis.

2.4. Fluorescence-based vesicle fluctuation spectroscopy method

The flicker noise spectroscopy is based on the analysis of a vesicle shape fluctuations in time. The reliability of the method depends on the image quality, acquisition time, probing frequency and number of images collected. Whereas phase contrast microscopy is capable of delivering a large number of instantaneous, good quality images the CLSM produces limited number of smeared images due to extended in time acquisition and photo-bleaching effect. The acquisition speed and number of available images can be radically increased by application of SDM. However, due to shorter exposure times the SDM requires application of higher laser power causing photo-destruction of fluorescent probes. Using the SDM series of 5000–10,000 images were recorded with 33 Hz probing frequency, while 1000–2500 images were acquired with 2–3 Hz probing frequency using the standard CLSM. Example of such an image is presented in Fig. 1a. Prior any membrane fluctuation analysis images were pre-processed to remove background noise using the rolling ball algorithm (radius 10) with disabled smoothing using the ImageJ software. [34] Extraction of the membrane fluctuation spectrum required the determination of the membrane contour location. Typically, this is done by detecting contour extremes and defining contour location as equivalent to the half-height position of the sigmoidal-shape of the radial fluorescence intensity profile, [20,35] by the location of a largest gradient in the signal intensity profile, [23] or by fitting the intensity profile with the Lorentzian
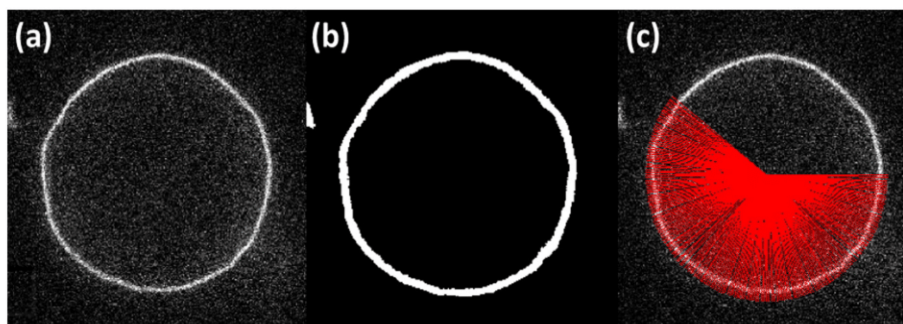
Fig. 1. The main steps of image processing leading to the vesicle contour determination. Panel a shows an example of a fluorescence image of a vesicle. Panel b demonstrates the processed image from panel a prior to the vesicle contour centre determination. Panel c shows linear intensity profiles on vesicle image that are used to determine vesicle cross-section centre location.

function. [36] In the paper, initially the grey-scale images were smoothed using a mean filter matrix of size 5. Next, images were binarized using either Otsu or Triangle algorithms (Fig. 1b). The approximate position of the vesicle contour was determined with the procedure based on the algorithm proposed by Suzuki. Threshold and contour determinations were performed using a software written in C++ with OpenCV (image processing library) [37]. A circle was fitted to predetermined initial vesicle contour using an algebraic procedure based on the Taubin method [38]. This provided the location of the vesicle centre. Next, using the initial non-smoothed image radial intensity profiles (typically 300) were collected and distances between the contour and the vesicle centre were calculated using the Bresenham algorithm as illustrated in Fig. 1c. Specifically, the intensity maximum along the radius of the circle was identified and the Lorentzian function was fitted to pixel intensity values around the intensity maximum. The fit was performed using the Levenberg–Marquardt algorithm [39]. Despite application of well establish image-processing methods, occasional local errors in contour detection may occur. This is due to the low level of the image/background ratio, especially frequent in images generated using the SDM. In order to eliminate such events three image processing procedures were tested. For that purpose 9 β-BODIPY-labelled POPC vesicles suspended in 75 mOsm sucrose solution were used and series of images collected using the SDM. Fig. 2 shows plots of the contour radial position as a function of the angle for DOPC vesicle, when three different image-processing methods were used. The first (smoothing) method is based on the calculation of the first-degree polynomial regression for the contour fragment. Intensities, which differ by more than six standards deviations from the mean intensity value, were eliminated from further analysis. In the second (polynomial) method the intensity value at each point was extrapolated with polynomial function (of 9th degree) fitted to the whole contour. In cases where the intensity value differed significantly from the extrapolated value it was replaced by the value of the polynomial function. In the third (quadratic) method the quadratic interpolation of the two neighbouring contour points was used to determine contour value at a given radial angle. The three image processing methods were tested and compared on the same large set of images. Selected image of vesicles, represented as distances between the membrane contour and the vesicle centre in polar coordinates, are presented in Fig. 2. To calculate the bending rigidity coefficient from a set of time-lapsed images a correlation between the two dimensional images and three dimensional membrane elasticity model had to be established [14]. This was achieved by means of the angular autocorrelation function $\xi(\gamma, t)$ defined by Eq. 2 [21,36].

$$\xi(\gamma, t) = \frac{1}{2\pi^2 R^2} \int_0^{2\pi} [\rho(\phi + \gamma, t) - \rho(t)] \cdot [\rho(\phi, t) - \rho(t)] d\phi \qquad (2)$$

Cross-sectional radius $\rho(\phi, t)$ is the position of vesicle bilayer at a given angle φ and at a given time t; $\rho(t)$ is an averaged vesicle radius of a given image recorded at time t using Eq. 3 as proposed by Pecreaux et al. [20] $R = \langle \rho(t) \rangle$ is the vesicle radius.

$$\rho(t) = \frac{1}{4\pi} \sum_{i=1}^{N} (\rho_i + \rho_{i+1}) \cdot (\phi_{i+1} - \phi_i) \qquad (3)$$

Selected autocorrelation curves for the three image processing method are presented in Fig. 3. Thermally driven membrane undulations were then used to calculate mechanical parameters, the bending rigidity coefficient κ and membrane tension σ of the lipid membrane. All calculations were performed using the MATLAB™ 7 software.
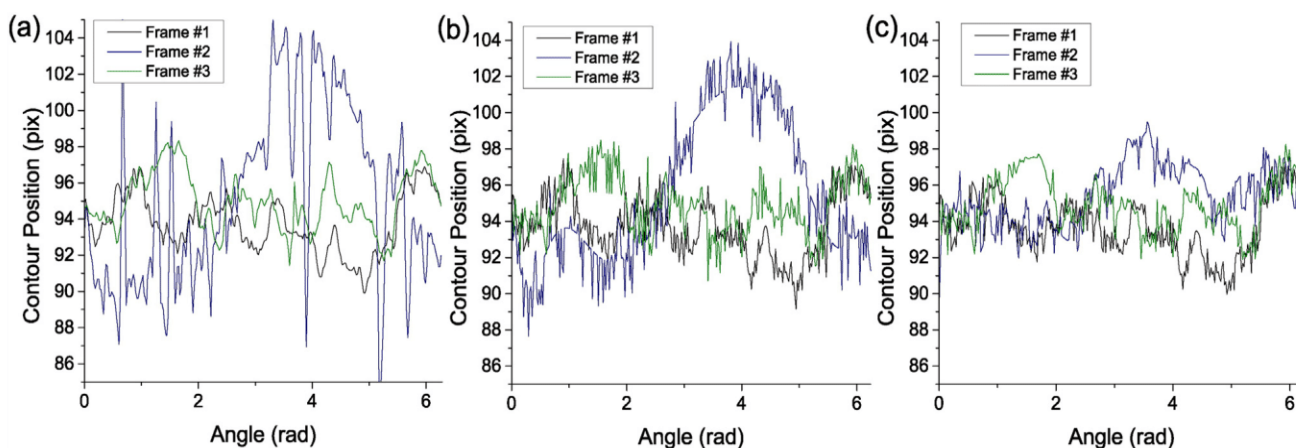
Fig. 2. The radial positions of three fluorescently labelled POPC membranes in 75 mOsm sucrose solution recorded using SDM were selected from a large (more than 5000) set of time-lapse images. Panels a, b and c show results of the smoothing and polynomial extrapolation, and quadratic interpolation image processing method, respectively.
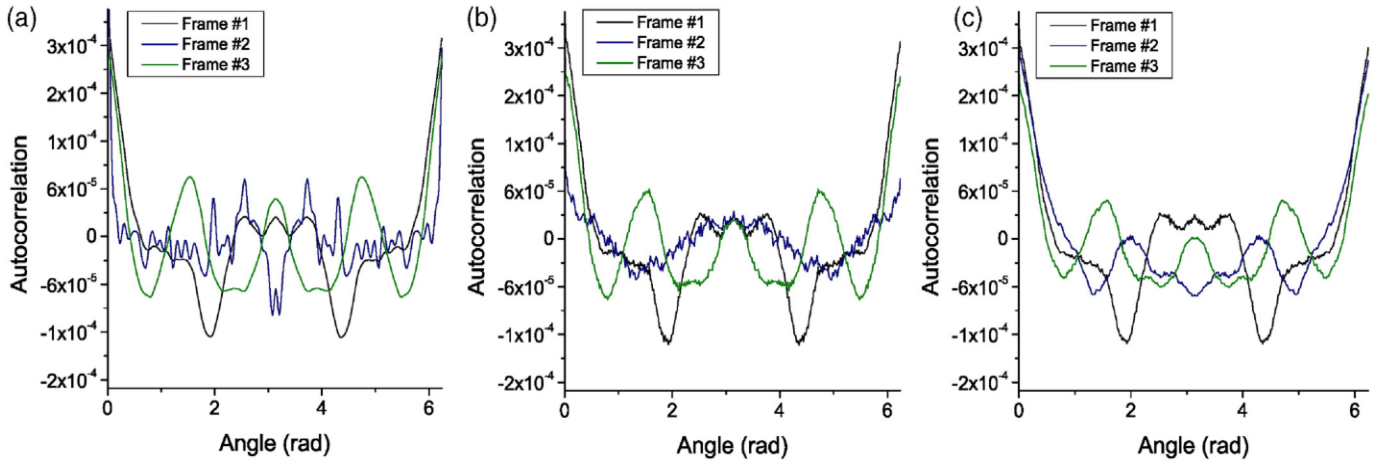
Fig. 3. Examples of autocorrelation functions calculated for selected images of POPC vesicles in 75 mOsm sucrose solution treated with (a) smoothing, (b) polynomial extrapolation and (c) quadratic interpolation image processing methods. The images were obtained using SDM.

3. Results and discussion

3.1. The optimization of the image processing procedure

Membrane undulations have been quantified using two procedures: average-based and statistical approaches. [21,24,27,35] In the average-based approach the angular autocorrelation curve is represented as the Legendre polynomials according to Eq. 4, where P_n are Legendre polynomial of nth degree, n_{max} is an upper mode cutoff defined as a square root of the number of lipid molecules in a membrane of a single vesicle N_{lip} (this value is usually limited to 30 due to smearing of the membrane contour in recorded images [36]) and coefficients $B_n(t)$ are interpreted as amplitudes derived in the decomposition of the angular correlation function in the Legendre polynomial series.

$$\xi(\gamma, t) = \langle B_0 \rangle \cdot P_0(cos\gamma) + \sum_{n=2}^{n_{max}} B_n(t) \cdot P_n(cos\gamma) \tag{4}$$

Since only positive values of $B_n(t)$ had physical meaning, $\langle B_n(t) \rangle$ is an average over positive $B_n(t)$. The numerical values of coefficients $\langle B_n(t) \rangle$ extracted from experimental images are related to physical events such as changes of the vesicle radius $\rho(t)$ (n = 0) or changes of the position of the vesicle centre of mass (n = 1). Thermal fluctuations were assigned to second and higher modes. Recorded GUV images have been averaged over the image acquisition time t_s, therefore, it was not possible to obtain the exact values of B_n coefficients, instead, only the averaged values were available $B'_n = f_n^{corr} B_n$. [24] The correction factor f_n^{corr} is defined by Eq. 5, where t_s is the image acquisition time, a value specific for each type of microscope (for the SDM $t_s = 30$ ms), and τ_n^m is the correlation time defined by Eq. 6, where η is the viscosity of the medium surrounding the vesicle membrane, k is Boltzmann constant and T is temperature. By combining Eq. 5 with definition of B'_n the Eq. 7 is obtained. The Eq. 7 can be used to calculate the correlation time τ_n^m. For images obtained using the SDM correction factors, for all modes and all image processing methods, were equal or higher than 0.999 indicating the high quality of the recovered vesicle contour.

$$f_n^{corr} = 2 \left(\frac{\tau_n^m}{t_s}\right)^2 \left[exp\left(-\frac{t_s}{\tau_n^m}\right) - \left(1 - \frac{t_s}{\tau_n^m}\right) \right] \tag{5}$$

$$\tau_n^m = \frac{4\pi\eta R^3}{k_b T} \left(2 - \frac{1}{n(n+1)}\right) B_n(\kappa, \overline{\sigma}) \tag{6}$$

$$B'_n = 2 \left(\frac{t_n^m}{t_s}\right)^2 \left[exp\left(-\frac{t_s}{\tau_n^m}\right) - \left(1 - \frac{t_s}{\tau_n^m}\right) \right] \cdot \left(\frac{k_b T \tau_n^m}{4\pi\eta R^3}\right) \cdot \left(2 - \frac{1}{n(n+1)}\right)^{-1} \tag{7}$$

Fitting Eq. 8 to experimental values of amplitudes using the Levenberg–Marquardt algorithm produced the bending rigidity κ and membrane tension σ values. In the fitting procedure the first few modes were omitted since their high level of uncertainty would distort the value of the calculated bending rigidity. High modes (n > 30) were also discarded due to their low detection levels. In Eq. 8 reduced membrane tension $\overline{\sigma}$ defined by Eq. 9 was used to maintain the same magnitude of numerical values. This has reduced the occurrence of the 'machine epsilon' effect in computations.

$$B_n(\kappa, \overline{\sigma}) = \frac{2n+1}{4\pi} \cdot \frac{kT}{\kappa(n+2)(n-1)[\overline{\sigma} + n(n+1)]} \quad for \ n > 1 \tag{8}$$

$$\overline{\sigma} = \frac{\sigma R^2}{\kappa} \tag{9}$$

Values of $\langle B_n(t) \rangle$ coefficients plotted as a function of mode, along with fitted theoretical curves, are presented in Fig. 4. For contours, determined using the smoothing method, the calculated value of the bending rigidity coefficient (determined for 9 POPC vesicles in sucrose) equalled to $(175 \pm 210) \cdot k_b T$ (corresponding to $\kappa = (72 \pm 86) \cdot 10^{-20} J$) and the value of the reduced membrane tension $\overline{\sigma}$ equalled to 1.7. For the contour of vesicles cross-sections, processed using the polynomial extrapolation method, the bending rigidity coefficient equalled to $(31 \pm 11) \cdot k_b T$ (corresponding to $\kappa = (13.0 \pm 4.5) \cdot 10^{-20} J$) and the value of the reduced membrane tension, $\overline{\sigma}$, equalled to 1.4. When contour was determined using the quadratic interpolation method, bending coefficient was equal to $(48 \pm 38) \cdot k_b T$ (corresponding to $\kappa = (20.0 \pm 15.7) \cdot 10^{-20} J$) and reduced membrane tension, $\overline{\sigma}$, equalled to 1.8. Only contours treated with extrapolation method provided the measured bending coefficient values within the range expected for POPC vesicles.

The statistical approach, proposed by Meleard et al., [36] took into account overall distribution of shape fluctuations, which were used for the determination of the bending rigidity coefficient κ. [40,41] In this approach autocorrelation curves represented by the Eq. 10 were represented as a Fourier series, in which sine components were omitted (curves are even functions).

$$\xi(\gamma, t) = \sum_{0 < m}^{n_{max}} \chi^m(t) \, cos(m\gamma) \tag{10}$$
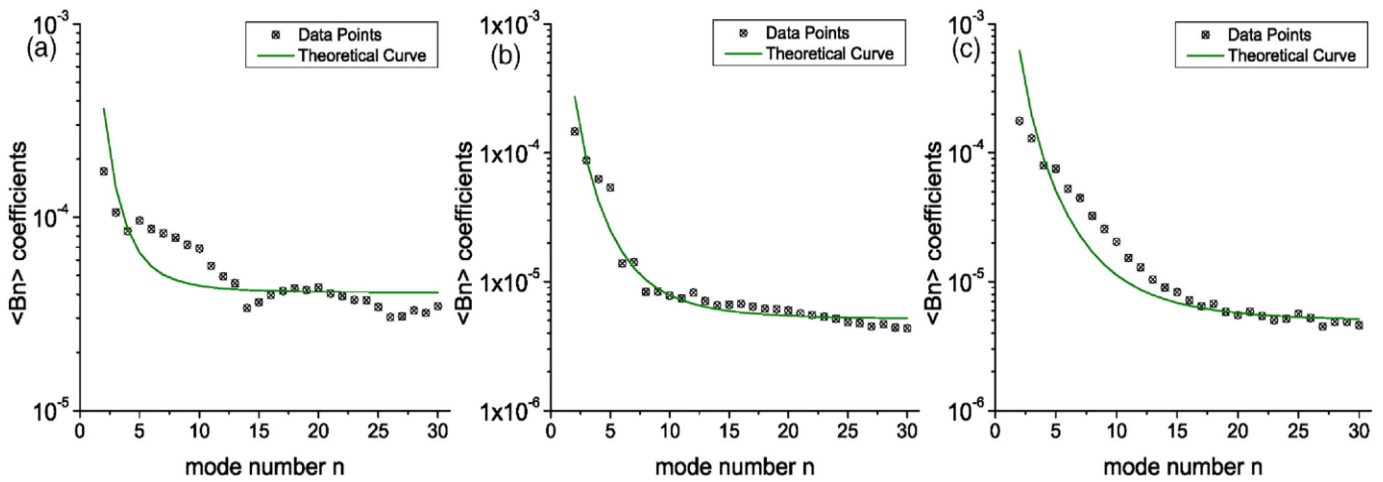
Fig. 4. The dependence of B_n coefficients on the mode number along with the fit of the Eq. 8. Panels a, b and c show experimentally determined values of coefficients B_n for contours determined using smoothing, polynomial extrapolation and quadratic interpolation methods, respectively. Images of POPC vesicles in 75 mOsm sucrose solution were rescored using SDM.

Amplitudes of cosine functions for each frame of a given mode m, $\chi^m(t)$, were histogrammed and fitted by mono-exponential distributions $\Gamma^m(\chi^m)$ (Eq. 11, Fig. 5). Frequencies in the distribution were adjusted with a normalization factor equal to the number of counts of the largest frequency.

$$\Gamma^m = a \cdot \exp\left(-R^m\left(\frac{\kappa}{kT}, \overline{\sigma}\right) \cdot \frac{\chi^m}{2}\right) \tag{11}$$

The mono-exponential character of distributions suggests that the model adequately describes the thermal fluctuation of the membrane. Fig. 5 shows frequency distributions Γ^m of shape fluctuations for selected amplitudes when images were treated with different image processing methods. The figure shows that the polynomial extrapolation method produced results that were best fitted with the mono-exponential function. For that reason the polynomial extrapolation method was used for further analysis. To determine bending rigidity coefficient from distributions, decays were fitted using mono-exponential function. Fits were carried out for Γ^m ranging from 0.6 to 0.08 as suggested by Meleard et al. [36]. Amplitudes bigger than 0.6 were omitted since they are statistically insignificant due to the low probability of occurrence. Amplitudes smaller than 0.08 are too close to the resolution

limit therefore they are also omitted. The quality of fitting was evaluated with residual values calculated according to Eq. 12.

$$\Delta\Gamma^m = \frac{R^m}{\sqrt{N}} \cdot \sqrt{\sum_i \left(\ln\left[\Gamma^m\left(\frac{\chi_i^m}{2}\right)\right] - \ln(a) + R^m \cdot \frac{\chi_i^m}{2}\right)^2} \tag{12}$$

In order to derive Eq. 12, Eq. 11 was linearized as $\ln(\Gamma^m) = \ln(a) - R^m(\frac{\kappa}{kT}, \overline{\sigma}) \cdot (\chi^m/2)$. The part of Eq. 12 under square root is the linearized distribution residuals while $R^m/\sqrt{N}$ is related to uncertainty of Γ^m slope.

The bending rigidity coefficient can be determine by fitting the Eq. 13 to experimentally determined R^m values, where σ_{wh} is a superposition of white noise, defined by the optical resolution of microscope, and the electronic noise, generated by the video camera, as defined by H. Bouvrais [42]. $\mathcal{P}_n^m$ are, normalized according to Eq. 14, Legendre polynomials P_n^m. Finally, $\lambda_n(\overline{\sigma})$ is the function dependent on the reduced membrane tension as defined by Eq. 15.

$$R^m\left(\frac{\kappa}{kT}, \overline{\sigma}, \sigma_{wh}\right) = \frac{1}{\frac{\kappa}{kT}\left(\sum_{n \geq m}^{n_{max}} \frac{[\mathcal{P}_n^m(0)]^2}{\lambda_n(\overline{\sigma})}\right) + \sigma_{wh}^2} \tag{13}$$
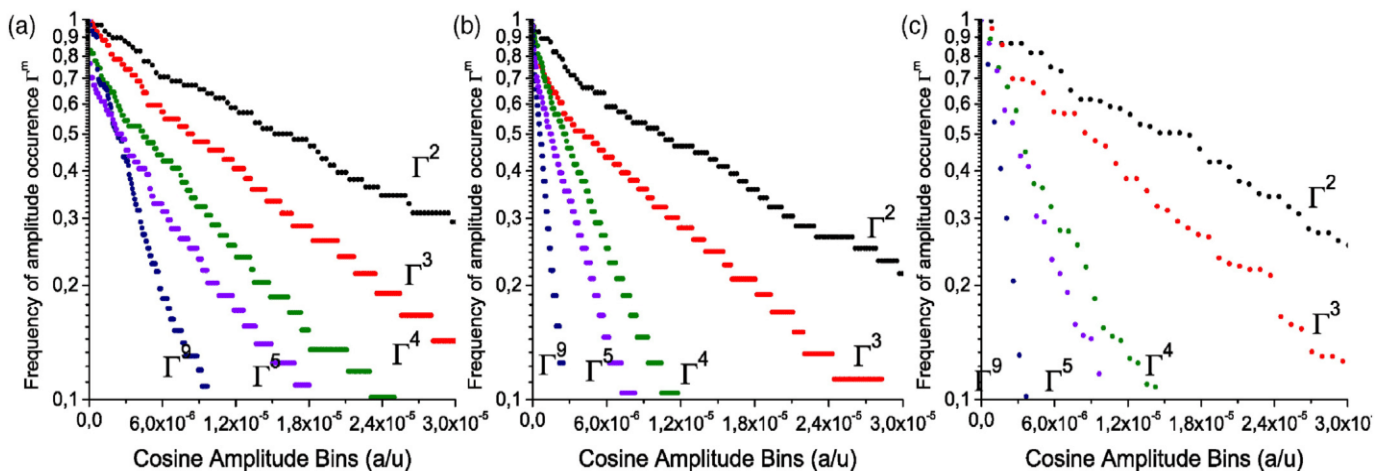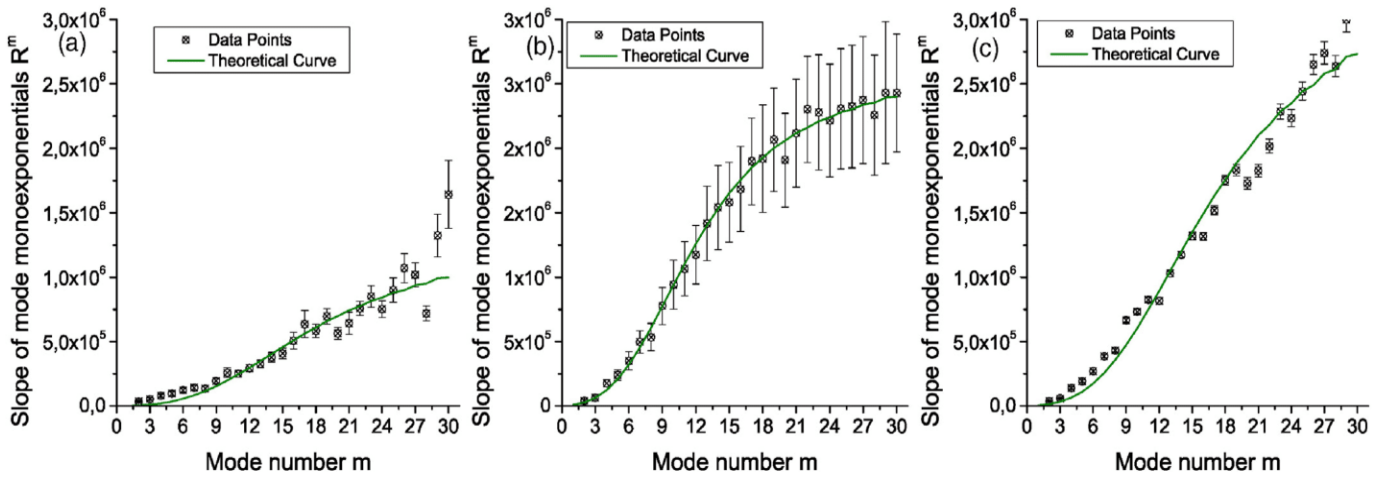

Fig. 5. Distributions Γ^m of shape fluctuations for selected mth orders acquired from contours derived using (a) smoothing, (b) polynomial extrapolation and (c) quadratic interpolation methods. The images of POPC vesicles in 75 mOsm sucrose solution were recorded using SDM.

Fig. 6. The dependence of R^m parameter (Eq. 11) as a function of mode m. Best fits of the theoretical curve (Eq. 13) are also presented. Plots in panels a, b and c were derived from contours extracted from images using smoothing, polynomial extrapolation and quadratic interpolation image processing methods, respectively. The images of POPC vesicle in 75 mOsm sucrose solution were recorded using SDM.

$$\mathcal{P}_n^m(x) = (-1)^m \sqrt{\frac{(2n+1)(n-m)!}{4\pi(n+m)!}} P_n^m(x) \qquad (14)$$

$$\lambda_n(\overline{\sigma}) = (n+1)(n+2)[\overline{\sigma} + n(n+1)] \qquad (15)$$

The R^m values plotted as a function of mode, along with fitted Eq. 13, are presented in Fig. 6. The calculated value of the bending rigidity coefficient depends on the method used to process vesicle images. Specifically, when the liposome image was processed using the smoothing method the value of bending rigidity coefficient of 9 analysed vesicles was equal to $(5 \pm 3) \cdot k_b T$ ($\kappa = (1.9 \pm 1.3) \cdot 10^{-20} J$) and the value of the reduced membrane tension $\overline{\sigma}$ equalled to 1.9. When vesicle image was treated with the polynomial extrapolation method the derived value of bending rigidity coefficient was equal to $(37 \pm 15) \cdot k_b T$ ($\kappa = (15.1 \pm 6.3) \cdot 10^{-20} J$) and the value of the reduced membrane tension $\overline{\sigma}$ was equal to 1.9, but when the interpolation method was used the value of the bending rigidity coefficient was equal to $(19 \pm 9) \cdot k_b T$ ($\kappa = (8 \pm 4) \cdot 10^{-20} J$) and the value of the reduced membrane tension $\overline{\sigma}$ was equal to 2. In both, interpolation and smoothing, image processing methods values of bending rigidity coefficient calculated using the average-based and statistical approaches were differed. Only the polynomial image processing method delivered consistent results therefore it has been selected for further analysis.

3.2. The effect of geometrical uncertainty of vesicle image reconstruction on the determined values of bending rigidity coefficient

The accuracy of the bending rigidity coefficient measurements depends mainly on the shape of autocorrelation curve, which is related to recurrence of fluctuations of given mode. This depends on the precision of the reconstruction of the vesicle geometry. It has been demonstrated previously by Loftus et al. [29] that certain alterations of membrane images did not affect much the value of the bending rigidity coefficient. The effect of image imperfections on autocorrelation curve and consequently the value of the bending rigidity coefficient was tested using controlled image distortion procedure. Specifically, the contour fragment was substituted with a set of random intensity values drown from the range of all intensities of the contour to simulate either poorly illuminated vesicle fragment or miss-detection of the bilayer edge. The increasing fraction of the vesicle contour was altered and the bending rigidity coefficient calculated. The dependence of the bending rigidity coefficient value on the size of the image distortion, calculated using both, average-based and statistical approaches, are presented in Fig. 7. Results show that the statistical approach is more resilient to contour distortion than averaged-based approach since distorted contour length of 0.13 rad (2% of the whole contour length) was required to alter significantly the value of the bending rigidity coefficient. The average-based approach was more sensitive to the contour
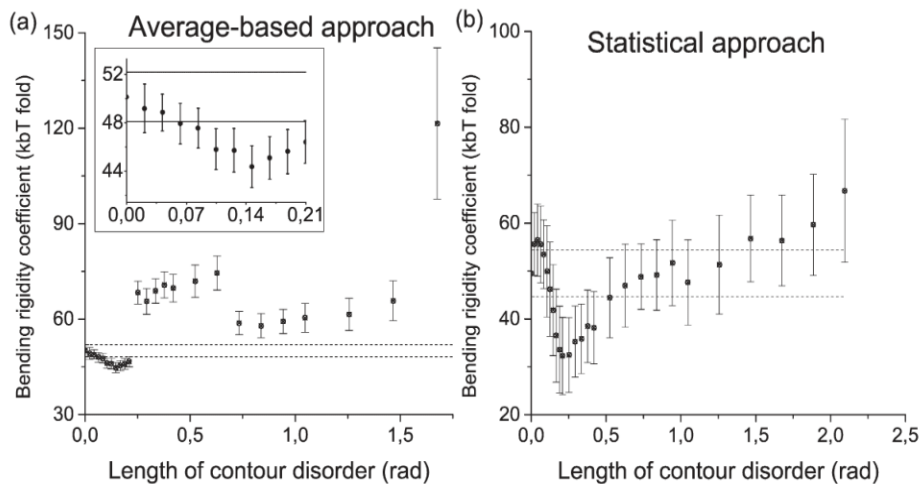
Fig. 7. The effect of the size of the vesicle contour distortion on the value of the calculated bending rigidity coefficient when average-based (a) or statistical (b) method was used. Inset in panel a shows a magnified part of the curve. The images of POPC vesicles were recorded using SDM.

---

distortion since 0.06 rad distortion (1% of the whole contour) was sufficient to alter bending rigidity coefficient value.

Since radial distances, used to evaluate the membrane fluctuation, may be affected by the precise location of vesicle centre we assessed the dependence of the value of the bending rigidity coefficient on the distortion of the centre positioning. Fig. 8 shows the effect of the vesicle centre repositioning on the determined value of the bending rigidity coefficient calculated with both; average-based and statistical approaches. We found that the value of bending rigidity coefficient, determined using the statistical method, was not sensitive to changes in the location of the vesicle centre. The variation in the vesicle centre location resulted only with an increase of an uncertainty value of the bending rigidity coefficient (Fig. 8b). The average-based approach, on the other hand, was very sensitive to the repositioning of the vesicle centre being detectable when the centre position was changed by as little as 3 pixels (Fig. 8a). The presented results demonstrate the importance of the image processing method and the model of membrane elasticity used for the evaluation of bending rigidity coefficient of the membrane.

3.3. Effects of imaging acquisition method and fluorescent probe type on the determined bending rigidity value

The evaluation of the lipid bilayer mechanical properties using the flicker noise spectroscopy requires acquisition of a series of a large number of images. To increase the probing frequency, which is low for the standard CLSM, the SDM was used. Improved sampling rate, resulting from the increased acquisition speed, was accompanied by the decreased image quality and elevated photo-damage of the fluorophore. Surprisingly, the determined value of the bending rigidity coefficient has not depended on the image acquisition time showing that the probing frequency of the fluctuating membrane is insignificant, as long as enough images were collected so the distribution functions would be correctly determined. The other source of experimental uncertainty may result from the construction of the experimental system itself. All images used for the analysis were based on the fluorescence of a probe incorporated into or associated with the membrane. The fluorescence intensity is sensitive to variety of factors such as photobleaching, polarity of the immediate vicinity of the fluorescent moiety or properties of the aqueous phase, which may affect the probe location with respect to the membrane surface [43,44]. It has been demonstrated previously that fluorescent probes at concentrations up to 2 mol% do not affect mechanical properties of the lipid bilayer [36]. To confirm this observation in our experimental setups POPC liposomes in 75 mOsm sucrose solution were labelled with four different fluorescent moieties (Atto-DOPE 488, β-BODIPY FL DHPE, NBD-PC and Rhodamine-

PE). All tested fluorophores were covalently attached to lipid molecules albeit at different locations with respect to the membrane surface. Specifically, β-BODIPY and NBD moieties are located within the interface of the lipid bilayer [45,46]. Hydrophobic Atto moiety is located in the membrane hydrophobic core, [47,48] whereas hydrophilic rhodamine is located in the aqueous phase adjacent to the membrane surface [49]. Such diversified set of fluorescent probes enabled testing the effect of their physicochemical and optical properties on the determined value of the bending rigidity coefficient. The fluorescent images were acquired using both, the SDM and CLSM as described in the Methods section. The values of the bending rigidity coefficient for individual vesicle as well as their averaged values are presented in Fig. 9. The determined value of bending rigidity coefficient did not depend on calculation method used or on the fluorophore type. The only exception was the sample where membranes were labelled with NBD-PC fluorophore and when images were acquired using the SDM. This is likely due to photobleaching of the dye, since NBD is prone to oxidation and the energy of laser used was much higher in the spinning disk system.

3.4. The effect of aqueous phase composition on the bending rigidity coefficient of DOPC and POPC membranes

DOPC and POPC lipid bilayers have been frequently used as models in biophysical studies, therefore numerous experimental data are available in the literature [17]. These data were used to evaluate the consistency of fluorescent-based image acquisition technique with the traditional, phase contrast-based method. There is an excellent agreement between experimental values of bending rigidity coefficient determine for POPC bilayer using phase contrast microscopy and fluorescence confocal microscopies. In the other experiment images of POPC and DOPC vesicles, labelled by fluorescent probe, were acquired for vesicles formed in water or 75 mOsm sucrose solution using both SDM and CLSM. The bending rigidity coefficients were calculated using both; the average-based and statistical methods. For each sample ten randomly selected vesicles were analysed. The obtained values of bending rigidity coefficients are summarized in Table 1.

Data presented in Table 1 indicates that the bending rigidity coefficients of membrane formed from DOPC in water is smaller than the bending rigidity coefficient of POPC bilayer, which is in agreement with the data presented by others [17,50]. The effect of sucrose on the bending rigidity coefficient of POPC membrane was similar to that observed by others for l-stearoyl-2-oleoyl-sn-glycero-3-phosphocholine (SOPC) bilayers [51,52]. Specifically the presence of sucrose has reduced the POPC membrane stiffness. Identical effect has been observed for DOPC membranes by us and others [53]. Those data show that the
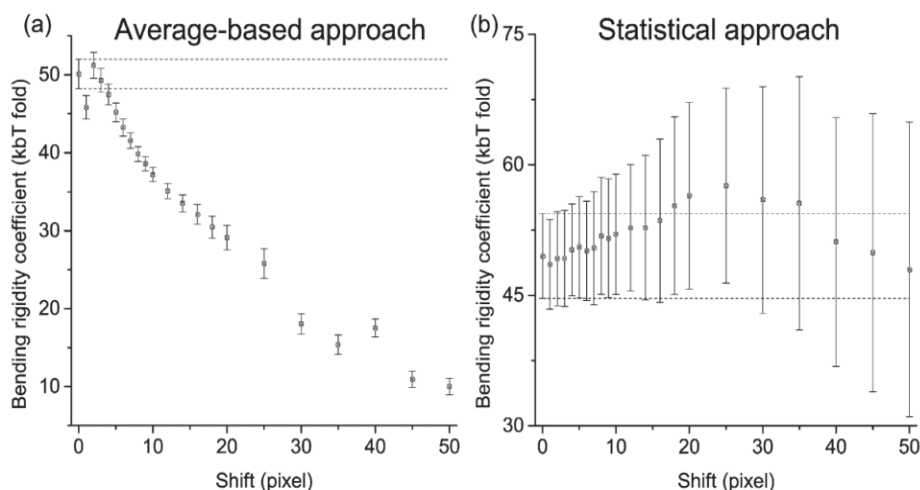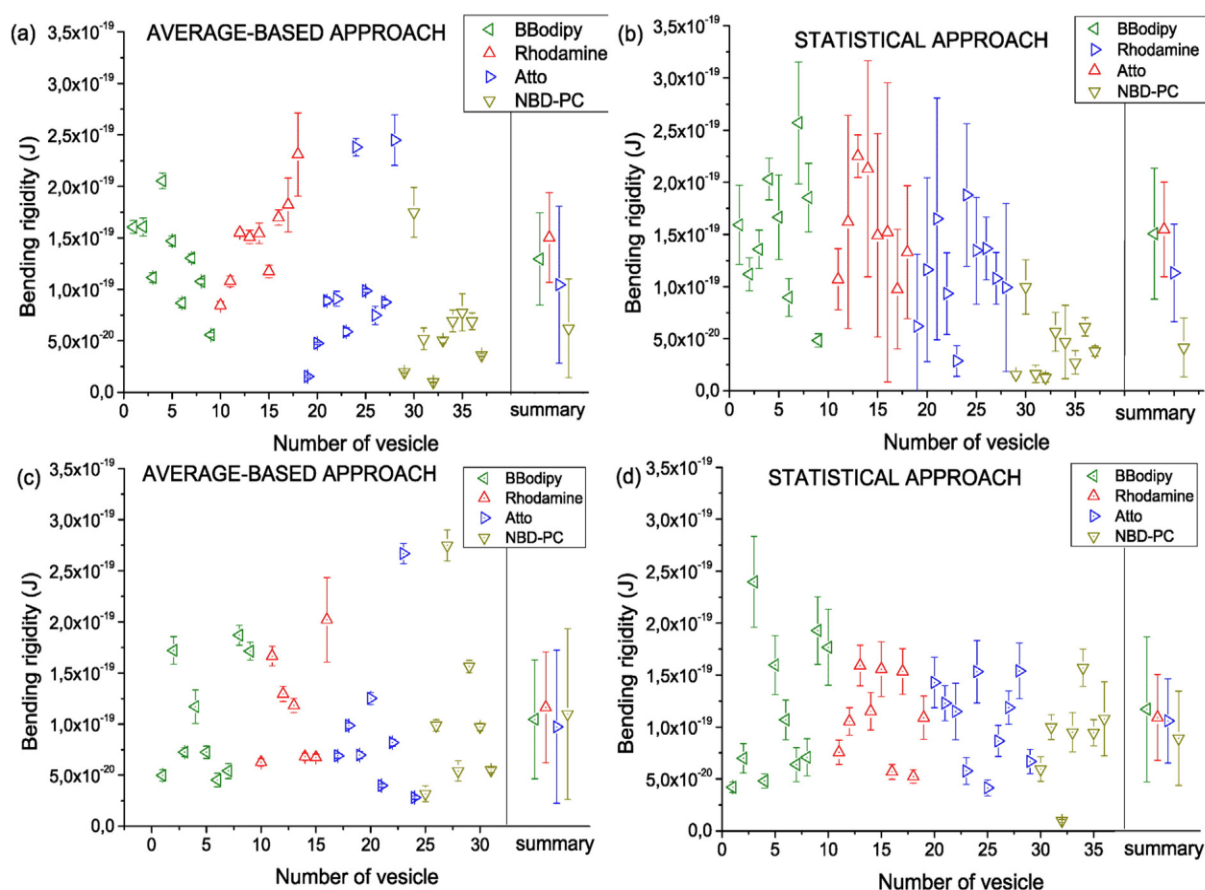

Fig. 8. The effect of the repositioning of the vesicle centre on the bending rigidity coefficient when calculated using the average-based (a) and statistical (b) methods. Dotted lines represent the lower and upper uncertainty level as defined in the text. The images of POPC vesicle were recorded using SDM.

Fig. 9. The effect of fluorescent probe used for POPC vesicle labelling on the bending rigidity coefficient. Vesicles were labelled with β-BODIPY (◄), Rhodamine (▲), Atto (►) and NBD-PC (▼) probes. Images were collected using SDM (top panels) and CLSM (bottom panels). The bending rigidity coefficient was calculated using average-based approach (panels a and c) or statistical approach (panels b and d). The left part of each plot shows values of bending rigidity coefficients obtained for single vesicles whereas the right part shows averaged values.

mechanical properties of the lipid bilayer are the result of a complex interdependences between physical parameters of the sample (temperature), lipid organization and local deformation of lipids (depending on the type of lipid used) and/or interface state (for instance organization of water adjacent to the membrane surface) [17,54–57].

Conclusions

The flicker noise spectroscopy is a method used for the determination of mechanical properties of lipid membranes. The method is based on the quantification of membrane thermal fluctuations from a series of images acquired by phase contrast microscopy. The phase contrast microscopy is an experimental technique performing well when the analysed membrane is homogeneous. The experimental procedure presented in the paper is a modified version of the standard flicker noise spectroscopy, which uses the fluorescence as a contrast for the vesicle contour determination. The fluorescence labelling makes the visualization of any membrane heterogeneities possible. However, the image acquisition using CLSM used for the bending rigidity coefficient determination is inherently slow. To overcome this limitation SDM was used. Despite differences in image acquisition the

measured values of the bending rigidity coefficient were similar for all imaging techniques used. This shows that fluorescence-based slow imaging techniques have no effect on the determined value of the bending rigidity coefficient. In addition the sensitivity of the determined value of the bending rigidity coefficient to various image imperfections, image acquisition time and fluorescence probe used was evaluated. When the membrane lipid was changed from POPC to DOPC the value of the bending rigidity coefficient decreased, showing the direct correlation between membrane mechanical properties and molecular organization of lipids. When the POPC and DOPC membranes were immersed in sucrose solution their rigidity decreased in a matter similar to that reported previously for membranes formed from SOPC. Nevertheless, the experimental protocol described in the paper opens the possibility for studies of membranes having intrinsic tendency for domain formation or where its inhomogeneity is induced by the membrane modifications with surface-active compounds (amphiphiles, peptides or proteins).

Transparency document

The Transparency document associated with this article can be found, in online version.

Table 1
The effect of the lipid and aqueous phase composition on the value of the bending rigidity coefficient [J]. The bending rigidity coefficient of POPC and DOPC lipid bilayers were determined by using the average-based and statistical approaches from images collected by a spinning disk microscope and CLSM.

Sample (T = 24 °C)	SDM — Average-based	SDM — Statistical	CLSM — Average-based	CLSM — Statistical
POPC in sucrose	$13.0 \pm 4.5 \cdot 10^{-20}$	$15.1 \pm 6.3 \cdot 10^{-20}$	$10.5 \pm 5.8 \cdot 10^{-20}$	$11.7 \pm 7.0 \cdot 10^{-20}$
POPC in water	$22.3 \pm 4.2 \cdot 10^{-20}$	$21.2 \pm 9.7 \cdot 10^{-20}$	$20.4 \pm 5.7 \cdot 10^{-20}$	$19.5 \pm 5.7 \cdot 10^{-20}$
DOPC in sucrose	$14.1 \pm 5.4 \cdot 10^{-20}$	$13.3 \pm 4.9 \cdot 10^{-20}$	$13.3 \pm 5.8 \cdot 10^{-20}$	$13.8 \pm 5.7 \cdot 10^{-20}$
DOPC in water	$17.5 \pm 9.8 \cdot 10^{-20}$	$17.8 \pm 8.2 \cdot 10^{-20}$	$16.6 \pm 5.6 \cdot 10^{-20}$	$17.1 \pm 5.6 \cdot 10^{-20}$

Acknowledgements

Appendix A. Supplementary data

Supplementary data to this article can be found online at http://dx.doi.org/10.1016/j.bbamem.2015.11.020.

References

[1] A. Anishkin, S.H. Loukin, J.F. Teng, C. Kung, Feeling the hidden mechanical forces in lipid bilayer is an original sense, Proc. Natl. Acad. Sci. USA 111 (2014) 7898–7905.

[2] C.J. Miller, L.A. Davidson, The interplay between cell signalling and mechanics in developmental processes, Nat. Rev. Genet. 14 (2013) 733–744.

[3] E. Moeendarbary, A.R. Harris, Cell mechanics: principles, practices, and prospects, WIREs Syst. Biol. Med. 6 (2014) 371–387.

[4] J. Fels, P. Jeggle, I. Liashkovich, W. Peters, H. Oberleithner, Nanomechanics of vascular endothelium, Cell Tissue Res. 355 (2014) 727–737.

[5] H. Mohammadi, C.A. McCulloch, Impact of elastic and inelastic substrate behaviors on mechanosensation, Soft Matter 10 (2014) 408–420.

[6] J. Oldenburg, J. de Rooij, Mechanical control of the endothelial barrier, Cell Tissue Res. 355 (2014) 545–555.

[7] N.V. Bukoreshtliev, K. Haase, A.E. Pelling, Mechanical cues in cellular signalling and communication, Cell Tissue Res. 352 (2013) 77–94.

[8] H. Sprong, P. van der Sluijs, G. van Meer, How proteins move lipids and lipids move proteins, Nat. Rev. Mol. Cell Biol. 2 (2001) 504–513.

[9] R.S. Cantor, Lipid composition and the lateral pressure profile in bilayers, Biophys. J. 76 (1999) 2625–2639.

[10] R.S. Cantor, The influence of membrane lateral pressures on simple geometric models pf protein conformational equilibria, Chem. Phys. Lipids 101 (1999) 45–56.

[11] J.W. Shaevitz, D.A. Fletcher, Load fluctuations drive actin network growth, Proc. Natl. Acad. Sci. USA 104 (2007) 15688–15692.

[12] K.J. Van Vliet, G. Bao, S. Suresh, The biomechanics toolbox: experimental approaches for living cells and biomolecules, Acta Mater. 51 (2003) 5881–5905.

[13] S.J. Singer, G.L. Nicolson, The fluid mosaic model for the structure of cell membranes, Science 175 (1972) 720–731.

[14] W. Helfrich, Elastic properties of lipid bilayers: theory and possible experiments, Z. Naturforsch. 28 (1973) 693–703.

[15] S.A. Safran, Curvature elasticity of thin films, Adv. Phys. 48 (1999) 395–448.

[16] M. Angelova, D.S. Dimitrov, A mechanism of liposome electroformation, Progr. Colloid Polym. Sci. 76 (1988) 59–67.

[17] R. Dimova, Recent developments in the field of bending rigidity measurements on membranes, Adv. Colloid Interf. Sci. 208 (2014) 225–234.

[18] D. Boal, Mechanics of the Cell, Cambridge Univer. Press, New York, 2012.

[19] F.L.H. Brown, Continuum simulations of biomembrane dynamics and the importance of hydrodynamic effects, Q. Rev. Biophys. 44 (2011) 391–432.

[20] J. Pecreaux, H.-G. Dobereiner, J. Prost, J.-F. Joanny, P. Bassereau, Refined contour analysis of giant unilamellar vesicles, Eur. Phys. J. E 13 (2004) 277–290.

[21] J.F. Faucon, M.D. Mitov, P. Meleard, I. Bivas, P. Bothorel, Bending elasticity and thermal fluctuations of lipid membranes. Theoretical and experimental requirements, J. Phys. France 50 (1989) 2389–2414.

[22] S. Penic, A. Iglic, I. Bivas, F. M., Bending elasticity of vesicle membranes studied by Monte Carlo simulations of vesicle thermal shape fluctuations, Soft Matter (2015).

[23] J. Henriksen, A.C. Rowat, J.H. Ipsen, Vesicle fluctuation analysis of the effects of sterols on membrane bending rigidity, Eur. Biophys. J. 33 (2004) 732–741.

[24] J. Genova, V. Vitkova, L. Aladgem, P. Meleard, M.D. Mitov, Using stroboscopic illumination to improve the precision of the bending modulus measurement, Bulg. J. Phys. 31 (2004) 68–75.

[25] H. Bouvrais, P. Meleard, T. Pott, K.J. Jensen, J. Brask, J.H. Ipsen, Softening of POPC membranes by magainin, Biophys. Chem. 137 (2008) 7–12.

[26] H.P. Duwe, E. Sackmann, Bending elasticity and thermal excitation of lipid bilayer vesicles: modulation by solutes, Phys. A 163 (1990) 410–428.

[27] J. Henriksen, J.H. Ipsen, Thermal undulations of quasi-spherical vesicles stabilized by gravity, Eur. Biophys. J. 9 (2002) 365–374.

[28] R.S. Gracia, R.L. Knorr, R. Lipowsky, R. Dimova, Effect of cholesterol on the rigidity of saturated and unsaturated membranes: fluctuation and electrodeformation analysis of giant vesicles, Soft Matter 6 (2009) 1472–1482.

[29] A.F. Loftus, S. Noreng, V.L. Hsieh, R. Parthasarathy, Robust measurement of membrane bending moduli using light sheet fluorescence imaging of vesicle fluctuations, Langmuir 29 (2013) 588–594.

[30] R. Parthasarathy, J.T. Groves, Curvature and spatial organization in biological membranes, Soft Matter 3 (2007) 24–33.

[31] L. Bagatolli, P.B.S. Kumar, Phase behavior of multicomponent membranes: experimental and computational techniques, Soft Matter 5 (2009) 3234–3248.

[32] N.C. Megoulas, M.A. Koupparis, Twenty years of evaporative light scattering detection, Crit. Rev. Anal. Chem. 35 (2005) 301–316.

[33] D.G. Watson, C. Atsriku, E.J. Oliveira, Review role of liquid chromatography–mass spectrometry in the analysis of oxidation products and antioxidants in biological systems, Anal. Chim. Acta 492 (2003) 17–47.

[34] J. Schindelin, I. Carreras-Arganda, E. Frise, V. Kaynig, M. Longair, T. Pietzsch, S. Preibisch, C. Rueden, S. Saalfeld, B. Schmid, J.-Y. Tineves, D.J. White, V. Hartenstein, K. Eliceiri, P. Tomancak, A. Cardona, Fiji: an open-source platform for biological-image analysis, Nat. Methods 9 (2012) 676–682.

[35] I. Bivas, P. Hanusee, P. Bothorel, J. Lalanne, O. Aguerre-Chariol, An application of the optical microscopy to the determination of the curvature elastic modulus of biological and model membranes, J. Physique 48 (1987) 855–867.

[36] P. Meleard, T. Pott, H. Bouvrais, J.H. Ipsen, Advantages of statistical analysis of giant vesicle flickering for bending elasticity measurements, Eur. Biophys. J. E 34 (2011) 1–14.

[37] G. Bradski, The OpenCV Library, Dr. Dobb's Journal of Software Tools, 2000.

[38] G. Taubin, Estimation of planar curves, surfaces and nonplanar space curves defined by implicit equations, with applications to edge and range image segmentation, IEEE Trans. PAMI 13 (1991) 1115–1138.

[39] D.W. Marquardt, An algorithm for least-squares estimation of nonlinear parameters, J. Soc. Ind. Appl. Math. 11 (1963) 431–441.

[40] H. Bouvrais, T. Pott, L.A. Bagatolli, J.H. Ipsen, P. Meleard, Impact of membrane-anchored fluorescent probes on the mechanical properties of lipid bilayers, Biochim. Biophys. Acta 1798 (2010) 1333–1337.

[41] H. Bouvrais, M. Holmstrup, P. Westh, J.H. Ipsen, Analysis of the shape fluctuations of reconstitued membranes using GUVs made from lipid extracts of invertebrates, Biology Open 0 (2013) 1–6.

[42] H. Bouvrais, Bending Rigidities of Lipid Bilayers: Their Determination and Main Inputs in Biophysical Studies, Elsevier Inc., Oxford, UK, 2012.

[43] G.B. Behera, B.K. Mishra, P.K. Behera, M. Panda, Fluorescent probes for structural and distance effect studies in micelles, reversed micelles and microemulsions, Adv. Colloid Interf. Sci. 82 (1999) 1–42.

[44] A.P. Demchenko, Y. Mely, G. Duportail, A.S. Klymchenko, Monitoring biophysical properties of lipid membranes by environmental-sensitive fluorescent probes, Biophys. J. 96 (2009) 3461–3470.

[45] R. Sachl, I. Boldyrev, L.B.A. Johansson, Localisation of BODIPY-labelled phosphatidyl-cholines in lipdi bilayers, Phys. Chem. Chem. Phys. 12 (2009) 27–34.

[46] D. Huster, P. Muller, K. Arnold, A. Hermann, Dynamics of membrane penetration of the fluorescent 7-nitrobenz-2-Oxa-1,3-diazol-4-yl (NBD) group attached to an acyl chain of phosphatidylocholine, Biophys. J. 80 (2001) 822–831.

[47] A.S. Klymchenko, R. Kreder, Fluorescent probes for lipid rafts: from model membranes to living cells, Chem. Biol. 21 (2014) 97–113.

[48] T. Tabarin, A. Martin, R.J. Forster, T.E. Keyes, Poly-ethylene glycol induced super-diffusivity in lipid bilayer membranes, Soft Matter 8 (2012) 43–51.

[49] A. Kyrychenko, A molecular dynamics model of rhodamine-labeled phospholipid incorporated into a lipid bilayer, Chem. Phys. Lett. 485 (7 December 2009) 95–99.

[50] N. Kucerka, S. Tristram-Nagle, J.F. Nagle, Structure of fully hydrated fluid phase lipid bilayers with monounsaturated chains, J. Membr. Biol. 208 (2005) 193–202.

[51] J. Genova, A. Zheliaskova, M.D. Mitov, The influence of sucrose on the elasticity of SOPC lipid membrane studied by the analysis of thermally induced shape fluctuations, Colloids Surf.,A 282–283 (2005) 420–422.

[52] J. Genova, A. Zheliaskova, M.D. Mitov, Monosaccharides (fructose, glucose) and disaccharides (sucrose, trehalose) influence the elasticity of SOPC membranes, J. Optoelectron. Adv. Mater. 9 (2006) 427–430.

[53] J.F. Nagle, M.S. Jablin, S. Nagle-Tristram, A. Kiyotaka, What are the true values of the bending modulus of simple lipid bilayers? Chem. Phys. Lipids 185 (2015) 3–10.

[54] L.A. Bagatolli, D. Needham, Quantitative optical microscopy and micromanipulation studies on the lipid bilayer membranes of giant unilamellar vesicles, Chem. Phys. Lipids 181 (2014) 99–120.

[55] D.D. Lasic, D. Needham, The "stealth" liposome: a prototypical biomaterial, Chem. Rev. 95 (1995) 2601–2628.

[56] A. Velikonja, S. Perutkova, E. Gongadze, P. Kramar, A. Polak, A. Maček-Lebar, A. Iglič, Monovalent ions and water dipoles in contact with dipolar zwitterionic lipid headroups — theory and MD simulations, Int. J. Mol. Sci. 14 (2013) 2846–2861.

[57] E. Gongadze, A. Velikonja, Š. Perutkova, P. Kramar, A. Maček-Lebar, V. Kralj-Iglič, A. Iglič, Ions and water molecules in an electrolyte solution in contact with charged and dipolar surfaces, Electrochim. Acta 126 (2014) 42–60.

Supporting information: The modified fluorescence based vesicle fluctuation spectroscopy technique for determination of lipid bilayer bending properties

Dominik Drabik,[a,b]†* Magda Przybyło,[a,b]† Grzegorz Chodaczek,[c] Aleš Iglič[d] and Marek Langner[a,b]

[a] Laboratory for Biophysics of Lipid Aggregates, Department of Biomedical Engineering, Wrocław University of Technology, 50-377 Wrocław, Pl. Grunwaldzki 13, Poland.
[b] Lipid Systems sp. z. o. o. [Ltd], ul. Duńska 9, Wrocław, Poland
[c] Wrocaw Research Centre EIT+, ul Stabłowicka 147, 54-066 Wrocław, Poland.
[d] Laboratory of Biophysics, Faculty of Electrical Engineering, University of Ljubljana, Tržaška 25, SI-1000 Ljubljana, Slovenia.
† authors contributed equally

ABSTRACT: Lipid bilayer is the main constitutive element of biological membrane, which confines intracellular space. The mechanical properties of biological membranes may be characterized by various parameters including membrane stiffness or membrane bending rigidity, which can be measured using flicker noise spectroscopy. The flicker noise spectroscopy exploits the spontaneous thermal undulations of the membrane. The method is based on the quantitative analysis of a series of microscopic images captured during thermal membrane fluctuations. Thus, measured bending rigidity coefficient depends on the image quality as well as the selection of computational tools for image processing and mathematical model used. In this work scanning and spinning disc confocal microscopies were used to visualize fluctuating membranes of giant unilamellar vesicles. The bending rigidity coefficient was calculated for different acquisition modes, using different fluorescent probes and different image processing methods. It was shown that both imaging approaches gave similar bending coefficient values regardless of acquisition time. Using the developed methodology the effect of fluorescent probe type and aqueous phase composition on the value of the membrane bending rigidity coefficient was measured. Specifically it was found that the bending rigidity coefficient of DOPC bilayer in water is smaller than that determined for POPC membrane. It has been found that the POPC and DOPC bending rigidities coefficient in sucrose solution was lower than that in water. Fluorescence imaging makes possible the quantitative analysis of membrane mechanical properties of inhomogeneous membrane.

Depth of focus

All experiments have been performed using dedicated PTT chamber, which allows for the focusing everywhere within the chamber volume. In addition, to ensure that during the image acquisition the vesicle cross-section has been recorded, the vesicle radius has been calculated. Image was discarded from further analysis when the radius variation was large as shown in figure S.1.
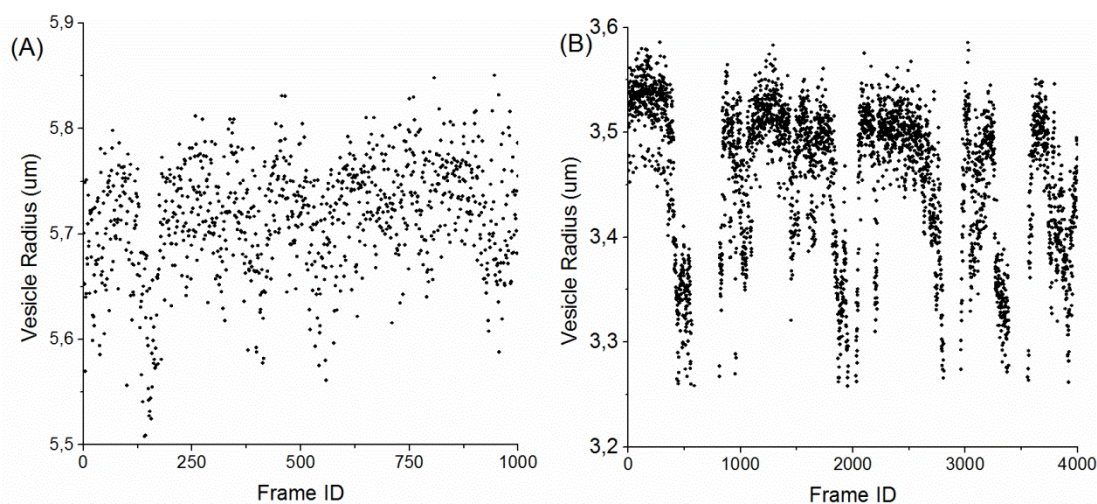

Figure S.1 Examples of vesicle radius variations in subsequent images. Panel A shows the acceptable fluctuation of vesicle radius while fluctuation presented in panel B was considered as unacceptable.

Detailed results for POPC and DOPC systems using Spinning Disk Microscopy (SDM) and Confocal Laser Scanning Microscopy (CLSM)
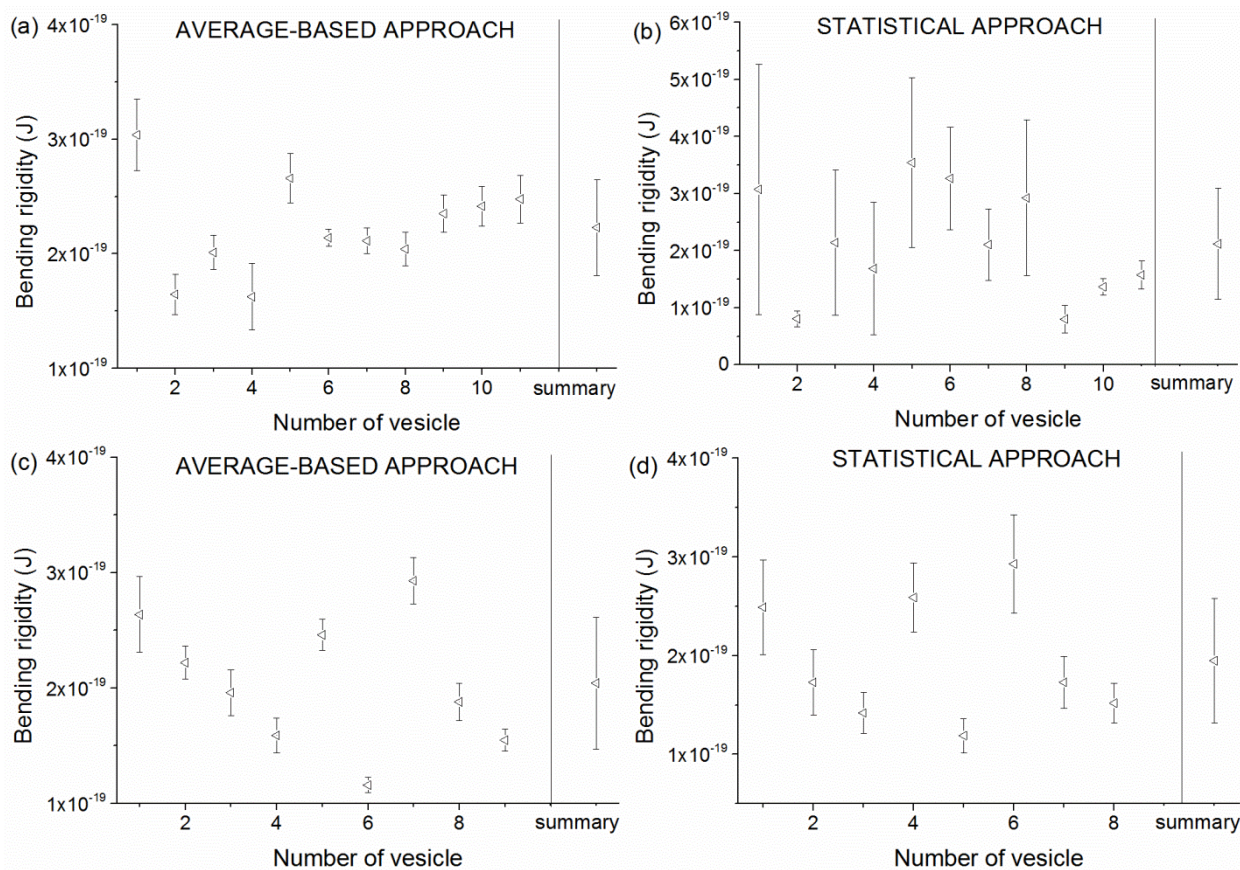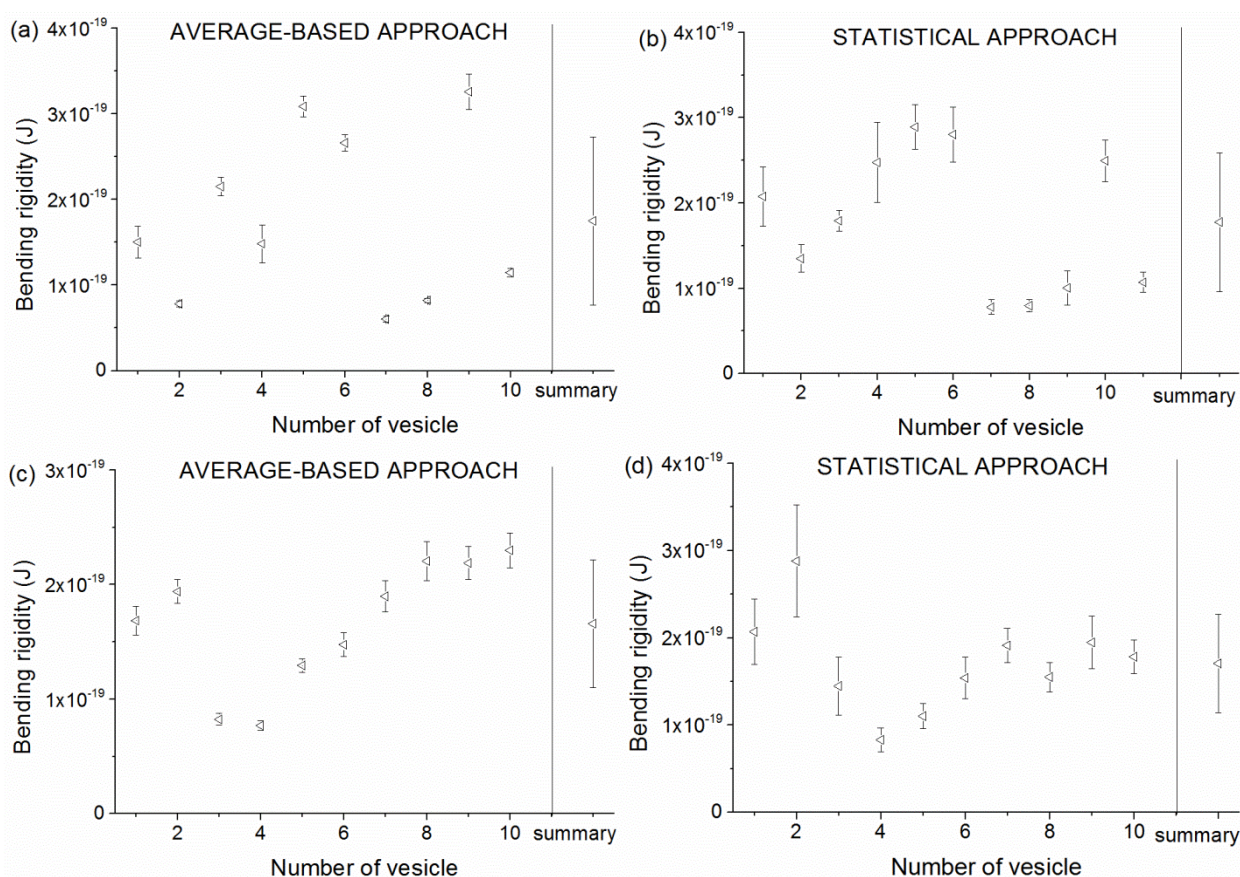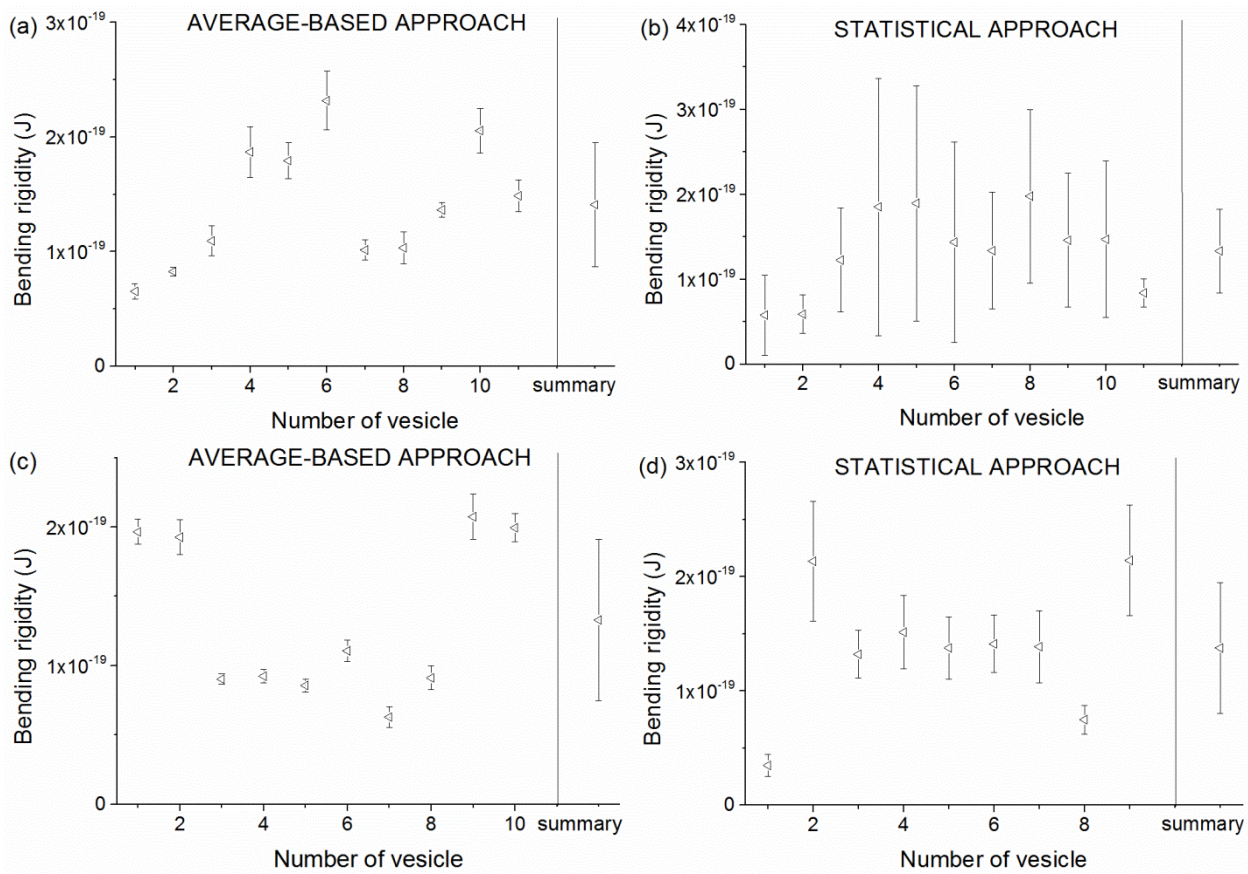
Figure S.2 Bending rigidity coefficients determined for POPC vesicles in water. Images were collected using SDM (top panels) and CLSM (bottom panels). The bending rigidity coefficient was calculated using average-based approach (panels a and c) or statistical approach (panels b and d). The left side of each graph shows values of bending rigidity coefficients obtained for a series of vesicles whereas the right side shows the averaged value. βBodipy FL DHPE was used to label the vesicles.

Figure S.3 Bending rigidity coefficients determined for DOPC vesicles in water. Images were collected using SDM (top panels) and CLSM (bottom panels). The bending rigidity coefficient was calculated using average-based approach (panels a and c) or statistical approach (panels b and d). The left side of each graph shows values of bending rigidity coefficients obtained for a series of vesicles whereas the right side shows the averaged value. βBodipy FL DHPE was used to label the vesicles.

Figure S.4 Bending rigidity coefficients determined for DOPC vesicles in 75mOsm sucrose. Images were collected using SDM (top panels) and CLSM (bottom panels). The bending rigidity coefficient was calculated using average-based approach (panels a and c) or statistical approach (panels b and d). The left side of each graph shows values of bending rigidity coefficients obtained for a series of vesicles whereas the right side shows the averaged value. βBodipy FL DHPE was used to label the vesicles.

LANGMUIR

Article

Mechanical Properties Determination of DMPC, DPPC, DSPC, and HSPC Solid-Ordered Bilayers

Dominik Drabik,* Grzegorz Chodaczek, Sebastian Kraszewski, and Marek Langner

Cite This: https://dx.doi.org/10.1021/acs.langmuir.0c00475

Read Online

ACCESS | Metrics & More | Article Recommendations | Supporting Information

ABSTRACT: Lipid bilayers are active participants in many crucial biological processes. They can be observed in different phases, liquid and solid, respectively. The liquid phase is predominant in biological systems. The solid phase, both crystalline and gel phases, is under investigation due to its resilience to mechanical stress and tight packing of lipids. The mechanical properties of lipids affect their dynamics, therefore influencing the transformation of cell plasma and the endomembrane. Mechanical properties of lipid bilayers are also an important parameter in the design and production of supramolecular lipid-based drug delivery systems. To this end, in this work, we focused on investigating the effect of solid phases of lipid bilayers on their structural parameters and mechanical properties using theoretical molecular dynamics studies on atomistic models of whole vesicles. Those include area per lipid, membrane thickness, density vesicle profiles, bending rigidity coefficient, and area compressibility. Additionally, the bending rigidity coefficient was measured using the flicker noise spectroscopy. The two approaches produced very similar and consistent results. We showed that, contrary to our expectations, bending rigidity coefficients of solid-ordered bilayers for vesicles decreased with an increase in lipid transition temperature. This tendency was reverse in planar systems. Additionally, we have observed an increase of membrane thickness and area compressibility and a decrease of area per lipid. We hope these results will provide valuable mechanical insight for the behavior in solid phases and differences between spherical and planar confirmations.
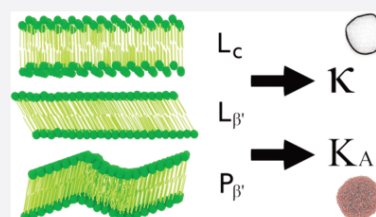
■ INTRODUCTION

Over past few years, lipids have been acknowledged as diverse active participants in many biological processes rather than being simple building blocks of cells components.[1] Lipids and their aggregates, apart from their barrier function, participate in metabolic processes, cytoplasm compartmentalization, and the formation of a dynamic infrastructure for the rearrangement of aqueous compartments. In the fluid mosaic membrane model, disordered bilayers are built by freely moving lipids subject to lateral diffusion. While the model is an effective tool for understanding molecular-level processes, it is unable to rationalize lipid bilayer properties. This is especially relevant in cell physiology, where the occurrence of local defects, the size, and both mechanical and electrostatic properties are necessary for ensuring local molecular homeostasis.[2] The other important feature of the biological membrane is its heterogeneity with respect to lipid composition and physicochemical properties. This gave rise to the membrane raft concept, also sometimes referred to as microdomains. They differ from the surrounding lipid matrix with respect to lipid composition and molecular packing.[3] Furthermore, individual lipid mobility and collective lipid dynamics (i.e., the packing structure and organization) depend on the activity of the surrounding water.[4] The effect of microdomains on the mechanical properties has not been thoroughly investigated.[5] The mechanics of heterogeneous lipid bilayers can be simplified by the investigation of homogeneous lipid bilayers with different lipid dynamics and different hydrocarbon chain

lengths. Typically, there are four states in which the bilayer can be in the crystalline phase, gel phase (together referred to as solid phase), ripple phase, and liquid phase. When the cell membrane is fully hydrated, it is predominantly in the liquid phase. However, it transitions into the gel phase with a reduction in temperature below the so-called main transition temperature (T_m).[6]

The gel phase is mostly observed in long and saturated fatty acid chains. In that phase, the lipid head groups are very tightly packed; the lipid acyl chains become straighter and ordered, and the bilayer thickness increases.[7] The lipid bilayer formed from lipids, whose phase is well-defined at a specific temperature, is a convenient experimental model. For instance, the coexistence of gel and fluid phases has been demonstrated on membranes formed from the mixture of lipids with different T_m's. Such cases were reported for DMPC (1,2-dimyristoyl-*sn*-glycero-3-phosphocholine)−DSPC (1,2-distearoyl-*sn*-glycero-3-phosphocholine), 20:0 DMPC−PC (phosphocholine), and DMPC−DPPC (1,2-dipalmitoyl-*sn*-glycero-3-phosphocholine) mixtures using quick-freeze differential scanning calorimetry[8]

A

as well as for different two-component mixtures of DSPC, DLPC, DMPC, or DAPC using model simulations.[9] From a biological perspective, the membrane is formed from lipids that are mostly unsaturated, and organisms adapt their fatty acid composition to the environment to prevent the formation of solid phases. Despite detecting solid phases in very specific cases of biological membranes like the myelin sheath or stratum corneum,[10] where it is required to form a mechanically resistant lipid barrier, it is generally considered that they do not occur in biological membranes.[11] The lipid bilayer mechanics is also a very significant property for the design of the targeted delivery system. It has been demonstrated that endocytosis depends on the nanoparticle stiffness and shape.[12] The drug carrier mechanics is also important for its stability in serum, specifically by protecting it from undesired interactions such as the interaction with lipoproteins (which are known to interact with lipids and to induce structural changes) and/or blood key proteins.[13]

In this Article, we have focused on mechanical properties of solid phase bilayers as a means to provide information about their behavior. From a general mechanical point of view, lipid systems possess a peculiar combination of elastic properties. The stretching elasticity of the lipid bilayer is described by the area compressibility modulus (K_A; N/m). It is understood that energy is necessary to stretch the bilayer into a direction perpendicular to the bilayer itself. The shear elasticity of the lipid bilayer is understood as the shear between individual lipid molecules. It is negligible in liquid-ordered phases but significant for crystallized membranes. However, the ability to bend under very low stress, the bending elasticity, is perhaps the most interesting one of the mechanical properties.[14] This ability is described by bending elasticity, κ. It is very challenging to measure this parameter as its value is very small (on the order of 10^{-19}–10^{-20} J). Due to the pioneering work of Helfrich,[15] the membrane thermal flickering phenomenon was initially observed in red blood cell membranes.[16] This discovery sparked a significant number of studies involving membrane mechanics and allowed for different approaches to determine the bending elasticity in membrane systems.[5] In this work, we have used two different techniques to determine the mechanical properties of the investigated bilayers. These bilayers consist of lipids with T_m higher than the ambient temperature often used in experimental measurements. We selected four such lipids: DMPC, DPPC, DSPC, and an HSPC (L-α-phosphatidylcholine, mixture of 11.4% DPPC and 88.6% DSPC) mixture. The measuring temperature in the experiments and simulations was selected at 295 K (22 °C). As a result, each of the investigated bilayers are measured in different solid phases. The DMPC bilayer is only 2 K below the transition temperature ($T_m = 297$ K) but, at the same time, higher than both subtransition and pretransition temperatures (287 and 289 K, respectively), which results in a rippled $P_{\beta'}$ gel phase. In the rippled phase, the regions in the gel phases are separated by liquid phases.[17] The DPPC bilayer is measured below its transition and pretransition temperatures (314 and 307 K, respectively) but higher than its subtransition temperature (294 K), which results in the $L_{\beta'}$ gel phase. The DSPC bilayer is measured below the subtransition, pretransition, and transition temperatures (301, 324, and 328 K, respectively), which results in either an L_c stable crystalline phase or a metastable phase transitioning into it. The HSPC bilayer is a mixture of 11.4% DPPC and 88.6% DSPC, which means that there are two

fractions, one of them being in the crystalline/metastable phase and the second one in the gel phase.[6,18] First, we used an experimental flicker noise spectroscopy, a measuring technique that links spontaneous bilayer fluctuations with its mechanical properties. The second technique was molecular dynamics (MD) simulations of small unilamellar vesicles. Due to its nature, it allows great insight into vesicle dynamics. To our knowledge, this is the first approach to measure an HSPC mixture using two different techniques.

■ EXPERIMENTAL METHODS AND PROCEDURES

Materials. Lipids DMPC (1,2-dimyristoyl-sn-glycero-3-phosphocholine), DSPC (1,2-distearoyl-sn-glycero-3-phosphocholine), DPPC (1,2-dipalmitoyl-sn-glycero-3-phosphocholine), and HSPC (L-α-phosphatidylcholine, mixture of 11.4% DPPC and 88.6% DSPC) were purchased from Avanti Polar Lipids (USA). The fluorescent probe Atto488-DOPE was purchased from Atto-Tech (Germany).

Preparation of Giant Unilamellar Vesicles (GUVs). A modified electroformation method was used to model the formation of lipid membranes.[19] Briefly, 20 μL of the chosen lipid in chloroform (3 mM) was deposited in small quantities (as 2 μL droplets) onto platinum electrodes. Two electrodes were set parallel to one another at a distance of 5 mm. The electrodes were kept for 1 h under reduced pressure to remove traces of organic solvents. Next, the electrodes were immersed in preheated pure aqueous solution. As we recently demonstrated,[20] a sufficient electroformation protocol consists of 4 h of electroformation with a 1 Hz AC electrical field applied in an electroformation chamber with the electrical field voltage set to 1 V for the first hour, 2 V for the second hour, 3 V for the third hour, and finally 4 V for the remaining time of the electroformation. In order to obtain GUVs from the investigated lipids, the temperature of the solvent was set at least 20 °C above the transition phase temperature of the investigated lipids (for example, it was 80 °C for HSPC). To this end, a custom glass electroformation chamber similar in design to thermal glasses combined with a heated bath (Lab. Companion RW-0525G, Poland) was used. After electroformation, the sample was left at the elevated temperature for an additional hour without the electrical field applied to allow the descent of the vesicles from the electrodes. Finally, the solution with GUVs was transferred to an unheated glass vial to induce a free decrease of solvent temperature to room temperature.

Acquisition and Assessment of Microscopic Images. The Cell Observer SD spinning disk confocal microscope (Zeiss, Germany) was used for vesicle recording. It was equipped with an α Plan-Apochromat 100×/1.46 oil immersion objective (Zeiss, Germany). 512 × 512 pixel images were recorded with an EMCCD camera (iXon3885, Andor, UK) using 2 × 2 binning with a 0.133 μm pixel size at a rate of 33 frames per second (fps) with a video integration time of 30 ms. At least 5000 images were recorded for each of the vesicles. Samples were illuminated with a 488 nm laser, and emitted light passed through the 527/54 filter. All samples were measured at 22 ± 1 °C (295 K). All measurements have been performed in a dedicated PTFE observation chamber with very limited height (equal to 300 μm) to reduce the effect of uncontrolled vesicle movements. The value of depth of focus was equal to 0.85 μm. To improve further quality of the analysis, the radius of the vesicle was calculated for each image, and when the fluctuations of the radius were unacceptable, as a result of misdetection caused by noise or other reasons described in previous work,[19] the image in the series was discarded from further analysis.

Flicker Noise Spectroscopy Analysis. The flicker noise spectroscopy technique is based on the analysis of vesicle shape fluctuations over time. In short, a membrane fluctuation spectrum was extracted from every single recorded image of the same lipid vesicle. This was performed using custom software.[19] To calculate the bending rigidity coefficient from a set of time-lapsed images, a correlation between the two-dimensional fluctuations and three-dimensional membrane elasticity model was established. This was

B

achieved by calculating the angular autocorrelation function $\xi(\gamma, t)$ defined by eq 1. The cross-sectional radius $\rho(\Phi, t)$ is the position of the vesicle bilayer at a given angle Φ and time t; $\rho(t)$ is an averaged vesicle radius of a given image recorded at time t using eq 2. $R = \langle \rho(t) \rangle$ is the vesicle radius.

$$\xi(\gamma, t) = \frac{1}{2\pi^2 R^2} \int_0^{2\pi} [\rho(\phi + \gamma, t) - \rho(t)] \times [\rho(\phi, t) - \rho(t)] \, d\phi \tag{1}$$

$$\rho(t) = \frac{1}{4\pi} \sum_{i=1}^{N} (\rho_i + \rho_{i+1}) \times (\phi_{i+1} - \phi_i) \tag{2}$$

The bending rigidity coefficient can be determined using two approaches, the statistical approach[19,21] and the averaged-based approach (AVB),[19,22] respectively. In the first one, autocorrelation curves are decomposed as cosine components of Fourier series. Since curves are even functions, sine components were not calculated. The amplitudes of cosine functions for each frame of a given mode m, $\chi^m(t)$, were next histogrammed and fitted by monoexponential distributions $\Gamma^m(\chi^m)$ according to eq 3.

$$\Gamma^m = a \times \exp\left(-R^m\left(\frac{\kappa}{kT}, \overline{\sigma}\right) \times \frac{\chi^m}{2}\right) \tag{3}$$

The monoexponential character of the distribution indicates that the model adequately describes the thermal fluctuations of the membrane. To bridge the bending rigidity coefficient with the obtained distributions, the decays were fitted using the monoexponential function for Γ^m ranging from 0.6 to 0.08. Higher values are omitted due to the low probability of the occurrence, while lower values were omitted due to being too close to the resolution limit. The uncertainty of the Γ^m value was calculated according to eq 4.

$$\Delta\Gamma^m = \frac{R^m}{\sqrt{N}} \times \sqrt{\sum_i \left(\ln\left[\Gamma^m\left(\frac{\chi_i^m}{2}\right)\right] - \ln(a) + R^m \times \frac{\chi_i^m}{2}\right)^2} \tag{4}$$

The bending rigidity coefficient can be determined by fitting eq 5 to the experimentally determined Γ^m values, where σ_{wh} is related to white noise generated by the limited optical resolution of the microscope and the electronic noise generated by the camera. $\mathcal{P}_n^m$ is the normalized Legendre polynomial, and $\lambda_n(\overline{\sigma})$ is the function related to the reduced membrane tension ($\overline{\sigma}$) defined by eq 6.

$$R^m\left(\frac{\kappa}{kT}, \overline{\sigma}, \sigma_{wh}\right) = \frac{1}{\frac{\kappa}{kT}\left(\sum_{n \geq m}^{n_{max}} \frac{[\mathcal{P}_n^m(0)]^2}{\lambda_n(\overline{\sigma})}\right) + \sigma_{wh}^2} \tag{5}$$

$$\lambda_n(\overline{\sigma}) = (n+1)(n+2)[\overline{\sigma} + n(n+1)] \tag{6}$$

In the average-based approach, angular autocorrelation curves (eq 1) are decomposed in the Legendre polynomial series. The decomposition is described by eq 7, where $B_n(t)$ with physical meaning (only positive values) is averaged over the position to obtain $\langle B_n \rangle$. Obtained $\langle B_n \rangle$ values are then plotted as a function of fluctuation mode number, and the bending rigidity coefficient is determined (eq 8). In the equation, k_B is the Boltzmann constant.

$$\xi(\gamma, t) = \langle B_0 \rangle \times P_0(\cos\gamma) + \sum_{n=2}^{n_{max}} B_n(t) \times P_n(\cos\gamma) \tag{7}$$

$$\langle B_n \rangle \cong B_n(\kappa, \overline{\sigma}) = \frac{2n+1}{4\pi} \times \frac{k_B T}{\kappa(n+2)(n-1)[\overline{\sigma} + n(n+1)]}$$

for $n > 1$ \tag{8}

Molecular Dynamics Simulations.
The full-atomistic molecular dynamics simulations were performed using NAMD 2.9[23] software with CHARMM36 united-atom force field[24] under NPT conditions (constant: number of particles, pressure, and temperature). The bending rigidity coefficient and area compressibility were determined

for POPC, DMPC, DSPC, DPPC, and HSPC lipid vesicles. Each of the vesicles was modeled separately as a liposome with a 10 nm radius, and both sides were hydrated with TIP3P water molecules, giving a final simulation box of 30 nm³. Three dimensional periodic boundary conditions were applied in order to deal with potential energy disruption due to the origin cell discontinuity. The vesicle system was created using a custom script in MATLAB. The starting area per lipid (APL) value was chosen to be 65.7 Å² for DPPC, 70 Å² for DMPC, 68.1 Å² for POPC, and 63.8 Å² for DSPC on average, respectively.[25] The APL was corrected to account for the effect of the vesicle's curvature by multiplying the APL value by 0.95 and 1.05 for inner and outer leaflets, respectively. This correction is a result of conclusions drawn by Braun and Sachs.[26] Vesicle systems, after the standard equilibration procedure, were subjected to at least the 10 ns production run and then analyzed. In order to determine a stable time point of equilibration, six selected parameters (mean values and standard deviations of both inner and outer leaflets, vesicle radius, and the thickness of the lipid bilayer) were continuously monitored. This was followed by determination of the order parameter drift. More detailed information regarding the setup of the systems and their properties are presented in Section 1 of the Supporting Information. Additionally, planar bilayers were simulated under the same conditions with 648 lipid molecules and a hydration level of 20 Å for comparison (details are presented in Section 4 of the Supporting Information).

Determination of Bending Rigidity Coefficient in MD. The bending rigidity of model lipid vesicles was determined according to the algorithm developed by Braun and Sachs.[26] It has an advantage over other approaches,[27] as it determines mechanical properties based on fluctuations of the bilayer within the vesicle. In short, each lipid is described by a vector spreading from the head (phosphorus atom) up to the tail position (midpoint of both 16th carbon atoms in each of the tails). This is followed by discrete surface representation θ, φ using a grid. For each time point, the surface of the fluctuations is established by the detection of the origin point of the fitted sphere, the conversion of the bilayer fluctuations into spherical coordinates, and the subtraction of the radius value. Finally, the average of both the inner and outer leaflet fluctuations is calculated. This is followed by spectral harmonics analysis (SPHA) for calculated fluctuations $f(\theta, \varphi)$. The fluctuations are represented as a linear combination of spherical harmonics with degree l and order m. Eventually, Helfrich's approach can be employed as described by eq 9, where a_{lm} is the spherical harmonic coefficient and Y_{lm} is the spherical harmonic basis function described by eq 10. The term $\tilde{P}_l^m$ defines the fully normalized associated Legendre polynomials.

$$f(\theta, \varphi) = \sum_{l,m} a_{lm} Y_{lm} \tag{9}$$

$$Y_{lm} = \tilde{P}_l^m(\cos\theta) e^{im\varphi} \tag{10}$$

In order to determine the values of the spherical harmonic coefficient, inverse transformation is used. To this end, matrix $\mathbf{P}$ for a given θ, φ distribution is generated, as presented in eq 11, where $l_i \in 0, ..., l_{max}$,

$$\mathbf{P}_{l_i}^m = \begin{bmatrix} \begin{pmatrix} \tilde{P}_0^m(\cos\theta_1) & \cdots & \tilde{P}_{l_i}^m(\cos\theta_1) \\ \vdots & \ddots & \vdots \\ \tilde{P}_0^m(\cos\theta_N) & \cdots & \tilde{P}_{l_i}^m(\cos\theta_N) \end{pmatrix} \end{bmatrix}^T \tag{11}$$

from which the matrix $\mathbf{Y}$ can be written as the spherical harmonic forward transformation (eq 12). In this equation, a_{lm}^1 is a recasting of spherical harmonic coefficients a_{lm} with dimensions corresponding to the row construction of $\mathbf{Y}$, and $f_{\theta,\varphi}^1$ is the matrix of the bilayer position.

$$Y a_{lm}^1 = f_{\theta,\varphi}^1 \tag{12}$$

In order to calculate the inverse transformation (eq 13), the FACTORIZE package[28] in MATLAB was used. This allowed one to
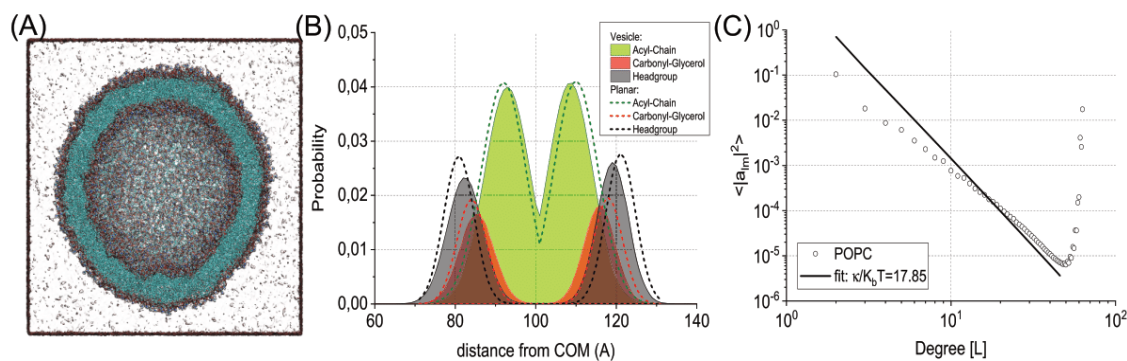
Figure 1. Molecular dynamics simulations of POPC membrane systems at 295 K. (A) A snapshot of the POPC vesicle cross-section in the water box. (B) Comparison of bilayer profiles for the POPC vesicle and the POPC planar system. (C) Undulation power spectra for the POPC vesicle system with the corresponding bending rigidity fit.

compute the approximation of the pseudoinverse of $\mathbf{Y}$ and apply it to determine a_{lm}^1.

$$\mathbf{Y}^{-1} f_{\theta,\varphi}^1 = a_{lm}^1 \tag{13}$$

From a_{lm}^1, the undulation power spectrum can be obtained by the binning modulus of the spherical harmonic coefficients across degree l. The resulting profile can be interpreted according to the Helfrich continuum model for undulations on a sphere with vanishing spontaneous curvature (eq 14), where T is temperature and k_B is the Boltzmann constant.

$$|a_{lm}|^2 = \frac{k_B T}{\kappa[l^2(l+1)^2 - 2l(l+1)]} \tag{14}$$

Determination of Basic Structural Parameters. Additional structural parameters were determined from MD simulations. Those include membrane thickness (MT), area per lipid (APL), and vesicle density profiles. For each frame, a sphere fit to the phosphorus atoms in the inner leaflet and in the outer leaflet and to all phosphorus atoms was done in order to obtain the radius for the inner leaflet, for the outer leaflet, and for the whole vesicle, respectively. MT was calculated as a difference between the radius of the outer and inner layers. APL, for the whole vesicle and each of the leaflets separately, was calculated according to eqs 15−17 as proposed by Braun and Sachs.[26]

$$\text{ALP}_{\text{vesicle}} = \frac{4\pi r_{\text{vesicle}}^2}{\frac{1}{2}(n_{L,\text{inner}} + n_{L,\text{outer}})} \tag{15}$$

$$\text{APL}_{\text{inner}} = \frac{4\pi r_{\text{inner}}^2}{n_{L,\text{inner}}} \tag{16}$$

$$\text{APL}_{\text{outer}} = \frac{4\pi r_{\text{outer}}^2}{n_{L,\text{outer}}} \tag{17}$$

In order to determine the density vesicle profiles, three crucial zones of each vesicle in the lipid molecule particles were distinguished: headgroups, carbonyl−glycerol, and acyl chains. The vesicle center of mass is established with respect to all lipid molecule particles, which is followed by calculating the distance between particles and the established center of mass. This was done for at least the 100 last frames of the system. Eventually, the positions of the particles were histogrammed and fitted with a normal distribution.

Determination of Area Compressibility in Molecular Dynamics. In order to determine area compressibility (K_A), a method by Waheed and Edholm was used.[29] It allows one to separate the contributions from area fluctuations and undulations. First, the apparent area compressibility is calculated using eq 18, where A is the area of the system (calculated from the radius of the vesicle) and $\langle \delta A^2 \rangle$ is its mean square displacement.

$$K_A^{\text{app}} = \frac{A \times k_B T}{\langle \delta A^2 \rangle} \tag{18}$$

Undulations and area changes in the curved surface occur independently of each other. The true value of area compressibility is determined using eq 19 for systems with low surface tension and eq 20 for systems with high surface tension.

$$\frac{1}{K_A^{\text{true}}} = \frac{1}{K_A^{\text{app}}} - \frac{A \times k_B T}{32\pi^3 \kappa^2} \tag{19}$$

$$\frac{1}{K_A^{\text{true}}} = \frac{1}{K_A^{\text{app}}} - \frac{A \times k_B T}{16.6\pi^3 \kappa^2} \tag{20}$$

■ RESULTS AND DISCUSSION

Validation of the Numerical Approach. In order to verify whether the numerical approach was correctly adapted, a well-characterized POPC lipid bilayer (TT = −2 °C, Figure 1A) was used as a reference.[5] The simulation system was equilibrated for 98 ns followed by an analysis time of 65 ns. Calculated membrane thickness (MT) was equal to 3.425 ± 0.008 nm. This result is slightly larger than in NMR experimental work, where it was equal to 3.05[30] or 2.98 nm.[31] On the other hand, the result was smaller than the membrane thickness (MT) obtained by X-ray scattering, which was equal to 3.9 ± 0.1 nm.[25] The calculated value of MT is also slightly smaller than the results from the MD studies of planar lipid bilayers ranging from 3.8[32] to 3.95 nm.[33] Since the result is within the range of reported values, it is considered correctly calculated.

The calculated area per lipid (APL) was equal to 57.7 ± 0.1 A°² in the inner leaflet and 65.4 ± 0.1 A°² in the outer leaflet. The APL calculated for the whole vesicle was equal to 61.4 ± 0.1 A°². Similar results were reported in the literature 40−65 A°².[27a,34]

The calculated vesicle density profile is presented in Figure 1B. For comparison, a profile calculated from the planar lipid bilayer is also included in the plot. While positions of the peaks representing membrane regions are similar for both systems, the distributions are different. In the planar system, the distributions are broader than these calculated for a vesicle. This indicates a higher mobility of lipids in a model system characterized by a lower curvature. This can be easily observed by looking at the peak of the carbonyl−glycerol groups (red dashed curve and red area in Figure 1B). In most experimental techniques, lipid vesicles are used as a model, for instance, to determine MT. Quantitative values of structural parameters

calculated using the presented simulation model of the POPC vesicle are in good agreement with experimental data and simulations presented by others.

Finally, the bending rigidity coefficient was calculated and was equal to 7.40×10^{-20} J (which corresponds to $17.85\kappa/K_{b}T$ as shown in Figure 1C). This result is in good agreement with the bending rigidities obtained from other molecular dynamics studies.[27a,34] It was also within the limits of the reported experimental value based on the number of vesicles ($N = 10$) and equal to $(10.5 \pm 5.8) \times 10^{-20}$ J.[19] Calculated area compressibility (K_{A}) was equal to 0.23 N/m. Again, determined values for the vesicle model were in excellent agreement with other computational (0.24−0.28 N/m)[35] and experimental studies (0.18−0.33 N/m).[36] In summary, the presented computational approach delivers structural and mechanical data for the POPC (liquid) lipid bilayer, which is in good agreement with the results presented by others. Next, the computational approach combined with the experimental studies will be employed to characterize lipid bilayers in solid phases.

Basic Structural Properties. Table 1 presents calculated basic structural properties of the investigated solid-phase lipid vesicles. When one compares the results of APL obtained from vesicle simulations with literature data, significant differences in parameters can be observed.[25] In the investigated bilayers, it was determined that the APL for DPPC and DSPC systems is lower than for the corresponding measured experimental value by 20 and 17 Å², respectively. In the DMPC system, the value of the APL was in agreement with the membrane in the fluid phase. Additionally, this agreement was also confirmed by another MD simulation[26] and the experiment at 303 K.[37] Furthermore, for each of investigated vesicles, it was determined that the APL in the inner monolayer is higher than the one in the outer layer with the exception for DSPC and POPC systems. Such a difference was already reported in the literature. It was presumed by Braun and Sachs that its occurrence is caused by greater tension in the inner leaflet and tighter position distribution (as a result of unbalance in water density or lipid density across the vesicle).[26] Interestingly, during DMPC simulation, an occurrence of a spontaneous water pore was observed. It remained open until the balance of water densities inside and outside the lipid vesicle was reached, which has been followed by its closure. The observation is in good agreement with data presented by others.[38] Such an event can be explained by the fact that the DMPC membrane is in the rippled-gel phase, where the existence of interdigitated regions occurs. The starting points of the vesicle systems are lipids set opposite to each other. During the initial stages of simulation, an interdigitated region would need to emerge, which could result in high lateral pressure, resulting in spontaneous water pores and/or lack/excess of water to allow the appropriate confirmation for the interdigitated regions to emerge. Interestingly, a significant difference between the APL for the inner and outer layers was observed in the DMPC system. It was not observed in any other of the investigated systems. Hence, we believe that the difference is imposed by the system itself. Interestingly, the APL of the DMPC system is closer to the POPC system rather than the gel systems, which might suggest a high influence of the interdigitated regions in the rippled-gel phase. For liposomes consisting of lipids with high T_{m} (HSPC, DPPC, and DSPC), the determined APL was lower by about 20 Å² than that of the DMPC/POPC system. This well-known dependency[39] can be

Table 1. Summary of Calculated Parameters from a Molecular Dynamics (MD) Study and Flicker Noise Spectroscopy Measurements for Gel Phase Lipid Vesicles[a]

| lipid type	membrane thickness [nm]	APL of vesicle [Å²]	APL of inner membrane [Å²]	APL of outer membrane [Å²]	κ (MD, vesicle) [J]	κ (flicker, AVB) [J]	κ (flicker, SA) [J]	K_{A} (MD) [N/m]	κ (MD, planar) [J]
POPC	(3.425 ± 0.008)	(61.4 ± 0.1)	(57.7 ± 0.1)	(65.4 ± 0.1)	7.40×10^{-20}	$(12 \pm 7) \times 10^{-20}$	$(10.5 \pm 2.2) \times 10^{-20}$	0.23	$(10.8 \pm 0.3) \times 10^{-20}$
DMPC	(3.140 ± 0.007)	(60.5 ± 0.1)	(72.1 ± 0.1)	(56.3 ± 0.1)	7.22×10^{-20}	$(6.0 \pm 2.0) \times 10^{-20}$	$(5.3 \pm 2.2) \times 10^{-20}$	0.25	$(11.7 \pm 0.4) \times 10^{-20}$
DPPC	(4.059 ± 0.003)	(45.6 ± 0.1)	(47.2 ± 0.1)	(46.8 ± 0.1)	4.28×10^{-20}	$(5.3 \pm 3.0) \times 10^{-20}$	$(5.0 \pm 3.3) \times 10^{-20}$	0.31	$(23 \pm 1) \times 10^{-20}$
DSPC	(4.297 ± 0.004)	(46.8 ± 0.1)	(47.4 ± 0.1)	(48.5 ± 0.1)	3.74×10^{-20}	$(4.5 \pm 2.6) \times 10^{-20}$	$(5.0 \pm 2.4) \times 10^{-20}$	0.57	$(19.9 \pm 1.1) \times 10^{-20}$
HSPC	(4.290 ± 0.006)	(46.1 ± 0.1)	(45.6 ± 0.1)	(48.4 ± 0.1)	3.55×10^{-20}	$(3.5 \pm 1.8) \times 10^{-20}$	$(2.9 \pm 2.0) \times 10^{-20}$	0.26	$(23.2 \pm 1.8) \times 10^{-20}$

[a]APL, area per lipid; κ, bending rigidity coefficient; AVB, average-based approach; SA, statistical approach; K_{A}, true value of area compressibility.

E
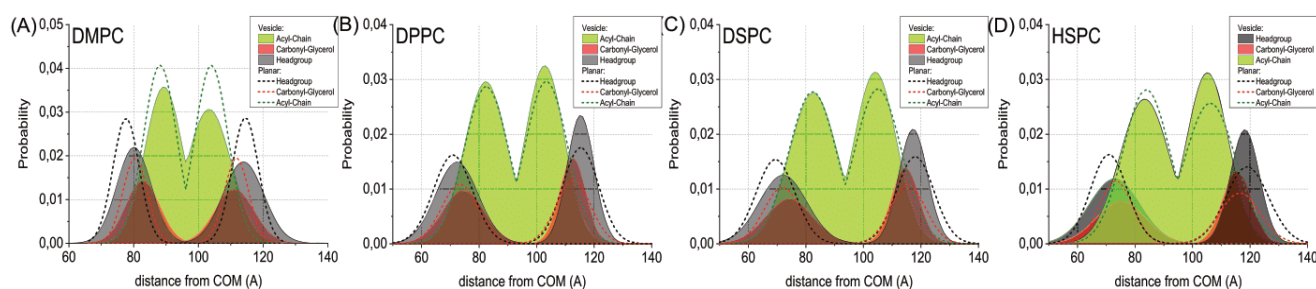
Figure 2. Comparison of component atom probabilities for (A) DMPC, (B) DPPC, (C) DSPC, and (D) HSPC lipid bilayers in molecular dynamics vesicle studies.
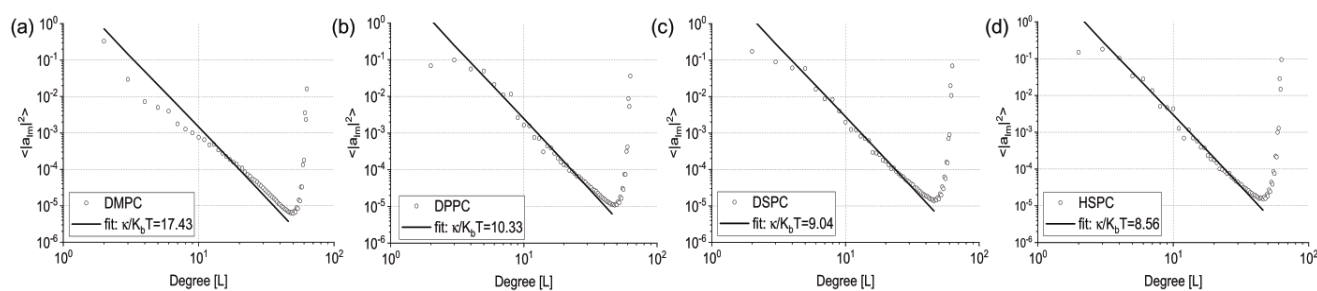
Figure 3. Fluctuations of the power spectra for (A) DMPC, (B) DPPC, (C) DSPC, and (D) HSPC vesicle systems with the corresponding bending rigidity (κ) fit.

explained by denser packing of lipid tails when the membrane is at a temperature substantially lower than the T_m. In the case of membrane thickness, a simple dependency is known: the higher the transition temperature of lipids, the higher is the membrane thickness of the bilayer.[39] Our results are in agreement with it. Similar conclusions can be drawn when analyzing density vesicle profiles in Figure 2. It can be observed that the main influence of the membrane thickness comes from the width of the acyl chain position population. The population width is smaller in DMPC, resulting in smaller MT contrary to other investigated bilayers. Furthermore, the profile does not change when the bilayer becomes heterogeneous as can be observed in the case of the HSPC bilayer. Profiles determined for the DSPC and DPPC lipids also remain the same in the case of the HSPC bilayer. All of the investigated vesicles sustained their quasi-spherical geometry.

Mechanical Parameters Determination. The bending rigidity coefficient was obtained using both computational and experimental approaches. The determined bending rigidity coefficients are presented in Table 1. The power spectra of the investigated lipid bilayers obtained using MD studies along with model fits are shown in Figure 3. Additionally, mechanical properties were determined for planar systems using the real-space fluctuation method (details are presented in Section 4 of the Supporting Information).

The value of the bending rigidity coefficient from the MD simulations for the DMPC lipid bilayer was equal to 7.22×10^{-20} J at 295 K. This value is slightly lower than the values for the DMPC bilayers obtained in our simulation of the flat-patch system (-1.2×10^{-19} J). The obtained values of the DMPC bending in the literature are for the bilayer in the liquid phase; however, they are presented to show the effect of the different phases. The obtained values for the ripple phase are lower than those reported in the literature for the liquid phase: -1.3×10^{-19} J for vesicle and 2.1×10^{-19} J for the flat-patch system ($T = 303$ K),[26] 1.45×10^{-19} J for the flat-patch system ($T = 303$

K),[40] and 1.22×10^{-19} J for the flat-patch system ($T = 303$ K).[35] Such a variation of the bending rigidity coefficient for the DMPC bilayers can be somewhat explained by the phase, topology, and/or water model. As reported in ref 41, the mechanical properties of the DMPC lipid bilayer, especially in gel/rippled phases, are very sensitive to temperature changes, especially when near T_m. A difference of 1 order of magnitude was reported in bending rigidity coefficient values of the DMPC lipid bilayer when changing the temperature from 293 to 296 K. It was shown that changes in the topology of the lipid bilayer influence the bending rigidity coefficient. For instance, vesicle systems tend to show generally smaller values compared to flat-patch systems in the MD simulation, although simulations were performed in the liquid phase (303 K).[26] It was also reported[26] that a small increase in the number of water molecules in the initial system can influence the obtained bending rigidity coefficient from 6.1×10^{-20} J up to 1.3×10^{-19} J for the DMPC system. Furthermore, as reported by Levine et al.,[27b] the value of the bending rigidity for another bilayer type, a DPPC bilayer, can differ significantly from 3.0×10^{-20} J up to 1.9×10^{-19} J, depending on the numerical approach used. All these factors can, in extreme cases, sum up to the difference of the magnitude in the value of the bending rigidity coefficient. Therefore, it is crucial to compare calculated values with experimental ones. According to the calculations, the area compressibility was equal to 0.25 N/m for the DMPC system. While this value is well within the range of values reported in the literature, a significant discrepancy in the literature can be found. The area compressibility for DMPC using the MD simulations was reported to be 0.25 N/m,[35] 0.23 N/m with a micropipette (temperatures not provided),[42] and decreased from 0.56 to 0.40 N/m with an increase of temperature from 300 up to 340 K with Neutron Spin Echo spectroscopy.[43]

In our MD simulations, the obtained value of the bending rigidity coefficient for the DPPC bilayer was equal to $4.28 \times$

F
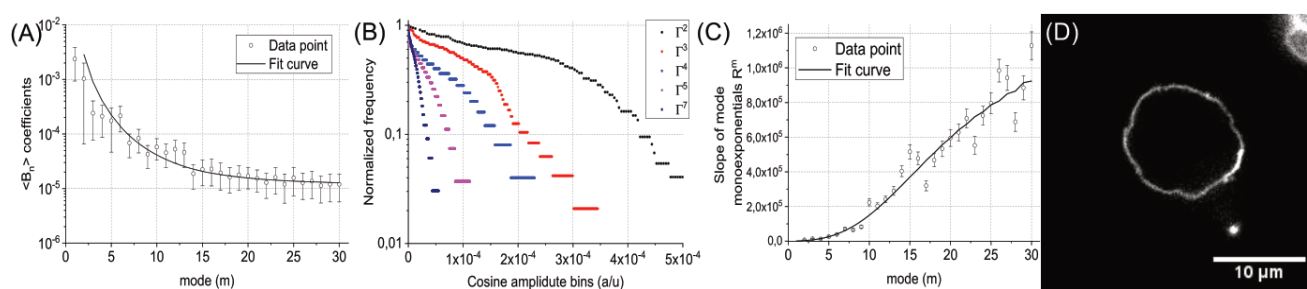
Figure 4. Flicker noise analysis of the HSPC vesicle. (A) Model fit of the $\langle B_n \rangle$ dependency on mode in the average-based approach. (B) Distribution Γ_m of shape fluctuations acquired by cosine decomposition in the statistical approach. (C) Model fit of slope R_m dependency on mode in the statistical approach. (D) Image of an HSPC vesicle with an oddly rectangular shape.

10^{-20} J at 295 K. This value is an order lower than the one we obtained for the flat-patch system (-2.3×10^{-19} J). Furthermore, this result differs by 1 order of magnitude from the values for the DPPC bilayer reported in the literature, which are 1.52×10^{-19} J for the flat-patch system ($T = 303$ K),[40] 1.56×10^{-18} J for the flat-patch system ($T = 323$ K),[27b] and 1.58×10^{-19} J for the flat-patch system ($T = 323$ K),[35] but we also found a much closer value to our finding of 4.52×10^{-20} J in the flat-patch system ($T = 323$ K).[44] It has to be noted that systems in the literature are above T_m; therefore, the comparison should be understood as an effect of phase change rather than a direct value comparison. Interestingly, the bending rigidity obtained for our flat-patch system is slightly higher than for those reported in the literature; however, this can also be explained by the phase difference. The area compressibility was equal to 0.31 N/m with our MD study. Similarly, the discrepancy can be observed with the area compressibility for DPPC equal to 0.21−0.23 N/m, depending on the size of the system in the MD studies,[35] 0.23 N/m with micropipette measurements (temperatures not provided),[42] and 0.56 N/m in 320 K with Neutron Spin Echo spectroscopy.[43]

Finally, bending rigidity coefficients for the DSPC and HSPC lipid bilayers obtained by the MD simulations were equal to 3.74×10^{-20} and 3.55×10^{-20} J, both at 295 K, respectively. Those values, yet again, were lower than the bending rigidities obtained in our flat-patch simulations. Those were equal to 2.0×10^{-19} and 2.3×10^{-19} J for DPSC and HSPC, respectively. No literature value for the bending rigidity coefficient was found for those bilayers. Area compressibility values were equal to 0.57 and 0.26 N/m for DSPC and HSPC lipid bilayers, respectively. Only the area compressibility for DSPC is available from the literature; it was reported to decrease from 0.50 down to 0.45 N/m with the temperature rising from 330 to 340 K using Neutron Spin Echo spectroscopy.[43] These results are consistent with ours since the temperature set in our simulations is 295 K. Therefore, the value of area compressibility should be higher, considering the dependence provided in the literature.

The calculated parameters were confronted with experimental values of the bending rigidity coefficient determined with the flicker noise technique. The experimental values presented in Table 1 are averaged over at least 10 vesicles. They are calculated using two different approaches: statistical and average-based (AVB) ones. An example of fluctuation distribution and model fits using both approaches is presented in Figure 4A−C. The details on individual measurements are presented in the Supporting Information in Section 3. Additionally, it should be noted that GUVs created from

lipids with a T_m higher than room temperature tend to form oddly rectangular shapes rather than typical quasi-spherical ones. This is shown in Figure 4D and was not observed in our MD studies. The reason for this is probably due to the small size of the simulated vesicles and/or lack of the lipid bilayer rapid phase change in MD simulations.

Using flicker noise spectroscopy, the obtained values of the bending rigidity coefficient for the DMPC lipid bilayer using AVB and statistical approaches were equal to $(5.3 \pm 2.2) \times 10^{-20}$ and $(6.0 \pm 2.0) \times 10^{-20}$ J, both at 295 K, respectively. When compared to the literature, the values can be either within the range of error or even an order of magnitude higher, depending on the temperature, method, and data processing used. Using spin echo spectroscopy, the value of the bending rigidity coefficient for the DMPC bilayer was equal to 1.5×10^{-19} J at 300 K and 9.4×10^{-20} J at 340 K.[43] Using an optical dynamometry study, the value decreased from 2×10^{-18} to 4×10^{-20} J by increasing the temperature from 293 to 296 K.[41] Using flicker noise spectroscopy, the value was reported to be 1×10^{-19} J for 298 K.[45] Using the all-optical method, the value was equal to $(1.41 \pm 0.13) \times 10^{-19}$ J for 300 K and $(1.33 \pm 0.12) \times 10^{-19}$ J for 303 K,[46] respectively.

The experimentally determined bending rigidity coefficients for the DPPC lipid bilayer obtained with AVB and statistical approaches were equal to $(5.0 \pm 3.3) \times 10^{-20}$ and $(5.3 \pm 3.0) \times 10^{-20}$ J, both at 295 K, respectively. The measured value is lower than those reported with other experimental results. Specifically, with AFM indentation, the value of the bending rigidity coefficient for the DPPC bilayer was equal to 1.55×10^{-18} J for the vesicle system and 2.03×10^{-19} J for the supported lipid bilayer system at 293 K.[47] In another AFM study, the value was equal to $(1.3 \pm 0.1) \times 10^{-18}$ J.[48] Using spin echo spectroscopy, the value was equal to 2.08×10^{-19} J for 320 K.[43]

For the DSPC bilayer, the bending rigidity coefficient was equal to $(5.0 \pm 2.4) \times 10^{-20}$ and $(4.5 \pm 2.6) \times 10^{-20}$ J at 295 K using AVB and statistical approaches, respectively, in our study. Using spin echo spectroscopy, the value was equal to 2.28×10^{-19} J for 330 K.[43] There was no agreement between the results, probably due to the temperature difference.

Finally, for the HSPC bilayer, the values were equal to $(3.5 \pm 1.8) \times 10^{-20}$ and $(2.9 \pm 2.0) \times 10^{-20}$ J for 295 K using AVB and statistical approaches, respectively. No literature data regarding the bending rigidity of the HSPC bilayer is available.

It is well-known that different techniques yield inconsistent values for the bending rigidity coefficient.[49] Such discrepancies in the reported data are not surprising. On the other hand, the difference in the reported values of the bending rigidity between both vesicle simulation and flicker noise spectroscopy

G

and both flat-patch simulations and the literature value is quite puzzling, especially given the fact that values of membrane thickness and APL are in agreement with the literature; additionally, there is an agreement for bending rigidity values between performed experimental calculations and simulations. It also should be noted that the obtained bending rigidity modulus from flicker noise spectroscopy compares very well with our theoretical simulations of the vesicles. When T_m of the investigated lipids is taken into account, an additional dependency can be found. It can be observed that the bending rigidity coefficient of the bilayers consisting of low T_m lipids are almost twice the value of bilayers consisting of lipids with higher T_m (difference between 7.22×10^{-20} and 3.55×10^{-20} J). This is, however, contrary to what we got when the bending rigidity was determined for flat-patch systems. This is also contrary to what one might expect, as a bilayer in the gel phase exhibits shear elasticity between individual lipid molecules and the effective energy required to bend the bilayer should be much higher than in the bilayers without it.[15] Another puzzling phenomena is the time constant deviation from the sphere shape observed in the vesicles, which bilayer is built from lipids with a high T_m, such as DPPC, DSPC, and HSPC (see Section 6 in the Supporting Information regarding the time stability of solid-ordered vesicles shapes). To this end, a different explanation is proposed, which could explain this discrepancy and phenomena. Since vesicles are formed by electroformation in high temperatures above T_m and then slowly cooled down, the phase-transition process is not rapid enough to cause the rupture of vesicles. What is happening is the slow stiffening of individual, small, flat patches, which rapidly meet at angles, slowly driven by the occurrence of another force, shear elasticity, which has been reported in bilayers below T_m. The system then is slowly reaching new minimal-energy config-uration and, as result, the vesicle we are observing has a considerable deviation from sphericity. This would be extremely visible where the rigid flat patches meet. This would explain why, when analyzing the flat patch, the bending rigidity coefficient is very high, but when treating a system globally (as a vesicle), the system is hardly rigid at all. It would also explain the oddly rectangular shapes of the vesicles we were observing. It is also possible that these phenomena are observed only in a metastable phase, leading to the subgel phase of the membrane. However, this confirmation was observed for considerable amounts of time (at least hours), and the mechanical properties of the membrane in such a state are also worth investigating.

For area compressibility, the simple tendency in homoge-neous lipid bilayers can be found; area compressibility increases with T_m. However, interesting phenomena can be observed in the case of heterogeneous HSPC. Despite both being a mixture of DPPC and DSPC and having a high T_m, its area compressibility is almost equal to that of DMPC (0.26 N/m) and is significantly lower than its component lipids. This result suggests that the heterogeneity of the lipid bilayers can influence the area compressibility in an unexpected nonlinear way.

SUMMARY AND CONCLUSIONS

In this paper, we have investigated the basic structure parameters (membrane thickness, area per lipid of both layers, and vesicle profiles) as well as mechanical properties (bending rigidity coefficient and area compressibility) of selected lipid bilayers. We have selected lipids on the basis of their transition temperature with an aim to investigate solid-ordered bilayers in physiological temperatures. To this end, lipids such as DMPC, DPPC, DSPC, and HSPC were chosen. Each of the bilayers built from those lipids are considered in different phases: rippled P_β gel phase, L_β gel phase, L_c stable crystalline or metastable phase, and the mixture of crystalline and gel phase lipids, respectively. Furthermore, POPC was chosen as a reference for the MD setup verification. Our results of area per lipid (APL) analysis confirmed that the parameter is lower for gel bilayers. We also reconfirmed that the higher value of membrane thickness is larger in solid-ordered than in liquid-ordered bilayers. Bending rigidity coefficients were determined using both flicker noise spectroscopy and 3D fluctuations spectra from MD studies. There was agreement in the parameters from experimental and computational techniques. For homogeneous bilayers, the bending rigidity coefficient decreased with an increase in the transition temperature of the lipids. These results are against intuition, as it could be argued that lipid bilayers are more resilient to mechanical stress when in the solid phase. Additionally, the obtained values of the bending rigidity coefficient were lower than in our flat-patch systems and in the literature data. Opposite dependencies were reported as well. We propose the explanation that the vesicle consists of rigid small patches. When analyzed locally, the bending rigidity is quite high, but when the system is analyzed globally, as for a vesicle, the value decreases, as individual small patches easily bend between each other. This view is additionally strengthened by the high deviation from sphericity observed in the investigated GUVs. Instead of the typical quasi-spherical shape, lipids with a higher T_m formed oddly rectangular shapes. This was mostly visible in HSPC and DSPC vesicles (crystalline phase or metastable phase), seen slightly less in DPPC (gel phase), and almost unobserved in DMPC (rippled gel phase). In the case of area compressibility, the parameter increased with T_m, suggesting that the presence of shear elasticity indeed limits stretching. Surprisingly, for the HSPC bilayer, the value of the bending rigidity was lower than both of its components and, at the same time, area compressibility was higher than both of its components. This suggests that the mechanical properties of the mixed bilayers cannot be straightforwardly calculated, due to either shear elasticity or the topology of the system. We hope that this work will prove valuable in further studies on solid-ordered bilayers as well as starting points to more detailed studies on the effect of bilayer topology from the mechanical point of view at the molecular level.

ASSOCIATED CONTENT

SI Supporting Information

The Supporting Information is available free of charge at https://pubs.acs.org/doi/10.1021/acs.langmuir.0c00475.

> (1) Details of molecular dynamics simulations, (2) calculation of the order parameter for vesicle systems, (3) flicker noise analysis approach for molecular dynamics studies, (4) planar bilayer MD simulations details and mechanical parameters determination, (5) details of flicker noise measurements, and (6) time-stability of solid-ordered vesicles shapes (PDF)

■ AUTHOR INFORMATION

Corresponding Author

> **Dominik Drabik** − *Department of Biomedical Engineering, Faculty of Fundamental Problems of Technology, Wrocław University of Science and Technology, 50-377 Wrocław, Poland;* ⊙ orcid.org/0000-0003-4568-4066; Email: Dominik.Drabik@pwr.edu.pl

Authors

> **Grzegorz Chodaczek** − *PORT − Polish Center for Technology Development, 54-066 Wrocław, Poland*
>
> **Sebastian Kraszewski** − *Department of Biomedical Engineering, Faculty of Fundamental Problems of Technology, Wrocław University of Science and Technology, 50-377 Wrocław, Poland*
>
> **Marek Langner** − *Department of Biomedical Engineering, Faculty of Fundamental Problems of Technology, Wrocław University of Science and Technology, 50-377 Wrocław, Poland*

Complete contact information is available at:
https://pubs.acs.org/10.1021/acs.langmuir.0c00475

Author Contributions

The manuscript was written through contributions of all authors. All authors have given approval to the final version of the manuscript.

Notes

The authors declare no competing financial interest.

■ ABBREVIATIONS

T_m, transition temperature; MD, molecular dynamics; AVB, averaged-based approach; APL, area per lipid; SPHA, spherical harmonics analysis; MT, membrane thickness

■ REFERENCES

(1) Stillwell, W. Introduction to Biological Membranes. In *An Introduction to Biological Membranes*; Gonzalez, P., Ed.; Elsevier: United Kingdom, 2013; pp 3−6.

(2) Humphrey, J. D.; Dufresne, E. R.; Schwartz, M. A. Mechanotransduction and extracellular matrix homeostasis. *Nat. Rev. Mol. Cell Biol.* **2014**, *15* (12), 802−12.

(3) Alonso, M. A.; Millan, J. The role of lipid rafts in signalling and membrane trafficking in T lymphocytes. *J. Cell Sci.* **2001**, *114*, 2957−2965.

(4) Milhaud, J. New insights into water−phospholipid model membrane interactions. *Biochim. Biophys. Acta, Biomembr.* **2004**, *1663* (1−2), 19−51.

(5) Dimova, R. Recent developments in the field of bending rigidity measurements on membranes. *Adv. Colloid Interface Sci.* **2014**, *208*, 225−234.

(6) Marsh, D. Phase Transition Temperatures. In *Handbook of lipid bilayers*; Taylor & Francis Group: New York, 2013; pp 539−600.

(7) (a) Nagle, J. F. Theory of the main bilayer phase transition. *Annu. Rev. Phys. Chem.* **1980**, *31*, 157−195. (b) Bagatolli, L.; Sunil Kumar, P. B. Phase behavior of multicomponent membranes: Experimental andcomputational techniques. *Soft Matter* **2009**, *5*, 3234−3248.

(8) (a) Melchior, D. L. Lipid domains in fluid membranes: a quick-freeze differential scanning calorimetry study. *Science* **1986**, *234* (4783), 1577−80. (b) Lentz, B. R.; Barenholz, Y.; Thompson, T. E. Fluorescence depolarization studies of phase transitions and fluidity in phospholipid bilayers. 2. Two-component phosphatidylcholine liposomes. *Biochemistry* **1976**, *15* (20), 4529−4537. (c) Mabrey, S.; Sturtevant, J. M. Investigation of phase transitions of lipids and lipid mixtures by sensitivity differential scanning calorimetry. *Proc. Natl. Acad. Sci. U. S. A.* **1976**, *73* (11), 3862−3866.

(9) Jørgensen, K.; Sperotto, M. M.; Mouritsen, O. G.; Ipsen, J. H.; Zuckermann, M. J. Phase equilibria and local structure in binary lipid bilayers. *Biochim. Biophys. Acta, Biomembr.* **1993**, *1152* (1), 135−145.

(10) (a) Ruocco, M. J.; Shipley, G. G. Interaction of cholesterol with galactocerebroside and galactocerebroside-phosphatidylcholine bilayer membranes. *Biophys. J.* **1984**, *46* (6), 695−707. (b) Norlen, L. Skin barrier structure and function: the single gel phase model. *J. Invest. Dermatol.* **2001**, *117* (4), 830−836.

(11) Jouhet, J. Importance of the hexagonal lipid phase in biological membrane organization. *Front. Plant Sci.* **2013**, *4*, 494.

(12) Yi, X.; Gao, H. Kinetics of receptor-mediated endocytosis of elastic nanoparticles. *Nanoscale* **2017**, *9* (1), 454−463.

(13) (a) Ishida, T.; Harashima, H.; Kiwada, H. Liposome clearance. *Biosci. Rep.* **2002**, *22* (2), 197−224. (b) Moghimi, S. M.; Hunter, A. C.; Murray, J. C. Long-circulating and target-specific nanoparticles: theory to practice. *Pharmacol. Rev.* **2001**, *53* (2), 283−318. (c) Lombardo, D.; Calandra, P.; Barreca, D.; Magazu, S.; Kiselev, M. A. Soft Interaction in Liposome Nanocarriers for Therapeutic Drug Delivery. *Nanomaterials* **2016**, *6* (7), 125.

(14) Bouvrais, H.; Holmstrup, M.; Westh, P.; Ipsen, J. H. Analysis of the shape fluctuations of reconstitued membranes using GUVs made from lipid extracts of invertebrates. *Biol. Open* **2013**, *2*, 373−378.

(15) Helfrich, W. Elastic Properties of Lipid Bilayers: Theory and Possible Experiments. *Z. Naturforsch., C: J. Biosci.* **1973**, *28* (c), 693−703.

(16) Brochard, F.; Lennon, J. F. Frequency Spectrum of the Flicker Phenomenon in Erythrocytes. *J. Phys. (Paris)* **1975**, *36* (11), 1035−1047.

(17) Akabori, K.; Nagle, J. F. Structure of the DMPC lipid bilayer ripple phase. *Soft Matter* **2015**, *11* (5), 918−26.

(18) (a) Silvius, J. R. *Thermotropic Phase Transitions of Pure Lipids in Model Membranes and Their Modifications by Membrane Proteins*; John Wiley & Sons, Inc.: New York, 1982. (b) Lewis, R. N. A. H.; Mak, N.; McElhaney, R. N. A differential scanning calorimetric study of the thermotropic phase behavior of model membranes composed of phosphatidylcholines containing linear saturated fatty acyl chains. *Biochemistry* **1987**, *26* (19), 6118−6126.

(19) Drabik, D.; Przybyło, M.; Chodaczek, G.; Iglič, A.; Langner, M. The modified fluorescence based vesicle fluctuation spectroscopy technique for determination of lipid bilayer bending properties. *Biochim. Biophys. Acta, Biomembr.* **2016**, *1858* (2), 244−252.

(20) Drabik, D.; Doskocz, J.; Przybyło, M. Effects of electroformation protocol parameters on quality of homogeneous GUV populations. *Chem. Phys. Lipids* **2018**, *212*, 88−95.

(21) Meleard, P.; Pott, T.; Bouvrais, H.; Ipsen, J. H. Advantages of statistical analysis of giant vesicle flickering for bending elasticity measurements. *Eur. Phys. J. E: Soft Matter Biol. Phys.* **2011**, *34*, 116.

(22) Pecreaux, J.; Döbereiner, H.-G.; Prost, J.; Joanny, J.-F.; Bassereau, P. Refined contour analysis of giant unilamellar vesicles. *Eur. Phys. J. E: Soft Matter Biol. Phys.* **2004**, *13*, 277−290.

(23) Phillips, J. C.; Braun, R.; Wang, W.; Gumbart, J.; Tajkhorshid, E.; Villa, E.; Chipot, C.; Skeel, R. D.; Kale, L.; Schulten, K. Scalable molecular dynamics with NAMD. *J. Comput. Chem.* **2005**, *26* (16), 1781−1802.

(24) Lee, S.; Tran, A.; Allsopp, M.; Lim, J. B.; Hénin, J.; Klauda, J. B. CHARMM36 United Atom Chain Model for Lipids and Surfactants. *J. Phys. Chem. B* **2014**, *118* (2), 547−556.

(25) Kučerka, N.; Nieh, M.-P.; Katsaras, J. Fluid phase lipid areas and bilayer thicknesses of commonly used phosphatidylcholines as a

function of temperature. *Biochim. Biophys. Acta, Biomembr.* **2011**, *1808*, 2761−2771.

(26) Braun, A. R.; Sachs, J. N. Determining Structural and Mechanical Properties from Molecular Dynamics Simulations of Lipid Vesicles. *J. Chem. Theory Comput.* **2014**, *10*, 4160−4168.

(27) (a) Khelashvili, G.; Johner, N.; Zhao, G.; Harries, D.; Scott, H. L. Molecular origins of bending rigidity in lipids with isolated and conjugated double bonds: The effect of cholesterol. *Chem. Phys. Lipids* **2014**, *178*, 18−26. (b) Levine, Z. A.; Venable, R. M.; Watson, M. C.; Lerner, M. G.; Shea, J.-E.; Pastor, R. W.; Brown, F. L. H. Determination of Biomembrane Bending Moduli in Fully Atomistic Simulations. *J. Am. Chem. Soc.* **2014**, *136*, 13582−13585. (c) Kawamoto, S.; Nakamura, T.; Nielsen, S. O.; Shinoda, W. A guiding potential method for evaluating the bending rigidity of tensionless lipid membranes from molecular simulation. *J. Chem. Phys.* **2013**, *139*, No. 034108.

(28) Davies, T. A. Algorithm 930: FACTORIZE: An object-oriented linear system solver for MATLAB. *ACM Transactions on Mathematical Software* **2013**, *39* (4), 28.

(29) Waheed, Q.; Edholm, O. Undulation Contributions to the Area Compressibility in Lipid Bilayer Simulations. *Biophys. J.* **2009**, *97*, 2754−2760.

(30) Harzer, U.; Bechinger, B. Alignment of Lysine-Anchored Membrane Peptides under Conditions of Hydrophobic Mismatch: A CD, ^{15}N and ^{31}P Solid-State NMR Spectroscopy Investigation. *Biochemistry* **2000**, *39*, 13106−13114.

(31) Nezil, F. A.; Bloom, M. Combined influence of cholesterol and synthetic amphiphillic peptides upon bilayer thickness in model membranes. *Biophys. J.* **1992**, *61*, 1176−1183.

(32) Pasenkiewicz-Gierula, M; Murzyn, K; Rog, T; Czaplewski, C Molecular dynamics simulation studies of lipid bilayer systems. *Acta Biochimica Polonica* **2000**, *47*, 601−611.

(33) Tsai, H.-H. G.; Lee, J.-B.; Huang, J.-M.; Juwita, R. A Molecular Dynamics Study of the Structural and Dynamical Properties of Putative Arsenic Substituted Lipid Bilayers. *Int. J. Mol. Sci.* **2013**, *14*, 7702−7715.

(34) MacDermaid, C. M.; Kashyap, H. K.; DeVane, R. H.; Shinoda, W.; Klauda, J. B.; Klein, M. L.; Fiorin, G. Molecular dynamics simulations of cholesterol-rich membranes using a coarsegrained force field for cyclic alkanes. *J. Chem. Phys.* **2015**, *143*, 243144.

(35) Venable, R. M.; Brown, F. L. H.; Pastor, R. W. Mechanical properties of lipid bilayers from molecular dynamics simulation. *Chem. Phys. Lipids* **2015**, *192*, 60−74.

(36) Nagle, J. F.; Tristram-Nagle, S. Structure of lipid bilayers. *Biochim. Biophys. Acta, Rev. Biomembr.* **2000**, *1469* (3), 159−195.

(37) Petrache, H. I.; Dodd, S. W.; Brown, M. F. Area per lipid and acyl length distributions in fluid phosphatidylcholines determined by (2)H NMR spectroscopy. *Biophys. J.* **2000**, *79* (6), 3172−92.

(38) Lis, M.; Wizert, A.; Przybylo, M.; Langner, M.; Swiatek, J.; Jungwirth, P.; Cwiklik, L. The effect of lipid oxidation on the water permeability of phospholipids bilayers. *Phys. Chem. Chem. Phys.* **2011**, *13* (39), 17555−63.

(39) Kinnun, J. J.; Mallikarjunaiah, K. J.; Petrache, H. I.; Brown, M. F. Elastic deformation and area per lipid of membranes: atomistic view from solid-state deuterium NMR spectroscopy. *Biochim. Biophys. Acta, Biomembr.* **2015**, *1848* (1 Pt B), 246−259.

(40) Doktorova, M.; Harries, D.; Khelashvili, G. Determination of bending rigidity and tilt modulus of lipid membranes from real-space fluctuation analysis of molecular dynamics simulations. *Phys. Chem. Chem. Phys.* **2017**, *19*, 16806.

(41) Dimova, R.; Pouligny, B.; Dietrich, C. Pretransitional Effects in Dimyristoylphosphatidylcholine Vesicle Membranes: Optical Dynamometry Study. *Biophys. J.* **2000**, *79* (1), 340−356.

(42) Rawicz, W.; Olbrich, K. C.; McIntosh, T.; Needham, D.; Evans, E. Effect of chain length and unsaturation on elasticity of lipid bilayers. *Biophys. J.* **2000**, *79* (1), 328−39.

(43) Nagao, M.; Kelley, E. G.; Ashkar, R.; Bradbury, R. D.; Butler, P. D. Probing Elastic and Viscous Properties of Phospholipid Bilayers

Using Neutron Spin Echo Spectroscopy. *J. Phys. Chem. Lett.* **2017**, *8* (19), 4679−4684.

(44) Hofsäß, C.; Lindahl, E.; Edholm, O. Molecular Dynamics Simulations of Phospholipid Bilayers with Cholesterol. *Biophys. J.* **2003**, *84* (4), 2192−2206.

(45) Meleard, P.; Gerbeaud, C.; Pott, T.; Fernandez-Puente, L.; Bivas, I.; Mitov, M. D.; Dufourcq, J.; Bothorel, P. Bending Elasticities of Model Membranes: Influences of Temperature and Sterol Content. *Biophys. J.* **1997**, *72*, 2616−2629.

(46) Lee, C.-H.; Lin, W.-C.; Wang, J. All-optical measurements of the bending rigidity of lipid-vesicle membranes across structural phase transitions. *Phys. Rev. E: Stat. Phys., Plasmas, Fluids, Relat. Interdiscip. Top.* **2001**, *64*, No. 020901(R).

(47) Et-Thakafy, O.; Delorme, N.; Gaillard, C.; Mériadec, C.; Artzner, F.; Lopez, C.; Guyomarc'h, F. Mechanical properties of membranes composed of gel-phase or fluid-phase phospholipids probed on liposomes by atomic force spectroscopy. *Langmuir* **2017**, *33* (21), 5117−5126.

(48) Delorme, N.; Fery, A. Direct method to study membrane rigidity of small vesicles basedon atomic force microscope force spectroscopy. *Phys. Rev. E* **2006**, *74*, No. 030901(R).

(49) Nagle, J. F. Introductory Lecture: Basic quantities in model biomembranes. *Faraday Discuss.* **2013**, *161*, 11−29.

Supporting Information for:

Mechanical properties determination of DMPC, DPPC, DSPC and HSPC solid-ordered bilayers

Dominik Drabik,[a*] Grzegorz Chodaczek,[b] Sebastian Kraszewski,[a] Marek Langner[a]

[a] Department of Biomedical Engineering, Faculty of Fundamental Technical Problems, Wrocław University of Science and Technology, 50-377 Wrocław, Pl. Grunwaldzki 13, Poland.

[b] PORT – Polish Center for Technology Development, Stabłowicka 147, 54-066 Wrocław, Poland.

* Corresponding author: Dominik.Drabik@pwr.edu.pl

Number of:

pages - 12

figures - 20

tables - 1

1. Molecular Dynamics simulation details of vesicle systems

All full-atomic simulation simulations were performed with the NAMD[1] software and united-atom CHARMM36 force field under NPT conditions. Each of vesicles was modelled with 10nm radius. United atom chain models were used for lipids[2]. The system was hydrated with TIP3P water molecules giving a final simulation box of 30 nm³. Ions were not added to system. It was our aim to recreate experimental setup, where deionized water is used, at accurately as possible. Furthermore ions are charged particles which increase significantly simulations time, as they require calculation of additional electrostatic interactions. Due to significant volume of systems such option was choose in order to avoid prolonged simulation time. Three dimensional periodic boundary conditions were applied in the simulations. Vesicle system was created using custom script in Matlab. Starting area per lipid (APL) value was assumed based on literature data[3]. APL was adopted to account for the effect of vesicle's curvature – multiplied by respectively 0.95 and 1.05 for inner and outer leaflet. Simulations were analysed for at least the last 10ns of
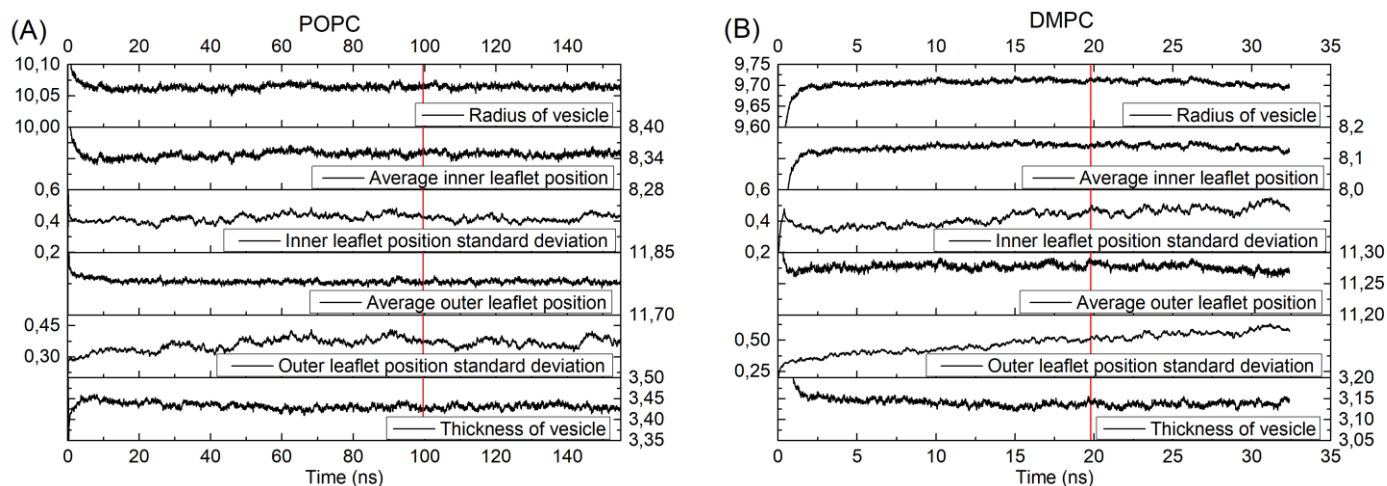
Figure S1. Visualization of six parameters used for equilibration determination for (A) POPC and (B) DMPC vesicle systems. Red line represents the starting point of data used for bending rigidity determination.

equilibrated system. In order to determine equilibration six selected parameters were monitored. Those were vesicle radius, thickness of lipid bilayer, mean values and standard deviations of both inner and outer leaflets. All calculation of this parameters is based on location of phosphorus atom in lipid molecules. The simulations were run with time-step equal to 2fs. The simulated POPC system consisted of 3637 lipid molecules (269 139 atoms) and 748 344 water molecules (2 245 032 atoms). Adopted Area per lipid (APL) was equal to 68.1 Å². There were 1521 lipid molecules in inner leaflet and 2 116 in outer leaflet. As a reference simulation it was carried out for the longest time - total 163 ns simulation time. Final simulation unit cell was equal to 298Å in each of xyz axis. The equilibration parameters are presented in figure S1.A. Last 65 ns of simulation were used for bending rigidity determination. The simulated DMPC system consisted of 3556 lipid molecules (241877 atoms) and 720 421 water molecules (2 161 263 atoms). Adopted APL was equal to 70 Å². There were 1156 lipids in inner leaflet and 2 400 in outer. The simulation was carried out for 32 ns. Final simulation unit cell was equal to 293Å in each of xyz axis. The equilibration parameters are presented in figure S1.B. At the beginning of equilibration spontaneous water pore has opened. It closed itself at the end of equilibration time. Last 13 ns of simulation were used for bending rigidity determination. The simulated DSPC system consisted of 4251 lipid molecules (323077 atoms) and 678 524 water molecules (2 035 572 atoms). Adopted APL was equal to 68.1 Å². There were 1 443 lipids in inner leaflet and 2808 in outer. The simulation was carried out for 35 ns. Final simulation unit cell was equal to 293Å in each of xyz axis. The equilibration parameters are presented in figure S3.A. Last 15 ns of simulation

were used for bending rigidity determination. The simulated DPPC system consisted of 4251 lipids (306 073 atoms) and 693 076 water molecules (2 079 228 atoms). Adopted APL was equal to 65.7 Å². There were 1443 lipid molecules in inner leaflet and 2 808 in outer. The simulation was carried out for 32 ns. Final simulation unit cell was equal to 294Å in each of xyz axis. The equilibration parameters are presented in figure S3.B. Last 12 ns of simulation were used for bending rigidity determination. The simulated HSPC system, as a mixture of 11.4% of DPPC and 88.6% DSPC, consisted of 4328 lipid molecules (326 949 atoms) and 682 785 water molecules (2 048 355 atoms). From those lipid molecules 495 of them was DPPC and 3833 DSPC. Adopted APL was equal to weighted average of DPPC and DSPC APLs. There were 1520 lipids in inner and 2808 it outer leaflet. The simulation was carried out for 31 ns. Final simulation unit cell was equal to 294Å in each of xyz axis. The equilibration parameters are presented in figure S3.C. Last 12 ns of simulation were used for bending rigidity determination.
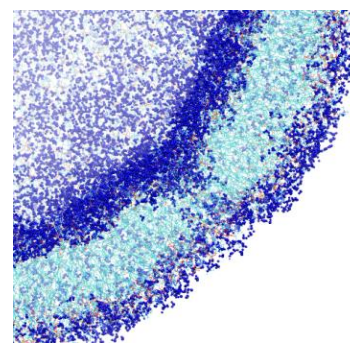

Figure S2. Spontaneous water pore observed during DMPC vesicle equilibration.
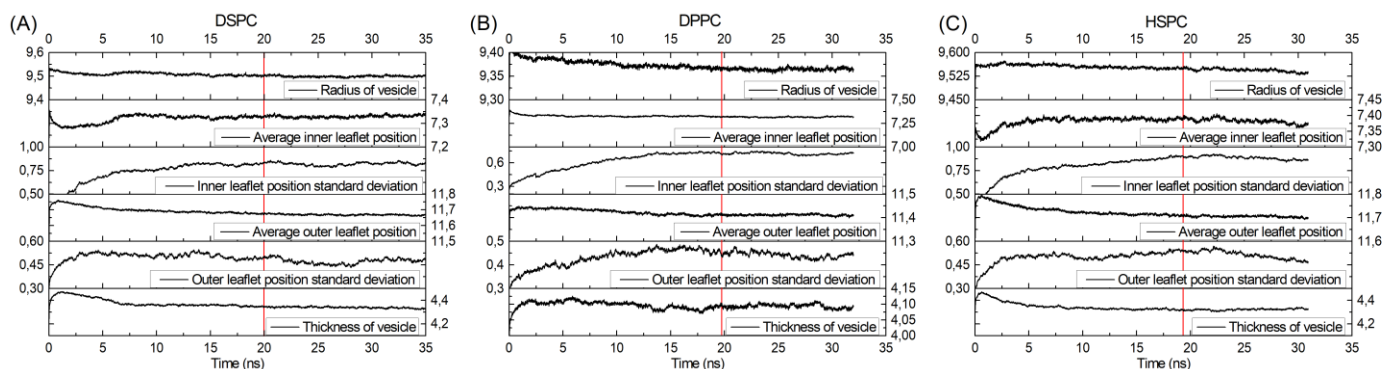
Figure S3. Visualization of six parameters used for equilibration determination for (A) DSPC, (B) DPPC and (C) HSPC vesicle systems. Red line represents the starting point of data used for bending rigidity determination.
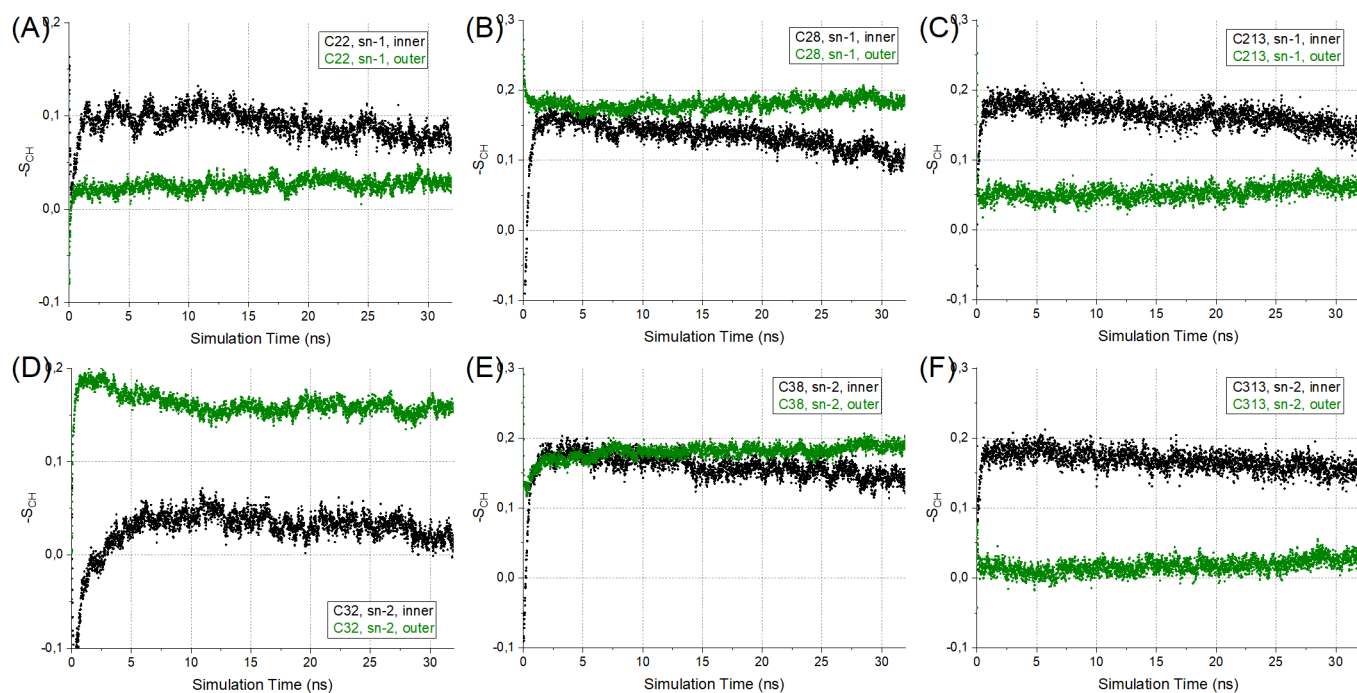
2. Calculation of order parameter for vesicle systems

Carbon-hydrogen order parameter of lipid tails is often used to assess force field accuracy. In this section we are presenting the change of order parameter throughout whole simulation for both inner and outer membranes. Three carbons were selected on both tails – second (C22, C32), eighth (C28,C38) and fifteenth (C215,C315). For DSPC vesicle system thirteen carbon (C213,C313) was selected instead of fifteenth for obvious reasons. Order parameter was calculated by established protocol for united-atom[4] with slight adaptation for vesicle systems. Namely, the vector between vesicle center and position of phosphorus atom for given lipid is treated as membrane normal.
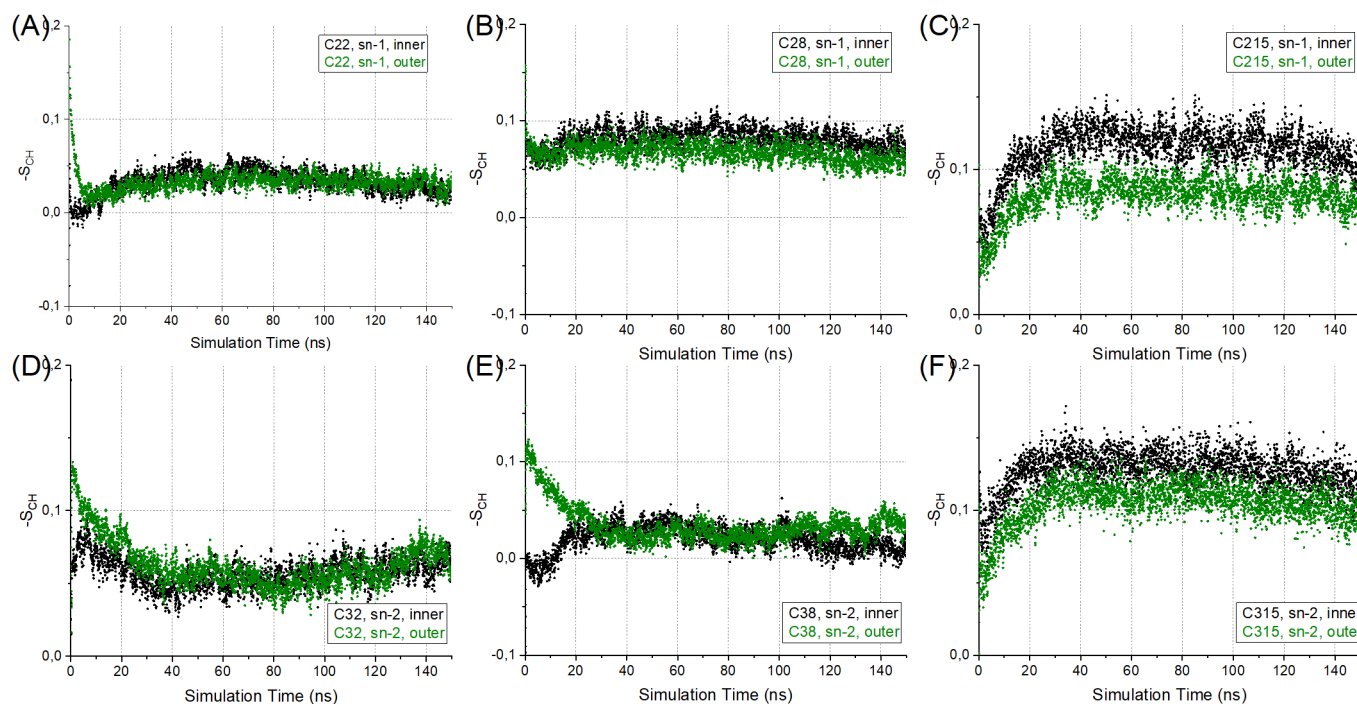
Figure S4. Order parameter for selected carbon atoms in function of simulation time for POPC vesicle system.

Carbon atoms for POPC system located closer to lipid head (namely C22,C32,C28 and C38) became stable after 20 ns of simulations. For C215 and C315 order parameter semi-stabilized after 20 ns, after which constant small drift could be observed. However such drift is to be expected in carbon atoms at the end of carbon tails. Parameter evolution is presented in Figure S4.

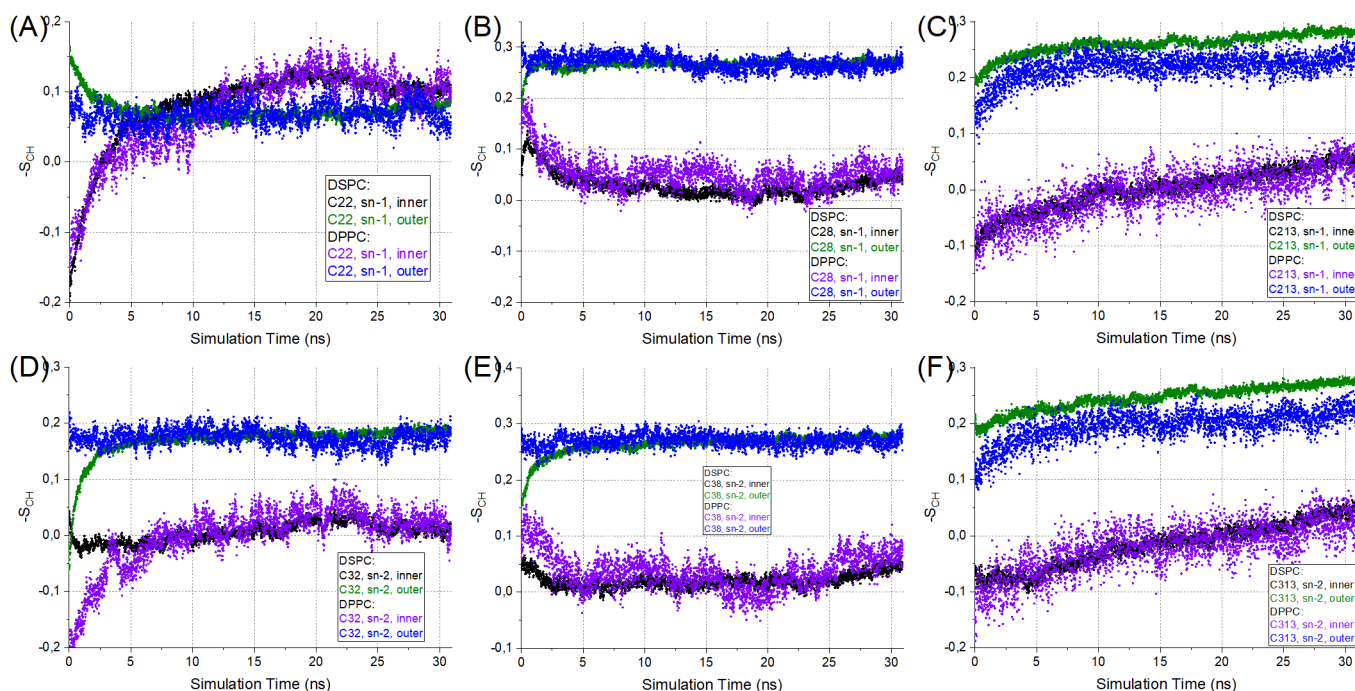**Figure S5.** Order parameter for selected carbon atoms in function of simulation time for DMPC vesicle system.

Carbon atoms in DMPC vesicle system located closer to lipid head (namely C22,C32,C28 and C38) became stable after 10 ns of simulations for sn-2 tail and after 8 ns for sn-1 tail. For carbon atoms at the end of tails the order parameter semi-stabilized almost instantly after less than 2 ns, after which remain constant when a small drift could be observed around 28 ns. Additionally, significant difference was observed in parameter value between the inner and outer leaflets. This was not observed only for middle carbon atom. However it can be concluded that system is thermally stable. Order parameter evolution in time is presented in Figure S5.
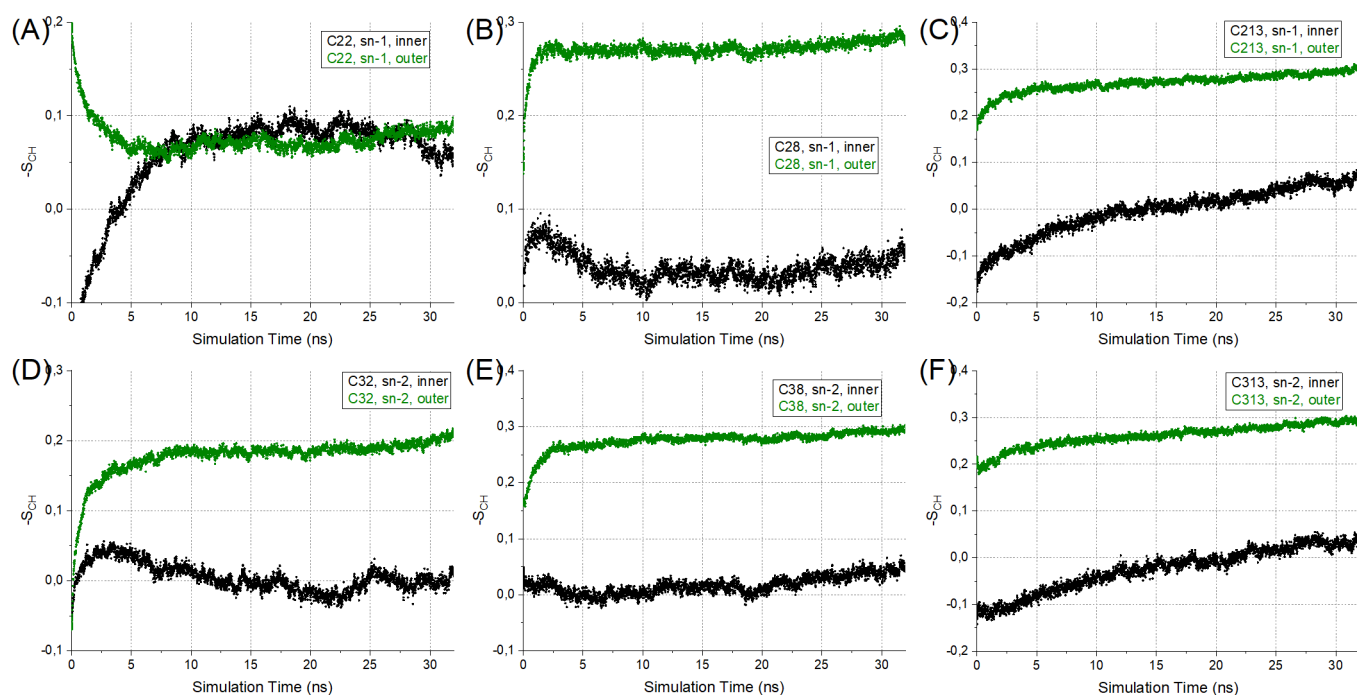

Figure S6. Order parameter for selected carbon atoms in function of simulation time for DSPC vesicle system.

For DSPC system atoms closest to head, namely C22 and C23, obtained stability after 10 ns for both inner and outer leaflets. However the fluctuation of the parameter in time was much higher than observed for POPC or DMPC systems. Similar tendency was observed for C28 and C38 atoms. Additionally it takes longer for inner leaflet to obtain stability. A constant drift was observed for last carbon atoms in tails, the drift was higher in inner leaflet. Except for C22 atom, order parameter values were different between the inner and outer leaflet. Despite that the parameters and stable, therefore system can be treated as thermally stable as well. Order parameter evolution in time is presented in Figure S6.
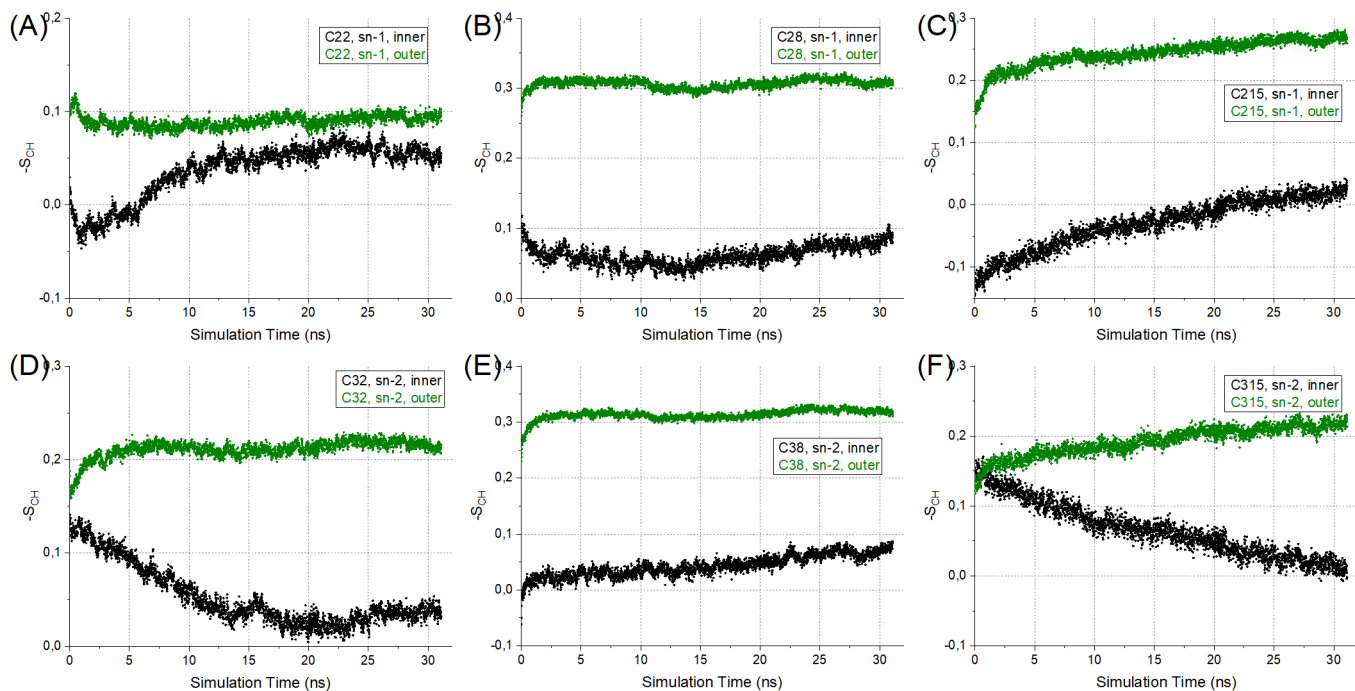
Figure S7. Order parameter for selected carbon atoms in function of simulation time for DPPC vesicle system.

For DPPC system and carbon atoms closest to head, stability was obtained after 15 ns for inner leaflet and after 5ns for outer leaflet. For C28 and C38 stability was obtained relatively quick after 5 ns. However, either small drift or high fluctuation can be observed for carbon atom in inner leaflet. A constant drift was observed for last carbon atoms in tails, after obtaining semi-stability at around 3 ns. It can be concluded that system can be treated as thermally stable after 15 ns. Order parameter evolution in time is presented in Figure S7.

Figure S8. Order parameter for selected carbon atoms in function of simulation time for HSPC vesicle system.

For HSPC system two different lipid types can be found. It can be observed that order parameter value is the same for both DSPC and DPPC lipid molecules. Only exception from this tendency can be observed in C213 and C313 atoms in outer leaflet. For carbon atoms closes to head as well as for middle carbon atoms stability was observed after 8ns. For carbon atoms at the end of tail semi-stability was observed after 4 ns for outer and 10 ns for inner leaflet. However constant small drift was present in both cases. Nevertheless, it can be safely assumed that systems are thermally stable after 10 ns of simulations. Order parameter evolution in time is presented in Figure S8.

3. Flicker-noise analysis approach for Molecular Dynamics simulation

For bending rigidity determination in case of molecular dynamics study the fluctuation analysis is done on whole liposome. However, in case of flicker-noise spectroscopy, only cross-section is analysed and used to mathematically re-establish fluctuations on whole vesicle. To compare accuracy of such approach, fluctuation contour of cross-section of vesicle in molecular dynamics studies was extracted and analysed similarly to flicker-noise images. Fluctuation spectra was collected for range of 3 nm and under five different angles as visualized in Figure S9. Bending rigidity calculated using Braun and Sachs[5] approach was equal to $\kappa=17.86 \cdot k_B T$. When analysed the slice under 0 degree angle it was equal to $17.9 \pm 0.6 \cdot k_B T$ and $17 \pm 3 \cdot k_B T$ from average-based and statistical approaches respectively. In other angles result were within margin of error: for 30 degree slice it was equal to $17.2 \pm 0.7 \cdot k_B T$ and $16 \pm 4 \cdot k_B T$, for 45 degree slice - $16.6 \pm 0.6 \cdot k_B T$ and $15.5 \pm 4.3 \cdot k_B T$ and for 90 degree slice - $17.7 \pm 0.7 \cdot k_B T$ and $17 \pm 4 \cdot k_B T$. In each case first result from average-based approach is presented followed by statistical approach. Only in case of 60 degree angle slice result was slightly different - $13.9 \pm 0.5 \cdot k_B T$ and $14.3 \pm 3.4 \cdot k_B T$. Despite this single discrepancy, it can be concluded that determination of fluctuation spectra from cross section is accurate.
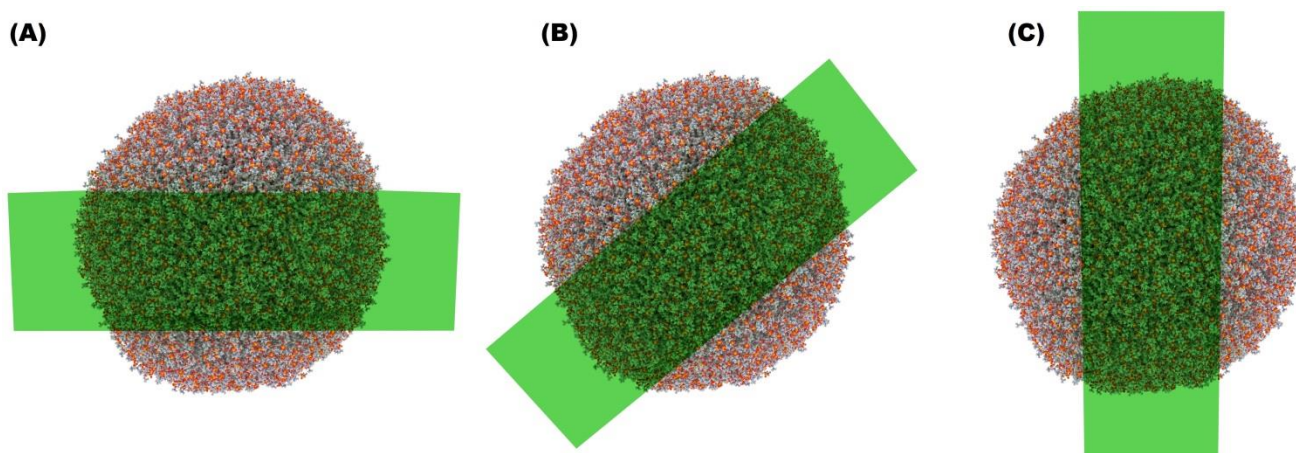
Figure S9. Liposomes used for contour determination in (a) 0 (b) 45 and (c) 90 degree cross-sections. Images were rendered using Blender software.

## 4. Planar bilayer MD simulations details and mechanical parameters determination

Mechanical parameters for investigated lipids were also determined in planar lipid bilayer configuration. All full-atomic simulations were performed with the NAMD[1] software and united-atom CHARMM36 force field[2] under NPT conditions. Specifically, planar lipid bilayers were generated using CHARMM-GUI membrane builder, which was followed with hydrogen removal to reflect united-atom force field. Each investigated bilayer consisted of 648 lipids (324 for each leaflet). For HSPC system the bilayer consisted of 574 DSPC molecules and 74 DPPC molecules. Other options were the same as in vesicle system simulations. Planar bilayer simulations were run for at least 100 ns. Last 50 ns were used for mechanical parameter determination.

To determine mechanical parameters (focusing on bending rigidity coefficient, but also tilt modulus) a real-space fluctuation (RSF) method was used[6]. Specifically, a probability distribution for both tilt and splay is determined for all lipids over all analyzed time steps. Tilt θ is defined as an angle between the lipid director (vector between lipid head – midpoint between C2 and P atoms – and lipid tail – midpoint between last carbon atoms) and bilayer normal. Lipid splay S_r is defined as divergence of an angle formed by the directors of neighboring lipids providing that they are weakly correlated. The method, along with equations and calculations, is thoroughly described in given references. APL in planar bilayer simulation is simply determined by dividing box area over number of lipids, which is followed by averaging over analyzed time steps. In table 1 obtained parameters are presented. In figures S10-S14 obtained probabilities $P(\theta)$ and $P(S_r)$ along with model fit to the potential of mean force (PMF) for each bilayers are presented. Area compressibility is determined using same algorithm as for vesicle systems[7].

Table S1. Mechanical parameter determination from planar lipid bilayer simulations using RSF method.

| Lipid type	APL [Å^2]	κ [J]	κ_t [J]	K_A [N/m]
POPC	62.4 ± 0.6	$(10.8 \pm 0.3) \times 10^{-20}$	$(2.80 \pm 0.04) \times 10^{-20}$	0.18
DMPC	59.4 ± 0.5	$(11.7 \pm 0.4) \times 10^{-20}$	$(2.69 \pm 0.06) \times 10^{-20}$	0.30
DPPC	51.3 ± 0.5	$(23 \pm 1) \times 10^{-20}$	$(3.8 \pm 0.3) \times 10^{-20}$	0,55
DSPC	49.2 ± 0.4	$(19.9 \pm 1.1) \times 10^{-20}$	$(5.3 \pm 0.1) \times 10^{-20}$	0.88
HSPC	49.6 ± 0.2	$(23.2 \pm 1.8) \times 10^{-20}$	$(5.61 \pm 0.32) \times 10^{-20}$	0.48

APL, Area per lipid; κ, bending rigidity coefficient; κ_t, thermodynamic tilt modulus; K_A, area compressibility;
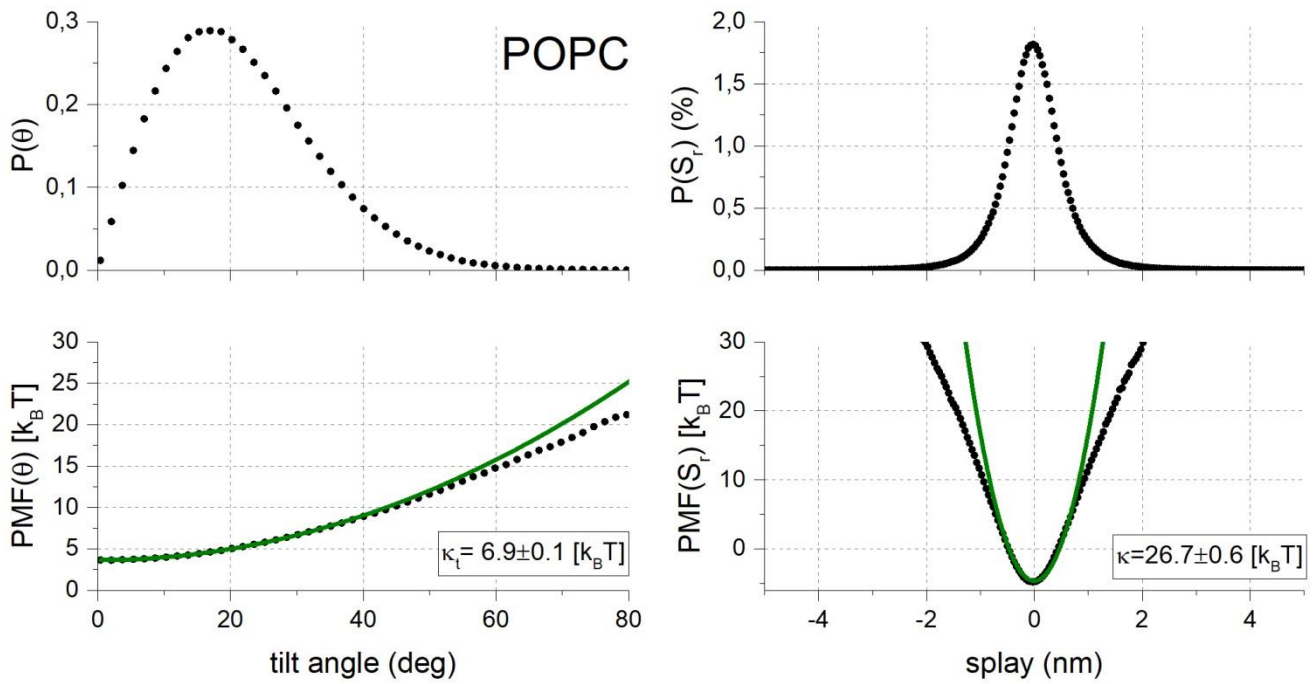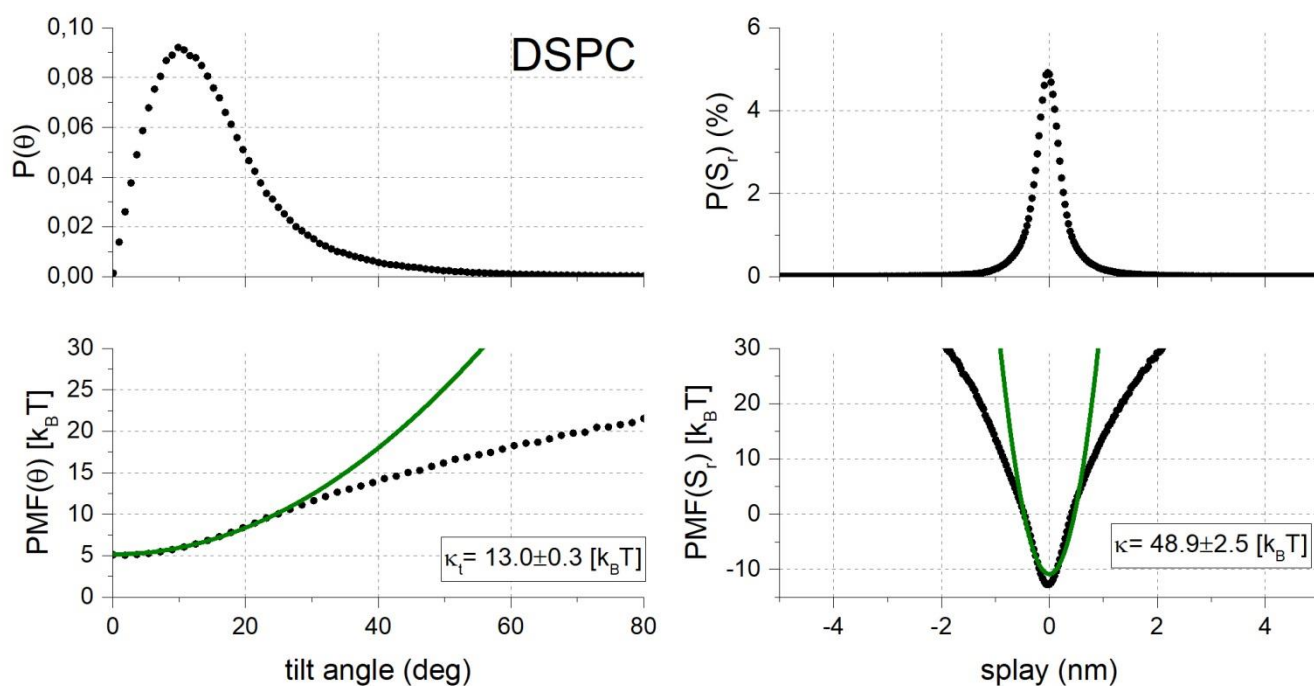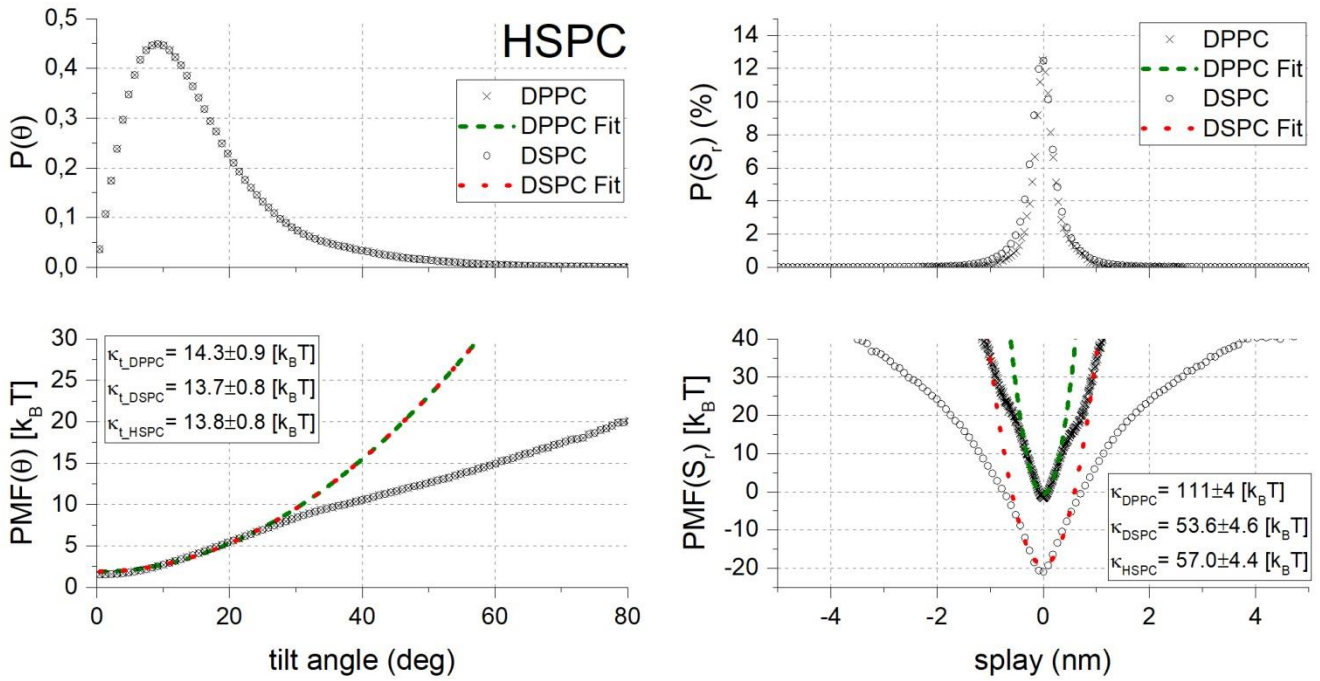
Figure S10. Visualization of the fitting procedure used for the determination of the tilt and splay moduli on example of **POPC** bilayer. Both probability distributions and PMFs of tilt angle θ and lipid splay S are presented. A quadratic function is fitted to PMF in range of [μ-σ, μ+σ] to obtain either tilt of bending moduli in low tilt/splay region. Values of tilt and splay modulus in function of fold k_BT are also included.
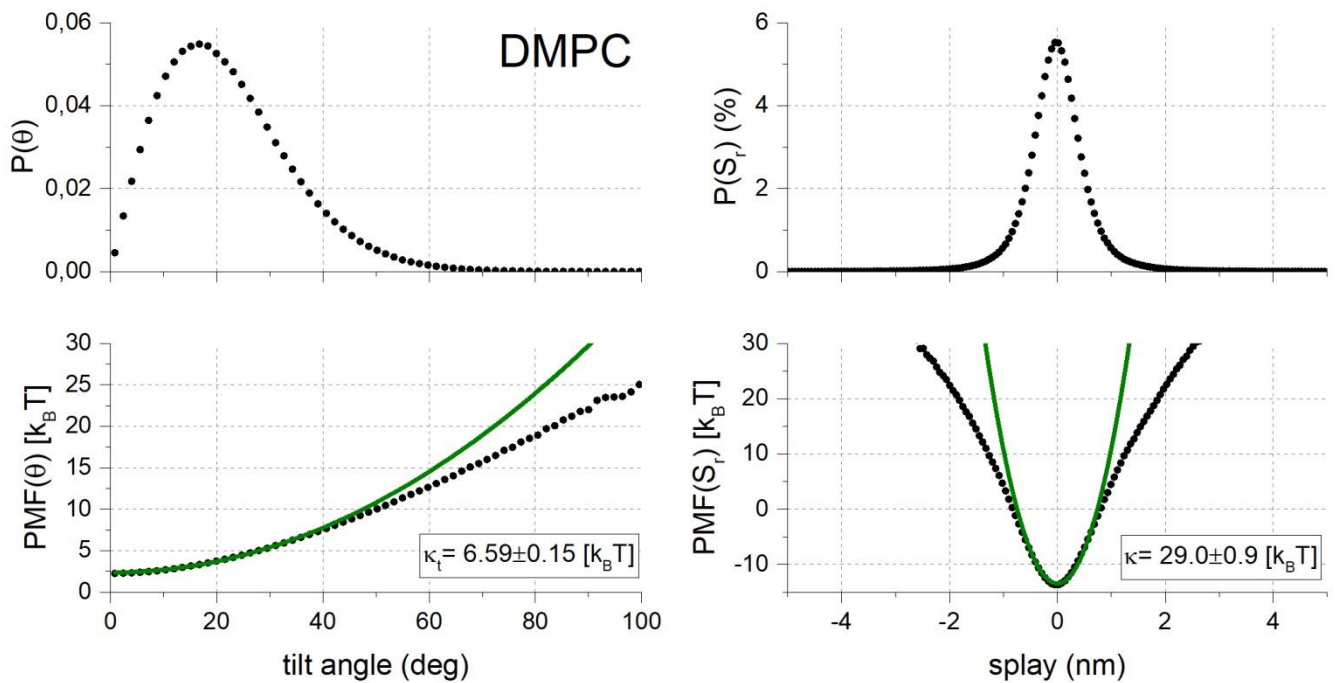

Figure S11. Visualization of the fitting procedure used for the determination of the tilt and splay moduli on example of **DMPC** bilayer. Both probability distributions and PMFs of tilt angle θ and lipid splay S are presented. A quadratic function is fitted to PMF in range of [μ-σ, μ+σ] to obtain either tilt of bending moduli in low tilt/splay region. Values of tilt and splay modulus in function of fold k_BT are also included.
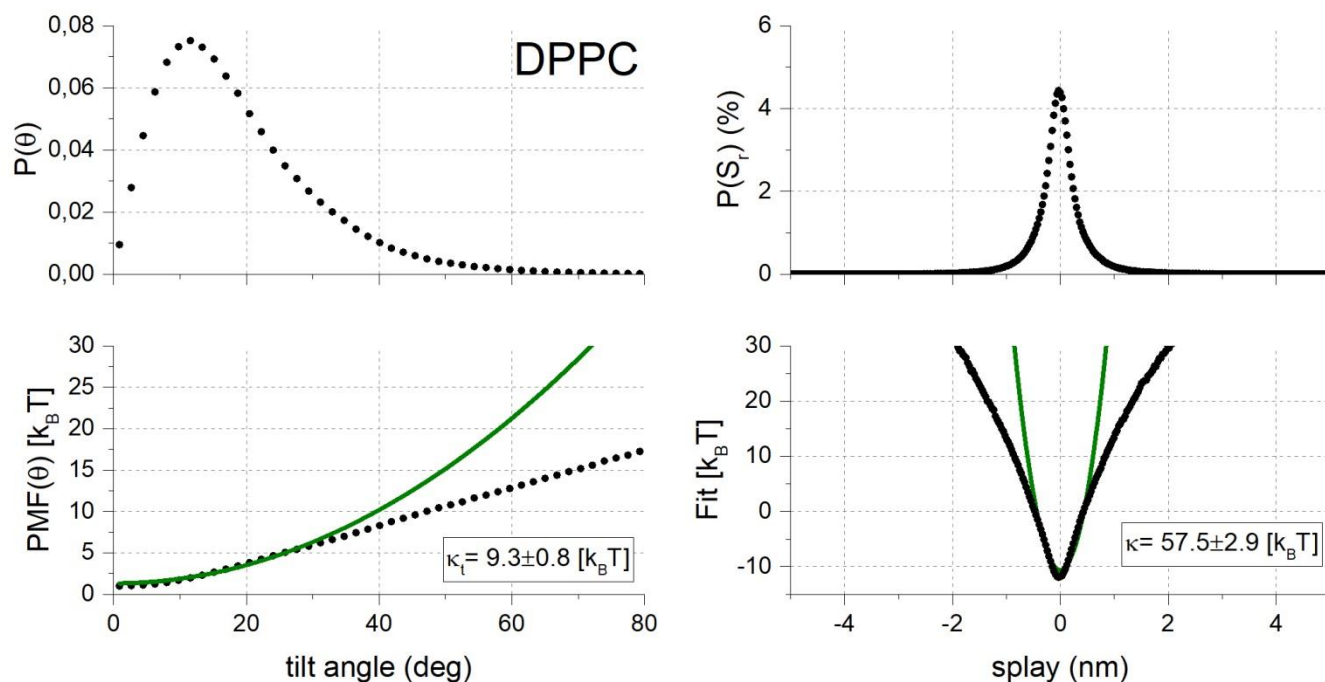
Figure S12. Visualization of the fitting procedure used for the determination of the tilt and splay moduli on example of **DPPC** bilayer. Both probability distributions and PMFs of tilt angle θ and lipid splay S are presented. A quadratic function is fitted to PMF in range of [μ-σ, μ+σ] to obtain either tilt of bending moduli in low tilt/splay region. Values of tilt and splay modulus in function of fold k_BT are also included.

Figure S13. Visualization of the fitting procedure used for the determination of the tilt and splay moduli on example of **DSPC** bilayer. Both probability distributions and PMFs of tilt angle θ and lipid splay S are presented. A quadratic function is fitted to PMF in range of [μ-σ, μ+σ] to obtain either tilt of bending moduli in low tilt/splay region. Values of tilt and splay modulus in function of fold k_BT are also included.

Figure S14. Visualization of the fitting procedure used for the determination of the tilt and splay moduli on example of **HSPC** bilayer. Both probability distributions and PMFs of tilt angle θ and lipid splay S are presented. A quadratic function is fitted to PMF in range of [μ-σ, μ+σ] to obtain either tilt of bending moduli in low tilt/splay region. Values of tilt and splay modulus in function of fold k_BT for individual lipid types are also included, as well as final parameters calculated according to phenomenological dependency established to heterogeneous bilayers.

5. Flicker-noise detailed results

Presented in main paper bending rigidity coefficients determined in flicker noise spectroscopy were averaged values. They are averaged over at least 10 individual vesicles. However average value do not fully show the diversity of individual measurements. To this end the values of bending rigidity coefficient for individual vesicles as well as their average values are presented in this paragraph (Figures S15-18). They are presented for both average-based approach and statistical one. Furthermore image of vesicles are shown to further emphasize the difference in their shape, which is stated in main paper.
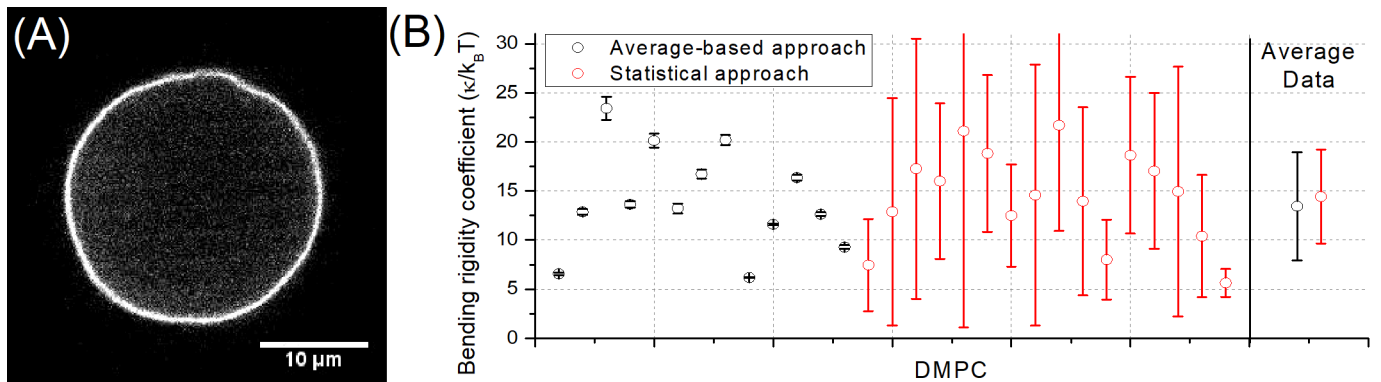
Figure S15. (A) Image of DMPC vesicle and (B) bending rigid coefficient values for individual measurements.
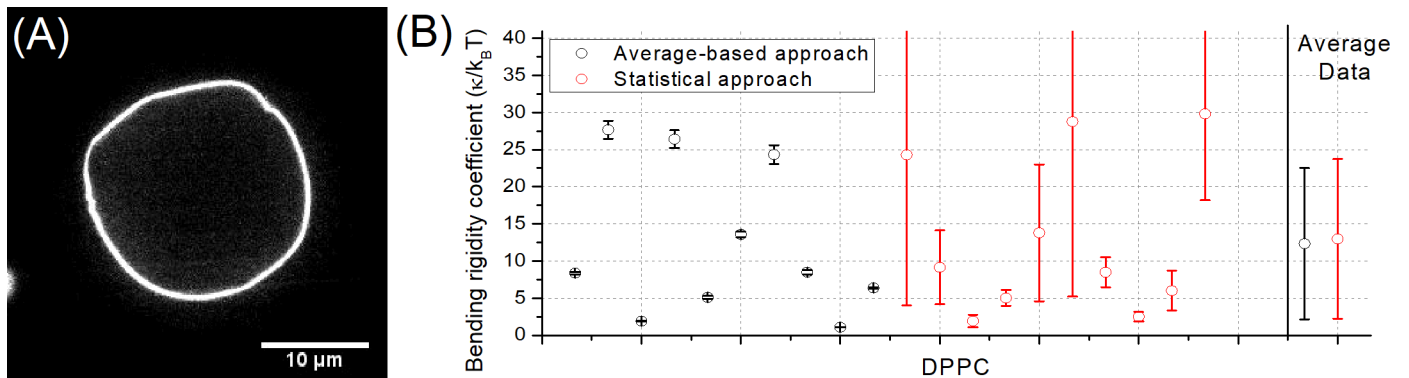
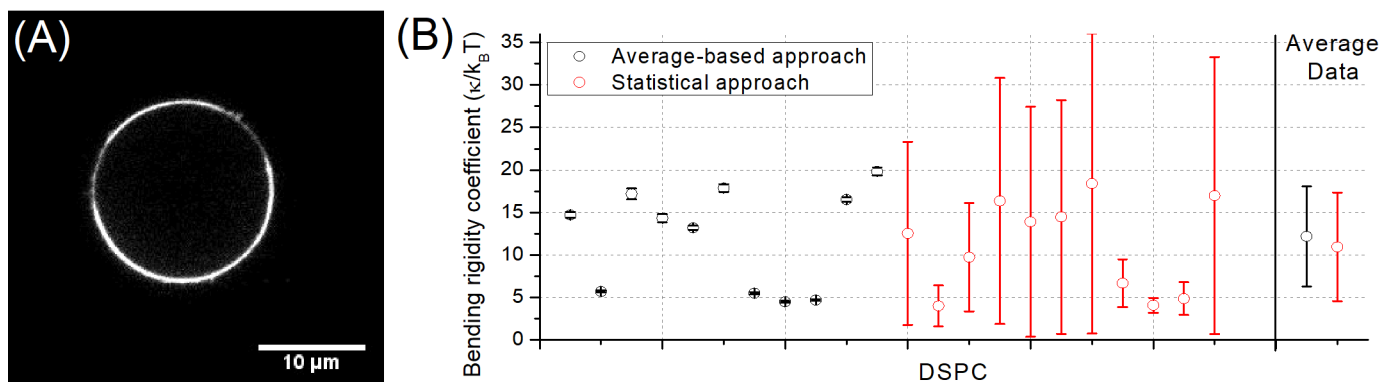Figure S16. (A) Image of DPPC vesicle and (B) bending rigid coefficient values for individual measurements.

Figure S17. (A) Image of DSPC vesicle and (B) bending rigid coefficient values for individual measurements.
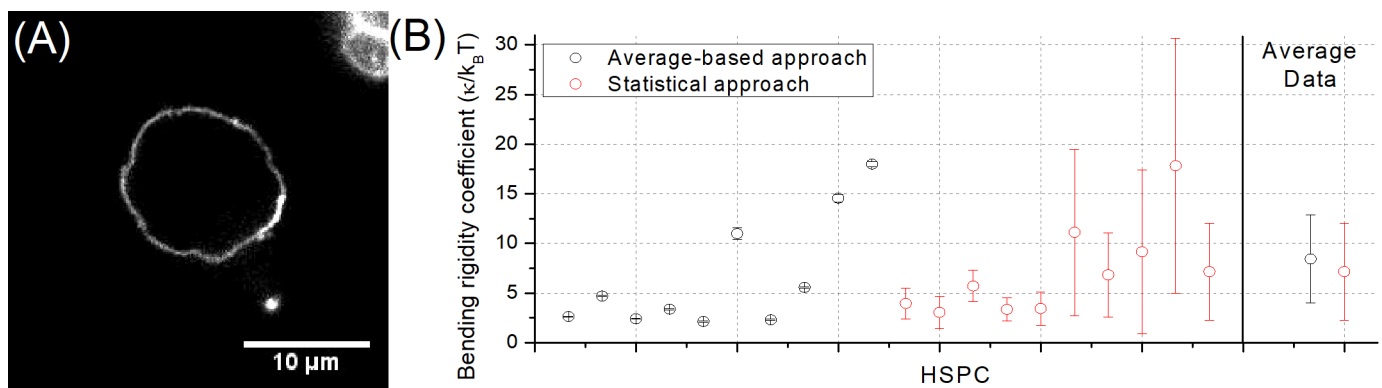

Figure S18. (A) Image of HSPC vesicle and (B) bending rigid coefficient values for individual measurements.

6. Time-stability of solid-ordered vesicles shapes

Vesicles created from lipids with T_m higher than room temperature exhibited oddly-rectangular shape rather than typical quasi-spherical one. This was more visible the higher was the T_m of lipid – namely observed 'bilayer wrinkles' were common view in DSPC, DPPC and HSPC, while they were less visible in DMPC. In this section time stability of this peculiar bilayer shape are shown. As one can see in Figures S9 and S10, visible 'wrinkles' can be seen stable for over a minute. Furthermore, the changes in the vesicle shape is mostly due to rotation of vesicle rather than change of individual *wrinkles*.
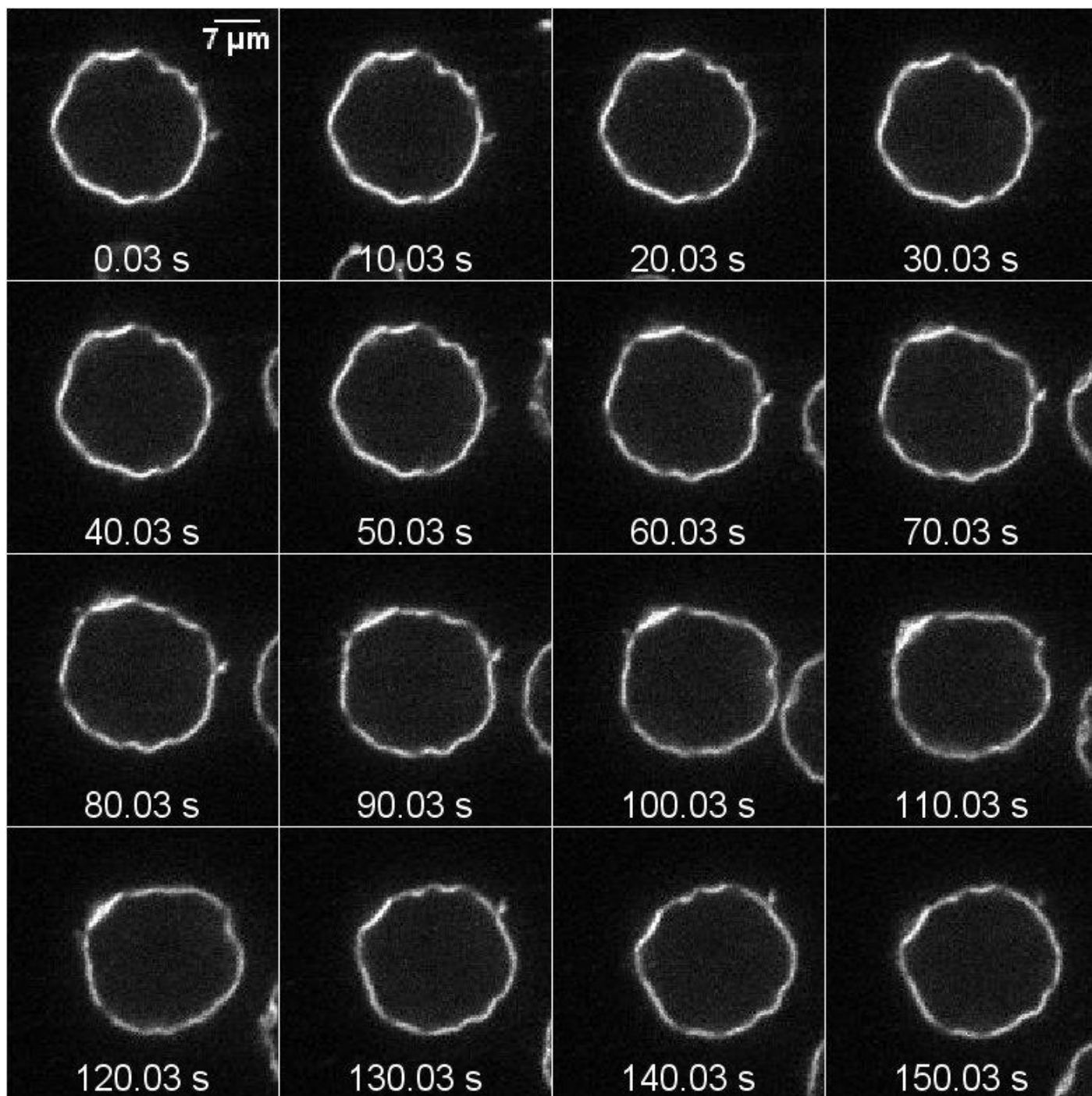
Figure S19. Time evolution of selected DPPC vesicle shape.
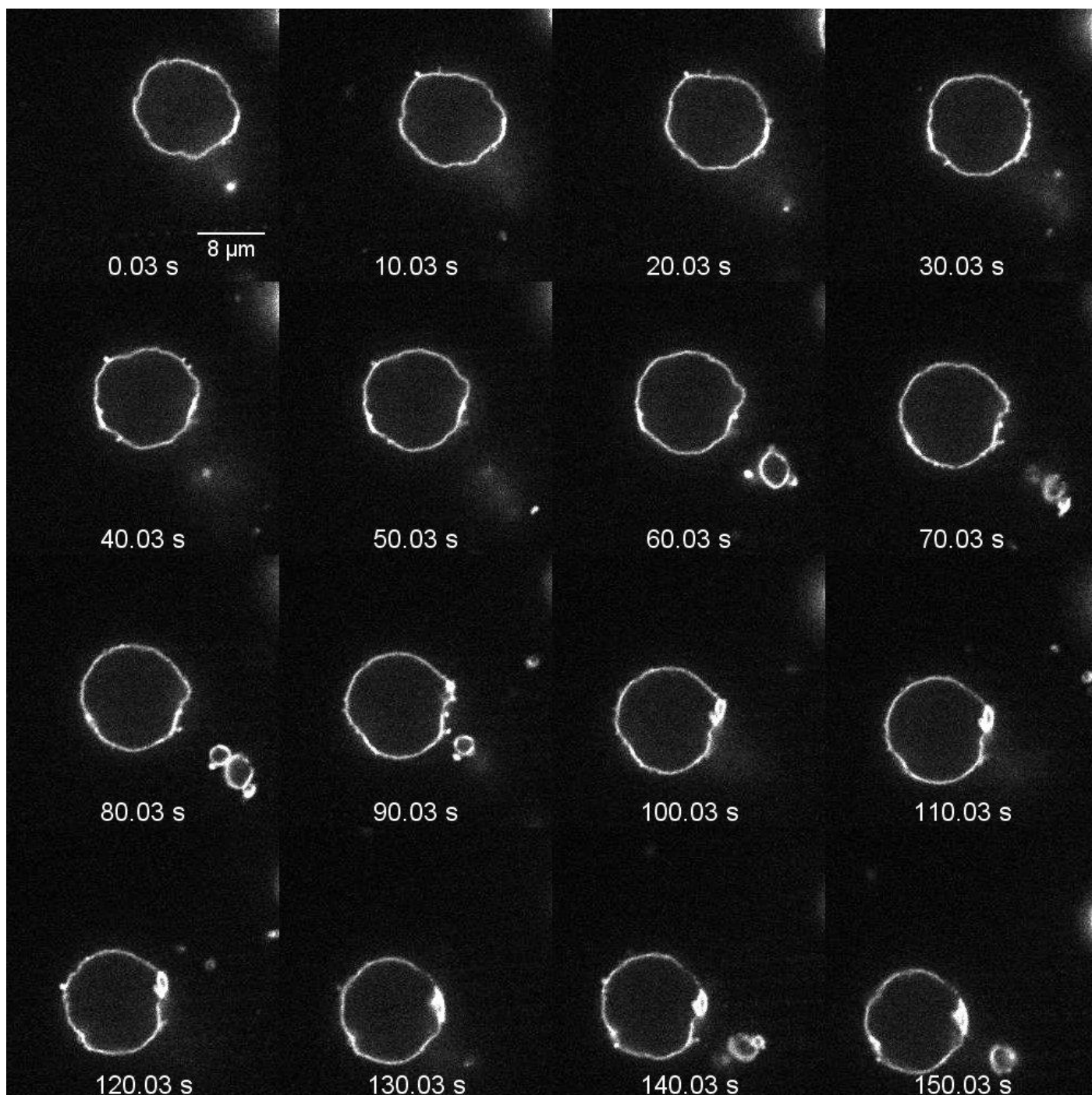
Figure S20. Time evolution of selected HSPC vesicle shape.

6. Bibliography

1.	Philips, J. C.; Braun, R.; Wang, W.; Gumbart, J.; Tajkhorsid, E.; Villa, E.; Chipot, C.; Skeel, R. D.; Kalé, L.; Schulten, K., Scalable molecular dynamics with NAMD. *Journal of Computational Chemistry* **2005**, 26 (16), 1781-1802.

2.	Lee, S.; Tran, A.; Allsopp, M.; Lim, J. B.; Hénin, J.; Klauda, J. B., CHARMM36 United Atom Chain Model for Lipids and Surfactants. *J. Phys. Chem. B* **2014**, 118 (2), 547-556.

3.	Kučerka, N.; Nieh, M.-P.; Katsaras, J., Fluid phase lipid areas and bilayer thicknesses of commonly used phosphatidylcholines as a function of temperature. *Biochimica et Biophysica Acta* **2011**, 1808, 2761-2771.

4.	Piggot, T. J.; Allison, J. R.; Sessions, R. B.; Essex, J. W., On the Calculation of Acyl Chain Order Parameters from Lipid Simulations. *Journal of chemical theory and computation* **2017**, 13 (11), 5683-5696.

5.	Braun, A. R.; Sachs, J. N., Determining Structural and Mechanical Properties from Molecular Dynamics Simulations of Lipid Vesicles. *J. Chem. Theory Comput.* **2014**, 10, 4160-4168.

6.	(a) Doktorova, M.; Harries, D.; Khelashvili, G., Determination of bending rigidity and tilt modulus of lipid membranes from real-space fluctuation analysis of molecular dynamics simulations. Phys. Chem. Chem. Phys. 2017, 19, 16806; (b) Johner, N.; Harries, D.; Khelashvili, G., Curvature and Lipid Packing Modulate the Elastic Properties of Lipid Assemblies: Comparing HII and Lamellar Phases. *The journal of physical chemistry letters* **2014**, 5 (23), 4201-6.

7.	Waheed, Q.; Edholm, O., Undulation Contributions to the Area Compressibility in Lipid Bilayer Simulations. *Biophys J* **2009**, 97, 2754-2760.

5. Acknowledgments

Thank you to my family and loved ones for patience, support and understanding.